King County Combined Sewer Overflow Water Quality Assessment for the Duwamish River and Elliott Bay

Appendix B1: Hydrodynamic and Fate and Transport Numerical Model for the Duwamish River and Elliott Bay

Prepared by the

Duwamish River and Elliott Bay

Water Quality Assessment Team

February 1999

Parametrix, Inc.
5808 Lake Washington Boulevard, NE
Kirkland, Washington, 98033-7350

King County Department of Natural Resources
Wastewater Treatment Division &
Water and Land Resources Division
821 Second Avenue
Seattle, Washington 98104-1598

TABLE OF CONTENTS

Page

TABLE OF CONTENTS (CONTINUED)

Page

ACCOMPANYING VOLUMES

LIST OF FIGURES

Page

LIST OF FIGURES (CONTINUED)

Page

LIST OF TABLES

Page

LIST OF TABLES (CONTINUED)

Page

LIST OF ACRONYMS

ACOE	Army Corps of Engineers
BC	Boundary conditions
BCF	Bioconcentration factor
COD	Coefficient of Determination
COPCs	Chemicals of potential concern
CSOs	Combined sewer overflows
EDRP	Elliott Bay/Duwamish River Restoration Program
EFDC	Environmental Fluids Dynamic Computer Code
IC	Initial concentrations
JD	Julian days
MDL	Method detection limit
MLLW	Mean lower low water
NOAA	National Oceanic and Atmospheric Administration
PAHs	Polyaromatic hydrocarbons
PCB	Polychlorinated biphenyls
PSD	Power spectral density
QA/QC	Quality Assurance/Quality Control
RDLs	Reporting Data Limits
REM	Relative Error of the Means
SAIC	Science Applications International Corp
SPMD	Semi-permeable Membrane Devices
TBT	Tributyltin
TOC	Total Organic Carbon
TSS	Total suspended solids
USGS	United States Geological Survey
WLRD	Water and Lands Resource Division
WQA	Water Quality Assessment
WSDOE	Washington State Department of Ecology
WTD	Wastewater Treatment Division

1. INTRODUCTION

This report documents the constituents of potential concern (COPC) selection process, a data bibliography of the field sampling programs and the hydrodynamic and fate and transport numerical modeling methodology used for the Combined Sewer Overflow Water Quality Assessment for the Duwamish River and Elliott Bay. This Water Quality Assessment (WQA) is an assessment of the ecological and human risks from exposure to pollutants in the Duwamish River and Elliott Bay, and of what part of these risks are from combined sewer overflows (CSOs). Figure 1-1 shows the study area, which encompasses Elliott Bay and part of the Duwamish/Green River. The area of particular interest for the risk assessment extends from the Duwamish Head in Elliott Bay to the turning basin in the Duwamish River. Risks to wildlife, aquatic life, and human health were assessed based on results from the computer model and field data.

COPCs for the risk assessment were:

- Metals: arsenic, cadmium, copper, lead, nickel, zinc, mercury, tributyltin
- Organic Compounds: 1,4 dichlorobenzene, 4 methylphenol, bis(2-ethylhexyl)phthalate, fluoranthene, phenanthrene, total PCBs, pyrene, benzo(k)fluoranthene, chrysene, benzo(b)fluoranthene
- fecal coliform bacteria

The computer model was used (primarily) for two purposes:

1. As a mass balancing tool to estimate chemical contributions from other sources given CSO, ambient, and boundary chemical loads.
2. To estimate chemical concentrations for conditions with and without CSO discharges. The estimates will be used to determine the change in risk to human health, wildlife, and aquatic life for conditions without CSOs.

1.1 The Duwamish Estuary

The Duwamish Estuary is defined as the body of water from Elliott Bay up to 18.5 kilometers upstream in the Duwamish River. The Duwamish River is located in the heart of Seattle's industrial area south of downtown and flows north into the southern tip of Elliott Bay. It is a heavily used shipping port and is a significant habitat area for salmon and other wildlife. Most of the river is dredged for shipping with dredging extending upstream to the turning basin approximately 12.5 kilometers upstream from the mouth. The river is well stratified (salt wedge type) when freshwater inflow rates are greater than 1,000 cfs; but when flows are less than 1,000 cfs, the lower 5.5 kilometers of the estuary grades into the partly mixed type.

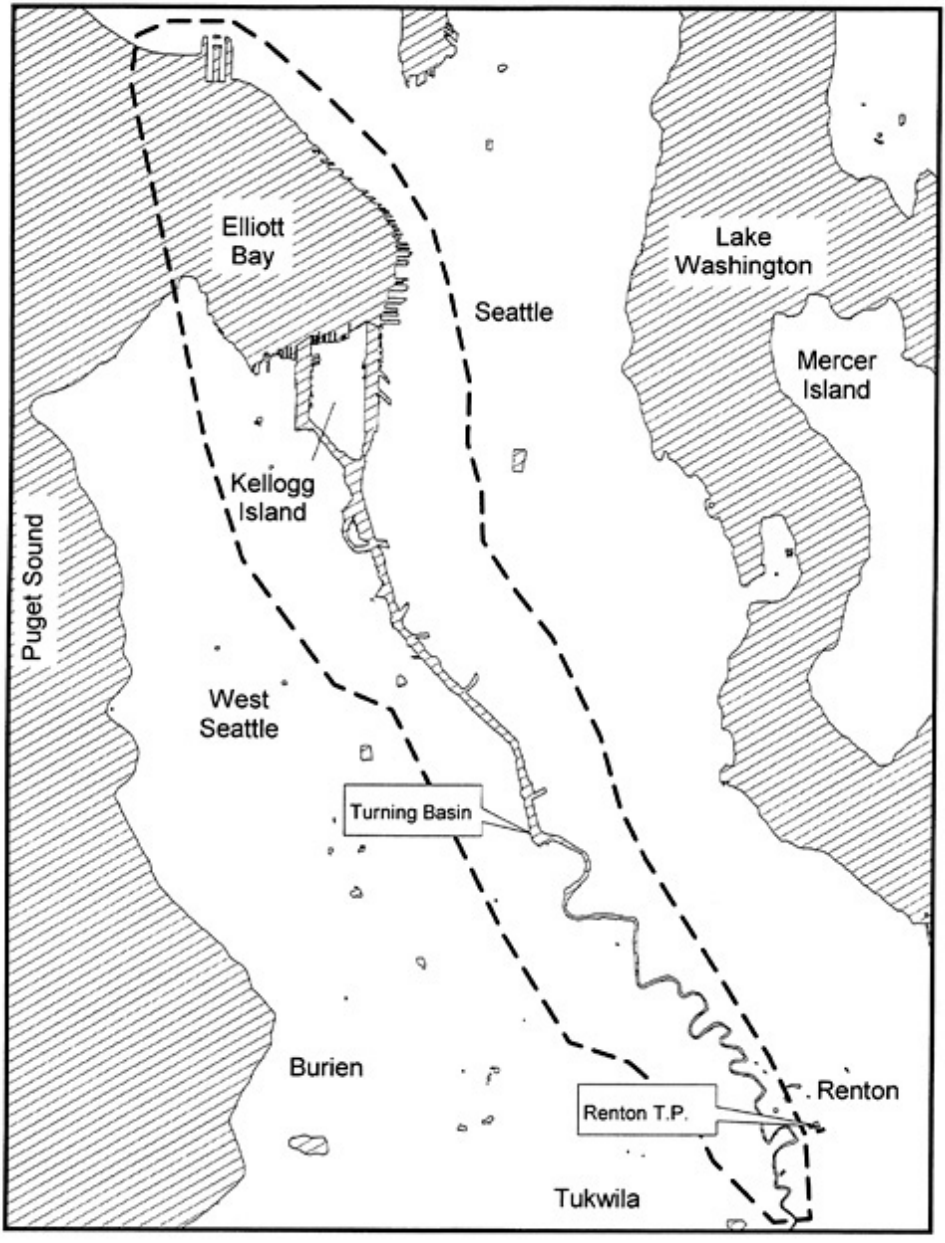

Water Quality Assessment Area - - - - -

King County/Duwamish/55-1521-27(07) 1/99

Figure 1-1.
Water Quality
Assessment Study Area

The cross-channel salinity distribution is generally uniform for a given location and depth. Salinity migration is controlled by tides and freshwater flow. The upstream extent of the wedge is dependent upon freshwater inflow and tide height, except that flows greater than 1,000 cfs will prevent intrusion of the wedge farther than 12.6 km upstream, regardless of tide height. At freshwater inflow less than 600 cfs and at tide heights greater than ten feet above mean lower low water (MLLW), the salt wedge has extended upstream approximately 16 km above the mouth. Dye studies indicate that downward vertical mixing over the length of the salt wedge is almost nonexistent.

Freshwater flow into the Duwamish River comes from the Green River. The Green River is regulated at the Howard Hanson dam for flood control. However, flow rates do vary considerably day to day because of storm runoff and snow melt. Upstream tidal flow reversal has been observed in the Green River 21 km upstream of the mouth of the estuary.

Water depth in the dredged sections of the Duwamish River vary from 15 meters MLLW at the mouth to four meters at 14th Avenue bridge (9.5 km). The channel above the turning basin is not dredged and varies in depth from 1 to 1.5 meters MLLW. Elliott Bay, at its deepest location, is about 160 meters MLLW. Tides in the Duwamish River have ranged from minus 1.4 to plus 4.5 meters from MLLW.

1.2 Modeling Objective

The objective of the WQA was to determine the change in risk to humans, wildlife and aquatic life when CSOs were removed from the estuary and bay. To estimate how things would change when CSOs were removed required the use of a computer model. It was also necessary to use the model as a tool to estimate mass loading contributions from other sources. Once the other source components were sufficiently quantified, the model was used to determine how chemical concentrations in the water and sediments changed when CSOs were removed.

In using the model to estimate other source loads to the area, it was assumed there were only three general chemical sources in the estuary; boundaries, CSOs, and other sources (which include but are not limited to, storm drains, groundwater, over-land flow, etc.). The model was used to estimate other sources because of limited financial resources, the County only had funds enough to collect field information on CSO chemical compounds and ambient chemical concentrations. Knowing two of the three sources, the computer model was employed as the third equation to estimate inputs from the other chemical sources. The model was configured to represent physical features, chemical and flow conditions at the boundaries; to CSO discharges and concentrations, and an initial set of other source loads.

Before the model was used to estimate the other sources and simulate conditions without CSO discharges, it had to be calibrated for hydrodynamic processes. Calibration is the process of comparing model predictions against measured field data and adjusting certain model parameters until the model predictions adequately match field data. The

hydrodynamic calibration process is described later in the report in the Hydrodynamic Calibration section.

Hydrographs used to describe other source load inputs were estimated from the basin model the County uses to determine sewage flows to the West Point Treatment Plant. Details of how the hydrographs were developed are given later in the report in the Stormwater Hydrology section.

Once the other source loads had been estimated and the hydrodynamic calibration was completed, the model was used to estimate chemical mass contributions to the estuary and bay. Simulated chemical concentrations from the model were compared to measured concentrations from the field monitoring program. Other source chemical loads were adjusted until model predicted chemical concentrations were comparable to observed chemical concentrations in the field. This process was termed the "mass calibration". When the mass calibration was completed, the model was used to separate water and sediment contaminant concentrations from CSOs and from other sources by simulating two scenarios: one scenario operated with all chemical inputs estimated in the calibration (boundary, CSOs, and other sources) discharging into the estuary; the other scenario operated with only boundary and other sources (CSOs were omitted). Differences in chemical concentrations between the two scenarios were ascribed to CSOs.

The model was configured to simulate a one-year scenario to look at differences in risk between CSOs and other sources in the water and sediments. Chemical concentrations were saved at one-hour intervals for use in the risk assessment.

The one-year simulations are of sufficient duration to understand how the various sources affect concentrations in the water, but provides only an estimate of how the sediments would be affected. Sediments respond very slowly to changes from chemical sources. They may take tens of years to fully respond to changes. To understand how existing discharges could potentially affect sediment concentrations, the model was configured to repeat the one-year simulation over ten cycles, or ten one-year periods. The ten cycles would allow for some type of equilibrium between sediments and water column under existing discharges. Ten cycles were chosen because the model required such large amounts of computer time to simulate multiple chemicals at the given spatial resolution that the number of simulations had to be limited in order to finish the modeling in a timely manner.

1.3 COPC Identification and Data Collection Bibliography

The first steps in predicting baseline and without CSO chemical concentrations in the study area required selecting which chemicals posed potential risks to the receptors and collecting sufficient data on these chemicals to calibrate the hydrodynamic model. This section presents the results of the Constituents of Potential Concern (COPC) selection process.

1.3.1 Selection of Candidate COPCs

Selecting candidate COPCs involved a number of steps—(1) determining the presence and quantity of chemicals in the study area as well as analytical detection limit goals; (2) identifying water and sediment criteria for use in screening these value; and (3) developing surrogate approaches to handle the number of chemicals that were eventually selected. King County's 1997 sampling program analyzed a total of forty-five candidate chemical COPCs, as well as fecal coliforms (Table 1-1).

Table 1-1. Candidate COPCs[a] Evaluated for Inclusion in EFDC Model

1,4-Dichlorobenzene	Benzo(e)pyrene	Dibenzo(a,h)anthracene	Nickel
2-Methylphenol	Benzo(g,h,i)perylene	Dibenzofuran	Pentachlorophenol
4-Methylphenol	Benzo(k)fluoranthene	Dieldrin	Phenanthrene
Aldrin	Benzoic Acid	Fecal Coliforms	Pyrene
Antimony	Benzyl Alcohol	Fluoranthene	Silver
Arochlor 1254	Benzyl Butyl Phthalate	Gamma-BHC (Lindane)	Total HPAHs
Arsenic	Beryllium	Heptachlor	Total PCBs
Barium	Bis(2-ethylhexyl)phthalate	Hexachlorobenzene	Tributyltin
Benzidine	Cadmium	Indeno(1,2,3-cd)Pyrene	Vanadium
Benzo(a)anthracene	Chromium (Total)	Iron	Zinc
Benzo(a)pyrene	Chrysene	Lead	
Benzo(b)fluoranthene	Copper	Mercury	

[a] While not a chemical, fecal coliforms were included in this list as they could be evaluated using the EFDC model.

These chemicals were screened following the approach outlined in the Analysis Plan (Appendix A3). Chemicals were initially screened for frequency of detection, with infrequently detected chemicals then further evaluated to determine if the method detection limit (MDL) was less than the detection goal[1]. Infrequently detected chemicals

[1] The detection goal the lowest concentration of this chemical that would produce a hazard quotient of one for the most sensitive receptor, based on the identified exposure pathway for that receptor.

with MDLs greater than detection goals were not selected as candidate COPCs, and instead have been identified as posing uncertain risk[2].

Frequently detected chemicals were then compared against water and sediment criteria (Analysis Plan Citation) after calculating the appropriate 95th percentile (the sample 95th percentile for the water column and the 95th percentile on the mean for sediments). Chemicals with percentiles exceeding the criteria were selected as being candidate COPCs requiring further evaluation in the detailed risk assessment (Table 1-2). Those with percentiles less than criteria were not selected for further evaluation because they posed no risks (Table 1-3).

Table 1-2. Chemicals Selected as Candidate COPCs for Use in the EFDC Model

Chemical	Reason for Selection
1,4-Dichlorobenzene	Exceeded sediment criterion, 1997 sampling data
4-Methylphenol	Exceeded sediment criterion, Duwamish/Diagonal Study
Arsenic	Exceeded sediment criterion, Duwamish/Diagonal Study; present in mussel tissue, 1996-1997 sampling data
Benzo(a)anthracene	Known human carcinogen, present in mussel tissue, 1996-1997 sampling data
Benzo(a)pyrene	Known human carcinogen
Benzo(b)fluoranthene	Known human carcinogen, present in mussel tissue, 1996-1997 sampling data
Benzo(g,h,i)perylene	Exceeded sediment criterion, Norfolk Study
Benzo(k)fluoranthene	Known human carcinogen
Bis(2-ethylhexyl)phthalate	Exceeded sediment criterion, 1997 sampling data, present in mussel tissue, 1996-1997 sampling data
Cadmium	CSO concentrations exceeded water criterion and present in mussel tissue, 1996-1997 sampling data
Chrysene	Known human carcinogen, present in mussel tissue, 1996-1997 sampling data
Copper	CSO concentrations exceeded water criterion and present in mussel tissue, 1996-1997 sampling data
Dibenzo(a,h)anthracene	Known human carcinogen
Fecal Coliforms	Indicator of pathogen contamination, present in mussel tissue,

[2] Risk is uncertain because the high MDLs automatically generate hazard quotients greater than one, without regard to the actual concentrations of this chemical in the environment.

	1996-1997 sampling data
Fluoranthene	Exceeded sediment criterion and present in mussel tissue, 1996-1997 sampling data
Indeno(1,2,3-cd)pyrene	Exceeded sediment criterion, 1997 sampling data
Lead	CSO concentrations exceeded water criterion and present in mussel tissue, 1996-1997 sampling data
Mercury	Exceeded sediment criterion, Duwamish/Diagonal Study; present in mussel tissue, 1996-1997 sampling data

Table 1-2. Chemicals Selected as Candidate COPCs for Use in the EFDC Model (continued)

Chemical	Reason for Selection
Nickel	CSO concentrations exceeded water criterion and present in mussel tissue, 1996-1997 sampling data
Phenanthrene	Exceeded sediment criterion and present in mussel tissue, 1996-1997 sampling data
Pyrene	Present in mussel tissue, 1996-1997 sampling data
Total PCBs	Exceeded sediment criterion, 1997 sampling data
Tributyltin	Present in mussel tissue, 1996-1997 sampling data
Zinc	CSO concentrations exceeded water criterion and present in mussel tissue, 1996-1997 sampling data; Sediment exceedance, Duwamish/Diagonal Study.

Table 1-3. Chemicals Not Selected as Candidate COPCs for Use in the EFDC Model

Chemical	Reason Not Selected	Comment
2-Methylphenol	Not detected in sediment or water	Present in mussel tissue, 1996-1997 sampling data
Aldrin	Not detected in any media	Exceeded detection limit goals[a]
Antimony	No state criteria for evaluation	But Draft USEPA 1988 Acute AWQC = 30 µg/L, Chronic AWQC = 88 µg/L
Aroclor 1254	Not detected in sediment or water	Present in mussel tissues, 1997 sampling data. Included in Total PCBs
Barium	Overall toxicity is low	Exceeds water criterion in CSO effluent
Benzidine	Overall toxicity is low	Exceeds 1997 sampling data detection limit goals in background water, CSO effluent, mussel tissue
Benzo(e)pyrene	Not detected in any media	Exceeded detection limit goals
Benzoic Acid	Overall toxicity is low	Sediment exceedance in Norfolk Study, detected in mussel tissue, 1997 sampling data

Table 1-3. Chemicals Not Selected as Candidate COPCs for Use in the EFDC Model (continued)

Chemical	Reason Not Selected	Comment
Benzyl Alcohol	Not detected in sediment or water	Identified in 1995 WQA report, present in mussel tissue, 1996-1997 sampling data
Benzyl Butyl Phthalate	Not detected in sediment or water	Sediment exceedance in Duwamish/Diagonal Study, present in mussel tissue, 1996-1997 sampling data
Beryllium	Not detected in any media	Exceeded minimum detection limit goals in background water and CSO effluent
Chromium (Total)	Not detected in sediment or water	Only present in mussel tissue as chromium III.
Dibenzofuran	Not detected in any media	All non-detects in sediment, background water and CSO effluent, 1996-1997 sampling data.
Dieldrin	Not detected in any media	Exceeded detection limit goals
Gamma-BHC (Lindane)	Not detected in any media	Exceeded detection limit goals
Heptachlor	Not detected in any media	Exceeded detection limit goals
Hexachlorobenzene	Not detected in any media	Exceeded detection limit goals and exceeded sediment criterion in the Duwamish/Diagonal Study
Iron	Infrequently detected	What data is available has 95th percentile greater than criteria and exceeded background water detection limit goals.
Pentachlorophenol	Not detected in any media	Exceeded detection limit goals in background water and CSO effluent
Silver	Not detected in any media	Identified in 1995 WQA report
Total HPAHs	Not detected in any media	Identified in sediments in Duwamish/Diagonal Study and 1995 WQ report. Assessed as individual chemicals.
Vanadium	Overall toxicity is low	Exceeded water criterion in CSO effluent

[a] Detection limit goals are defined in the following section.

1.3.2 Detection Limit Goals

Detection limit goals were developed for water column (Table 1-4) and tissue measurements (Table 1-5). These goals were derived from exposures for aquatic life, wildlife, and people by back-calculating water and tissue concentrations from toxicity effects thresholds that would not represent risks to these receptors. Non-detect measurements determined by analytical protocols with Reporting Data Limits (RDLs) greater than these values would represent uncertain, "paper" risks to these receptors. That this, as these non-detects would be greater than the toxicity thresholds, they would represent a highly uncertain risk to receptors. Detection limit goals were used only for chemicals with low levels of detection in the relevant media as presented above.

Table 1-4. Minimum Water Column Detection Goals Necessary to Reduce Analytical Uncertainty in the Risk Assessment

Chemical	Minimum Water Detection Goal (µg/L)	Current King County Water RDL	Is Current King County Water RDL Adequate?
Antimony	10.00	0.002	Yes
Arsenic	1.91	0.002	Yes
Beryllium	0.04	0.002	Yes
Cadmium	0.60	0.002	Yes
Chromium	2.61	0.002	Yes
Copper	2.90	0.002	Yes
Lead	0.77	0.002	Yes
Mercury	0.012	0.00060	Yes
Nickel	8.30	0.002	Yes
Selenium	2.31	0.002	Yes
Silver	0.12	0.002	Yes
Thallium	1.13	0.002	Yes
Zinc	58.91	0.002	Yes
Benzene	6.07		N/AP
Vinyl chloride	0.75		N/AP
Anthracene	0.79	0.00024	Yes
Benzidine	0.00031	0.011	No

Table 1-4. Minimum Water Column Detection Goals Necessary to Reduce Analytical Uncertainty in the Risk Assessment (continued)

Chemical	Minimum Water Detection Goal (µg/L)	Current King County Water RDL	Is Current King County Water RDL Adequate?
Benzo(a)pyrene	0.00077	0.00047	Yes
Hexachlorobenzene	0.000015	0.00024	No
Pentachlorophenol	0.094	0.00047	Yes
Aldrin	0.0000013		N/AP
Lindane	0.0064		N/AP
Chlordane	0.00011		N/AP
Dieldrin	0.000018		N/AP
Heptachlor	0.000032		N/AP
Polychorinated Biphenyls	0.00000017		N/AP

Table 1-5. Minimum Tissue Detection Goals Necessary to Reduce Analytical Uncertainty in the Risk Assessment

Chemical	Minimum Detection Goal (mg/kg)	King County Tissue RDL (mg/kg)	Is Current King County Tissue RDL Adequate?
Antimony	0.19	0.0704	Yes
Arsenic	0.0023	0.0704	No
Beryllium	0.00080		N/AP
Cadmium	0.40	0.0704	Yes
Chromium	0.39	0.22	Yes
Copper	45.65	0.0704	Yes
Lead	0.40	0.0704	Yes
Mercury	0.44	0.0162	Yes
Nickel	22.00	0.0704	Yes
Selenium	0.24		N/AP

Table 1-5. Minimum Tissue Detection Goals Necessary to Reduce Analytical Uncertainty in the Risk Assessment (continued)

Chemical	Minimum Detection Goal (mg/kg)	King County Tissue RDL (mg/kg)	Is Current King County Tissue RDL Adequate?
Silver	7.37	0.0704	Yes
Thallium	0.12		N/AP
Zinc	17.39	0.22	Yes
Benzene	0.12		N/AP
Vinyl chloride	0.0018		N/AP
Anthracene	0.6105		N/AP
Benzidine	0.000015		N/AP
Benzo(a)pyrene	0.00047	0.0267	No
Hexachlorobenzene	0.0021	1.28	No
Pentachlorophenol	0.029	0.0533	No
Aldrin	0.00020	0.0267	No
Lindane	0.0026	0.0533	No
Chlordane	0.0026		N/AP
Dieldrin	0.00021		N/AP
Heptachlor	0.00076		N/AP
Polychorinated Biphenyls	0.00045		N/AP

1.3.3 Grouping Chemicals to Overcome Computing Limitations

The selection process described above resulted in the selection of more candidate COPCs than could be logistically addressed by the EFDC model and King County's WAVE computer. This system was capable of predicting the concentrations of 21 parameters, will the above selection process identified 24 candidate COPCs. In order to be able to predict concentrations for all 24, we investigated whether it was possible to identify surrogate chemicals for use in predicting concentrations of chemicals that could not be included in the model.

The polyaromatic hydrocarbons (PAHs) measured in the 1997 sampling effort—benzo(a)anthracene, benzo(a)pyrene, benzo(b)fluoranthene, benzo(g,h,i)perylene,

benzo(k)fluoranthene, chrysene, dibenzo(a,h)anthracene, and indeno(1,2,3-cd)pyrene, pyrene—were determined to be appropriate for this purpose. This was based on observation that this group has very similar environmental fate and transport characteristics. Chemicals with similar partitioning coefficients and half-lives will move through and persist in the environment at the same rate. If we know the ratio of these chemicals in the environment at the beginning of a model run, then we will be able to use this ratio to adjust the concentrations at the end of the model run. Thus, it would be possible to include a small number of surrogate PAHs in the model, and then use a post processing adjustment factor to predict the concentrations of PAHs not included in the model.

1.3.4 PAH Groups Based on Chemical Properties

PAHs were grouped based on their partitioning coefficients and half-lives in the environment. Chemicals will portion into the aqueous dissolved phase given its partition coefficient and the total suspended solids concentration. Review of the ambient field study conducted over the winter of 1997 indicated that TSS values between 5.79 and 17.38 mg/l are a reasonable representation of TSS in the River.

Partitioning coefficients for pyrene, benzo(a)anthracene, chrysene, and benzo(a)pyrene indicated that they would partition primarily into the dissolved phase, while the remainder would partition into the particulate phase. The partition coefficient will determine where or how the chemical is transported in the estuary. One group would reside in the water column, the second group would be half in the water and half in the sediments, and the third would partition strongly into the sediments. Review of the half-life of individual PAHs indicated that they could be grouped into three groups—short, moderate, and long-lived. Combining the results of the partition coefficient and half-life analyses resulted in four groups, identified in Table 1-6.

Table 1-6. PAH Groupings

Group	Chemicals	Reason for Grouping
Group 1	Pyrene	Partitions mostly into the dissolved phase but is very persistent in the sediments
Group 2	Benzo(k)fluoranthene	Partitions mostly into particulate phase and very persistent in the sediments.
Group 3	Benzo(a)anthracene Chrysene Benzo(a)pyrene:	Partitions evenly between dissolved and particulate and moderately persistent in sediments
Group 4	Benzo(b)fluoranthene Dibenzo(a,h)anthracene Benzo(g,h,i)perylene Indeno(1,2,3-cd)pyrene:	Partitions mostly in the particulate phase and moderately persistent in the sediments.

As groups 1 and 2 had only one PAH each, these were included in the model. As groups 3 and 4 had more than one PAH, it was necessary to identify which to include in the modeling effort. Data on PAH water concentrations was available from Semi-permeable Membrane Devices (SPMD) that had been deployed by King County into several stations in the Duwamish River and Elliott Bay (see the Sampling and Analysis Plan for further details). Review of the back-calculated water concentrations indicated that chrysene had the overall highest concentration for Group 3, and benzo(b)fluoranthene had the highest concentrations for Group 4 (Table 1-7). Consequently, these analytes were also included in the model runs.

Table 1-7. Back Calculated Water Concentrations for PAHs.

Compound	PAH Group	Sample 1 ng/L	Sample 2 ng/L	Sample 3 ng/L	Sample 4 ng/L
Benzo(a)anthracene	3	0.360	0.207	0.215	0.167
Benzo(a)pyrene	3	0.033	0.030	0.024	0.020
Chrysene	3	0.397	0.237	0.206	0.166
Benzo(b)fluoranthene	4	0.149	0.109	0.095	0.081
Benzo(g,h,i)perylene	4	0.048	0.061	0.030	0.027
Dibenzo(a,h)anthracene	4	0.004	0.005	0.003	0.003
Indeno(1,2,3-c,d)pyrene	4	0.022	0.019	0.015	0.009

After the model runs were completed, the concentrations in sediments and the water column of the five PAHs not included in these runs were predicted by multiplying the average water column ratio (Table 1-8) to the predicted concentration of their group surrogate PAH. This approach assumes that these chemicals are in equilibrium in all media in the environment (water, sediment, and tissues) and that the one-month SPMD deployment allowed these devices to reach equilibrium with the water column.

Table 1-8. Average PAH Water Column Ratio

Compound	Sample 1 Ratio	Sample 2 Ratio	Sample 3 Ratio	Sample 4 Ratio	Average	STD
Benzo(a)anthracene	0.91	0.87	1.04	1.01	0.96	0.08
Benzo(a)pyrene	0.08	0.13	0.12	0.12	0.11	0.02
Chrysene	1.00	1.00	1.00	1.00	1.00	0.00
Benzo(b)fluoranthene	1.00	1.00	1.00	1.00	1.00	0.00
Benzo(g,h,i)perylene	0.32	0.56	0.31	0.34	0.38	0.12

Dibenzo(a,h)anthracene	0.03	0.05	0.04	0.03	0.04	0.01
Indeno(1,2,3-c,d)pyrene	0.15	0.18	0.16	0.12	0.15	0.03

1.4 Computer Model Description

King County selected the Environmental Fluids Dynamic Computer Code (EFDC), developed by Dr. John Hamrick, for application to the WQA. It was selected over other models because: (1) it can simulate highly stratified flows for both nutrients and toxic compounds; (2) it has been applied to many estuarine studies; and (3) it is non-proprietary. The County reviewed 13 different models for application to the Duwamish Estuary. They were rated against a set of requirements defined by the County that were based on the needs of the WQA and observed conditions within the estuary. A final report of the selection process can be obtained from King County (1996).

The model equations used in the EFDC model are the horizontal momentum equations:

$$\partial_t(m_x m_y H v)+\partial_x(m_y H u v)+\partial_y(m_x H v v)+\partial_z(m_x m_y w v)-f_e m_x m_y H u$$
$$=-m_x H\partial_y(p+p_{atm}+\phi)+m_x(\partial_y z_b+z\partial_y H)\partial_z p+\partial_z\left(m_y m_x\frac{A_v}{H}\partial_z v\right)+Q_y \qquad \text{Equation 1-1}$$

$$\partial_t(m_x m_y H u)+\partial_x(m_y H u u)+\partial_y(m_x H v u)+\partial_z(m_x m_y w u)-f_e m_x m_y H v$$
$$=-m_x H\partial_x(p+p_{atm}+\phi)+m_y(\partial_x z_b+z\partial_x H)\partial_z p+\partial_z\left(m_y m_x\frac{A_v}{H}\partial_z u\right)+Q_x \qquad \text{Equation 1-2}$$

$$m_x m_y f_e = m_x m_y f - u\partial_y m_x + v\partial_x m_y \qquad \text{Equation 1-3}$$

$$(\tau_{xz},\tau_{yz})=A_v H^{-1}\partial_z(u,v) \qquad \text{Equation 1-4}$$

where *u* and *v* are the horizontal velocity components in the curvilinear horizontal coordinates *x* and *y*, respectively. The scale factors of the horizontal coordinates are m_x and m_y. The vertical velocity in the stretched vertical coordinate *z*, is *w*. The physical vertical coordinates of the free surface and bottom bed are z_s* and z_b* respectively. The total water column depth is *H*, and ϕ is the free surface potential which is equal to gz_s*. The effective Coriolis acceleration f_e incorporates the curvature acceleration terms according to Equation 1-3. The *Q* terms in Equations 1-1 and 1-2 represent optional horizontal momentum diffusion terms. The vertical turbulent viscosity A_v relates the shear stresses to the vertical shear of the horizontal velocity components by Equation 1-4.

The kinematic atmospheric pressure, referenced to water density is p_{atm}, while the excess hydrostatic pressure in the water column is given by:

$$\partial_z p = -gH(\rho - \rho_0)\rho_0^{-1} \qquad \text{Equation 1-5}$$

Where ρ and ρ_o are the actual and reference water densities and b is the buoyancy. The three-dimensional continuity equation in the stretched vertical and curvilinear horizontal coordinate system is:

$$\partial_t(m_x m_y H) + \partial_x(m_y Hu) + \partial_y(m_x Hv) + \partial_z(m_x m_y w) = Q_H \qquad \text{Equation 1-6}$$

With Q_H representing volume sources and sinks including rainfall, evaporation, infiltration, and lateral inflows and outflows having negligible momentum fluxes. The generic three-dimensional transport and transformation equation for a dissolved or suspended material represented by the concentration variable C is:

$$\begin{aligned}&\partial_t(m_x m_y HC) + \partial_x(m_y HuC) + \partial_y(m_x HvC) + \partial_z(m_x m_y wC)\\ &= \partial_x\left(\frac{m_y}{m_x} HA_H \partial_x C\right) + \partial_y\left(\frac{m_x}{m_y} HA_H \partial_y C\right) + \partial_x\left(\frac{m_y m_x}{H} A_b \partial_z C\right) + m_x m_y HR_c\end{aligned} \qquad \text{Equation 1-7}$$

Where A_H and A_b are horizontal and vertical turbulent mass diffusion coefficients and R_c represents physical and biogeochemical sources and sinks. The horizontal mass diffusion terms in Equation 1-7 are generally omitted in the numerical solution when the model is configured for three-dimensional simulation.

Vertical boundary conditions for the solution of the momentum equations are based on the specification of the kinematic shear stresses:

$$(\tau_{xz}, \tau_{yz}) = (\tau_{bx}, \tau_{by}) = c_b \sqrt{u_1^2 + v_1^2}\,(u_1, v_1) \qquad \text{Equation 1-8}$$

And

$$(\tau_{xz}, \tau_{yz}) = (\tau_{sx}, \tau_{sy}) = c_s \sqrt{U_{w1}^2 + V_{w1}^2}\,(U_w, V_{w1}) \qquad \text{Equation 1-9}$$

At the bottom, $z=0$, and free surface, $z=1$, respectively, with U_w and V_w being the components of the wind velocity at ten meters above the water surface. The subscript *1*

$$c_b = \left(\frac{\kappa}{\ln(\Delta_1 / 2z_0)}\right)^2 \qquad \text{Equation 1-10}$$

refers to velocity and elevation at the mid-point of the bottom layer. The bottom drag coefficient is given by:

Were κ, is the von Karman constant, Δ_1 is the dimensionless thickness of the bottom layer, and $z_o=z_o*/H$ is the dimensionless roughness height. The wind stress coefficient is given by:

$$C_s=0.001\frac{\rho_a}{\rho_w}\left(0.8+0.065\sqrt{U_w^2+V_w^2}\right) \qquad \text{Equation 1-11}$$

Wind velocity components are meters per second, with ρ_a and ρ_w denoting air and water densities respectively. A no flux vertical boundary condition is used for the transport Equation 1-7, when C represents salinity. Turbulent viscosity and diffusion coefficients in the momentum and transport equations, respectively, are determined using turbulence closure model (Galperin et al. 1988; Mellor and Yamada 1982). The numerical solution procedures used in the EFDC model are documented by Hamrick (1992) and summarized in Hamrick and Wu (1997).

1.5 Initial and Boundary Condition Requirements

The hydrodynamic and transport equations given above simulate the movement of water, dissolved salt (salinity), chemicals, and sediments within the model domain. The equations are first order in time and second order in space. Their solution requires a known initial value (initial conditions) at an arbitrary point in time and a known value at two points in space (boundary condition) for all time. An initial condition must be specified for each transported variable at each cell, thus requiring knowledge of their spatial distribution also. Initial conditions describe the state of the model at the start, or time equal to zero. Boundary conditions specify what comes in and out of the model. Other sources like CSOs, storm water, and other input sources can also be considered a boundary effect. Boundaries can be constant or time varying.

To set up the model for the WQA, the geophysical and geochemical features of the study area must be defined within the model domain. This included defining the initial concentrations (IC) and boundary conditions. The IC data were pretty sparse, missing areas of data within the model domain had to be filled to define the initial character for each model cell. This was typically accomplished using simple linear interpolation between known points. Below is a summary of the geophysical and geochemical features that must be defined in the model.

1.5.1 Geophysical

- Initial water depth
- Initial water velocity
- Bottom elevation (bathymetry)
- Initial suspended solid concentration

- Initial sediment depth (mass)
- Suspended solids settling velocity (usually spatially constant)
- Critical sediment resuspension and deposition shear stresses (usually spatially constant)
- Water elevations or flows over time (boundary condition)
- Wind speeds over time (boundary condition)
- Suspended solid concentrations over time (boundary condition)

1.5.2 Geochemical

- Initial chemical concentration in water and sediments
- Chemical partitioning in water and sediment columns (usually spatially constant)
- Chemical decay in water and sediment columns (usually spatially constant)
- Initial salinity
- Chemical and salinity concentrations over time (boundary condition)

2. FIELD MONITORING PROGRAM

To determine the feasibility of performing an appropriate field sampling program for the proposed modeling project, King County did a pilot study to see if it was possible to collect the number of samples required and if current laboratory analytical techniques were appropriate. The pilot study revealed:

1. The saline water of the estuary interfered with measuring metal concentrations.

2. Most all of the organic compounds were below detection limits.

As a result, the County instigated new laboratory procedure that removed the saline matrix and pre-concentrated the water samples; lowering metal detection levels by an order of magnitude. Difficulties in detecting low organic concentrations were overcome by employing a relatively new method using Semi-Permeable Membrane Devices (SPMD), very simply described as thin sheets of plastic. They provide a time-averaged estimate of water concentrations over the deployment period. The SPMDs were deployed at two locations: near the Brandon CSO and near the Duwamish/Diagonal storm drain for two weeks. Organic grab samples were still collected as part of the field-monitoring program approximately once per month using conventional methods. Except for bis(2-ethylhexyl)phthalate, all other organic COPCs were below detection levels in the grab samples for the duration of the monitoring program. Even bis(2-ethylhexyl) phthalate was detected sporadically.

Field monitoring was started during the wet season on October 31, 1996, and terminated June 4, 1997. Approximately 28 sampling trips were performed during this time period. There was no intent to sample in the estuary under similar tidal conditions and flows (e.g., slack tide after flood). Rather, it was considered more important to try and capture different conditions within the estuary that would give a broader view of transport processes and more varied conditions for model calibration.

Samples were taken either once or three times per week. If the three largest CSOs were not discharging (ie., a non-storm event), one sample was collected for that week. If the three CSOs were discharging (storm event), then sampling occurred over three consecutive days. During non-storm events, the field sampling trip was scheduled for every Wednesday during the afternoon. This was determined by the availability of the research boat. Storm events didn't necessarily occur every Wednesday afternoon. As a result, personnel were put on 24 hour alert, seven days a week, to mobilize for storm sampling. For safety reasons, it was decided that sampling would only occur during daylight hours. Because of this, some storm sampling trips did not commence until the tail end of the storm period when CSO discharges had diminished considerably.

Sampling locations were selected along the length and width of the estuary (Figure 2-1). Sample depth, number of stations across the width and total number of samples collected

at each site are summarized in Table 2-1. In addition to the grab sampling, caged mussels were deployed as part of the WQA biological assessment study. The mussels were used

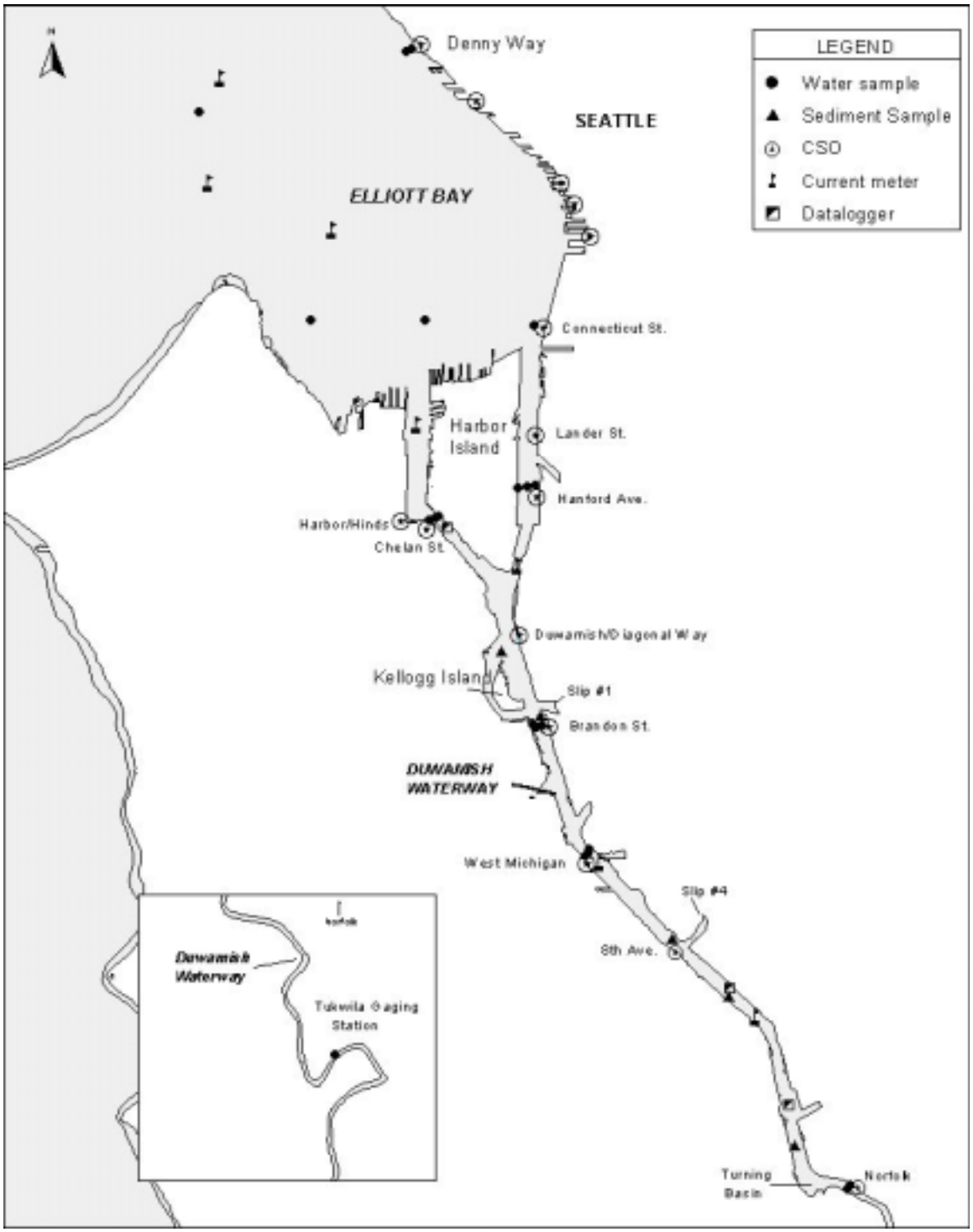

Figure 2-1. Locations of WQA Sampling and Field Instrument Sites

in a method similar to the SPMDs to estimate water concentrations. COPCs and parameters measured are summarized in Table 2-2.

Table 2-1. Station Names and Number of Samples Per Station

Station Number (see Fig. 2-1)	Field Station	Depths at Which Water Samples Were Drawn	Number of Field Sample Sites	
			Per Station	Total
1	Tukwila, tidal gauging station	1 M below surface	1	1
2	Norfolk, east of west bank	1 M below surface	2	2
3	Michigan, east bank, center, and west bank	1 M below surface 1 M above bottom	3	6
4	Brandon, east bank, center, and west bank	1 M below surface 1 M above bottom	3	6
5	Chelan, east bank, center, and west bank	1 M below surface 1 M above bottom	3	6
6	Hanford, east bank, center, and west bank	1 M below surface 1 M above bottom	3	6
7	Connecticut, east bank, center, and west bank	1 M below surface 15,20,20 M below surface	3	6
8	Duwamish Head	1 M below surface 20 M below surface	1	2
9	Denny Way Cap	1 M below surface 16 M below surface	1	2
9	Denny Way Outfall	1 M below surface	1	1

Table 2-2. Properties Measured During Field Monitoring Program

Constituent of Potential Concern	Collection Technique	Measured Quantity	
		Water	Sediments
Metals			
Arsenic Cadmium Copper Lead Nickel Zinc	Grab	T,D	T,TOC,TS
Organics			
1,4-Dichlorobenzene	Grab	T,D,TV,S	T, TOC,TS
4- Methylphenol	Grab	T,D,TVS	T, TOC,TS
Bis(2-ethylhexyl)phthalate	Grab	T,D,TVS	T, TOC,TS
Total PCBs	SPMD,Mussels	TAT,TVS	T, TOC,TS
Pyrene	SPMD,Mussels	TAT,TVS	T, TOC,TS
Benzo(k)fluoranthene	SPMD,Mussels	TAT,TVS	T, TOC,TS
Fluoranthene	SPMD,Mussels	TAT,TVS	T, TOC,TS
Phenanthene	SPMD,Mussels	TAT,TVS	T, TOC,TS
Chrysene	SPMD,Mussels	TAT,TVS	T, TOC,TS
Benzo(b)fluoranthene	SPMD,Mussels	TAT,TVS	T, TOC,TS
Others			
Mercury	Ultra-Clean Methods	T,D	T,TVS
Fecal coliform bacteria	Grab	T	
Tributyltin	Mussels	TAT	
Total Suspended Solids	Grab	0.45	PD

T = Total concentration

D = Dissolved concentration

TOC = Total organic carbon

TS = Total sulfides

TVS = Total volatile solids

TAT = Total time averaged concentration

PD = Phi size distribution

0.45 = Total suspended solids (0.45µ filter)

Five of the largest CSOs that discharge along the Duwamish River were selected for sampling: Brandon, King, Hanford, Connecticut, and Chelan. The sampling program was designed to test whether chemical concentrations changed over the duration of the discharge event (first flush effects), across the depth of the CSO pipe, or between CSO outfalls. Additionally, the Denny Way/Lake Union CSO Control Project, Field Monitoring Report (Herrera 1997) sampled the Denny Way CSO for chemical analysis

and solids separation testing to study how metals partition to suspended solids, and estimate settling velocities.

2.1 Geochemical Sampling

Collection of water samples started before the County had developed the new analytical techniques to remove the saline matrix and pre-concentrate the sample. The new technique lowered detection levels an order of magnitude. While this was good, it also proved to be problematic. Laboratory techniques had improved but sampling methods had not. The lower detection limit increased the degree to which sample contamination could be observed. Standard QA/QC revealed that significant field blank contamination (sample results are less than five times the field blank response) had occurred in most samples for lead, copper, and zinc. A field blank is a sample of distilled water that was passed through the sample collection device and indicates how much cross contamination could occur between samples or from sampling techniques. Standard blank correction methods would not work because only two field blanks were collected during each field sampling trip, one before sampling started and one upon completion. The two blanks gave no quantitative indication of field contamination in each sample. It indicated that some of the samples could be contaminated. To remedy possible contamination and to keep the fieldwork that had been completed, a method for blank correction was developed.

The 26 weeks of samples were divided into two periods. The field blank values in each period were grouped and the median value was computed. Sample data in each period were blank corrected by subtracting the median blank value. It was postulated that removing the median of the group would on average produce the same effect as blank correcting individual samples and blanks, preserving the total mass of the system.

Correction of the field data in this manner resulted in negative values for some samples. Corrected samples with negative values were handled two ways, negative values at the Elliott Bay and Green River boundaries were replaced with the mean value of the positive numbers. Negative values at all other field locations were not used in the mass calibration.

Field bland contamination and the correction or non-correction of field samples could affect the risk assessment in the following ways (it is assumed that blank contamination occurs independent of other storm-related sources that discharge into the estuary and bay).

No Blank Correction and Field Samples are Contaminated: Existing risk would be estimated higher than true risk, resulting in over-prediction of the risk. The relative risk of CSOs compared to other sources and existing boundary sources would be less because of the additional chemical mass included in the blank contamination. This additional chemical mass would be attributed to other sources during the calibration process. The mass calibration did not adjust CSO mass inputs.

Over-Correction of Blank Contamination: Existing risk estimates would be less than true risk, resulting in under-prediction of the risk. The relative risk from CSOs compared to existing sources would appear greater because some of the mass from other sources would be erroneously removed due to over correction. Since CSO inputs are determined from field monitoring and not adjusted during the mass calibration, over-correction would remove part of the mass associated with the other sources, resulting in less mass input. The relative mass contribution from CSOs would be relatively greater.

Under-correction of blank contamination lies somewhere between the two scenarios listed above. Correction of field blank contamination increases the relative risk of CSOs compared to all other sources. Since one objective of this study was to determine the relative risk of CSOs compared to other sources, the more conservative approach of blank correcting the data were used. The downside of the blank correction method is it could possibly cause under-prediction of existing risk.

2.2 Bibliography of Field Sampling Data Reports and Quality Assurance Reviews

The following data reports and supporting quality assurance (QA) reviews are available upon request. Data reports are available as Microsoft® Excel 5.0 spreadsheets, either electronically or in hard copy. QA reviews are available as reports or technical memoranda in hard copy only either comb-bound or loose. It is recommended that, when requesting a data report, the associated QA review also be requested. This will allow the user to evaluate the data in the context of its overall quality. To receive copies of any of the following documents, please contact:

Scott Mickelson
King County Environmental Laboratory
322 West Ewing Street
Seattle, Washington 98119-1507
(206) 684-2377 (phone)
(206) 684-2395 (fax)
scott.mickelson@metrokc.gov (e-mail)

These data are also available on the Water Quality Assessment web site at http://splash.metrokc.gov/wlr/waterres/wqa/wqapage.htm.

2.2.1 Combined Sewer Overflow (CSO) Effluent Data

2.2.1.1 *Data Reports*

8014CB.XLS CSO Discharge Event of 03/29/96 to 04/01/96 (Brandon Street, Hanford Street, and Connecticut Street CSOs)

8015CB.XLS CSO Discharge Event of 04/15/96 to 04/16/96 (Brandon Street and Hanford Street CSOs)

8016CB.XLS CSO Discharge Event of 04/22/96 to 04/23/96 (Brandon Street, Chelan Avenue, Connecticut Street, Hanford Street, and King Street CSOs)

8017CB.XLS CSO Discharge Event of 05/22/96 (Brandon Street, Connecticut Street, and Hanford Street CSOs)

8018CB.XLS CSO Discharge Event of 08/02/97 (Brandon Street CSO)

8019CB.XLS CSO Discharge Event of 10/13/96 (Brandon Street CSO)

8020CB.XLS CSO Discharge Event of 10/17/96 (Connecticut Street, Hanford Street, and King Street CSOs)

8021CB.XLS CSO Discharge Event of 10/21/96 (Chelan Avenue and Hanford Street CSOs)

8022CB.XLS CSO Discharge Event of 10/28/96 (Hanford Street CSO)

8023CB.XLS CSO Discharge Event of 11/12/96 (Brandon Street CSO)

8024CB.XLS CSO Discharge Event of 12/04/96 (Brandon Street, Chelan Avenue, Connecticut Street, Hanford Street, and King Street CSOs)

8025CB.XLS CSO Discharge Event of 01/27/97 (Brandon Street, Hanford Street, and King Street CSOs)

8026CB.XLS CSO Discharge Event of 01/30/97 (Brandon Street, Hanford Street, and King Street CSOs)

8027CB.XLS CSO Discharge Event of 03/01/97 (Brandon Street, Hanford Street, and King Street CSOs)

8028CB.XLS CSO Discharge Event of 03/06/97 (Hanford Street and King Street CSOs)

8029CB.XLS CSO Discharge Event of 03/15/97 (Brandon Street, Chelan Avenue, Hanford Street, and King Street CSOs)

8030CB.XLS CSO Discharge Event of 04/19/97 (Brandon Street, Chelan Avenue, Connecticut Street, Hanford Street, and King Street CSOs)

8031CB.XLS CSO Discharge Event of 04/26/97 (Brandon Street CSO)

8032CB.XLS CSO Discharge Event of 05/31/97 (Brandon Street, Chelan Avenue, Connecticut Street, Hanford Street, and King Street CSOs)

2.2.1.2 *Quality Assurance Reviews*

Quality Assurance Review of Conventional Analytical Data for Water Samples (Technical Memorandum), June 27, 1997

Quality Assurance Review of Metals Data for CSO Storm Water Samples (Technical Memorandum), August 26, 1997

Quality Assurance Review of Organic Analytical Data for Water Samples (Technical Memorandum), June 18, 1997

2.2.2 Receiving Water Data

2.2.2.1 *Data Reports*

8033CB.XLS Receiving Water Analytical Data - Week One (10/30/96)

8034CB.XLS Receiving Water Analytical Data - Week Two (11/06/96)

8035CB.XLS Receiving Water Analytical Data - Week Three (11/13/96)

8036CB.XLS Receiving Water Analytical Data - Week Four (11/20/96)

8037CB.XLS Receiving Water Analytical Data - Week Five (11/25/96)

8038CB.XLS Receiving Water Analytical Data - Storm Event of 12/04/96 - Day One (12/05/96) - Week Six

8039CB.XLS Receiving Water Analytical Data - Storm Event of 12/04/96 - Day Two (12/06/96) - Week Six

8040CB.XLS Receiving Water Analytical Data - Storm Event of 12/04/96 - Day Three (12/07/96) - Week Six

8041CB.XLS Receiving Water Analytical Data - Week Seven (12/11/96)

8042CB.XLS Receiving Water Analytical Data - Week Eight (12/18/96)

8043CB.XLS Receiving Water Analytical Data - Week Nine (01/29/97)

8044CB.XLS Receiving Water Analytical Data - Week Ten (02/05/97)

8045CB.XLS Receiving Water Analytical Data - Week Eleven (02/19/97)

8046CB.XLS Receiving Water Analytical Data - Week Twelve (02/26/97)

8047CB.XLS Receiving Water Analytical Data - Week Thirteen (03/05/97)

8048CB.XLS Receiving Water Analytical Data - Week Fourteen (03/12/97)

8049CB.XLS Receiving Water Analytical Data - Storm Event of 03/15/97 - Day One (03/16/97) - Week Fifteen

8050CB.XLS Receiving Water Analytical Data - Storm Event of 03/15/97 - Day Two (03/17/97) - Week Fifteen

8051CB.XLS Receiving Water Analytical Data - Storm Event of 03/15/97 - Day Three (03/18/97) - Week Fifteen

8052CB.XLS Receiving Water Analytical Data - Week Sixteen (03/26/97)

8053CB.XLS Receiving Water Analytical Data - Week Seventeen (04/02/97)

8054CB.XLS Receiving Water Analytical Data - Week Eighteen (04/09/97)

8055CB.XLS Receiving Water Analytical Data - Week Nineteen (04/15/97)

8056CB.XLS Receiving Water Analytical Data - Storm Event of 04/19/97 - Day Two (04/21/97) - Week Twenty

8057CB.XLS Receiving Water Analytical Data - Storm Event of 04/19/97 - Day Three (04/22/97) - Week Twenty

8058CB.XLS Receiving Water Analytical Data - Week Twenty One (04/30/97)

8059CB.XLS Receiving Water Analytical Data - Week Twenty Two (05/07/97)

8060CB.XLS Receiving Water Analytical Data - Week Twenty Three (05/15/97)

8061CB.XLS Receiving Water Analytical Data - Week Twenty Four (05/20/97)

8062CB.XLS Receiving Water Analytical Data - Week Twenty Five (05/28/97)

8063CB.XLS Receiving Water Analytical Data - Storm Event of 05/31/97 - Day One (06/01/97) - Week Twenty Six

8064CB.XLS Receiving Water Analytical Data - Storm Event of 05/31/97 - Day Two (06/02/97) - Week Twenty Six

8065CB.XLS Receiving Water Analytical Data - Storm Event of 05/31/97 - Day Three (06/03/97) - Week Twenty Six

2.2.2.2 *Quality Assurance Reviews*

Final Data Package for Semipermeable Membrane Device Analytical Data (Technical Memorandum), July 28, 1997 (this package includes the quality assurance review and the analytical data report)

Quality Assurance Review of Conventional Analytical Data for Water Samples (Technical Memorandum), June 27, 1997

Quality Assurance Review of Low Level Mercury Data for Water Samples (Technical Memorandum), July 28, 1997 (this review includes the analytical data report)

Quality Assurance Review of Metals Analytical Data for Water Samples - First Thirteen Weeks (Technical Memorandum), August 29, 1997

Quality Assurance Review of Metals Analytical Data for Water Samples - Second Thirteen Weeks (Technical Memorandum), November 7, 1997

Quality Assurance Review of Organic Analytical Data for Water Samples (Technical Memorandum), June 18, 1997

2.2.3 Sediment Data

2.2.3.1 *Data Reports*

8008CB.XLS Brandon Street CSO Sediment Chemistry Data

8009CB.XLS Eighth Avenue CSO Sediment Chemistry Data

8010CB.XLS Hamm Creek Delta Sediment Chemistry

8011CB.XLS Kellogg Island Sediment Chemistry Data

8012CB.XLS South Park (16th Avenue South Bridge) Sediment Chemistry Data

8013CB.XLS Benthic Invertebrate Study Sediment Chemistry Data (Duwamish/Diagonal CSO and Kellogg Island)

2.2.3.2 *Quality Assurance Reviews*

Quality Assurance Review for Duwamish Estuary Water Quality Assessment Sediment Project Weeks One Through Six (Report), May 29, 1997

Quality Assurance Review for Duwamish Estuary Water Quality Assessment Sediment Project Weeks Seven Through Seventeen (Report), July 31, 1997

Quality Assurance Review for Duwamish/Estuary Benthic Invertebrate Study Sediment Chemistry (Report), December 23, 1997

Quality Assurance Review for Duwamish/Estuary Benthic Invertebrate Study Sediment Chemistry - Archived Samples (Report). March 4, 1998.

2.2.4 Tissue Data

2.2.4.1 *Data Reports*

8000CB.XLS Crab Tissue Chemistry Data

8001CB.XLS Invertebrate Tissue Chemistry Data

8002CB.XLS Large Fish Tissue Chemistry Data

8003CB.XLS Small Fish Tissue Chemistry Data

8004CB.XLS Squid Tissue Chemistry Data

8005CB.XLS Miscellaneous (Crab, Mussels, Prawns) Tissue Chemistry Data

8006CB.XLS Transplanted Mussel Study (Phase I) Chemistry Data

8007CB.XLS Transplanted Mussel Study (Phase II) Chemistry Data

2.2.4.2 *Quality Assurance Reviews*

Quality Assurance Review for Duwamish Estuary/Elliott Bay Crab Tissue Study (Report), October 22, 1997

Quality Assurance Review for Duwamish Estuary/Elliott Bay Invertebrate Tissue Study (Report), October 20, 1997

Quality Assurance Review for Duwamish Estuary/Elliott Bay Large Fish Tissue Study (Report), October 18, 1997

Quality Assurance Review for Duwamish Estuary/Elliott Bay Small Fish Tissue Study (Report), October 17, 1997

Quality Assurance Review for Duwamish Estuary/Elliott Bay Squid Tissue Study (Report), February 5, 1998

Quality Assurance Review for Duwamish Estuary/Elliott Bay Miscellaneous (Crab, Mussels, and Prawns) Tissue Study (Report), December 30, 1997

Quality Assurance Review for Duwamish Estuary Transplanted Mussel Study (Report), February 12, 1997

Quality Assurance Review for Duwamish Estuary Transplanted Mussel Study II (Report), October 27, 1997

Review of Quality Control Data for Potential Method Detection Limit Adjustments for Tissue, (Technical Memorandum), November 10, 1997

2.3 Geophysical Sampling

Water velocity, elevation, temperature, and salinity were the four physical parameters measured to characterize water transport within the bay and estuary. Acoustic doppler

profilers were employed to measure water velocity, and Hydrolabs were used to measure water elevation, salinity, and temperature. Station locations are shown in Figure 2-1.

2.3.1 Water Velocity

Three acoustic doppler meters were deployed on the bottom of the estuary at four sites shown in Figure 2-1 (velocity meters), they were rotated through the sites at three month intervals. The meters were configured to measure velocities every half-meter (0.5 m bins), at 15 minute intervals, across the observed water depth. They were deployed for approximately one year starting in late August 1996.

Two additional meters were used to measure water velocities in Elliott Bay at four sites shown in Figure 2-1, they were rotated through the sites at one month intervals. The meters were deployed on the bottom and configured to measure water velocities every four meters, at 15 minute intervals, across the observed water depth. Deployment was from January 1997 to June 1997.

By their design, the meters have limited ability to measure water velocity in the upper 10 percent to 15 percent of the water surface and in the first bin just above the meter. As a result, caution should be used when comparing observed and simulated water velocities near the surface and in the first bin.

2.3.2 Salinity, Water Elevation, and Temperature

Salinity, temperature, and water elevations were measured at three field stations as shown in Figure 2-1 (data loggers). Three instruments were deployed near the Spokane Street bridge with instruments placed one meter below water surface, five meters above the bottom, and one meter above the bottom. Two meters were deployed near the 16th Avenue bridge with instruments placed one meter below the water surface and one meter above the bottom. The third station at the Duwamish Yacht Club had a single instrument placed one meter below the surface. The meters were deployed from late August 1996 through early May 1997.

3. MODEL CONFIGURATION

3.1 Geophysical Features

3.1.1 Bathymetry

The model domain includes the Green River from the Interstate 405 Bridge through the Duwamish River to the western edge of Elliott Bay. The downstream boundary at Elliott Bay is along a shallow arc between Alki Point and Fourmile Rock. The study area was divided into 512 cells (Figure 3-1). Bathymetric features for Elliott Bay and the Duwamish River was obtained from National Oceanic and Atmospheric Administration (NOAA) bathymetry records with shore boundaries digitized from the NOAA navigational charts. Bathymetric data for the Green River were surveyed by a consultant for King County and boundary data were obtained from United States Geological Survey (USGS) maps. The model divides the depth into ten equal layers at each cell in the model domain.

3.1.2 Water level and flow boundary conditions

Boundary points for the model occur just outside of Elliott Bay and upstream of the City of Tukwila were I-405 crosses the Green River. The boundary at Elliott Bay was forced by a phased harmonic tidal series specifying water elevations. The harmonics where determined by back calculating tidal information collected at the Seattle ferry terminal. Phasing was determined from water elevation records located near Fourmile Rock and Alki Point. The phasing accounts for the time it takes the tidal wave to travel from Fourmile Rock to Alki Point.

At the upstream Tukwila boundary, tidal effects are negligible which allow the use of a simple flow time series boundary condition. Flow conditions were defined by measured flows at the USGS flow station at Auburn. Daily average flows were used.

Wind speed and direction information was obtained from the Sea-Tac Airport to define wind conditions within the model domain.

3.1.3 Initial sediment chemical concentrations and particle distribution

Sediment particle size for the estuary was obtained from GeoSea Consulting (1994) which gathered the data for the Elliott Bay/Duwamish Restoration Program. These data were also supplemented with particle information collected by Science Applications International Corp (SAIC 1991, Unpublished Report) for the U.S. Army Corps of Engineers (ACOE) dredging at the turning basin. Very little sediment chemistry and particle size information is available for the Green River section of the model. A small amount of particle size information was obtained from an in-field assessment of percent fines at four locations by County personnel. Anecdotal evidence from the USGS was

also used. The data was collated to initialize sediment concentrations and particle size distribution within all model cells. Multiple data points within a single model cell were averaged into a single value. Values for cells with no data points were interpolated from neighboring cells.

3.1.4 Initial sediment mass distributions

Sediment chemical concentrations are defined as the mass of chemical over the mass of sediment (mass chemical/mass sediment). To compute the total chemical mass, given the sediment chemical concentration, multiply the sediment concentration by the sediment mass in a given volume. The greater the sediment volume the greater the chemical. In the model, the initial mass of sediment in each cell must be defined. Since cell area remains constant over time, the depth of the sediment varies to account for sediment deposition or erosion. Sediments can act as a source of contamination; therefore it is important to know the available mass of a chemical in the sediment bed, as it determines the potential supply of the chemical into the overlying water.

Field sampling gives sediment concentration in units of mass chemical/mass sediment. As a result, the initial mass in the sediment bed implicitly defines the initial mass of sorbed chemical. Over-specification of the sediment mass will over-estimate effects of chemical transfer from the sediments to the water and increase the length of time of the effect. Under-specifying the sediment mass will have the opposite effect.

Sediment core sampling near the Duwamish/Diagonal Stormwater/CSO and Norfolk CSO indicated that some chemicals were measurable to depths of one meter below the sediment surface and thus, provide a larger chemical mass than sites with shallower chemical depths. Realizing that similar conditions might exist elsewhere, but not having the financial resources to collect core samples for each model cell, an alternative method was designed to estimate initial sediment depths. This technique entailed initializing the model with a 10-cm sediment layer everywhere and running it for 300 days. At the end of the 300-day simulation the resultant sediment depths were normalized to the maximum sediment depth. The normalized depths were then adjusted such that the maximum sediment depth was one meter. At locations where the adjusted depth was less than 10 cm, a 10 cm sediment was substituted. This allowed the definition of deposition and erosion areas based on the simulated hydrodynamics and the geomorphology defined in the model, and allowed the definition of spatial variability in the sediment depths and the implicit depth of chemical penetration. The model assumes that sediments can continually deposit in each cell without affecting water depth.

3.1.5 Sediment source concentrations

Review of the WQA estuary, bay, and CSO field sampling data, GeoSea and Elliott Bay/Duwamish River Restoration Program (EBDRP) sediment data indicated that the sediments could be divided into three general classes: fine sand to course silt, silts, and fine silt to clay. Solids concentrations at the Green River boundary for fine sand/course

silt class were generated using the ACOE Suspended Solids Loading Equation (ACOE 1981), given as Equation 3-1.

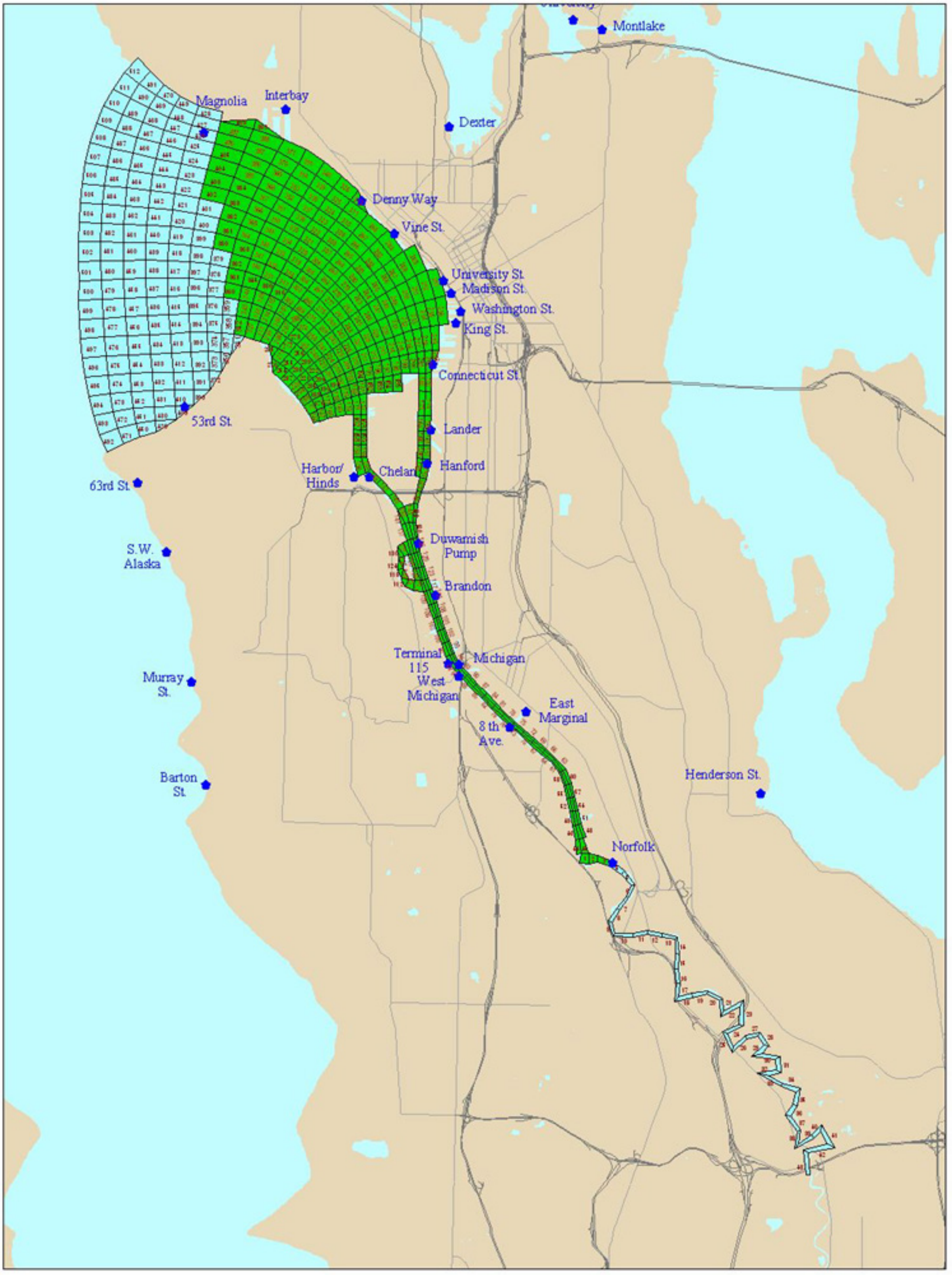

Fig. 3-1. Overlay of Model Cells on Study Area

$$SS\left[\frac{mg}{l}\right] = 0.964Q^{1.09} \quad \text{where Q is flow (cms)} \qquad \text{Equation 3-1}$$

Where cms is cubic meters per second.

Concentrations for the finer solids were generated from a similar regression equation (Equation 3-2) using TSS field data collected for the WQA and USGS Auburn flow data.

$$SS\left[\frac{mg}{l}\right] = 0.654Q^{1.09} \quad \text{where Q is flow (cms)} \qquad \text{Equation 3-2}$$

Field information collected from the WQA CSO monitoring program provided suspended solids concentrations for CSOs. Solids concentrations for other sources were obtained from existing storm water studies.

3.1.6 Critical Resuspension and Deposition Stresses

The model requires specifying a critical sediment stress at which resuspension and deposition occurs. No field measurements were made to estimate the critical resuspension stress value. Instead, values as suggested by Hamrick (1998 personal communication) were used. For the non-cohesives (fine sand, course silt and silt) and a critical shields stress of 1.6e-4 $(m/s)^2$ was used, and for the cohesives (fine silt to clay) the stress above which resuspension occurs was 1e-4 $(m/s)^2$.

3.2 Geochemical Features

3.2.1 Initial Sediment Chemical Concentrations

Sediment concentrations from Elliott Bay and the Duwamish River were obtained from the Washington State Department of Ecology (WSDOE) SedQual database. This data set was supplemented with data collected from the WQA. The data were collated to initialize sediment concentration distributions within all model cells. Multiple data points within a single model cell were averaged into a single value. Values for cells with no data points were interpolated from neighboring cells.

3.2.2 Chemical Concentration Boundary Conditions

Chemical data in the water columns gathered from the field monitoring program at the Tukwila and Duwamish Head field stations were used at the Green River and Elliott Bay boundaries, respectively, for model calibration. For the metals and fecal coliform calibration, the field sampling program produced approximately 28 data points over a 200 day period. To fill in missing data between observed field data, the model employed a linear interpolation scheme to estimate the boundary conditions during non-sampled periods.

For the one-year simulation, the data gaps between sampling periods were supplemented with synthetic data generated from a simple stochastic model developed from observed data. A statistical approach was used rather than using a mean value because of the concern of peak chemical concentrations to aquatic life. It was desired to simulate the potential combination of a peak load from the boundary and point sources rather than merely a static, average boundary condition. No synthetic data generation scheme for the organic compounds was developed because concentrations were below detection values.

Data at the upstream Tukwila boundary were checked against river flow and rainfall (using a non-parametric Spearman's test) to determine if a linear relationship existed between the observed chemical data and the two physical processes. No statistically significant correlation was found between the metals or fecal coliform bacteria and river flow or rainfall. The Elliott Bay data (both surface and depth samples) were checked against river flow, rainfall, and CSO events to determine if a mathematical relation existed between observed concentrations and the three possible sources. A statistically significant relationship did not exist for metals except for lead in the surface samples. The surface lead sample site was positively correlated to CSOs with a coefficient of determination of 0.19 at a 0.05 level (2-tailed).

The statistical analyses indicated that chemical conditions at the boundaries are not significantly affected by river flows, rainfall, or CSOs (with the exception of lead in the surface layer). This is not to say a relationship does not exist, just that one could not be found given the data and methods employed. A relation for lead to account for possible CSO and other source affects was not developed because no statistically significant relation was found for the other six metals, the relation was limited to the surface layer which composed about 1/10 of the surface area at the boundary.

At the time of this study, insufficient data existed to statistically study seasonal changes in chemical concentrations at the boundaries. It is suggested that a sampling program designed to test seasonal changes be implemented at a future date. However, as a result of the biological study conducted concurrent to this field program, it was observed that lower chemical concentrations where measured in mussels during September than in March (Strand et al. 1998).

The data collected to specify chemical boundary conditions at the Green River and Elliott Bay were used to generate a larger synthetic set for use in the one-year simulations. To show that the number of samples was sufficient to estimate distribution statistics for the stochastic time series, one can review the confidence intervals for the distribution statistics using the student *t* distribution to determine how sample size affects the confidence interval. Assuming the student *t*-test statistic use of a normal distribution is appropriate, then the student *t*-test statistic $t_{\alpha,v}$ approaches a value of 1.98 as the degrees of freedom approach infinity. For a sample size of 28 minus one degree of freedom for the calculation of the mean, the degrees of freedom is 27. The resultant *t* statistic at the 95 percent (2-tailed) confidence level is 2.05, which effectively increases uncertainty by 3.5 percent from the asymptotic minimum of 1.98. A sample population of 28 is deemed a reasonable number to estimate population distribution statistics.

Analysis of the chemical data at the Green River and Elliott Bay boundaries consisted of a primary and secondary assessment. In the primary approach, the underlying motivation for modeling metals for boundary conditions at Tukwila and the Duwamish Head was consideration of the statistical mixture or contamination model. The secondary approach looked at correlation between the chemical data. The most commonly used model for a process of this kind is to consider a parametric model, perhaps normal or lognormal, of the form F(X), where X is the statistical properties of the population. This model represents data that are described by, and perhaps generated by, one process. Frequency distributions of metals in the environment often do not fit this model. Metals often exhibit frequency distributions that do not test positive for the distributions of choice such as the normal or lognormal. In fact they sometimes are difficult to fit any known probability distributions.

Large data sets which show deviations from parametric models may be mixture of statistical contamination models of the form F(X) = G(X) + H(X). The components G(X) and H(X) represent two different distributions. They may both be parametric distributions of different types, or one of them may be an arbitrary distribution.

The existing metals data were tested for distributional fit. Most of the metals fit the model F(X) = G(X) + H(X). Some were simple parametric models, F(X). The model fits were made using computer software S+ (by StatSci a division of Mathsoft) and the Envirostats add-on to S+. Existing data for each metal were tested for distribution by using CDF.COMPARE, CDF.COMPARE.CENSORED, and CHISQ.GOF a goodness of fit test. As an example, arsenic in one of the sites exhibited a Weibull distribution with a shape parameter of 7.48 and a scale parameter of 0.00123 for the upper 88 percent of the data. The arsenic data that comprised the lowest 12 percent were fit by a uniform distribution. On the other hand, cadmium at the same site was represented by a normal distribution. The distributions that fit the data were Weibull, Gamma, Normal, and Uniform with the Weibull occurring most often and the Uniform the least.

After fitting distributions to the existing data, extended data sets were created by generating a set using the parameters and distributions of the existing data. For example, for the arsenic data described above, 88 per cent of 3,600 data points were generated using a Weibull distribution with parameters of shape = 7.48 and scale = 0.00123. In addition, 12 percent of 3,600 points were generated using a Uniform distribution with min = 0.00052 and max = 0.000698. The results were synthetic data sets of 3,600 data points that closely resembled the statistical properties of the boundary data set.

It was noted that at Tukwila especially, some metals were correlated with each other. At the Duwamish Head the correlations were weak and a model could not be fit using the secondary approach. At Tukwila, lead and copper were both correlated with zinc. It was determined that a model that described lead and copper as dependent on zinc would be a reasonable model. Generating data as described above in the primary approach would result in a lead data set that closely resembled the actual data but would not preserve the relationship between lead and zinc.

To preserve this association, a model was used that took advantage of the dependent relationship. Using lead as an example, a regression was fit to the lead and zinc data. The best fit was a non-linear regression of cubic form. Explicitly this model is represented by the formula:

$$\text{Lead} = 0.000074 - 0.114\ \text{Zinc} + 71.04\ \text{Zinc}^2 - 597\ \text{Zinc}^3.$$

This model yielded two components for an extended synthetic data set for lead: the coefficients of the fitted model, and a description of the residuals. The residuals for the model were retained and analyzed. The residuals were represented by a normal distribution with mean = 0 and standard deviation = 0.0004.

The extended data set of 3,600 data points were generated by applying the above cubic formula to the synthetic zinc data set. The zinc had been generated with the primary approach as described above. To this data a random component was added by generating a set of 3,600 residuals normally distributed with mean = 0 and standard deviation = 0.0004. The result was a synthetic data set that closely resembled the original lead data and that preserved the relationship between lead and zinc.

Fecal coliform data for the Green River and Elliott Bay boundaries were found to be log normally distributed when zeros were removed. A statistical set was generated using the same log normal mean and standard deviation and then added in the appropriate percentage of zero valued observations.

3.3 Chemical Properties

Chemical partition values for the metals arsenic, copper, cadmium, lead, nickel, and zinc were estimated from field data using the following equation (Thomann and Mueller 1987),

$$P = \frac{C_T - C_d}{C_d M} \qquad \text{Equation 3-3}$$

Where:

P	=	Partition coefficient
c_T	=	Total chemical concentration
c_d	=	Dissolved chemical concentration
m	=	Total suspended solids concentration

An average partition coefficient was computed for each metal at each sample site. The sample site averages were then combined to compute an average partition coefficient representing the whole estuary. Using the whole data pool, dependency of the partition coefficient on salinity was tested against linear and power functions using regression and optimization methods. None of the functions proved to be statistically significant.

Chemical partitioning for organic compounds tributyltin and mercury were provided by Hamrick. A constant partition coefficient was used for all chemicals.

Chemical decay rates for the organic compounds were obtained from literature references (Howard et al. 1991). Minimum rates were used for both water and sediment columns. A zero decay rate was used for unlisted chemicals. Partition and decay values are summarized in Table 3-1.

Table 3-1. COPC Decay Rate and Partitioning Coefficient

Chemical of Concern	Decay (1/sec)	Partition Coefficient (l/mg)	
		Water Column	Sediment Column
Arsenic [a]	None	0.02	0.005
Cadmium [a]	None	0.018	0.004
Copper [a]	None	0.11	0.025
Lead [a]	None	4.4	0.4
Nickel [a]	None	0.042	0.01
Zinc [a]	None	0.082	0.02
Tributyltin [c]	None	1.0e-3	1.0e-3
1,4-Dichlorobenzene [a]	None	8.1e-5	8.1e-5
4- Methylphenol [a]	None	2.4e-6	2.4e-6
Bis(2-ethylhexyl)phthalate [b]	3.5e-7	4.8e-3	4.8e-3
Fluoranthene [b]	3.1e-6	9.8e-3	9.8e-3
Phenanthrene [b]	7.7e-6	8.4e-4	8.4e-4
Total PCBs [b]	None	2.2e-3	2.2e-3
Pyrene [b]	9.4e-5	3.4e-3	3.4e-3
Benzo(k)fluoranthene [b]	3.9e-7	3.0e-1	3.0e-1
Chrysene [b]	1.5e-5	2.1e-2	2.1e-2
Benzo(b)fluoranthene [b]	2.7e-7	1.5e-1	1.5e-1
Mercury [c]	None	4.4e-4	4.4e-4
Fecal Coliforms	4.0e-6	None	None

[a] Calculated from Equation 3-3 in this document.

[b] Howard et al. (1991)

[c] Hamrick (1998 personal communication)

3.4 Combined Sewer Overflows

Currently 13 CSOs discharge into Elliott Bay and the Duwamish Estuary. They are South Magnolia, Denny Way, King, Connecticut, Lander, Hanford, Chelan, Duwamish/Diagonal, Brandon, South and West Michigan, Eighth Avenue, and Norfolk. Hydrographs used for the calibration are from flow data recorded over the 1996-97 year. The ten-year runs repeated the 1996-97 year hydrographs for each year of the extended simulation.

The CSO monitoring program collected metals concentration data at five of thirteen CSOs (Brandon, King, Hanford, Connecticut, and Chelan). Effects that were evaluated in the CSO data were as follows:

1. Variation of concentrations over the depth of the CSO effluent pipe
2. First flush effects
3. Differences between CSOs

3.4.1 Variation Over Depth

The Chelan Street CSO was the only one in which samples were taken at three different depths. Grab samples where taken at the surface, mid-depth, and bottom of the CSO stream. For the Chelan CSO, testing for differences at the 95 percent confidence level indicated none of the six COPC metals concentrations showed a significant difference with depth.

3.4.2 First Flush Effects

Testing all five CSOs for differences in first flush metals content, versus remainder of storm, indicated three of the six metals were statistically different at a significance level of 90 percent. The metals were cadmium, copper, and zinc. However, observation of box plots for these metals suggested that the differences were not of sufficient size to produce a noticeable effect in model simulations.

3.4.3 Differences Between CSOs

The evidence of the current data does not strongly suggest that the five CSOs are different. However, the data at the Brandon Street CSO can be shown to be statistically different (higher concentration) from the other CSOs, and that King Street can be shown to be statistically different (lower concentration) from the others.

In review of the statistical analysis it was decided to vary chemical input by CSO location using the average concentrations for each of the five CSOs for each of the COPCs. For the eight CSOs not included in the monitoring program, concentrations were estimated

from one of the five CSOs based on similar basin characteristics. Basin grouping, mean concentrations, and box plots showing chemical variability for each COPC at the five monitored CSOs are presented in Subappendix A.

3.5 Stormwater Model For the Duwamish River/Elliott Bay Catchment

In order to estimate the impact to the water quality of Duwamish River/Elliott Bay from the storm water pollutant loading, a computer model (Runoff and Transport Model) has been established to simulate the storm water runoff. The Runoff and Transport computer model developed by King County Wastewater Treatment Division (WTD) for the sewerage system was applied to the storm water drainage system of the Duwamish River and Elliott Bay basins. The model includes surface runoff, transport, and groundwater infiltration components.

To set up the model, basin parameters were estimated to reflect the average conditions of each of 129 subcatchments for the storm water runoff. A series of flow hydrographs was generated using the Runoff and Transport Model simulation results. The model-generated flow hydrographs were used as part of the loading inputs to the 3-D hydrodynamic and transport model for the Duwamish River/Elliott Bay water body.

Based on the simulation scenarios for the 3-D hydrodynamic and pollutant transport model, both one-year and ten-year hydrographs were prepared. The storm water hydrographs for the one-year simulation are corresponding to the period between June 1, 1996 to October 31, 1997. Due to the unavailability of rainfall data at the time of generating these hydrographs, the rainfall between June 1, 1981 to October 31, 1981 was used to represent the corresponding 1997 period.

Although ten separate years of stormwater hydrographs were generated, only the August 1, 1996 – May 31, 1997 and June 1, 1981- August 31, 1981 hydrographs were used, to expedite the long term modeling such that it was finished in time to be used in the risk assessment. For the ten-year simulation, historical rainfall data was used. Continuous simulations were carried out for stormwater events based on the rainfall records during the water years of 1978 to 1986, 1994 to 1995, and 1996 to May 31, 1997. Based on the model results, an analysis on annual stormwater flow volume was carried out. Table 3-2 summarizes total rainfall that occurred at each rain gauge station for the July 1,1996 to May 31,1997 time period.

The average rainfall for July through May is 35.5 inches at Sea-Tac Airport over the last 30 years. The extra rain during the 1996-97 simulation period occurred primarily during December, January, and March. The snowfall in late December followed by five days of heavy rainfall resulted in large volumes of stormwater and CSO flows and high river flows. The entire storm event has been estimated to have a return interval of greater than 30 years. Other large storm events during the Sept. 1996 to May 1997 period occurred in November (a three times/year event), March (a one time/year event), April (a twice/year event), and May (a four times/year event).

Table 3-2. Rainfall Record Summary (during July 1, 1996 to May 31, 1997)

Rain Gauge	Location	Total Rainfall (inch)
No. 14.	West Seattle	42.8
No. 15.	South Seattle	42.1
No. 16.	Boeing Field	42.6
No. 17.	White Center	46.3
No. 12.	Magnolia	43.5
No. 20.	Capital Hill	39.7
No. 11	Downtown Seattle	38.0

3.5.1 Subcatchments

Unless severely modified by human activities, the boundary for Duwamish River basins are based on the natural drainage defined by the contour map. Most of the stormwater subcatchment boundaries are based on the model for the sewerage system, which more or less follows the natural basin boundaries. The only exception is the separated sewer system subcatchments located north of Hanford Street in the upper Rainier Valley. A tunnel drains the stormwater collected from the area between East Columbia in the north to Hanford in the south of the Rainier Valley. The stormwater flow though the tunnel is directed to the Diagonal Avenue stormwater drain.

There are 129 subcatchments for the model simulation. The subcatchment area and its boundary are defined based on the sanitary and combined sewer segments. The area of the subcatchments ranges from 7 to 1,628 acres. Seventy-three of the 129 subcatchments flow directly into the Duwamish River or Elliott Bay and are only simulated by the Runoff Model. Fifty-six subcatchments are routed through the Transport Model and are routed through the Transport Model and combined with other subcatchments before flowing into the receiving water. Eight transport pipes were established in the model to represent Hanford and Diagonal Avenue storm water drainage, Longfellow Creek, Hamm Creek, and several other subcatchments combined by the storm water drains or natural surface streams for the transport model simulations.

3.5.2 Model Setup

The map in Figure 3-2 shows the subcatchment of the Runoff Model for the Duwamish River/Elliott Bay area. The total area for the Duwamish River/Elliott Bay basin is about 33 square miles. Some of the areas are serviced by a separated sewage system and some are serviced by a combined sewer system.

The Runoff Model for sanitary and combined sewage has been established and calibrated by Metro Staff in the late 1980s and early 1990s. The percentage of storm water-drained area for each subcatchment is determined based on the percentage not connected to the sanitary sewerage in the Runoff Model.

3.5.3 Subcatchment Parameters

Subcatchment parameters are required for Runoff and Transport Model simulations. The parameters are reflections of the geometry of the subcatchments, average hydrological conditions of the surface flow, and groundwater flow infiltration. The data required are area, width, slope, percent of impervious area, roughness coefficients, depression storage factor, and other components defining the soil permeability. It also includes parameters defining groundwater infiltration and base flow to the storm water drain. These parameters were determined based on the calibrated sanitary and combined sewerage Runoff model. Some of the parameters are calibrated using the storm water flow as is discussed in the next section. Table 3-3 lists some of the parameters used for the Runoff and Transport Model simulations. Locations of subcatchments, by numbers, are shown in Figure 3-2.

3.5.4 Precipitation Data

The rain data from the City of Seattle rain gauge stations were used for the model calibration and simulations. The data contain continuous rainfall records since 1978. The map in Figure 3-3 shows the locations of the city rain gauge stations. There are seven rain gauges involved for the Runoff and Transport model simulation listed in Table 3-3. The rain gauge data were examined for errors. If there were any unreasonable records or problems with the City gauge data, the records were edited basing edits/corrections on the corresponding rain data from a nearby King County WTD rain gauge station.

3.5.5 Model Calibration

There are only limited flow records for the storm water drains in this area. The storm water Runoff model was calibrated based on the level and flow measurement taken from Longfellow Creek collected by the City of Seattle and the data collected from Hamm Creek by the King County Water and Lands Division (WLRD).

The King County engineers had previously calibrated the Runoff Model to the sanitary and combined sewage areas. The only intensive calibration involved in the storm water model were the parameters for the groundwater component that define the base flow components. Since we do not have flow data from other storm drainage areas of Duwamish River/Elliott Bay area other than Longfellow Creek and Hamm Creek, the calibrated parameters for groundwater infiltration are assumed to be applicable to the whole Duwamish River/Elliott Bay basins.

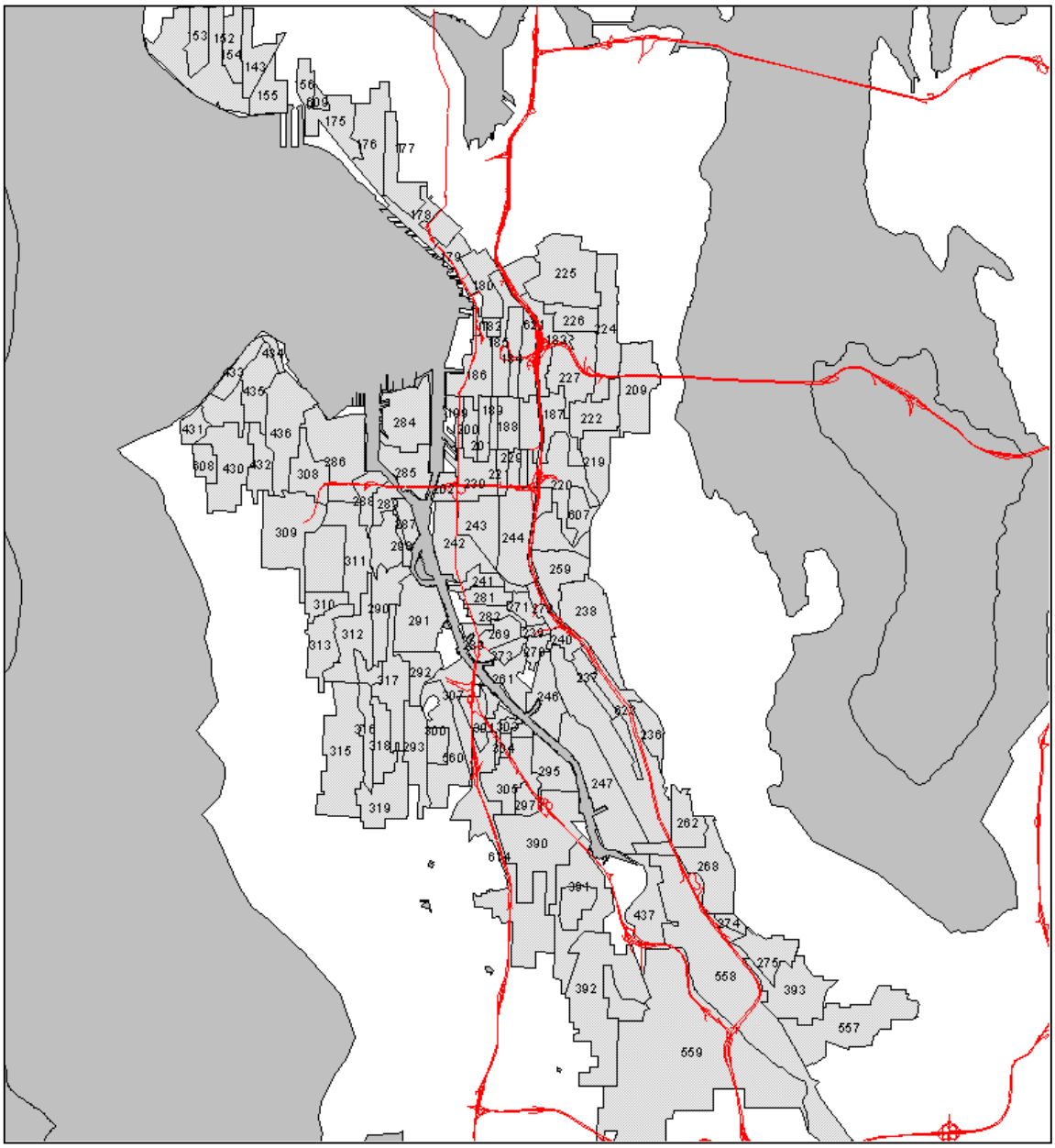

Figure 3-2. Subcatchment Map for Duwamish/Elliott Bay Catchment

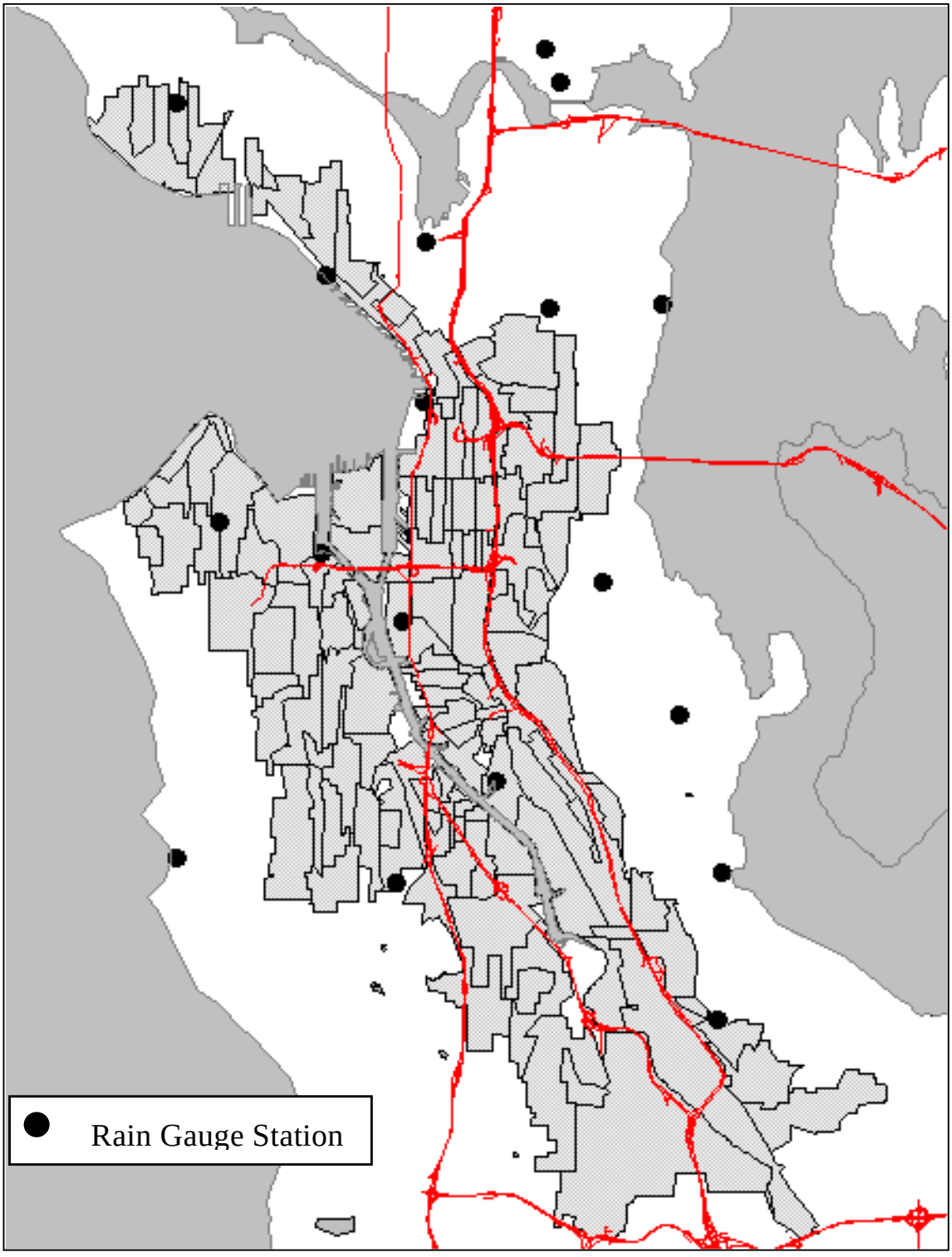

Figure 3-3. Location Map of the Rain Gauge Stations

3.5.6 Longfellow Creek

The City of Seattle Public Utilities have been collecting flow data from the Longfellow Creek since 1995. The monitoring site is located at SW Graham Street south of the West Seattle Golf Course. Water levels were continuously recorded in two minutes intervals. The City also evaluated some measurements of flow vs. level rating data pairs.

Since the measured level had a higher range than that for the rating data pairs, extrapolation was required. Based on the flow and level pairs, a rating curve was established to determine the flow rate based on the measurement of level as follows so that the level record can be extended.

The formula for the curve is expressed as follows:

$$Q\ cf(s) = 0.9 * H^{3} \qquad \text{Equation 3-4}$$

The curve is shown in Figure 3-4 in comparison to the data pairs from the rating table.

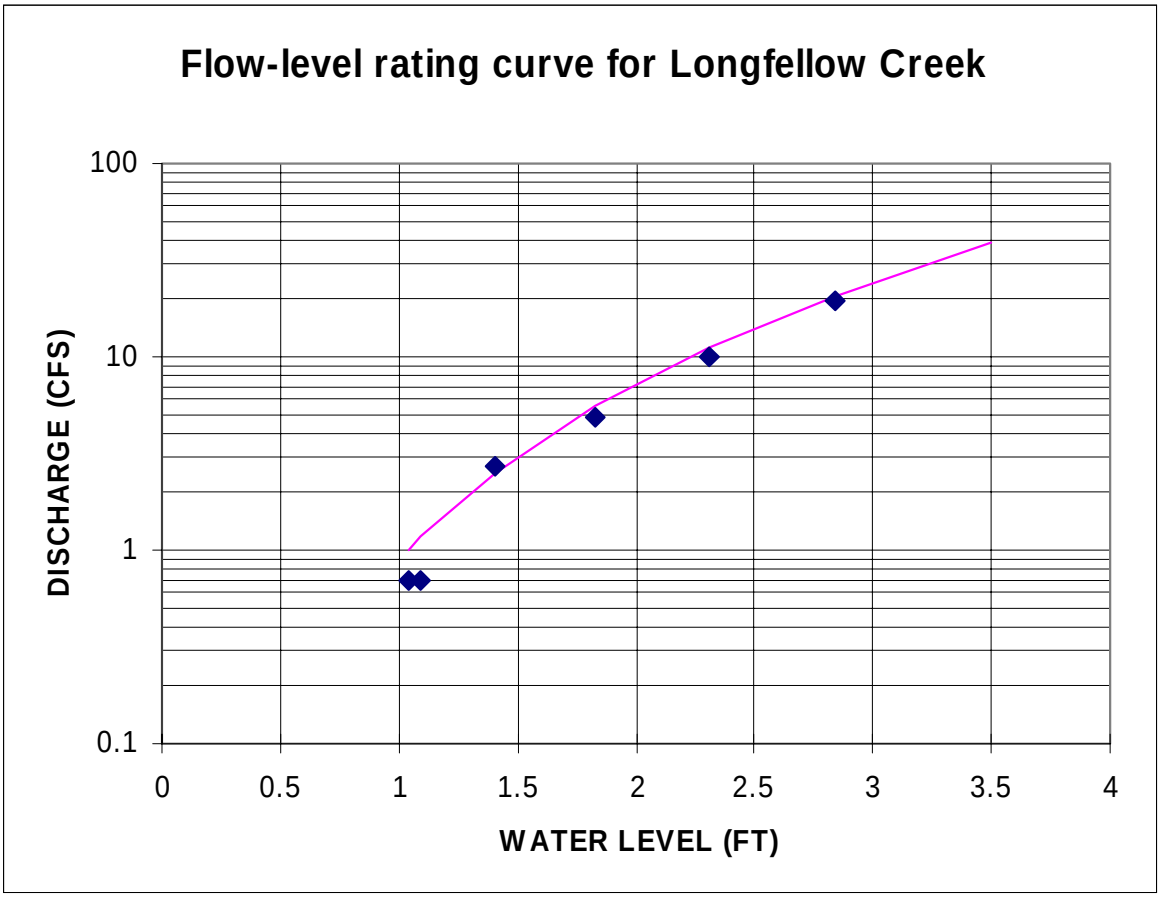

Figure 3-4. Flow-Level Rating Curve for Longfellow Creek

The curve appears to reasonably match the rating data pairs.

The basin map in Figure 3-5 shows part of subcatchments of Longfellow Creek upstream of the monitoring station for the Runoff Model calibration. The storm event between February 3 to February 10, 1996, which represents the heavy rainfall conditions, was selected for the calibration of the storm water drainage runoff model. The total rainfall during this period was 4.2 inches according to the records from rain gauge 14 (see Figure 3-3). The selection was made to emphasize the heavy and medium rain conditions so that the Runoff Model simulated flow would be more representative to overall conditions (Figure 3-6).

The calibrated model was then verified with the storm between February 17 and 21, 1996 as shown in Figure 3-7. The total rainfall was 2.23 inches during this period. It appears that the simulated flow generally matches the measurement well, especially during the high flow condition.

3.5.7 Hamm Creek

The Water and Land Resources Division of the County has been collecting flow data near the Hamm Creek storm water outfall since 1995. The flow data of the creek were recorded continuously in 15-minute intervals. With recorded rain data, the Runoff and Transport Model simulation can generate flow from the creek as well. The parameters of the subcatchments were adjusted to match the measured storm water flow.

Figure 3-8 shows the subcatchments for Hamm Creek Runoff model. Two storm events were selected for the Runoff and Transport Model calibration with subcatchments. The calibration of the Hamm Creek parameters for base flow of the Runoff Model is based on the parameters from the Longfellow Creek with minor modifications.

As shown in Figure 3-9 and Figure 3-10, the simulated flow from Hamm Creek is similar to the measured flow, especially at the high flow conditions. However, the comparison between the simulated and measured flow for the low flow conditions did not agree well with each other. There are several peaks based on the measurement which do not respond well with the rainfall record, suggesting that there might be some other factors influencing the flow processes.

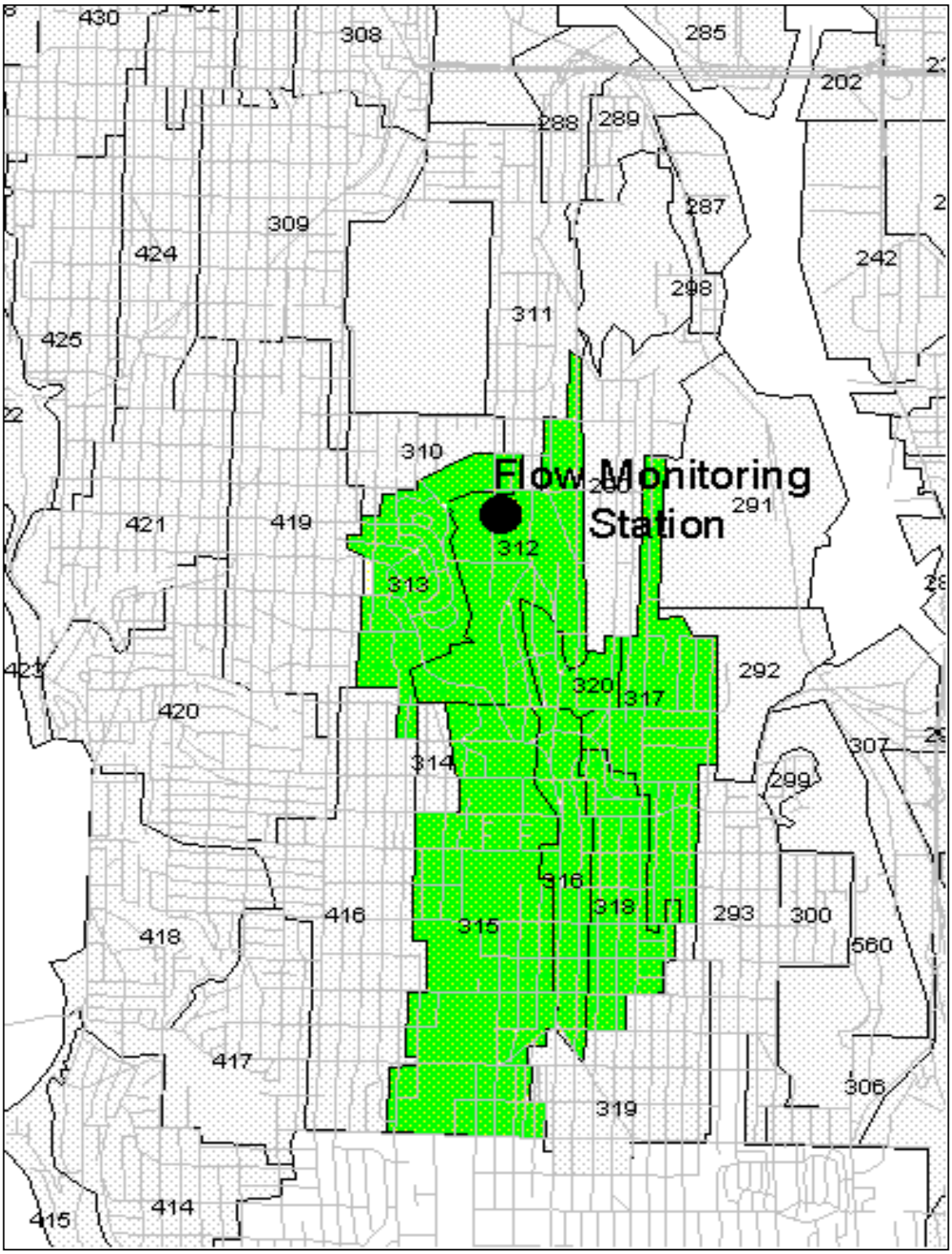

Figure 3-5. Location Map of Longfellow Creek Flow Monitoring Station

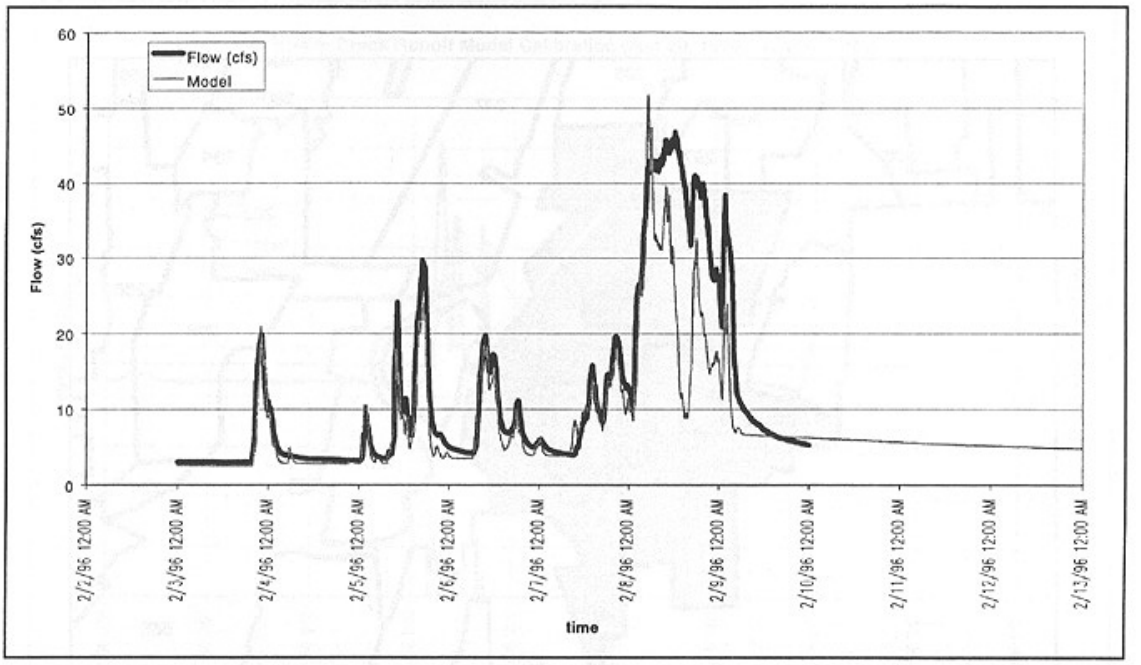

Figure 3-6. Comparison Between Measured and Model Simulated Flow in Longfellow Creek

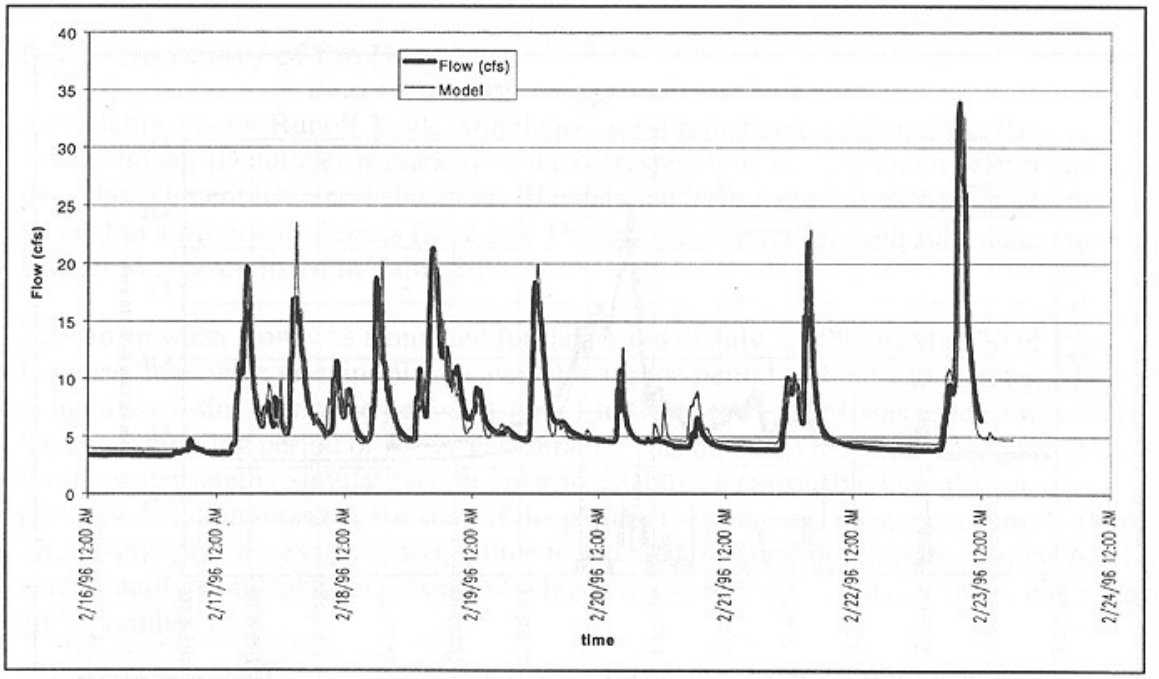

Figure 3-7. Comparison Between Measured and Model Simulated Flow in Longfellow Creek

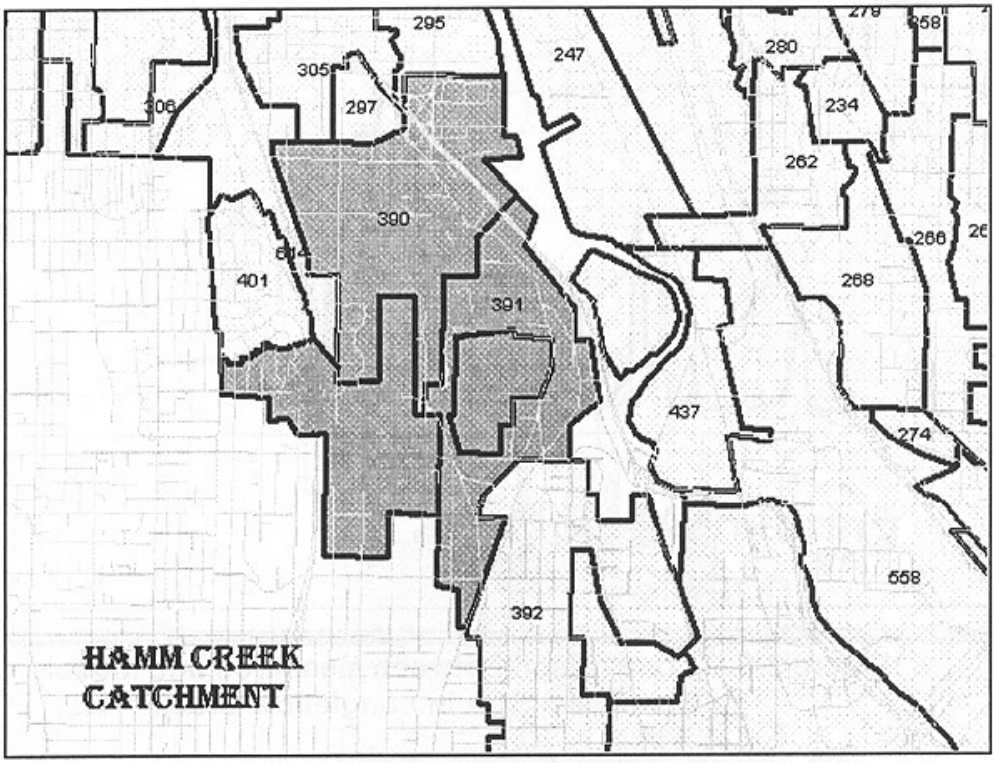

Figure 3-8. Location Map of Hamm Creek Subcatchments

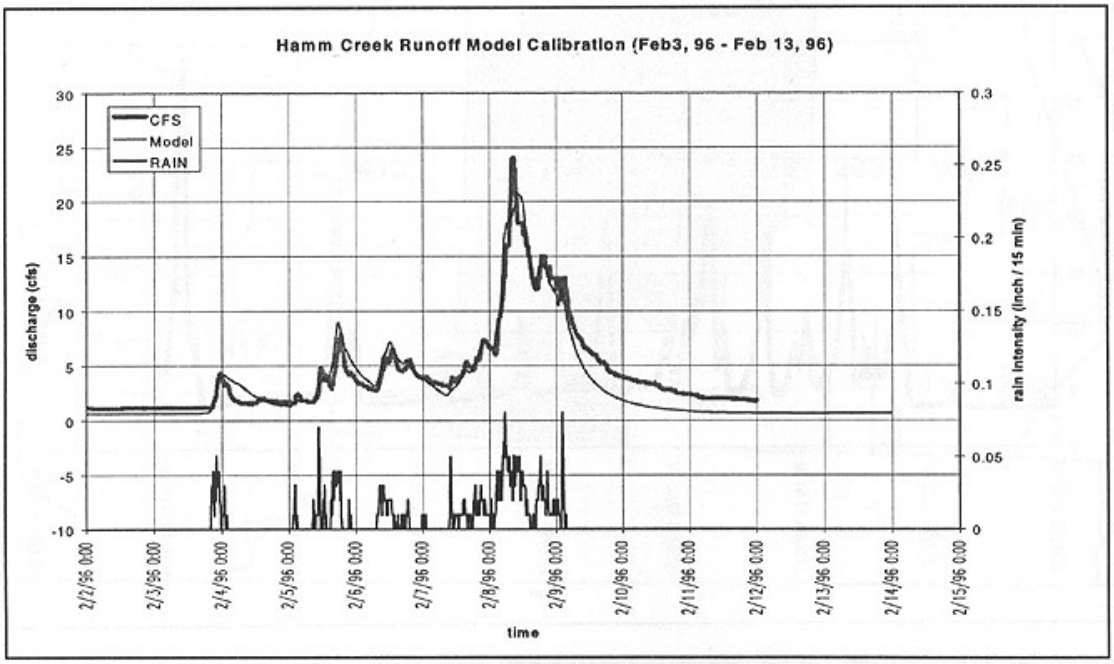

Figure 3-9. Comparison Between Measured and Model Simulated Flow in Hamm Creek, February 1996

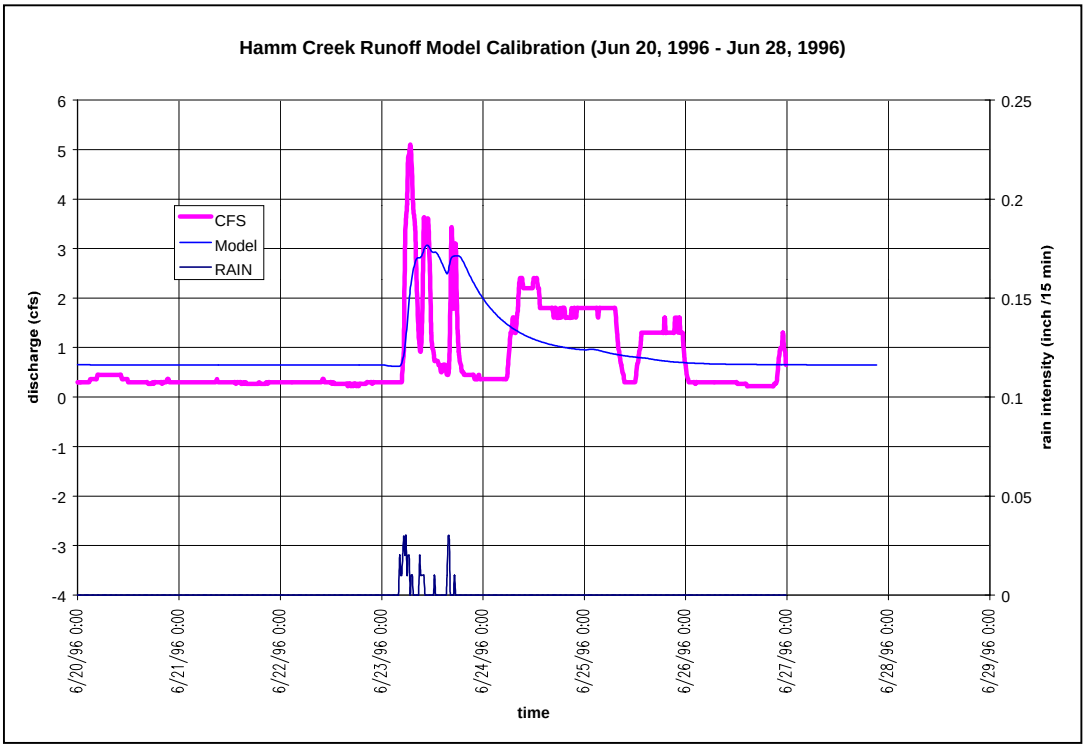

Figure 3-10. Comparison Between Measured and Model Simulated Flow in Hamm Creek, June 1996

3.5.8 Summary of the Results

Subcatchments for Runoff Model simulation are summarized in Figure 3-2. Each subcatchment ID number is marked on the corresponding location and is referenced in the subcatchment list (see Table 3-3). The detailed information of each subcatchment is located in a Microsoft Access Database. The key parameters for each subcatchment of the Runoff Model are listed in Table 3-3.

The storm water flow was simulated for the period of July 1, 1996 to May 30 of 1997. Because there were no rainfall data available for the period of June 1 to October 31, 1997 at the time of this work, the period of June 1 to October 31, 1981 was used to substitute the corresponding period of 1997. The duration was based on the simulation period used for the water quality simulations. In order to establish a reasonable base flow and groundwater component at the start of the period, the simulation began on June 1, 1996. This would give the system enough time to establish reasonable initial conditions for the water quality simulation, the results of which are used for the risk assessment, beginning on September 1.

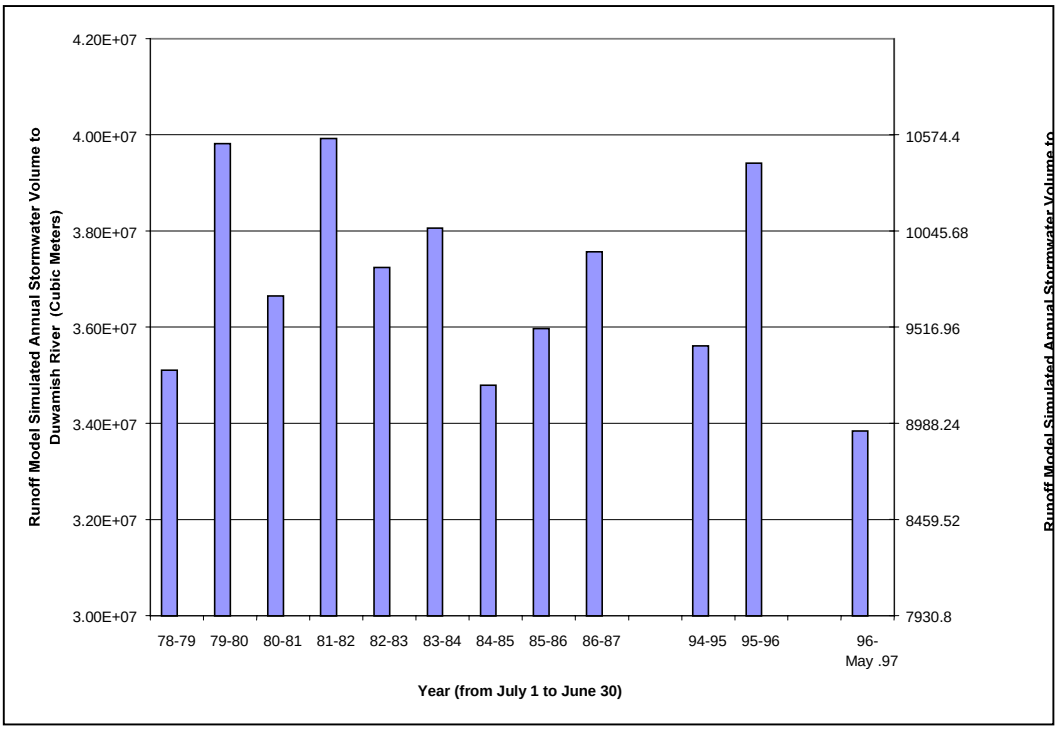

The storm water flow was also simulated for the Duwamish River/Elliott Bay catchment during mid-1978 to mid-1987, and mid-1994 to mid-1997. The simulated annual storm water volume is shown in the following charts (Figure 3-11). The simulation results are for the purpose of import to the water quality modeling effort.

Figure 3-11. Runoff Model Simulated Annual Stormwater Volume from Duwamish River/Elliott Bay Catchment

Based on the simulation results, the annual storm water volume for the periods of 1978 to 1986, 1994 to 1995 (starts from July 1 to June 30) and July 1, 1996 to April 30, 1997 are shown in Figure 3-11. Figure 3-12 through Figure 3-14 show the distribution of the storm water volume along the Duwamish River and Elliott Bay. In these figures, the storm water flow location along the river is defined based on the EFDC model cell number.

3.5.9 Discussion of Volume Balance

The average rainfall for the rain gauges involved is 42.1 inches during July 1, 1996 to May 31, 1997. Applying the average rainfall over the total basin area of about 33 square miles to determine the total rainfall volume during this period, results in about 24,150 million gallons. This volume of water is the source of combined sewer inflow, infiltration into sanitary sewerage, storm water drainage, evapotranspiration, groundwater storage variation, groundwater flow, and ground moisture variation.

In contrast, the model-simulated surface storm water outflow volume from the whole drainage basin was 8,940 million gallons, about 37 percent of the total rainfall volume. The other 63 percent would be transported through the combined sewerage, sanitary sewerage infiltration, groundwater flow, and evapotranspiration.

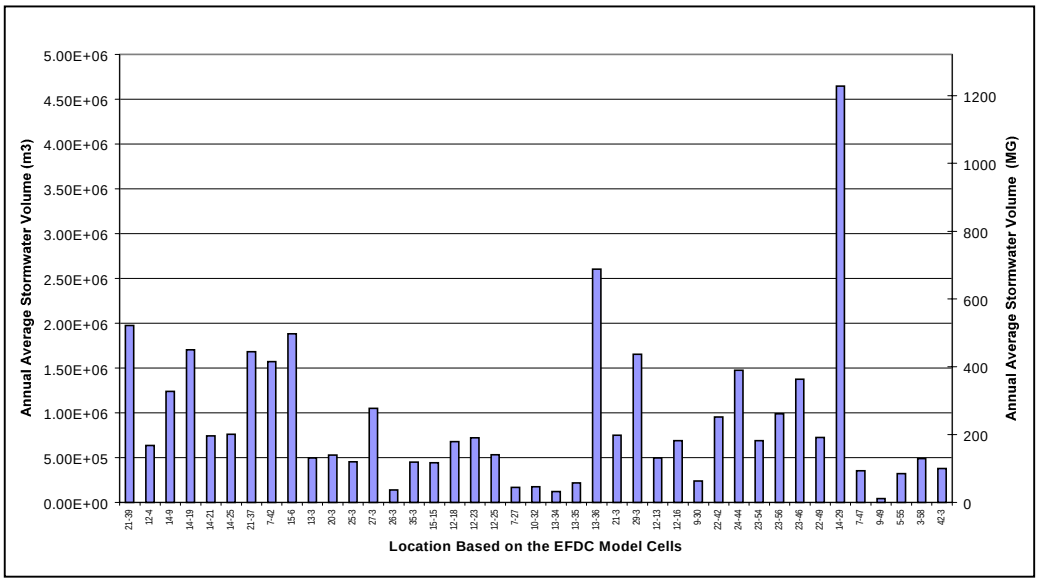

Figure 3-12. Runoff Model Simulated Stormwater Volume from Duwamish River /Elliott Bay Catchment (July 1, 1978 – June 1, 1986)

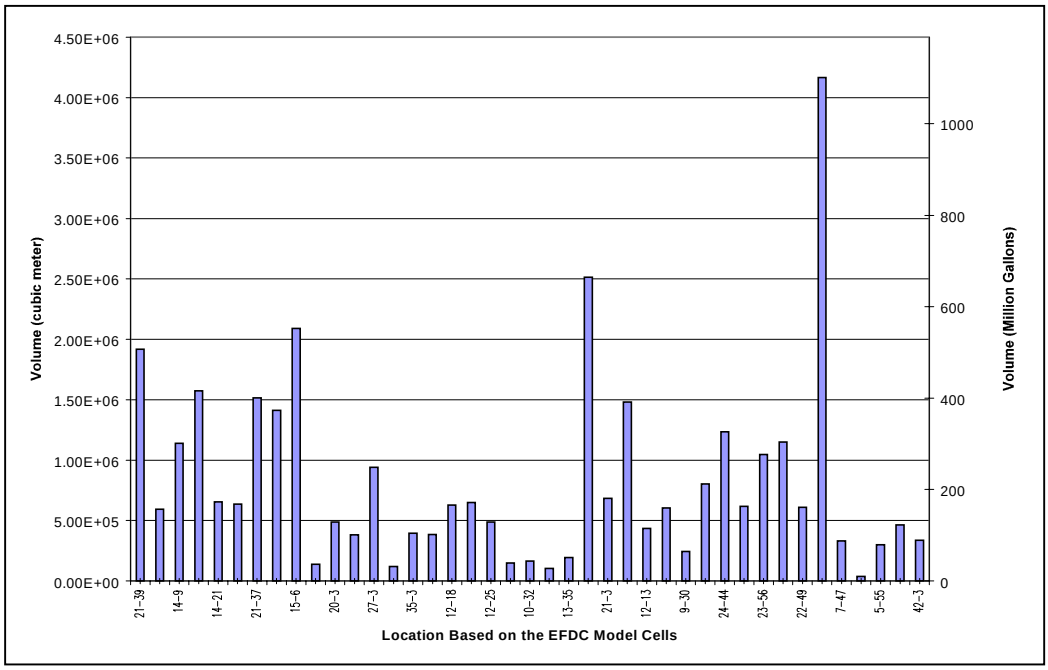

Figure 3-13. Runoff Model Simulated Stormwater Volume from Duwamish River/Elliott Bay Catchment (July 1994 – June 1995)

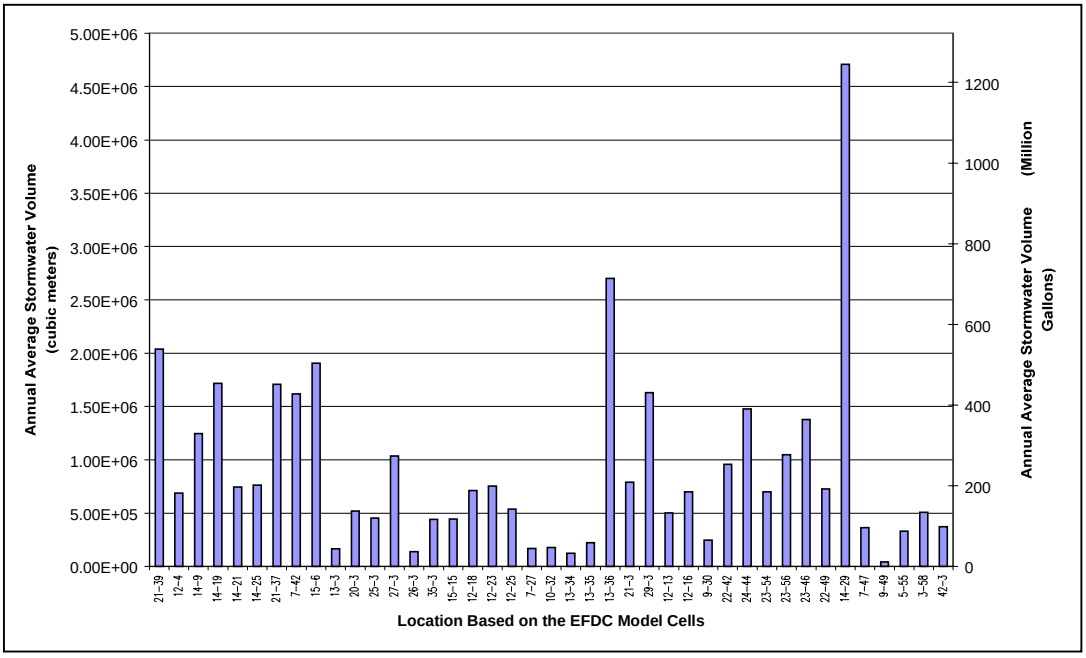

Figure 3-14. Runoff Model Simulated Stormwater Volume from Duwamish River/Elliott Bay Catchment (July 1996 – May 1997)

3.5.10 Chemical Inputs for Stormwater Runoff

Limited chemical data for the storm water chemical loads were obtained from historical storm water studies conducted within the Duwamish Estuary basin. The study sites included Longfellow Creek (collected since 1973) and Hamm Creek (collected between 1995 and 1996). Supplemental data were reviewed from the Densmore drain (collected between 1993 and 1996). The Densmore service basin however, is quite different from the Duwamish Estuary basin and may not be indicative of potential COPC loading to the estuary. Since one aspect of the modeling effort was to estimate chemical loads from other sources, and that those sources were adjusted until model predictions were comparable to observed, exact storm water concentrations were not required; only reasonable estimates were required. Use of the storm water data does not imply all loads from "other sources" are solely from storm water drains. The review did not provide chemical data for some of the COPCs. In these instances, CSO data were used in place of storm water data. Subappendix A summarizes initial chemical conditions for other sources in Tables A-1 through A-4.

4. HYDRODYNAMIC CALIBRATION

4.1 Introduction

The hydrodynamic model was configured to simulate three physical characteristics of the Elliott Bay/Duwamish River model; salinity, velocity, and water elevation. Temperature was not simulated for this study. As a condition to the solution of the equations used to predict the three variables, values for salinity, velocity, and water elevation must be specified at the model boundaries. Conditions at the Elliott Bay boundary were defined by a harmonic water elevation time series and a constant salinity profile. Conditions at the Green River boundary were defined by daily average river flow and fresh water (zero salinity). Fresh water flows at the Green River boundary was obtained from the U.S. Geological Survey (USGS) Auburn gage station, which recorded flows every 15 minutes.

There have been a number of geophysical sampling and modeling studies performed within the Puget Sound area in and around Elliott Bay prior to this study. The Pacific Marine Environmental Laboratory has done many studies of Elliott Bay measuring salinity, velocity, suspended solids, and various chemicals. King County (at the time Municipality of Metropolitan Seattle) has also collected a significant amount of information for the construction of the West Point and Renton Treatment Plant outfalls, and as part of it's Water Quality Monitoring Program. The studies, however, typically did not sample at a frequency fine enough, nor of sufficient duration to allow the development of a temporal equation to define conditions at the Elliott Bay boundary. Most of the studies were designed to either assess global flow, tides, and water quality characteristics, or to estimate generalized loading conditions in Elliott Bay. The studies are useful however in helping understand generalized patterns and interdependencies within and outside the bay.

The most detailed numerical study, known to date, of Puget Sound and Elliott Bay was performed by Jiing-Yih Liou and Wen-Sen Chu (1991). They developed a three dimensional model of Puget Sound and Elliott Bay. However, the study did not include density effects, and for Elliott Bay the simulations were limited to a single tidal cycle. The study was useful in showing a very complicated velocity field existed at the mouth of the bay.

Because of the interdependent salinity and flow structure that exists in the bay and sound (H. C. Curl et al. 1988, Stober and Chew 1984, Cannon et al. 1979, Silcox et al. 1981, Lavelle et al. 1985) and the difficulty in accurately defining it at the model boundary given existing information, a simplified approach was taken to describe the boundary. A harmonic water elevation was used to represent tidal forcing along with a constant salinity profile across the depth. A constant salinity of 31 parts per thousand was used based on average salinity observations collected during the Duwamish Head Baseline Study (Municipality of Metropolitan Seattle 1987).

This report documents the calibration of the Environmental Fluids Dynamic Computer Code (EFDC) hydrodynamic and transport model to simulate water surface elevation, horizontal currents, and salinity in Elliott Bay and the Duwamish River over a 240-day period between Julian Day 237, 1996 and Julian Day 112, 1997. The simulation period is characterized by increasing freshwater inflow as well as significant high-inflow events. Field observations of water surface elevations, horizontal currents, and salinity during this period are used in this study to provide a basis for calibration and validation of the EFDC model.

4.2 Model Configuration and External Forcings

The general procedure for the application of the EFDC model to Elliott Bay and the Duwamish River follows a sequence of steps beginning with model set-up or configuration. Model configuration involves the construction of a horizontal grid of the water body and interpolation of bathymetric data to the grid, construction of EFDC input files, and compilation of the source code with appropriate parameter specification of array dimensions. The EFDC input files include the master input file, efdc.inp; files specifying the grid and bathymetry, cell.inp, celllt.inp, dxdy.inp, lxly.inp, mask.inp, and moddxdy.inp; an atmospheric forcing file, aser.inp; an inflow-outflow file, qser.inp; a salinity boundary condition file sser.inp; an initial salinity file, salt.inp; and a screen print control file, show.inp (Hamrick 1996).

The horizontal grid constructed for Elliott Bay and the Duwamish River uses curvilinear horizontal grid cells and was constructed using an orthogonal mapping procedure (Ryskin and Leal 1983). Bathymetry data were provided by King County and supplemented by NOAA navigation chart data. Figure 3-1 shows the horizontal grid. The horizontal grid has 512 active water cells. Figure 2-1shows the location of field observation stations. The vertical model grid used ten stretched layers having equal fractional thickness' of 1/10.

Circulation in Elliott Bay and the Duwamish River is forced by water surface elevation at the western mouth of Elliott Bay, which opens into Puget Sound, freshwater discharge from the upper reach of the Duwamish River, and local winds. The forced radiation hydrodynamic boundary condition, which specifies incoming waves while allowing no reflection of outgoing waves, is used at the mouth of Elliott Bay. The condition is:

$$\zeta - \frac{n \bullet uH}{\sqrt{gH}} = 2\zeta_R \qquad \text{Equation 4-1}$$

where ζ is the water surface elevation relative to a sea-level data, **n** is the outward normal vector to the boundary, **u** is the horizontal barotropic velocity vector, H is the water depth, and ζ_R is the equivalent progressive incoming wave amplitude. In Elliott Bay and the Duwamish River water surface elevation is dominated by tidal variations and the boundary condition (Equation 4-2) was specified in harmonic form:

$$\zeta_R = \sum_{m=1}^{M} \left(\zeta_{RCm} \cos(\omega_m t) + \zeta_{RSm} \sin(\omega_m t) \right) \qquad \text{Equation 4-2}$$

for M tidal constituents where ζ_{RCm} and ζ_{RSm} are cosine and sine amplitudes at frequency ω_m. Six harmonics constituents (M2, S2, N2, K1, O1, and P1) were used. Since water surface elevation and horizontal velocity observations along the open boundary were not available, a variational inverse procedure was used to estimate cosine and sine harmonic constituent amplitudes such that the differences between observed and predicted water surface elevation tidal harmonic amplitudes at two interior observation locations, the Seattle Ferry Pier and the Spokane Avenue Bridge, were minimized in a least squares sense. The inverse procedure is based on the solution of the linear, barotropic hydrodynamic equations, and a corresponding set of adjoint equations in the frequency domain. A spatially uniform bottom roughness, equivalent to a roughness height of two cm, was used in the inverse procedure. The use of two interior observation stations allowed the harmonic amplitudes to vary linearly along the boundary with the inverse remaining well conditioned. When the boundary condition (Equation 4-1) was applied in the EFDC model, a spatially uniform two cm bottom roughness height was used. Figures B1 through B4, in Subappendix B, show observed and model predicted water surface elevations over a 29-day period at the Duwamish Yacht Club.

Density-driven circulation in Elliott Bay and the Duwamish River results from the dynamic interaction of high-salinity water entering the mouth of Elliott Bay and the freshwater discharge from the upper reaches of the Duwamish River. Figure 4-1 shows the Duwamish River discharge over the 240-day simulation period. The discharge is characterized by a relatively rapid increase in flow near the beginning of November and a number of subsequent high-flow events. Wind forcing was assumed to be spatially uniform and was based on NOAA observations at the Seattle Ferry Pier. Wind speed and

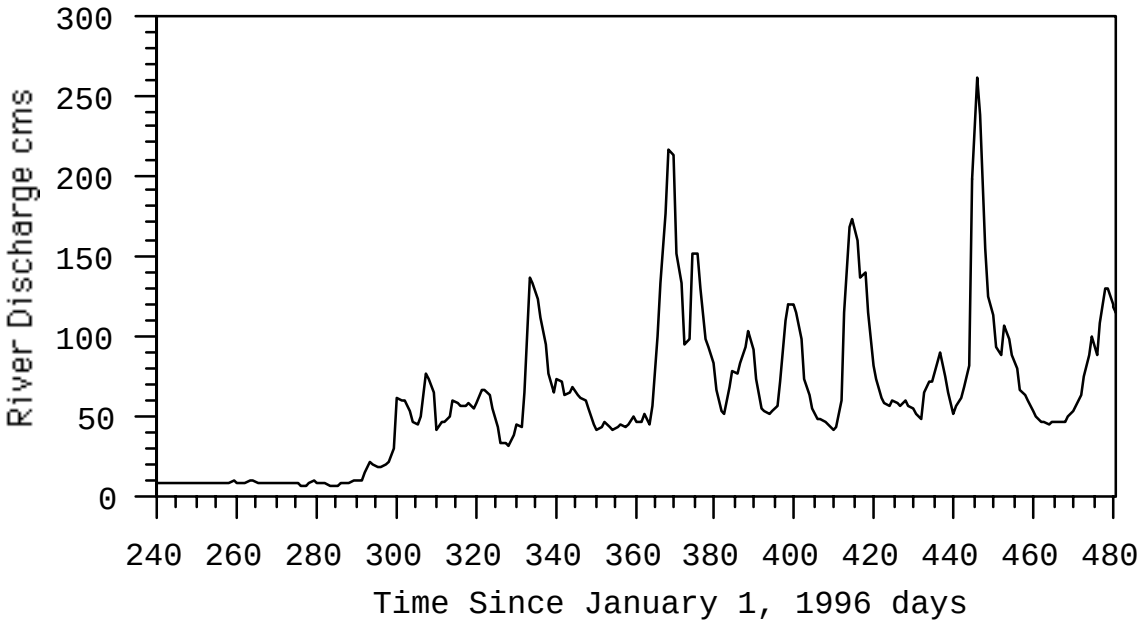

direction during the simulation period are shown in Figures 4-2 and 4-3, respectively.

Figure 4-1. Duwamish River Discharge

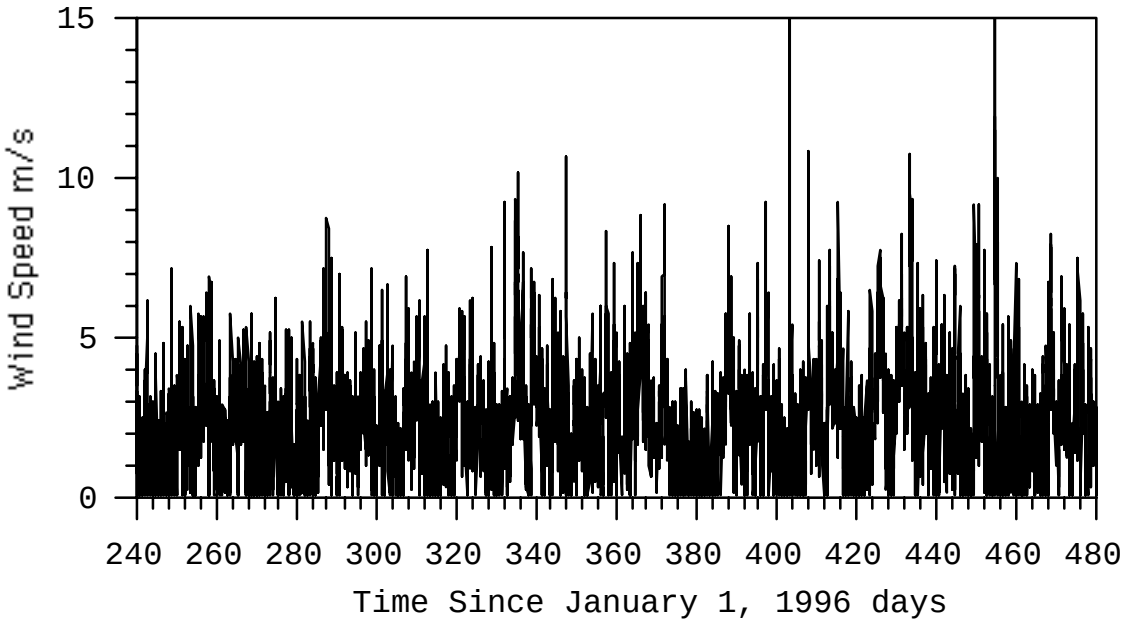

Figure 4-2. Seattle Ferry Pier Wind Speed

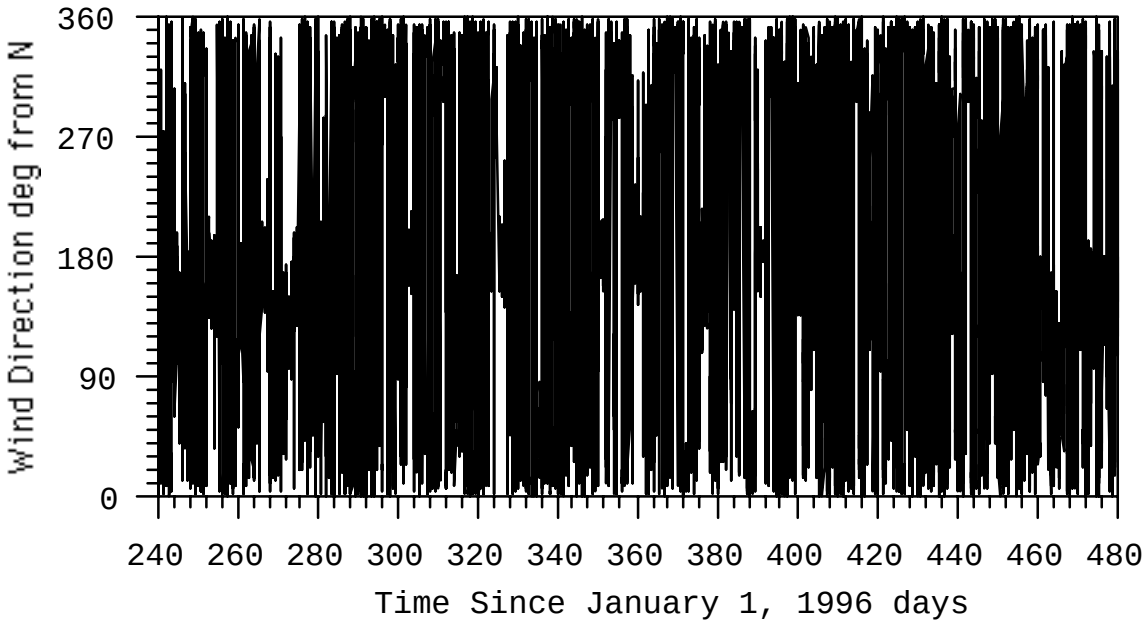

Figure 4-3. Seattle Ferry Pier Wind Direction (Bearing to)

4.3 Model Calibration and Verification Measures

To quantify the EFDC model's prediction of water surface elevation, salinity, and velocity, a number of statistical tests and time series analyses are used. This section summarizes general test and analysis procedures. Further discussion justifying the selection of particular tests and analyses for specific data types are presented in Section 4.4.

The statistical tests that can be used for evaluating model predictions include the mean error, mean absolute error, root mean square error, maximum absolute error, relative mean error and relative absolute mean error (Thomann 1982). Letting O and P denote observed and predicted values of a quantity at N observation times, the mean error is defined by:

$$ME = \frac{1}{N}\sum_{n=1}^{N}\left(O^{(n)} - P^{(n)}\right) \qquad \text{Equation 4-3}$$

Positive values of the mean error indicate that the model tends to under-predict the observations whereas negative values indicate that the model tends to over-predict observations. The mean absolute error is defined by:

$$MAE = \frac{1}{N}\sum_{n=1}^{N}\left|O^{(n)} - P^{(n)}\right| \qquad \text{Equation 4-4}$$

Although the mean absolute error provides no indication of over-prediction or under-prediction, it eliminates the canceling effects of positive and negative errors and can be viewed as a more extreme measure of observation-prediction agreement. The root mean square error is defined by:

$$RMS = \sqrt{\frac{1}{N}\sum_{n=1}^{N}\left(O^{(n)} - P^{(n)}\right)^2} \qquad \text{Equation 4-5}$$

The RMS can be interpreted as a weighted equivalent to the mean absolute error with larger observation-prediction differences given larger weightings. The square root operation recovers the units of the data quantities. The rms error is generally viewed as the most rigorous absolute error test. The maximum absolute error is defined by:

$$MAX = \max\left|O^{(n)} - P^{(n)}\right| : n = 1, N \qquad \text{Equation 4-6}$$

and provides information on the largest discrepancy between corresponding values of observed and predicted quantities over an interval of *N* measurements.

Relative error measures can be used to eliminate data units and to provide a measure of error relative to the magnitude of the observational data. The relative mean error and the relative mean absolute error are defined by:

$$RME = \frac{\sum_{n=1}^{N}(O^{(n)} - P^{(n)})}{\sum_{n=1}^{N}O^{(n)}} \qquad \text{Equation 4-7}$$

$$RMA = \frac{\sum_{n=1}^{N}\left|(O^{(n)} - P^{(n)})\right|}{\sum_{n=1}^{N}O^{(n)}} \qquad \text{Equation 4-8}$$

Caution should be employed in the use of these two relative error measures, particularly when observed and predicted quantities can have small values or values that have both positive and negative signs. An alternative relative error, hereafter referred to as the relative mean square error, is:

$$RSE = \frac{\sum_{n=1}^{N}(O^{(n)} - P^{(n)})^2}{\sum_{n=1}^{N}\left((O^{(n)} - \overline{O})^2 + (P^{(n)} - \overline{O})^2\right)} \qquad \text{Equation 4-9}$$

This error measure was proposed by Willmott (1982) and Willmott et al. (1982) and used by Blumberg and Goodrich (1990) to analyze the prediction skill of an estuarine model. The value of *RSE* always falls between zero and unity, with an increasing value corresponding to decreasing skill of the model.

Thomann (1982) suggested the use of linear regression for comparing model predictions with observations in the context of model calibration. Following Thomann, the linear equation relating observed and predicted values of the quantity *s* is written as:

$$S_o = \alpha + \beta s_p \qquad \text{Equation 4-10}$$

where alpha and beta are determined by:

$$\alpha = \frac{1}{N}\left(\sum_{n=1}^{N} s_o^{(n)} - \beta \sum_{n=1}^{N} s_p^{(n)} \right) \qquad \text{Equation 4-11}$$

$$\beta = \frac{\sum_{n=1}^{N}\left(s_o^{(n)} - s_o^{(avg)}\right)\left(s_p^{(n)} - s_p^{(avg)}\right)}{\sum_{n=1}^{N}\left(s_p^{(n)} - s_p^{(avg)}\right)^2} \qquad \text{Equation 4-12}$$

(Devore 1982). The null hypothesis for the linear regression is alpha, the intercept, equal to zero, and beta, the slope, equal to one. Also useful in the regression analysis is the correlation coefficient:

$$r = \frac{N\sum_{n=1}^{N} s_p^{(n)} s_o^{(n)} - \left(s_p^{(n)}\right)\left(s_o^{(n)}\right)}{\sqrt{N\sum_{n=1}^{N} s_p^{(n)} s_p^{(n)} - \left(\sum_{n=1}^{N} s_p^{(n)}\right)^2}\sqrt{N\sum_{n=1}^{N} s_o^{(n)} s_o^{(n)} - \left(\sum_{n=1}^{N} s_o^{(n)}\right)^2}} \qquad \text{Equation 4-13}$$

For a goodness of fit or correlation between observations and predictions, the correlation coefficient should be near one. The square of the correlation coefficient equals the fractional proportion of variation of observations explained by the regression relationship between the observations and predictions (Devore 1982).

Time series having deterministic periodic structure can be analyzed using least squares harmonic analysis. Consider a time series of the form:

$$\phi(t) = a_o + b_o t + \sum_{m=1}^{M} a_n \cos\left(\frac{2\pi t}{T_m}\right) + \sum_{m=1}^{M} b_n \sin\left(\frac{2\pi t}{T_m}\right) \qquad \text{Equation 4-14}$$

composed of a constant, a_0, a linear in time term $b_0 t$, and M periodic or harmonic components having periods T_m. Note that Equation 4-13 can also be written in the form:

$$\phi(t) = a_o - b_o t - \sum_{m=1}^{M} A_m \cos\left(\frac{2\pi t_n}{T_m}\left(t - \tau_m\right)\right) \qquad \text{Equation 4-15a}$$

$$A_m^2 = a_m^2 + b_m^2 \qquad \text{Equation 4-15b}$$

$$\tau_m = \frac{T_m}{2\pi}\arctan\left(\frac{b_m}{a_m}\right) \qquad \text{Equation 4-15c}$$

where A_m and τ_m are the amplitude and phase of the mth periodic or harmonic component of the time series. The a and b coefficients representing the time series can be determined from discrete values of ϕ at N times by minimization of the least squares functional:

$$E = \sum_{n=1}^{N} \left(\phi(t_n) - a_o - b_o t = \sum_{m=1}^{M} a_m \cos\left(\frac{2\pi t_n}{t_m} \right) - \sum_{m=1}^{M} b_m \sin\left(\frac{2\pi t_n}{T_m} \right)^2 \right) \quad \text{Equation 4-16}$$

with respect to the *a* and *b* coefficients. The minimization results in a system of *2N+1* equations for the *a* and *b* coefficients. For comparison of model predictions with observations, harmonic coefficients are determined for both model-predicted and observed time series, and the amplitudes and phases appropriately compared for each harmonic component.

For two-dimensional vector time series, the vector components, *u* and *v*, are separately analyzed to determine the coefficients in the expansions:

$$u(t) = u_0 + \sum_{m=1}^{M} uc_n \cos\left(\frac{2\pi t}{T_m} \right) + \sum_{m=1}^{M} us_n \cos\left(\frac{2\pi t}{T_m} \right) \quad \text{Equation 4-17a}$$

$$v(t) = v_0 + \sum_{m=1}^{M} vc_n \cos\left(\frac{2\pi t}{T_m} \right) + \sum_{m=1}^{M} vs_n \cos\left(\frac{2\pi t}{T_m} \right) \quad \text{Equation 4-17b}$$

The combined results can be cast in tidal velocity ellipse form with the major and minor axis amplitudes, the ellipse orientation, and the phase at which the velocity vector aligns with the major axis replacing the *uc*, *us*, *vc*, and *vs* coefficients for each constituent. The half-lengths, *ma* and *mi*, of the major and minor axes are given by:

$$ma = rp + rm \quad \text{Equation 4-18a}$$

$$mi = |rp - rm| \quad \text{Equation 4-18b}$$

$$rp = \sqrt{(uc + vs)^2 + (vc - us)^2} \quad \text{Equation 4-18c}$$

$$rm = \sqrt{(uc - vs)^2 + (vc + us)^2} \quad \text{Equation 4-18d}$$

for each constituent. The major axis orientation angle *ang*, in degrees counterclockwise from east, and the time phase *phe*, at which the velocity vector aligns with the major axis, are given by:

$$ang = \frac{90}{\pi}(ap + am) \quad \text{Equation 4-19a}$$

$$phe = \frac{T}{4\pi}(am - ap) \quad \text{Equation 4-19b}$$

$$ap = \tan^{-1}\left(\frac{vc - us}{us + vs} \right) \quad \text{Equation 4-19c}$$

$$am = \tan^{-1}\left(\frac{vc + us}{uc - vs} \right) \quad \text{Equation 4-19d}$$

for each constituent.

An alternative method for comparing time series of observed and model predicted quantities is the use of spectral analysis techniques. Spectral analysis is particularly useful for comparing the frequency domain structure of observed and predicted responses to random external model forcings such as wind. Spectral analysis can also be used for the analysis of time series composed of the sums of discrete harmonics and a random component. For a quantity s_k, observed or predicted at N discrete times $k\Delta t$ ($k = 0, N-1$) relative to a local time origin, the discrete Fourier transform S_n is given by:

$$S_n = \sum_{K=0}^{N-1} S_k \exp\left(\frac{2\pi ikn}{N}\right) \qquad \text{Equation 4-20}$$

where i is the unit imaginary number. Note that the standard Fourier transform convention of defining N data points from indices 0 to $N-1$ is employed here (Press et al. 1992). The discrete transform is defined at discrete frequencies:

$$f_n = \frac{n}{N\Delta t}; n = -\frac{N}{2}, \le 0 \le, \frac{N}{2} \qquad \text{Equation 4-21}$$

with S_0 corresponding to the discrete 0 frequency, S_n ($n = 1, N/2-1$) corresponding to the first $N/2-1$ positive frequencies, and S_n ($n = N/2+1, N-1$) corresponding to the first $N/2-1$ negative frequencies in reverse order. At n equals $N/2$, S_n defines the value at both the positive and negative Nyquist critical frequencies:

$$f_c = f_{N/2} = \frac{1}{2\Delta t} \qquad \text{Equation 4-22}$$

The inverse discrete transform is given by:

$$s_k = \frac{1}{N}\sum_{n=0}^{N-1} S_n \exp\left(\frac{2\pi ikn}{N}\right) \qquad \text{Equation 4-23}$$

The power spectral density function, P_{ss}, of the quantity s is defined, following Press et al. (1992), as:

$$P_{SS}(0) = P_{SS}(f_0) = \frac{1}{N^2}|S_0|^2 \qquad \text{Equation 4-24a}$$

$$P_{SS}(f_k) = \frac{1}{N^2}\left(|S_k|^2 + |S_{N-k}|^2\right), k = 1, \frac{N}{2} - 1 \qquad \text{Equation 4-24b}$$

$$P_{SS}(f_k) = P_{SS}(f_{N/2}) = \frac{1}{N^2}|S_{N/2}|^2 \qquad \text{Equation 4-24c}$$

for positive frequencies only and has the normalization property that its sum is equal to the mean square value of *s*:

$$\sum_{k=0}^{N/2} P_{ss}(f_k) = \frac{1}{N} \sum_{j=0}^{N-1} \left| S_j \right|^2 \qquad \text{Equation 4-25}$$

When *s* is the water surface elevation, the summed spectral density function is readily identified as twice the mean potential energy divided by the acceleration for gravity:

$$\frac{2PE}{g} = \sum_{k=0}^{N/2} P_{\zeta\zeta}(f_k) \qquad \text{Equation 4-26}$$

When *s* corresponds to velocity, the summed spectral density function is twice the component kinetic energy with the total kinetic energy defined by:

$$2KE = \sum_{k=0}^{N/2} \left(P_{uu}(f_k) + p_{vv}(f_k) \right) \qquad \text{Equation 4-27}$$

A useful measure of model performance is provided by the difference between observed and predicted power spectral density function of a particular quantity:

$$P_{dd}(f_k) = P_{oo}(f_k) - P_{pp}(f_k) \qquad \text{Equation 4-28}$$

with *d*, *o*, and *p* denoting the difference, observed, and predicted, quantities respectively.

4.4 Model Calibration and Verification

Formally, model calibration involves the adjustment of certain model input quantities in an attempt to achieve a specified level of model performance. Verification can be defined as the demonstration that a calibrated model meets specified performance measures or criteria, by quantitative comparison of model predictions with field observations. In this sense, calibration and verification may make use of the same set of observational data. Validation can be defined as the application of the calibrated and verified model to simulate an entirely different set of prototype conditions, with model performance measures, in relation to field observations, satisfying criteria similar to those specified for verification. It is desirable that the prototype conditions, including external model forcings, for the validation simulation be significantly different from calibration and verification conditions. For the present study, the hydrodynamic model is calibrated for water surface elevation at a single station. The subsequent verification evaluates the performance of the model in simulating observed water surface elevation at stations not used for calibration, and in simulating observed salinity and horizontal velocities. Since the salinity observations were taken over an extended period of time characterized by

significant variations in freshwater inflow, the salinity verification also encompasses elements of validation.

Calibration of the hydrodynamic model involved adjustment of the open boundary water surface elevation forcing, the bottom boundary roughness, and local bathymetry. Open boundary tidal elevation, specified as a linear variation of the tidal constituent amplitudes and phases, was adjusted until predicted amplitudes and phases agreed with those obtained from analysis of NOAA tide gauge records at the Seattle Ferry Pier. Table 4-1 compares the predicted and observed amplitudes and phases for six constituents at the Seattle Ferry Pier. Amplitudes for all constituents agree within 1 cm, and phases agree within ten minutes.

Table 4-1. Seattle Ferry Pier Water Surface Elevation Harmonic Analysis

Symbol	Observed Amplitude cm	Predicted Amplitude cm	Amplitude Error cm	Observed Phase sec	Predicted Phase sec	Phase Error Sec (deg)
M2	111	112	-1	2,687	2,615	69 (1)
S2	27	27	0	18,941	18,871	70 (1)
N2	22	22	0	14,794	14,567	230 (2)
K1	73	74	-1	35,380	34,831	549 (2)
O1	37	38	-1	9,564	10,194	-630 (-2)
P1	26	26	0	40,147	40,117	30 (0)

4.4.1 Water Surface Elevation Verification

The model is verified with respect to water surface elevation by analysis of observed and model-predicted water surface elevation time series at three interior locations - Spokane Avenue Bridge, 16th Avenue Bridge, and the Duwamish Yacht Club. Quantitative verification can be made by using any of the procedures presented in Section 4-3. For tidal waters, least squares harmonic analysis is the most commonly used procedure (Oey et al. 1985, Galperin and Mellor 1990, Cheng et al. 1993, Vemulakonda and Scheffner 1994, Peene et al. 1998, Shen et al. 1998). Tables 4-2 through 4-3 compare predicted and observed tidal harmonic amplitudes and phases at the three interior locations. Amplitudes at the furthermost upstream station, Duwamish Yacht Club, agree within 10 percent, while phases agree to within approximately 15 minutes. Figures B-1 through B-

4, in Subappendix B, graphically compare observed and predicted water surface elevations at Duwamish Yacht Club over a 28-day period. Tables 4-5 and 4-6 compare absolute observed amplitude and phase error ranges for the four Elliott Bay and Duwamish Estuary stations with the corresponding error ranges for the six previously cited studies. The comparison indicates that errors in amplitude and phase for this study are within the range of those reported for other multidimensional hydrodynamic modeling studies.

Table 4-2. Spokane Avenue Bridge Water Surface Elevation Harmonic Analysis

Symbol	Observed Amplitude cm	Predicted Amplitude cm	Amplitude Error cm	Observed Phase sec	Predicted Phase sec	Phase Error sec (deg)
M2	108	112	-4	3,097	2,626	471 (4)
S2	23	27	-4	19,425	18,886	539 (4)
N2	20	22	-2	15,289	14,577	712 (6)
K1	72	74	-2	35,732	34,851	881 (4)
O1	36	38	-2	9,443	10,228	-785 (-3)
P1	23	26	-3	41,079	40,152	927 (4)

Table 4-3. 16th Avenue Bridge Water Surface Elevation Harmonic Analysis

Symbol	Observed Amplitude cm	Predicted Amplitude cm	Amplitude Error cm	Observed Phase sec	Predicted Phase sec	Phase Error Sec (deg)
M2	105	114	-9	4,630	2,677	1,953 (16)
S2	24	27	-3	20,582	18,955	1,627 (14)
N2	18	22	-4	16,666	14,650	2,016 (16)
K1	71	75	-4	36,762	34,893	1,869 (8)
O1	34	38	-4	12,326	10,289	2,037 (8)
P1	29	27	2	38,072	40,175	-2,103 (-9)

Table 4-4. Duwamish Yacht Club Water Surface Elevation Harmonic Analysis

Symbol	Observed Amplitude cm	Predicted Amplitude cm	Amplitude Error cm	Observed Phase sec	Predicted Phase sec	Phase Error Sec (deg)
M2	106	114	-8	2,684	2,716	-32 (0)
S2	24	27	-3	18,053	19,043	-990 (-8)
N2	19	22	-3	15,287	14,675	613 (5)
K1	72	74	-2	34,943	34,915	28 (0)
O1	35	37	-2	9,573	10,311	-738 (-3)
P1	25	25	0	39,436	40,272	-836 (-4)

Table 4-5. Water Surface Elevation Harmonic Amplitude Error Ranges from This Study and Results from Previously Published Studies[a]

Symbol	Present Model	Oey et al. (1985)	Galperin & Mellor (1990)	Cheng et al. (1993)	Vem. & Scheff. (1994)	Peene et al. (1998)	Shen et al. (1998)
M2	1-9	1-10	3-19	0-5	9-60	1-6	0-3
S2	0-4	1-3	1-5	0-3	1-10	0-2	0-2
N2	0-4	0-1	1-7		2-10	1-4	0-3
K1	1-4	0-1	0-1	0-2	1-5	0-3	0-3
O1	1-4	0-2	0-2	0-2	1-3	0-1	0-2
P1	0-2				0-1		

[a] Absolute minimum and maximum errors in centimeters

Table 4-6. Water Surface Elevation Harmonic Phase Error Ranges from This Study and Results from Previously Published Studies[a]

Symbol	Present Model	Oey et al. (1985)	Galperin & Mellor (1990)	Cheng et al. (1993)	Vem. & Scheff. (1994)	Peene et al. (1998)	Shen et al. (1998)
M2	1-16	0-1	0-7	0-9	1-19	1-20	0-24
S2	1-14	3-7	1-41	0-6	1-16	1-25	3-33
N2	2-16	1-5	1-60		2-23	0-18	3-46
K1	2-8	0-4	0-12	0-5	1-4	0-22	5-26
O1	2-8	0-2	0-16	0-5	7-42	0-8	3-29
P1	0-9				1-32		

[a] Absolute minimum and maximum errors in degrees

Observed and predicted water surface elevation time series can also be quantitatively compared using time series statistical error measures. Tables 4-7 and 4-8 show the results for various statistical error measures and regression analysis for the four Elliott Bay and Duwamish Estuary stations. For a modeling study of the Chesapeake Bay, Blumberg and Goodrich (1990) report RMS errors ranging from 9 to 30 cm and RSE ranging from 7 to 30 percent. For a study of Tampa Bay, Hess and Bosley (1992) report RMS errors ranging from 1 to 6 cm. It should be noted, however, that the tidal water surface range in Elliott Bay and the Duwamish Estuary is over twice that in the Chesapeake Bay and four times that in Tampa Bay. Hess and Bosley suggested normalizing RMS water surface elevation errors by the mean tide range determined from the observed time series to define a relative error measure RMS/R, which is also shown in Table 4-7. Normalized RMS errors for Tampa Bay ranged from 3 to 12 percent. Hess and Bosley also suggested the root mean square error analysis of corresponding observed high and low water surface elevations and their times of occurrence for the evaluation of water surface elevation prediction. This error and a mean time lag error are defined by:

$$RMS = \sqrt{\frac{1}{N}\sum_{n=1}^{N}\left(O^{(n)} - P^{(n')}\right)^2} \qquad \text{Equation 4-29}$$

$$ME = \frac{1}{N}\sum_{n=1}^{N}\left(O^{(n)} - P^{(n')}\right) \qquad \text{Equation 4-30}$$

Table 4-7. Time Series Error Analysis of Water Surface Elevation

Station	MAE (cm)	RMS (cm)	RMS/R (%)	RSE (%)
Ferry Pier	14	18	8	2
Spokane Ave	13	17	7	1
16th Ave	34	41	18	8
Yacht Club	11	13	6	1

MAE = mean absolute error

MAX = maximum absolute error

RMS = root mean square error

RSE = relative square error

Table 4-8. Correlation Analysis of Water Surface Elevations

Station	Intercept (cm)	Slope	Correlation Coefficient
Ferry Pier	0.02	0.992	0.984
Spokane Ave	0.16	0.968	0.989
16th Ave	0.41	0.905	0.922
Yacht Club	0.28	0.935	0.993

where *n'* denotes the corresponding model prediction not necessarily occurring at the same time as the observation. Table 4-9 presents an analysis of these errors for the four Elliott Bay and Duwamish Estuary stations. Hess and Bosley reported RMS high and low elevation errors ranging from 2 to 4 cm, mean phase lag errors ranging from 3 to 15 minutes, and RMS phase lag errors ranging from 20 to 50 minutes. The time series error analyses and correlation analysis for water surface elevation again show that error measures for this study are well within the range of those reported for previous studies.

Table 4-9. Error Analysis of High and Low Waters and Their Times of Occurrence

Station	RMS Elev (cm)	ME Phase (minutes)	RMS Phase (minutes)
Ferry Pier	14	2.8	20.0
Spokane Ave	15	5.5	19.6
16th Ave	27	69	73
Yacht Club	13	-4.2	22.5

An estimate of error inherent in water surface elevation observations can be made from the b_0 coefficient in the time-linear term in Equation 29. The b_0 term, determined by the least squares harmonic analysis, is designed to detect changes in sensor elevation, which could occur during servicing, or to detect slow drift in the analogue sensor device. Table 4-10 summarizes the time trend terms for the observed and model-predicted water surface elevations. The small trend of 0.023 cm/day for the NOAA observations at the Seattle Ferry Pier is consistent with trends in the model predicted water surface elevation at all four stations, which range from 0.012 to 0.024 cm/day. The time trends at the other three observational stations are 20 to 30 times larger, ranging from 0.52 to 0.75 cm/day. The corresponding errors introduced over a 1-month interval at these three stations range from 15 to 20 cm. These errors are similar in magnitude to absolute errors summarized in Tables 4-5, 4-7, and 4-9. This is consistent with the common sense rationale that observation-prediction errors should at best be within the range of errors inherent in making the observations.

Table 4-10. Potential Water Surface Elevation Error Due to Change in Sensor Elevation or Sensor Drift

Station	Observed Trend Rate (cm/day)	Predicted Trend Rate (cm/day)	28 Day Difference (cm)
Ferry Pier	0.023	0.012	0.31
Spokane Ave	-0.52	0.017	-15.1
16th Ave	0.75	0.022	20.4
Yacht Club	0.73	0.024	19.9

Although no specific error criteria are widely accepted for water surface elevation predictions, a number of guidelines have been established. The National Ocean Service guidelines for tidal prediction (Hess and Bosley 1992) are prediction of high and low water elevations to within 15 cm and prediction of times of high and low water to within 15 minutes. The accuracy of the model-predicted water surface elevations in this study is consistent with these guidelines. The U.S. EPA's (1990) technical guidance for calibration and verification of estuary models for wasteload allocation studies specifies relative errors of less than 30 percent and correlation coefficients greater than 0.94 for hydrodynamic model variables. All of the RSE and RMS/R errors for this study (Table 4-7) are well below the 30 per cent guideline. All of the correlation coefficients (Table 4-8) are also above the 0.94 guideline.

4.4.2 Velocity Verification

Acoustic Doppler current profiler (ADCP) data was available at six stations - ARC, EWW, SBW, and BOE located in the estuary, and Deep101, and Deep201 located in the bay. All stations except EWW had time series of sufficient length for harmonic analysis of five tidal constituents - M2, S2, N2, K1, and O1 - and mean velocity. Station EWW was analyzed only for short period mean velocity. The ADCP data correspond to ten bins in the water column and all or portions of the data in the near bottom and near surface bins, one and ten, may be unreliable. Model predictions correspond to the ten stretched model layers. No attempt was made to exactly align the two data sets vertically. Absolute and relative errors between observed and model-predicted tidal velocity harmonic constituents for stations ARC, SBW and BOE are summarized in Tables 4-11, 4-12, and 4-13, respectively. Complete results of the harmonic analysis of observed and predicted velocities are presented in Subappendix C. The fourth and fifth columns in the tables show the observed major velocity axis amplitude (MAJ OBS) and the corresponding absolute difference between the observed and predicted major axis amplitudes (MAJ REL). The sixth column shows the relative error between observed and predicted major axis amplitude, defined by:

$$MAJ\ REL = \frac{\left| MAJ_{obs} - MAJ_{prd} \right|}{MAJ_{obs}} \qquad \text{Equation 4-31}$$

Table 4-11. Absolute Differences Between Observed and Predicted Velocity Harmonic Components at Station ARC

LAY	HAR	MAJ OBJ cm/s	MAJ ERR cm/s	MAJ REL ERR	MIN ERR cm/s	DIR ERR deg	PHASE ERR sec	PHASE ERR deg
1	M2	4.49	1.35	0.30	0.01	17.99	2,726.	21.94
	S2	1.14	0.54	0.47	0.05	21.98	63.	0.52
	N2	0.84	0.20	0.24	0.12	16.56	3,533.	27.91
	K1	1.78	0.87	0.49	0.06	21.89	6,294	26.30
	O1	2.11	1.64	0.78	0.02	17.34	8,982.	34.79
2	M2	6.93	1.81	0.26	0.19	11.89	3,414.	27.48
	S2	1.77	0.95	0.54	0.11	12.24	798.	6.65
	N2	1.25	0.38	0.30	0.23	18.78	4,818.	38.06
	K1	2.66	1.18	0.44	0.01	18.14	8,014.	33.48
	O1	3.00	2.30	0.77	0.10	16.76	10,874.	42.12
3	M2	7.31	1.29	0.18	0.02	10.60	3,392.	27.31
	S2	1.83	0.63	0.34	0.00	0.54	2,465.	20.54
	N2	1.34	0.20	0.15	0.32	20.90	5,877.	46.43
	K1	2.78	0.90	0.32	0.04	18.50	9,064.	37.87
	O1	2.74	1.85	0.68	0.05	13.50	13,717.	53.13
4	M2	7.45	1.11	0.15	0.51	9.24	3,018.	24.29
	S2	1.73	0.27	0.16	0.24	1.76	2,762.	23.02
	N2	1.45	0.08	0.06	0.49	17.48	6,560.	51.82
	K1	2.61	0.46	0.18	0.19	18.24	7,842.	32.76
	O1	2.09	0.96	0.46	0.02	0.53	13,878.	53.75
5	M2	7.41	1.02	0.14	0.91	7.87	2,176.	17.52
	S2	1.81	0.16	0.09	0.52	4.40	1,713.	14.28
	N2	1.45	0.06	0.04	0.73	14.71	6,806.	53.76
	K1	2.44	0.29	0.12	0.49	11.29	3,783.	15.81
	O1	1.36	0.01	0.01	0.03	12.46	11,763.	45.56

Table 4-11. Absolute Differences Between Observed and Predicted Velocity Harmonic Components at Station ARC (continued)

LAY	HAR	MAJ OBJ cm/s	MAJ ERR cm/s	MAJ REL ERR	MIN ERR cm/s	DIR ERR deg	PHASE ERR sec	PHASE ERR deg
6	M2	7.35	0.59	0.08	1.04	8.48	2,943.	23.70
	S2	1.98	0.04	0.02	0.55	7.63	1,930.	16.08
	N2	1.40	0.06	0.04	0.98	3.31	10,298.	81.35
	K1	2.62	0.27	0.10	0.66	12.89	2,118.	8.85
	O1	0.98	0.43	0.44	0.12	22.48	17,197.	66.61
7	M2	7.93	0.29	0.04	1.16	7.16	2,803.	22.57
	S2	2.17	0.11	0.05	0.47	4.17	1,436.	11.97
	N2	1.40	0.02	0.01	1.12	25.60	14,737.	116.42
	K1	3.23	0.03	0.01	0.65	7.56	1,301.	5.43
	O1	0.86	0.32	0.37	0.22	59.32	21,000.	81.33
8	M2	9.73	0.49	0.05	0.67	11.92	3,134.	25.24
	S2	2.69	0.08	0.03	0.14	1.83	1,897.	15.81
	N2	1.92	0.08	0.04	1.14	49.78	20,643.	163.08
	K1	4.41	0.38	0.09	0.83	9.73	4,898.	20.46
	O1	1.26	0.01	0.01	0.26	69.86	17,939.	69.48
9	M2	13.35	2.52	0.19	0.02	9.35	3,082.	24.82
	S2	3.60	0.79	0.22	0.10	4.39	1,188.	9.90
	N2	1.83	0.25	0.14	1.51	2.95	10,508.	83.02
	K1	6.23	1.98	0.32	0.77	4.07	8,523.	35.61
	O1	1.96	1.57	0.80	0.04	12.87	3,316.	12.84
10	M2	14.53	0.27	0.02	0.06	4.39	5,271.	42.44
	S2	4.89	0.79	0.16	0.10	4.01	2,291.	19.09
	N2	3.09	0.94	0.30	0.69	3.61	11,454.	90.48
	K1	7.62	0.11	0.01	0.71	0.28	7,498.	31.33
	O1	1.81	0.94	0.52	0.43	6.71	1,255.	4.86

The seventh column shows the absolute difference between observed and predicted minor velocity axis amplitudes (MIN ERR). The eighth column shows the absolute difference between the observed and predicted major axis direction (MAJ DIRECT). The last two columns show the absolute difference, in seconds and degrees, between the observed and predicted major velocity axis phase (MAJ PHASE).

Tables 4-11 and 4-13 indicate that observed and predicted axis amplitudes, orientation, and phase agree moderately well for stations ARC and BOE. Vertical variations in M2 major axis velocity amplitude at ARC and BOE, Figures D-1 and D-9, in Subappendix D, show reasonable qualitative agreement. Table 4-12 indicates consistently larger errors between observed and predicted axis amplitudes, orientation and phase at station SBW. The vertical variation in M2 major axis velocity amplitude at SBW (Subappendix D) shows poor agreement between observations and predictions. Agreement between observed and predicted harmonic axis amplitudes, directions, and phases is also poor at stations Deep101 and Deep201. Current amplitudes are small at these deep-water stations, which are also close to the open boundary. The artificial nature of the open boundary conditions, which require that currents be oriented normal to the boundary, likely, causes the discrepancies. Extending the model domain across Puget Sound and using open boundaries aligned across the sound, north and south of Elliott Bay would likely improve model prediction of currents in the western regions of Elliott Bay.

Table 4-12. Absolute Differences Between Observed and Predicted Velocity Harmonic Components at Station SBW

LAY	HAR	MAJ OBS cm/s	MAJ ERR cm/s	MAJ REL ERR	MIN ERR cm/s	DIR ERR deg	PHASE ERR sec	PHASE ERR deg
1	M2	2.19	4.61	2.11	0.27	1.89	5,751.	46.31
	S2	0.94	0.66	0.70	0.01	1.53	7,093.	59.11
	N2	0.75	0.98	1.31	0.00	1.36	1,880.	14.85
	K1	0.95	0.57	0.60	0.05	1.25	7,613.	31.81
	O1	0.45	0.33	0.73	0.03	8.35	19,208.	74.39
2	M2	24.24	12.46	0.51	0.48	3.21	956.	7.70
	S2	6.93	4.47	0.65	0.08	3.90	2,453.	20.44
	N2	3.52	1.59	0.45	0.07	7.70	2,217.	17.51
	K1	7.35	4.84	0.66	0.27	5.54	1,222.	5.10
	O1	2.94	1.81	0.62	0.08	1.32	9,700.	37.57
3	M2	28.17	12.84	0.46	0.18	3.58	794.	6.39
	S2	7.87	4.57	0.58	0.15	4.19	1,591.	13.26

Table 4-12. Absolute Differences Between Observed and Predicted Velocity Harmonic Components at Station SBW (continued)

LAY	HAR	MAJ OBS cm/s	MAJ ERR cm/s	MAJ REL ERR	MIN ERR cm/s	DIR ERR deg	PHASE ERR sec	PHASE ERR deg
	N2	4.27	1.53	0.36	0.13	6.82	2,566.	20.27
	K1	8.42	4.85	0.58	0.29	5.17	1,219.	5.09
	O1	3.68	2.08	0.57	0.09	3.45	12,026.	46.58
4	M2	31.78	14.04	0.44	0.27	4.36	354.	2.85
	S2	8.62	4.38	0.51	0.02	4.21	622.	5.18
	N2	4.97	0.84	0.17	0.20	5.27	3,709.	29.30
	K1	9.57	5.37	0.56	0.24	5.64	1,477.	6.17
	O1	4.43	2.52	0.57	0.10	5.75	9,434.	36.54
5	M2	34.21	14.25	0.42	0.30	4.83	331.	2.66
	S2	9.11	4.07	0.45	0.06	4.89	61.	0.51
	N2	5.89	0.81	0.14	0.27	3.60	4,843.	38.26
	K1	10.02	5.23	0.52	0.05	7.15	1,742.	7.28
	O1	4.79	2.98	0.62	0.02	10.82	8,135.	31.51
6	M2	33.61	11.27	0.34	0.33	3.41	919.	7.40
	S2	9.27	3.45	0.37	0.07	3.87	251.	2.09
	N2	6.89	1.58	0.23	0.35	2.31	4,774.	37.72
	K1	10.06	4.21	0.42	0.33	6.17	2,443.	10.21
	O1	4.43	2.31	0.52	0.08	7.98	7,409.	28.70
7	M2	29.67	4.63	0.16	0.86	1.90	1,502.	12.10
	S2	9.31	2.83	0.30	0.05	2.07	624.	5.20
	N2	6.68	1.14	0.17	0.03	0.05	3,511.	27.73
	K1	10.04	2.50	0.25	0.55	2.91	1,987.	8.30
	O1	4.83	1.81	0.37	0.06	3.24	7,386.	28.61
8	M2	24.88	3.25	0.13	0.61	1.32	2,488.	20.03
	S2	8.65	1.48	0.17	0.06	3.41	1,249.	10.41

Table 4-12. Absolute Differences Between Observed and Predicted Velocity Harmonic Components at Station SBW (continued)

LAY	HAR	MAJ OBS cm/s	MAJ ERR cm/s	MAJ REL ERR	MIN ERR cm/s	DIR ERR deg	PHASE ERR sec	PHASE ERR deg
	N2	4.63	0.95	0.21	0.06	0.96	2,378.	18.78
	K1	9.26	0.51	0.06	0.43	0.82	1,300.	5.43
	O1	5.17	0.82	0.16	0.13	2.53	5,997.	23.23
9	M2	19.88	10.28	0.52	0.20	0.84	3,481.	28.03
	S2	6.78	0.69	0.10	0.05	1.03	1,843.	15.36
	N2	3.02	2.47	0.82	0.06	0.05	4,297.	33.94
	K1	7.81	4.07	0.52	0.10	2.66	3,244.	13.55
	O1	4.38	1.81	0.41	0.06	1.18	3,355.	12.99
10	M2	17.79	13.29	0.75	0.74	0.54	5,398.	43.46
	S2	5.29	2.51	0.47	0.34	5.29	2,592.	21.60
	N2	3.34	2.98	0.89	0.47	1.62	7,198.	56.87
	K1	6.94	6.46	0.93	0.48	4.29	9,832.	41.08
	O1	3.36	4.19	1.25	0.25	9.57	3,388.	13.12

Table 4-13. Absolute Differences Between Observed and Predicted Velocity Harmonic Components at Station BOE

LAY	HAR	MAJ OBS cm/s	MAJ ERR cm/s	MAJ REL ERR	MIN ERR cm/s	DIR ERR deg	PHASE ERR sec	PHASE ERR deg
1	M2	0.42	2.94	7.00	0.23	11.07	6,614.	53.25
	S2	0.10	0.82	8.20	0.03	6.61	14,068.	117.24
	N2	0.26	0.74	2.85	0.01	13.94	20.	0.16
	K1	0.21	0.90	4.29	0.09	5.18	58,473.	244.31
	O1	0.29	0.55	1.90	0.12	13.89	33,960.	131.53
2	M2	23.87	13.75	0.58	0.21	13.13	1,407.	11.33
	S2	4.88	3.13	0.64	0.05	14.82	3,028.	25.23

Table 4-13. Absolute Differences Between Observed and Predicted Velocity Harmonic Components at Station BOE (continued)

LAY	HAR	MAJ OBS cm/s	MAJ ERR cm/s	MAJ REL ERR	MIN ERR cm/s	DIR ERR deg	PHASE ERR sec	PHASE ERR deg
	N2	2.64	1.14	0.43	0.05	12.69	466.	3.68
	K1	7.53	4.14	0.55	0.05	13.95	3,368.	14.07
	O1	2.85	0.90	0.32	0.15	11.57	7,297.	28.26
3	M2	27.70	10.70	0.39	0.05	12.41	307.	2.47
	S2	5.33	1.87	0.35	0.04	12.88	417.	3.47
	N2	3.04	0.61	0.20	0.14	11.34	749.	5.92
	K1	8.44	1.72	0.20	0.25	11.61	2,118.	8.85
	O1	3.40	1.13	0.33	0.16	15.07	13,748.	53.25
4	M2	31.42	6.42	0.20	0.37	11.97	1,621.	13.05
	S2	5.69	1.06	0.19	0.19	12.77	1,089.	9.07
	N2	3.66	0.35	0.10	0.00	11.61	1,641.	12.96
	K1	9.89	1.48	0.15	0.38	10.35	3,032.	12.67
	O1	4.05	1.37	0.34	0.15	10.61	16,317.	63.20
5	M2	33.78	1.93	0.06	0.57	11.66	2,255.	18.16
	S2	6.20	0.15	0.02	0.17	12.39	2,053.	17.11
	N2	4.46	0.19	0.04	0.08	11.70	4,312.	34.06
	K1	11.32	1.01	0.09	0.12	12.38	1,305.	5.45
	O1	4.78	0.05	0.01	0.27	10.45	11,974.	46.37
6	M2	32.84	2.68	0.08	0.68	9.54	2,009.	16.17
	S2	6.39	1.36	0.21	0.20	8.95	1,765.	14.70
	N2	5.29	0.58	0.11	0.19	8.74	6,002.	47.41
	K1	11.43	0.47	0.04	0.02	11.28	1,132.	4.73
	O1	5.12	0.31	0.06	0.65	9.16	6,548.	25.36
7	M2	28.25	7.19	0.25	0.32	8.72	2,072.	16.68
	S2	7.10	1.35	0.19	0.05	5.02	1,744.	14.54

Table 4-13. Absolute Differences Between Observed and Predicted Velocity Harmonic Components at Station BOE (continued)

LAY	HAR	MAJ OBS cm/s	MAJ ERR cm/s	MAJ REL ERR	MIN ERR cm/s	DIR ERR deg	PHASE ERR sec	PHASE ERR deg
	N2	4.87	1.87	0.38	0.20	8.90	5,512.	43.55
	K1	10.65	2.35	0.22	0.09	8.57	2,759.	11.53
	O1	4.82	1.01	0.21	0.46	6.14	1,948.	7.54
8	M2	23.52	9.01	0.38	0.00	8.52	2,936.	23.64
	S2	7.62	0.31	0.04	0.08	7.33	2,076.	17.30
	N2	4.41	2.87	0.65	0.02	7.80	3,741.	29.56
	K1	8.64	4.31	0.50	0.22	8.52	3,784.	15.81
	O1	3.19	3.40	1.07	0.28	5.03	4,520.	17.51
9	M2	19.41	9.68	0.50	0.02	8.00	3,113.	25.06
	S2	6.63	0.47	0.07	0.01	9.20	1,990.	16.59
	N2	3.68	3.55	0.96	0.07	7.33	3,890.	30.73
	K1	7.18	4.25	0.59	0.19	10.21	4,651.	19.43
	O1	2.58	3.33	1.29	0.19	4.72	7,524.	29.14
10	M2	16.48	11.03	0.67	0.06	10.64	3,056.	24.60
	S2	6.37	0.22	0.03	0.18	11.21	304.	2.53
	N2	2.53	4.05	1.60	0.07	2.91	5,071.	40.06
	K1	6.21	3.68	0.59	0.39	16.75	6,786.	28.35
	O1	1.91	2.75	1.44	0.77	2.56	5,393.	20.89

Table 4-14 summarizes the range of major velocity axis relative errors and the mean relative errors for all three stations by constituent. Tables 4-15 and 4-16 summarize the range of major velocity direction and phase errors and mean errors by constituent for all three stations. Harmonic analysis results from layers one and ten were not used in determining ranges and means since near-bottom and near-surface ADCP data are considered unreliable. Tables 4-17 and 4-18 compare the major axis relative error and major axis phase error ranges for this study with results from five previously published studies (Oey et al. 1985, Galperin and Mellor 1990, Cheng et al. 1993, Vemulakonda and Scheffner 1994, Peene et al. 1998) that used velocity harmonic analysis for comparing observations with model predictions. The error ranges for this study are reasonably consistent with those reported by the previous studies. No specific error criteria are

widely accepted for tidal velocity predictions. The U.S. EPA's (1990) technical guidance for calibration and verification of estuary models for wasteload allocation studies specifies relative errors of less than 30 percent for hydrodynamic model variables. As indicated by Table 4-14, the major velocity axis relative errors for four of the five constituents fall below or near the 30 percent guideline. The higher relative error for the K1 constituent is tolerable since it has the lowest major axis amplitudes of the five constituents analyzed. When phase errors (Table 4-16) are normalized by 180 degrees, three constituents, including the dominant M2, have relative phase errors of less than 10 percent, with the remaining two constituents having relative phase errors of less than 25 percent.

Table 4-14. Summary of Velocity Major Axis Relative Amplitude Errors

Symbol	Min Error	Max Error	Mean Error
M2	0.04	0.58	0.27
S2	0.02	0.65	0.26
N2	0.01	0.96	0.26
K1	0.01	0.66	0.31
O1	0.01	1.29	0.46

Table 4-15. Summary of Velocity Major Axis Direction Errors

Symbol	Min Error degrees	Max Error degrees	Mean Error degrees
M2	0.84	13.13	6.77
S2	0.54	14.82	6.16
N2	0.05	49.78	10.85
K1	0.82	18.50	9.31
O1	0.53	69.86	13.20

Table 4-16. Summary of Velocity Major Axis Phase Errors

Symbol	Min Error degrees	Max Error degrees	Mean Error
M2	2.47	28.03	16.94
S2	0.51	25.23	12.86
N2	3.68	163.08	44.39
K1	4.73	37.87	14.33
O1	7.54	81.33	39.22

Table 4-17. Range of Velocity Harmonic Major Axis Amplitude Relative Errors from this Study and Results from Previously Published Studies [a]

Symbol	Present Model	Oey et al. (1985)	Galperin & Mellor (1990)	Cheng et al. (1993)	Vem. & Scheff. (1994)	Peene et al. (1998)
M2	0.04 0.58	0.0 0.43	0.03 0.53	0.0 0.22	0.58 1.56	0.03 0.25
S2	0.02 0.65	0.08 0.53	0.11 0.54		0.7 1.96	0.06 0.21
N2	0.01 0.96	0.02 0.67	0.12 0.53		0.4 2.16	0.0 0.33
K1	0.01 0.66	0.18 0.62	0.21 0.51	0.02 0.36	0.17 2.0	0.4 0.54
O1	0.01 1.29	0.0 0.58	0.28 0.95		0.06 4.0	0.22 0.50

[a] Absolute difference/observed

Table 4-18. Range of Velocity Harmonic Major Axis Phase Errors from This Study and Results from Previously Published Studies

Symbol	Present Model	Oey, et al. (1985)	Galperin & Mellor (1990)	Cheng, et al. (1993)	Vem. & Scheff. (1994)	Peene, et al. (1998)
M2	2-28	0-14	1-10	2-16	10-31	3-21
S2	1-25	1-57	9-52		19-40	3-11
N2	4-90	2-23	1-20		1-22	3-12
K1	5-38	2-48	3-40	1-21	1-24	2-23
O1	8-81	3-60	11-40		7-203	2-28

[a] Absolute difference, degrees

Highly accurate agreement between point observations of tidal velocities and numerical model predictions is difficult to achieve for a number of reasons. In tidal channels like the Duwamish, considerable variation in velocity amplitude and phase can occur in the lateral or across-channel direction due to variations in bottom bathymetry. Velocities predicted by a model represent spatial averages over model grid cells. In the limit of a model grid fine enough to represent bathymetric variations, differences in predicted and observed velocities can arise due to differences in actual bathymetry and bathymetric data interpolated to the fine grid. Sparse bathymetric data or a coarser grid resolution introduce another source of bathymetric error due to the smoothing inherent in interpolating bathymetry to model grid cells. In this case errors arise due to the comparison of point observation with spatially averaged model predictions. For the present study, the lateral or across-channel grid cell width is approximately 100 m at station ARC and 50 m at stations SBW and BOE. The comparison of a point velocity with a spatially averaged model velocity has an inherent uncertainty in bathymetry equivalent to a lateral position uncertainty of one-half of a cell width. A relative lateral uncertainty can be estimated by dividing one-half by the number of cells resolving the channel in the lateral direction. Since two cells are used in the lateral direction at ARC and three cells are used at SBW and BOE, the corresponding relative uncertainties in lateral position are one-fourth and one-sixth.

Friedrichs and Hamrick (1998) investigated the effect of lateral depth variations on the cross-sectional distribution of longitudinal tidal and residual velocity. The essential results of their analysis are presented in Subappendix E for the idealized case of a triangular cross section. The analysis can be used to translate the 16 to 25 per cent lateral position or bathymetric uncertainty into ranges of errors inherent in the comparison of observed point velocities with model predictions influenced by spatial averaging and bathymetric data uncertainty. The analysis shows that lateral variability is controlled by a parameter, δ_o:

$$\delta_o = \sqrt{\frac{\omega h_o^2}{2A_v}} \qquad \text{Equation 4-32}$$

where ω is the tidal constituent frequency, h_o is the maximum depth, and A_v is the vertical eddy viscosity. Figures E-1 and E-2 show vertical profiles of current amplitude ratios and phase lags for δ_o equal to one at the deepest lateral position and a lateral position having a depth of 80 percent of the deepest position and representing a 20 percent uncertainty in lateral position. Figures E-3 and E-4 show similar profiles for δ_o equal to two. Note a doubling of δ_o is equivalent to doubling the depth or decreasing the vertical eddy viscosity by a factor of four. The value of δ_o equal to one produces vertical M2 phase lags on the order of those observed at station SBW, while vertical M2 phase lags observed at station ARC are better represented by the value of two. Observed vertical M2 phase lags at station BOE are intermediate, but somewhat closer to δ_o equal to one. Table E-1 summarizes a number of error measures obtained from the analysis for δ_o equal to one and two. For δ_o equal to one, the 20 percent relative change in lateral position or depth results in depth averaged absolute differences in velocity amplitude on the order of 18 percent of the surface velocity amplitude, depth averaged relative differences in velocity amplitude on the order of 25 percent and errors in phase on the order of 10 degrees. For δ_o equal to two, the 20 percent relative change in lateral position or depth results in depth-averaged absolute changes in velocity amplitude on the order of 5 percent of the surface velocity magnitude, depth-average relative changes in velocity amplitude on the order of 7 percent, and depth-averaged errors in phase on the order of 7 degrees. For the ARC station (Table 4-11) the depth-averaged relative error in M2 major axis amplitude (MAJ REL ERR) is 14 percent and less than the 25 percent estimated due to lateral position or bathymetric uncertainty. However, major axis phase errors are typically on the order of 25 degrees, larger than the 10 degrees estimated. For the SBW station (Table 4-12) the depth-averaged relative error in M2 major axis amplitude (MAJ REL ERR) is 37 percent, which is much larger than the 7 percent estimated due to lateral position or bathymetric uncertainty. At SBW the depth-averaged major axis M2 phase error is 11 degrees and compares reasonably with the estimated 7-degree error. For the BOE station (Table 4-13) the depth-averaged relative error in M2 major axis amplitude (MAJ REL ERR) is 31 percent, which is above the estimated 7 to 25 percent range due to lateral position or bathymetric uncertainty. The depth-averaged major axis M2 phase error at BOE is 16 degrees compared with the estimated range of 7 to 10 degrees. The primary conclusion to be drawn from the preceding discussion is that bathymetric or lateral position uncertainty associated with both bathymetric data and the spatial smoothing inherent in model-predicted velocities can account for a significant portion of the amplitude and phase errors between observed and model-predicted tidal velocities.

Observed and predicted mean or residual longitudinal velocities were determined at stations ARC, SBW, and BOE corresponding to the time interval of the harmonic analyses. Figures D-2, D-8, and D-10 show vertical profiles of the mean longitudinal velocities at these three stations. Agreement between observed and mean velocities over the upper portion of the water column is moderately good at all three stations. At station ARC in the west Harbor Island waterway, the agreement in the lower portion of the water

column is quite poor. Figures D-3 and D-4 show shorter averaging period mean velocity profiles at station ARC. These profiles also exhibit poor agreement over the lower portion of the water column. Figures D-5 and D-6 show mean vertical velocity profiles at station EWW, in the east Harbor Island waterway, corresponding to averaging periods approximately the same as those in Figures D-3 and D-4. Model predictions in the east waterway show significant landward flow over the lower portion of the water column and corresponding under-prediction of seaward flow in the upper portion of the water column. In light of the under-prediction of landward flow in the west waterway, the over-prediction in the east waterway points to a significant, but possibly compensating, error in the distribution of residual flow between the two Harbor Island waterways. As will be subsequently shown, density-driven mean or residual flow is extremely sensitive to bathymetric variability and, in turn, to errors or uncertainty in bathymetric data used by the model.

The introduction of an inherent error in comparing point observations and model predictions of mean or residual velocities follows the same line of reasoning as that presented for tidal velocities. However, since residual velocities are primarily driven by horizontal density gradients, they exhibit a greater level of variability with respect to bathymetric variations. Hamrick (1979) and Friedrichs and Hamrick (1966) investigated the effect of lateral bathymetric variations on the cross-sectional distribution of density-gradient driven longitudinal residual velocity in estuarine channels. An analysis of lateral residual velocity variability in a triangular cross section channel, based on Hamrick (1979) and Friedrichs and Hamrick (1966), is presented in Subappendix E. The essence of the analysis is presented in Figure 4-4 (also see Figure E-5), which shows the vertical distribution of residual velocity at the deepest point in the cross section (solid line) and a nearby point having a depth of 90 percent of that in the deepest point (dashed line). The analytical solution parameters upon which the profiles are based were estimated such that the deepest section profile approximates reasonably well the observed profiles at stations SBW and BOE (Figures D-8 and D-10, respectively).

The immediate conclusion from Figure 4-4 is that a slight change in point depth leads to a significant change in the vertical residual velocity profile, with the net landward near-bottom transport being almost eliminated at the slightly shallower point. Based on this analysis, it is very likely that disagreement between observed and model-predicted mean velocities is due to actual bathymetric data error or bathymetric smoothing inherent in the model grid. It is anticipated that improved prediction of mean velocities would result from the use of a combination of more accurate bathymetric data and grid refinement, (i.e., doubling the number of cells in the lateral direction in the Harbor Island and Duwamish channels).

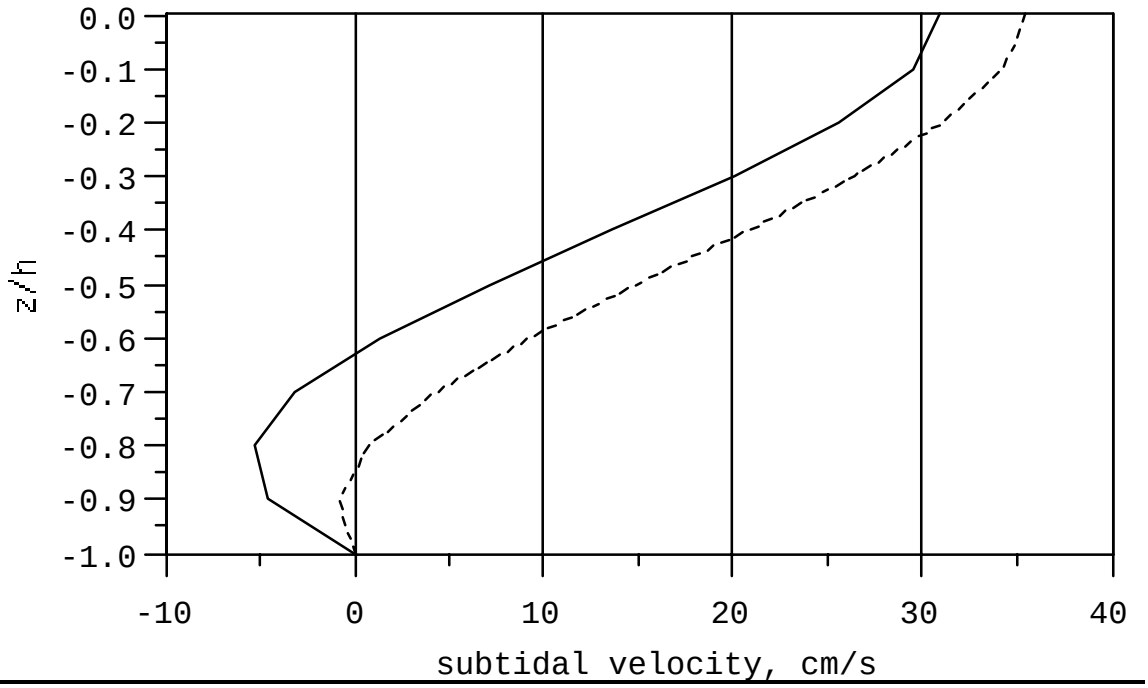

Figure 4-4. Vertical Profiles of the Residual Longitudinal Velocity for a Triangular Cross Section (solid line corresponds to lateral position of maximum depth, dashed line corresponds to lateral position having a local depth of 90% of maximum depth)

4.4.3 Salinity Verification

The ability of a numerical hydrodynamic model to predict the transient distribution of salinity in an estuary is viewed as the most important measure of the model's verification, if the ultimate use of the model is prediction of the transport and fate of dissolved contaminants. Since the salinity distribution is a direct consequence of physical transport by advection and turbulent diffusion, salinity verification substantiates advective and diffusive transport verification at a grid or flux scale rather than at the point scale addressed in the preceding sections. An acceptable salinity verification supports the accuracy of grid scale transport even under conditions of marginal verification of the model's ability to predict velocity at specific observation points. Observational salinity data for model verification was provided at three stations — S in the west Harbor Island waterway, B near the 16th Ave Bridge, and D at the Duwamish Yacht Club. Near-bottom, mid-depth, and near-surface observational time series were available at Stations S and B, while near-bottom and near-surface series were available at Station D. Observational periods include periods of gradual river flow variability and high-flow events. Observations and corresponding model predictions were divided into 23 pairs of hourly time series for analysis. Tables 4-19 through 4-21 list the 23 time series pairs by station, water column level (b-bottom, m-mid-depth, s-surface), and observation period

(elapsed days from midnight January 1, 1996). Instantaneous and low-pass filtered plots of the 23 time series pairs are presented in Subappendix F.

Table 4-19. Error Analysis of Observed and Predicted Salinity

STA[a,b]	MDL	Beg	End	MEAN	ME	RME	MAE	RMA	MAX	RMS	RSE
s_b	1/2	295	335	30.58	-0.24	-0.01	0.32	0.01	1.94	0.40	0.95
s_b	1/2	340	390	29.84	-0.59	-0.02	0.64	0.02	4.48	0.84	0.60
s_b	1/2	424	449	31.82	0.96	0.03	0.96	0.03	1.51	1.02	0.96
s_b	1/2	450	475	31.16	0.29	0.01	0.49	0.02	2.13	0.57	0.91
s_m	4/5	340	375	29.59	-0.54	-0.02	0.82	0.03	20.47	2.13	0.64
s_m	4/5	425	455	30.35	0.38	0.01	1.13	0.04	37.33	2.12	0.73
s_s	9/10	295	320	12.90	-2.30	-0.18	2.88	0.22	9.99	3.55	0.38
s_s	9/10	323	348	10.01	-2.79	-0.28	3.18	0.32	11.40	3.86	0.45
s_s	9/10	354	394	7.92	-3.57	-0.45	3.77	0.48	11.58	4.47	0.57
s_s	9/10	425	475	10.95	-0.75	-0.07	2.48	0.23	9.71	3.12	0.35
b_b	1/2	240	260	27.24	-0.68	-0.02	0.91	0.03	4.75	1.38	1.04
b_b	1/2	300	330	27.80	-0.19	-0.01	1.12	0.04	5.12	1.39	0.86
b_m	1/2	240	260	27.95	-1.12	-0.04	1.29	0.05	4.32	1.48	0.76
b_m	1/2	300	330	27.87	-0.15	-0.01	1.13	0.04	5.23	1.43	0.84
b_m	1/2	335	365	27.69	0.41	0.01	1.28	0.05	8.64	1.74	0.86
b_s	9/10	280	330	4.91	0.00	0.00	1.73	0.35	10.39	2.44	0.13
b_s	9/10	397	422	0.98	0.02	0.02	0.83	0.85	4.81	1.11	0.84
d_b	1/2	295	325	19.02	-2.37	-0.12	7.84	0.41	25.82	10.38	0.60
d_b	1/2	340	375	15.04	-0.82	-0.05	6.05	0.40	27.38	8.48	0.30
d_b	1/2	457	477	12.69	-4.99	-0.39	10.61	0.84	22.74	12.01	0.74
d_s	9/10	240	260	14.53	-0.16	-0.01	3.26	0.22	14.58	4.07	0.47
d_s	9/10	340	375	0.82	-0.30	-0.36	0.88	1.06	5.15	1.24	0.89
d_s	9/10	457	477	0.96	0.30	0.31	0.71	0.75	3.17	0.99	0.77
avg				18.81	-0.83	-0.07	2.36	0.28	10.98	3.05	0.68

[a] b_=16th ave bridge, d_=duwamish Yacht club, s_=spokane avenue bridge

[b] _b=bottom _m=mid-depth _s=surface

ME=mean error, RME=relative mean error, MAE=mean absolute error, RMA=relative mean absolute error, MAX=maximum absolute error, RMS=relative mean error, RSE=relative square error

Table 4-20. Error Analysis of Low-Pass Filtered Observed and Predicted Salinity

STA[a,b]	MDL	Beg	End	MEAN	ME	RME	MAE	RMA	MAX	RMS	RSE
s_b	1/2	295	335	30.43	-0.24	-0.01	0.30	0.01	0.88	0.34	0.02
s_b	1/2	340	390	29.74	-0.59	-0.02	0.62	0.02	1.83	0.79	0.15
s_b	1/2	424	449	31.60	0.96	0.03	0.96	0.03	1.38	1.00	0.13
s_b	1/2	450	475	30.94	0.29	0.01	0.43	0.01	0.85	0.47	0.03
s_m	4/5	340	375	29.47	-0.52	-0.02	0.61	0.02	3.49	0.92	0.13
s_m	4/5	425	455	30.16	0.38	0.01	0.60	0.02	1.89	0.75	0.09
s_s	9/10	295	320	12.80	-2.28	-0.18	2.29	0.18	5.81	2.77	0.33
s_s	9/10	323	348	9.94	-2.76	-0.28	2.76	0.28	6.99	3.03	0.37
s_s	9/10	354	394	7.85	-3.57	-0.45	3.57	0.45	8.28	3.88	0.55
s_s	9/10	425	475	10.93	-0.74	-0.07	1.61	0.15	4.45	1.94	0.21
b_b	1/2	240	260	27.03	-0.67	-0.02	0.81	0.03	2.84	1.28	0.21
b_b	1/2	300	330	27.64	-0.18	-0.01	0.48	0.02	1.32	0.58	0.07
b_m	1/2	240	260	27.73	-1.12	-0.04	1.24	0.04	2.25	1.37	0.20
b_m	1/2	300	330	27.71	-0.14	-0.01	0.43	0.02	1.24	0.52	0.05
b_m	1/2	335	365	27.52	0.40	0.01	0.67	0.02	2.12	0.86	0.14
b_s	9/10	280	330	4.90	0.00	0.00	0.83	0.17	4.71	1.18	0.04
b_s	9/10	397	422	0.97	0.02	0.02	0.49	0.51	1.28	0.58	0.44
d_b	1/2	295	325	18.91	-2.33	-0.12	3.13	0.17	9.87	3.73	0.51
d_b	1/2	340	375	14.96	-0.82	-0.05	2.22	0.15	5.90	2.66	0.08
d_b	1/2	457	477	12.59	-5.00	-0.40	5.00	0.40	10.51	5.56	0.63
d_s	9/10	240	260	14.40	-0.18	-0.01	1.50	0.10	4.06	1.71	0.41
d_s	9/10	340	375	0.82	-0.29	-0.36	0.34	0.41	1.27	0.45	0.40
d_s	9/10	457	477	0.95	0.30	0.31	0.32	0.33	0.76	0.36	0.26
Avg				18.81	-0.83	-0.07	1.36	0.15	3.65	1.60	0.24

[a] b_=16th ave bridge d_=duwamish yacht club s_=spokane avenue bridge

[b] _b=bottom _m=mid-depth _s=surface

ME=mean error. RME=relative mean error, MAE=mean absolute error, RMA=relative mean absolute error, MAX=maximum absolute error, RMS=relative mean standard error, RSE=relative square error

Table 4-21. Regression Analysis of Low-Pass Filtered Observed and Predicted Salinity

Station	MDL	BEG	END	ALPHA	BETA	R	R2
s_b	1/2	295	335	0.509	0.975	0.988	0.977
s_b	1/2	340	390	3.650	0.860	0.929	0.864
s_b	1/2	424	449	-0.648	1.052	0.990	0.979
s_b	1/2	450	475	-0.957	1.041	0.982	0.964
s_m	4/5	340	375	-3.038	1.084	0.922	0.851
s_m	4/5	425	455	0.114	1.009	0.936	0.875
s_s	9/10	295	320	-6.164	1.258	0.910	0.828
s_s	9/10	323	348	-3.208	1.035	0.915	0.837
s_s	9/10	354	394	-1.521	0.821	0.842	0.708
s_s	9/10	425	475	-3.070	1.200	0.863	0.744
b_b	1/2	240	260	5.066	0.793	0.839	0.703
b_b	1/2	300	330	2.925	0.888	0.941	0.886
b_m	1/2	240	260	3.357	0.845	0.926	0.857
b_m	1/2	300	330	2.369	0.910	0.951	0.905
b_m	1/2	335	365	4.941	0.833	0.887	0.787
b_s	9/10	280	330	-0.678	1.138	0.976	0.953
b_s	9/10	397	422	0.190	0.820	0.594	0.353
d_b	1/2	295	325	9.990	0.420	0.691	0.478
d_b	1/2	340	375	0.765	0.900	0.928	0.861
d_b	1/2	457	477	-2.127	0.837	0.761	0.579
d_s	9/10	240	260	6.042	0.574	0.595	0.354
d_s	9/10	340	375	-0.215	0.929	0.743	0.552
d_s	9/10	457	477	0.429	0.797	0.908	0.825

ALPHA-intercept, BETA-slope, R-regression coefficient, R2-regression coefficient squared.

The 23 time series pairs were analyzed to determine ME, RME, MAE, RMA, MAX, RMS, and RSE with the results summarized in Table 4-19. It should be noted that relative errors at b_s for days 397 to 422 and relative errors for station d_s for days 340 to 375 and 457 to 477 should be disregarded since mean salinities are less than one. Station B, near the 16th Avenue Bridge consistently has the lowest error measures at all three water column positions. Low error measures are also observed at the S bottom station in the west Harbor Island waterway. Highest error measures occur at the S surface station and at all three D stations. High error at the S surface station could be associated with error in distribution of mean flow between the west and east Harbor Island waterways. Station D, near the Duwamish Yacht Club, exhibits the highest error measures, with the bottom location errors being particularly high. Time series plots for the D bottom station, Figures F-18 through F-20 in Subappendix F, indicate that its location coincides with the toe of the saline wedge, with the large observed salinity variations corresponding to advection of the wedge toe back and forth across the sensor location.

The RMS is generally judged to be the most stringent error measure. Blumberg and Goodrich (1990) used RMS salinity errors to judge the prediction skill of a coarse-grid three-dimensional model of Chesapeake Bay. They reported RMS errors ranging from 1.14 to 1.37 psu over a one-month observational period at five locations in Chesapeake Bay. Since their observations corresponded to a low-flow period having little salinity variability, it is appropriate to compare their errors with only the S and B bottom and mid-depth stations, which exhibit similar variability. For the S and B bottom and mid-depth stations, the range of RMS errors is 0.4 to 2.12 psu and the mean RMS error is 1.32 psu. The U.S. EPA's (1990) technical guidance for calibration and verification of estuary models for wasteload allocation studies specifies relative mean absolute errors (RMA) of less than 25 percent for transport. The average RMA error for all 23 observational periods is 28 percent. This error is reduced to 18 percent when the three observational periods having mean salinities less than one are appropriately excluded.

Two primary non-sensor sources of error can be identified for model-predicted salinity. The first source is amplitude and phase error due to errors in model-predicted tidal velocities. The second source of error is potential errors or uncertainty in freshwater inflow. Both error sources lead to errors in model-predicted salinity at tidal frequencies, while uncertainty in freshwater discharge is the primary source of model-predicted salinity errors at subtidal frequencies. These error sources are readily illustrated using results from Hamrick (1990), who developed an analytical framework for analyzing mass transport mechanisms in strongly stratified estuaries. Hamrick (1990) showed that the instantaneous salinity is approximated by:

$$s = s_{hp} + s_{lp} \qquad \text{Equation 4-33}$$

the sum of a high-pass or tidal frequency component and a low-pass or slowly varying residual component. The high-pass component is approximately governed by:

$$\partial_t s_{hp} + \vec{u}_{hp} \nabla s_{lp} = 0 \qquad \text{Equation 4-34}$$

the first equation in a perturbation expansion leading to a closed three-dimensional transport equation for the low-pass or residual salinity. Equation 4-34 clearly indicates that amplitude and phase errors in model-predicted tidal velocities lead to corresponding errors in tidal frequency salinity. Equation 4-34 also indicates that errors in the residual salinity distribution influence tidal frequency salinity. The primary external driving mechanism determining the residual or low-pass salinity is the salinity open boundary condition and the net buoyancy or freshwater input to the estuary. Hamrick (1979) showed that the longitudinal distribution of residual salinity in moderately to strongly stratified simple channel estuaries can be characterized by a length of salinity intrusion, L_{IE}. The length of salinity intrusion, and in turn the longitudinal gradient of residual salinity, was shown to be inversely proportional to the freshwater discharge at the head of the estuary:

$$\frac{L_I}{L_{Io}} = \frac{Q_{fo}}{Q_f} \qquad \text{Equation 4-35}$$

Equation 4-35 indicates that a 10 to 20 percent error or uncertainty in freshwater inflow leads to a corresponding error in the length of salinity intrusion and a similar error in the longitudinal salinity gradient. This is particularly noteworthy for Station D, in that errors in freshwater inflow directly translate into significant changes in the mean position of the salt wedge toe observed to be in the vicinity of this station.

To isolate the two primary sources of error in model-predicted salinity, the observed and model-predicted salinities were filtered to partition them into high-pass and low-pass components. Time series plots of low-pass filtered observed and predicted salinity are shown in Subappendix G. The 23 low-pass filtered time series pairs were analyzed to determine ME, RME, MAE, RMA, MAX, RMS, and RSE, with the results summarized in Table 4-20. It should be noted that relative errors at b_s for days 397 to 422 and relative errors for station d_s for days 340 to 375 and 457 to 477 should be disregarded since mean salinities are less than one. As would be expected, error measures from the comparison of low pass filtered salinities are lower than those for instantaneous salinity. The average RMS error over all 23 series pairs is 1.6 psu. This compares favorably with the RMS low-pass salinity error ranging from 1.06 to 1.35 psu reported by Blumberg and Goodrich (1990) for conditions having much less variability. The average of the relative mean absolute (RMA) errors is 15 percent and reduces to 11 percent when the three cases having mean salinities less than one are eliminated. These relative errors are considerably lower than the 25 percent relative error guideline specified in the U.S. EPA's (1990) technical guidance for calibration and verification of estuary models for wasteload allocation. Linear regression analysis was also performed on the low-pass filtered time series pairs, with the results shown in Table 4-21. The null hypothesis for the slope parameter, beta, is a value of unity. All but three slopes fall within the range between 0.8 and 1.2. Fourteen of the regression coefficients were greater than 0.90, indicating a high degree of correlation between model predictions and corresponding field observations. The U.S. EPA's (1990) technical guidance for calibration and verification of estuary models for wasteload allocation studies specifies regression

coefficients greater than 0.84 for transport verification. Only 5 of the 23 regression coefficients in Table 4-21 fall below this guideline.

Visual comparison of low-pass filtered observed and predicted salinities, Subappendix G, also allows judgments of the model's ability to predict event responses to freshwater inflow. The S bottom station (Figures G-1 through G-4) generally responds to the open boundary condition. The drop in model-predicted salinity at this station just before day 375 (Figure G-2) is likely a response to the high river inflow event near day 370. The mid-depth S station (Figures G-5 and G-6) also shows responses to high freshwater inflow events near days 370 and 445. At the surface S station (Figures G-7 through G-10) the model predictions tend to be greater than observations. The model predictions do respond to high freshwater inflow events near days 332, 365, and 345. Low-pass filtered predicted and observed salinities at the bottom and mid-depth B stations (Figures G-11 through G-15) agree quite well. Model-predicted mid-depth salinities at the B mid-depth station prior to day 255 suggest that the constant river discharge used by the model prior to day 290 could be in error. For the B surface station, agreement between days 280 and 330 is quite good (Figure G-16). Visual agreement between days 395 and 425 appears poor (Figure G-17) until note is made that both observed and predicted salinities are below 2 psu. Figures G-18 through G-20 show comparisons at the D bottom station. The freshwater inflow event after day 365 and the subsequent rebound is well predicted by the model. Between days 455 and 477, the model's over-prediction of the bottom salinity is likely due to errors in exact prediction of the salt wedge toe location. Figures G-21 through G-23 show comparisons at the D surface station. Agreement over the high-salinity period between days 240 and 260 is reasonable. The agreement over the other two intervals is reasonable, considering that salinities over these intervals are below two psu.

To visually evaluate the correspondence between observed and predicted salinity variability in the tidal frequency band, power spectral density functions were computed for the 23 pairs of high-pass filtered series. The comparison of using power spectral density functions effectively eliminated observation-prediction errors associated with tidal velocity phase errors. Plots of the salinity spectral density functions are shown in Subappendix H. The frequency distribution of observed and predicted spectral amplitude is extremely consistent between the observations and predictions.

4.5 Summary, Conclusions and Recommendations

This report documents the calibration and verification of the EFDC model to simulate circulation and salinity in Elliott Bay and the Duwamish River. Verification of model-predicted water surface elevation, tidal and mean velocities and salinity was quantified using harmonic, time series error, and regression analyses. Water surface elevation and salinity verification is judged to be acceptable, with error measures well within a number of guidelines including the U.S. EPA's (1990) technical guidance for calibration and verification of estuary models for wasteload allocation. Error measures for water surface elevation and salinity were also consistent with those of a number of previous studies reported in the literature. Velocity verification for tidal velocity is judged to be

marginally acceptable based on harmonic analysis. Relative tidal velocity major axis amplitude errors were within the EPA technical guidance of 30 percent for four of the five constituents and consistent with results published for previous studies. A number of arguments and a theoretical analysis were presented to define errors inherent in comparing point velocity observations with spatially average model predictions. Model predictions of mean velocity were shown to qualitatively agree with observations in the upper portions of the water column. Disagreement in the lower portions of the water column was shown to be due to bathymetric smoothing inherent in the model's spatial resolution or errors in bathymetric data.

The primary purpose of the hydrodynamic model is to provide physical transport representation for simulating the transport and fate of sediment and toxic contaminants in Elliott Bay and the Duwamish River on time scales ranging from hours to years. The quantitative and qualitative comparisons of observed and predicted salinity transport presented herein substantiate the model's ability to predict transport processes at the spatial grid scale at tidal, seasonal, and annual time scales and to respond correctly to high freshwater inflow events.

5. WATER QUALITY MASS CALIBRATION

The sediment and chemical mass calibrations compared predicted mass concentrations to mass concentrations observed in the field. Four calibrations measures where used, three statistical measures and visual inspection. The statistics provide a quantitative measure and visual inspection provides a qualitative measure. Statistical measures used were:

1. **Slope:** The slope of a line linearly regressed between the points of predicted and observed concentrations. A slope of "one" implies the model mass approaches observed mass.

2. **Coefficient of Determination (COD)**: The square of the linear regression coefficient. A COD of "one" implies model predictions match observed.

3. **Relative Error of the Means (REM)**:

$$rem = \frac{\sum_{n=1}^{N} (s_o^n - s_p^n)}{\sum_{n=1}^{N} s_o^n} \qquad \text{Equation 5-1}$$

S_o = observed values n = sample number
S_p =potential values N = total # of observations

Zero REM implies the average mass of the model equals the average observed mass. A negative REM implies the model over-predicts the expected mass, and a positive REM implies the model under-predicts the expected mass.

Generally, the REM statistic and visual inspection where used to determine the optimum fit between predicted and observed values for the mass calibration. Chemical mass from other sources were adjusted until predicted results best fit observed and set the REM as close to zero as possible.

5.1 Suspended Sediment Calibration

The first constituent calibrated was the suspended solids. Sediment class distribution and suspended solids settling velocity were adjusted during the calibration process. At first, two sediment types were selected; a fine sand and a silt. Sediment samples from ACOE (SAIC 1991) pre-dredging studies indicated that most of the solids deposited in the turning basin are fine to medium sands. The silt component was used to account for observed suspended solids that travel beyond the turning basin and out into Elliott Bay. The Denny Way/Lake Union CSO (Herrera 1997) study indicated that most of the solids that metals partitioned to had settling velocities characteristic of silts and clays. Initial

solids distribution at the Green River boundary was distributed 67 percent to fine sands and 33 percent to silts. Suspended solids for the Elliott Bay boundary, CSOs and other sources were assigned to the silt and/or clay fraction. Silt fraction for CSOs were based on results from the Denny Way/Lake Union study, the same results were applied to other sources for lack of better information.

Analysis of the two-component solids distribution indicated simulated suspended solids were settling out too fast in the upper estuary and in Elliott Bay. A third solids class was added with a settling velocity similar to clays and flocculated material. Introduction of the third sediment class greatly improved the spatial distribution of suspended solids predicted by the model. The third sediment class also allowed division of the solids in the CSOs and other sources into two classes, a silt class and a clay class. Results from the Denny Way/Lake Union CSO (Herrera 1997) study suggested approximately 50 percent of the solids have a settling velocity less than 0.025 cm/s (typical for particles finer than medium silts). Therefore, suspended solids from the CSOs were at 50 percent silt and 50 percent clay. Solids distributions for the other sources and CSOs were divided into two classes.

Settling velocities and solids loads at the Green River boundary were adjusted for all three classes until an optimum fit between observed and predicted solids concentrations was reached. The best fit occurred with a suspended solids distribution at the Green River boundary of 78 percent fine sands, 15 percent silts, and 7 percent clays, and 100 percent clay at the Elliott Bay boundary. Suspended solids from CSOs and other sources were negligible compared to that from Green River. Final settling velocities for each class was 0.01 m/s for the fine sands, 0.004 m/s for silts, and $1x10^{-6}$ m/s for the clays.

5.2 Metals Mass Calibration

To reiterate the objectives of the modeling, the model was used as a tool to estimate contributions of chemical mass from other sources. There will be no attempt to state that the mass calibration has identified every specific source, other than CSOs, within the estuary. The mass calibration only identifies one possible loading condition to the area, it does not identify exact conditions. The mass calibration was essentially a process upon which other sources were back-calculated from observed field data and known CSO inputs.

The limitation of this approach is the assumption that variations in observed concentrations due to any other physical and chemical processes are small in comparison to changes in concentrations from other unknown sources. The data set used in the mass calibration was finite in both space and time. The intent was to get a reasonable fit between model predictions and field observations, and to get a reasonable estimate of CSO and other sources. The field data set does not capture every aspect and detail of the processes and conditions that could possibly occur. The important components of these processes are defined within the model and have been accepted by the scientific community. It was beyond the fiscal ability of the County to identify and characterize all possible sources and processes within the study area. Should additional funding become

available, more time and effort will be spent to characterize other input sources and processes to refine the current model.

Metals were calibrated after the suspended solids calibration was completed. Calibration entailed adjusting load inputs from other sources until simulated metals concentrations were comparable to observed. Metals loading from CSOs were not adjusted. It was assumed that inputs from CSOs had been adequately defined during the sampling effort.

The model simulated the transport of metals in two phases, dissolved and particulate. Division between the two phases was defined by the partition coefficients given in Table 3-1 and the suspended solids as given by Equation 3-3. It was assumed that the partition coefficients remained constant in both space and time. Given that the partition coefficient does not vary and that the suspended solids field has been defined, differences in simulated and observed metals concentrations were ascribed to other source loads. The model simulates chemical loads using a hydrograph and chemical concentration time series. It multiplies the flow rate by the chemical concentration to give a chemical flux into the cell. To adjust the load that discharges into the cell, either the flow rate or the chemical concentrations can be manipulated. For the EFDC model it is easier to manipulate the chemical concentration time series rather than the hydrograph.

Calibration was carried out in multiple steps, with each step refining the previous steps. The first steps were to match the general fit of model predictions to field observations. After the general fit was completed the next steps refined model predictions at specific points in the observed time series. This entailed adjusting either the existing hydrographs, chemical time series, or adding a separate hydrograph and chemical time series as needed to match observed field data.

The time field in the modeling analysis is numerated with the Julian day notation. Julian day 0.5 for this modeling project is defined as January 1, noon, 1996 and Julian day 1 is January 1, mid-night, 1996. Since 1996 was a leap year, there would be 366 Julian days (JD) in the year.

5.2.1 General Fitting of Model to Observed Conditions

Analysis of Run 1. The first simulation indicated that the model tended to over-predict metals concentrations throughout the estuary. Time series concentrations for all source loads other than CSOs were reduced accordingly.

Analysis of Run 2. Results indicated that concentrations at Elliott Bay would be better simulated by applying the 20 m depth field sample concentration time series over the nine bottom layers, and the surface field sample series to the surface layer. Review of historical salinity measurements near the model boundary indicated that salinity does not change much with depths below 20 meters, implying a uniformly mixed layer.

The model over-predicted lead and zinc on the same sample days that had been blank corrected and had been assigned a mean value (because they were negative). Blank corrected values were set to zero. Green River boundary field data for JD 422 measured

a very high concentration for lead and zinc. The model transported the elevated concentration on JD 422 through the entire estuary. However, field observation at other sample sites did not show elevated concentrations on this day. Because the river flows are several orders of magnitude larger than the CSO or other sources, small perturbations at the Green River boundary can reverberate throughout the model domain. If these perturbations are real, then one would expect to see some sort of perturbation at other locations influenced by the river. Since the perturbation imposed at the boundary on JD 422 was not observed at any of the downstream field sites it can be reasoned that the perturbation was not a true boundary condition, but perhaps a sampling anomaly. The difficulty in making such a determination is that the true boundary condition is not known and must be estimated from downstream conditions. Therefore, values for lead and zinc on JD 422 were reduced at the boundary based on conditions observed farther downstream.

Simulated copper, cadmium and arsenic were generally too low in the upper part of the estuary. All three were increased.

Subsequent to Run 2, a run was started in which all the other sources were shut off to determine how much effect other sources had to simulated concentrations. Results indicated that the model was sensitive to inputs from zinc, lead, and copper, and less so to arsenic, cadmium, and nickel.

Analysis of Run 3. Changes to chemical distributions at the Elliott Bay and Green River boundaries improved comparisons between predicted and observed chemical concentrations and distributions.

In general, model predictions were too high along the east side of estuary and that other source loads should be separated into an east and west side component. Simulated lead and zinc concentrations were too high and were reduced on both sides of the estuary, more so on the east side.

Green River boundary field data for JD 422 measured a high concentration for nickel. Model results showed the elevated concentration was transported through the estuary. However, field data at other sample sites did not show the an elevated concentration on this day. The JD 422 peak for nickel was reduced. A similar, but opposite condition existed at the Elliott Bay boundary for JD 429. The JD 429 at the Elliott Bay boundary was increased. The model also over-predicted nickel along the east side of the estuary. Nickel was decreased along the east side.

Copper, arsenic and cadmium tended to be under-predicted in the east waterway. Therefore, concentrations were increased along the east side for Run 4.

Analysis of Run 4. Lead and zinc were still too high along the east side. It was also apparent that zinc and lead concentrations were under-predicted on sample days before JD 400. This can be explained by the field blank correction methodology used to correct field samples. Blank correction was divided into two groups: the first group had samples from JD 303 through 400 and the second from JD 415 through 518. The model indicated

that blank correction over corrected field contamination in the first sample group. Zinc concentrations at the Elliott Bay boundary for JDs 436 and 505 were corrected to better fit observed conditions within the bay and estuary.

Nickel concentrations were over-predicted in the east waterway. Simulations without any of the other sources discharging indicated that nickel concentrations were not that sensitive to inputs from the other sources. Therefore, nickel concentrations along the east side were set to zero.

Modeled arsenic and copper distributions were fairly good. Cadmium was over-predicted in the upper reaches of the estuary and under-predicted in the east waterway. The same held true for arsenic but to a lesser degree. Cadmium was reduced.

Distributions for metals after Run 4 were generally good. Gross differences had been removed but as a result smaller differences became more obvious. The analysis was shifted to more isolated differences that persisted at a number of field locations. The model over-predicted all chemical concentrations on JDs 317 and 329 at the Norfolk sample location. At the Michigan and Brandon sites the model under-predicted concentrations on JDs 317 and 492.

5.2.2 Refined Fitting of Model to Observed Conditions

Comparison of results from Run 4 to observed conditions indicated the model was consistently under-predicting concentrations at the Michigan and Brandon sample sites on JDs 317 and 492. Rainfall records and other source hydrographs show that discharge events could and do occur on those days. Hydrograph discharges for other sources near the sampling sites were modified to increase the discharge flow for a brief period of time during the sampling interval.

Assessment of over-predicted concentrations at the Norfolk site during JDs 317 and 329 and review of simulated flow dynamics, showed reversing flow with significant sediment resuspension occurring on these days. The critical shear stress for the silt and clay components were increased to reduce resuspension for Run 5.

Analysis of Run 5. Increasing the critical shear significantly reduced sediment resuspension and chemical concentrations for the two periods without substantially changing predicted values at other times. The critical stress was increased from 1.0×10^{-4} to 3.0×10^{-4} (m^2/s^2). Review of the suspended solids calibration showed increasing the critical stress for the fines did not affect the calibration. The resuspension of sediments and corresponding chemicals was localized to the Norfolk sampling area. Review of suspended solids and metals concentrations on the same days, but at other sites, does not show the same peaks.

The model was still over-predicting zinc, lead, nickel, and copper in the east waterway and under-predicting arsenic and cadmium. It was speculated that the model was allowing too much river flow through the east waterway, even though acoustic doppler velocity data indicated otherwise. Bottom depths in model cells at the restriction near the

Spokane Street bridge [cells (146) and (149)] were decreased 4 and 2 meters, respectively, to increase flow resistance through the section.

Adjustment of other source hydrographs on JDs 317 and 492 did not increase model predictions. Day-317-observed concentration peaks were higher at the Brandon station than Michigan and decreased from the west to east banks. In addition, estuary flow was flood, indicating another source should be up-current of the Brandon site. Day-492-observed peaks were higher at the Michigan station than at Brandon and decreased from the east to west bank and flow was ebbing, indicating another source above the Michigan site. Two separate hydrographs were constructed for days 317 and 492, discharging slightly before and after the sampling event. Hydrograph 317 was placed at the Brandon station cell, on the west bank. Hydrograph 492 was placed upstream of the Michigan station cell on the east bank for Run 6.

Analysis of Run 6. Decreasing bottom depth at the east-waterway restriction did not change chemical concentrations in the east waterway. As a result, it was postulated that the model was not adequately mixing saline water into the freshwater lens. The model was under-predicting arsenic and cadmium in the freshwater layer in the east waterway, but was adequately predicting concentrations in the saline water. The primary source of arsenic and cadmium appears to come from the bay because average concentrations in the bay are greater than the average at the Green River boundary. For nickel, the model tended to over-predict in the freshwater layer in the east waterway, but was adequately predicting concentrations in the saline water. The primary source of nickel appears to be the Green River as average concentrations in the Green River are greater than the average concentrations in the bay. Given the observations of arsenic, cadmium, and nickel, the model may under-predict vertical mixing between the fresh and saline waters. Because the model employs a turbulent-eddy-viscosity and diffusion-solution scheme, the turbulent mixing between the fresh and saline waters cannot be adjusted directly. Constants used in the scheme are considered universal and should not be adjusted (Hamrick 1992). However, the model does use a minimum turbulent diffusion value that is invoked if the predicted value falls below the minimum turbulent value. The minimum turbulent diffusion value was increased from $1x10^{-9}$ to $1x10^{-6}$ (m^2/s). The minimum should not exceed $1x10^{-5}$ (m^2/s), or 0.1 (cm^2/s) (Hamrick 1998 personal communication).

Model predictions on sample days 317 and 496 were comparable to observed in the surface layer but were under-predicted at depth. Also, the model was not showing adequate horizontal transport across the estuary for both days. The discharge location for the JD 492 Michigan station was moved farther upstream to allow greater horizontal transport and both the discharge depth and flow were increased. An additional source location was placed above the JD 317 Brandon station and the discharge depth was increased as well.

Predictions of zinc and lead concentrations in the east waterway were too high in the surface layer and too low at depth. Discharge depths were increased for the two non-CSO sources in the east waterway and the one non-CSO source near the Duwamish/Diagonal CSO/storm drain. Also apparent was an over-prediction of zinc and lead on JD 339 at several sample locations along the east side of the river. The east side

chemical time series was modified to reduce zinc and lead concentration on JD 339 for Run 7.

Analysis of Run 7. Increasing the minimum turbulent diffusion value did not affect vertical mixing between the fresh and saline layers. It is possible that the cell resolution at the restriction near the Spokane Street bridge is not sufficient to resolve the hydrodynamic mixing that could be occurring in the area. As well, there is no field data in which to review the hydrodynamic processes to determine if significant mixing is occurring between the fresh and saline waters in this area. The minimum turbulent diffusion value was decreased to $1x10^{-8}$ (m^2/s) and was not adjusted again.

Adjustments to JD 317 hydrographs over-predicted zinc and lead concentrations at depth and under-predicted them in the surface. For JD 492, predicted concentrations at depth increased slightly but concentrations at the surface decreased. The discharge depth for the JD 317 hydrograph was lowered slightly, and the discharge volume for JD 492 hydrograph was increased with no adjustment to the discharge depth.

Increasing the discharge depths for the three non-CSO sources distributed the mass of zinc and lead between the surface and bottom layers more in accordance with observed data. However, concentrations were still a little high in the east waterway surface layer. Discharge depths for the Hanford and Lander CSOs were increased for Run 8.

Analysis of Run 8. Changes to JD 317 hydrographs reduced peak concentrations in the bottom sample layer and increased concentrations in the surface. Adjustments to JD 492 hydrograph also brought predicted concentrations more in line with observed concentrations, but the model still tended to under-predict concentrations at depth. Lowering of discharge depths for Hanford and Lander improved zinc and lead distributions in the east waterway, bringing predicted concentrations in line with observed values.

Mass calibrations for Run 8 were accepted as the final loading conditions. Chemical concentration time series and point source hydrographs used in calibration Run 8 were used for model simulations to determine the risk of CSOs and other sources. Final chemical time series concentrations for other source inputs are listed in Subappendix A, Table 2, and calibration plots for the six metals of concern are shown in Subappendix B.

5.3 Organic Compounds, Mercury, and Fecal Coliform Bacteria

Mass calibration for this section was broken into two groups. The first group consisted of: tributyltin (TBT), fluoranthene, phenanthrene, chrysene, pyrene, benzo(b)fluoranthene, benzo(k)fluoranthene, and total PCBs. The second group consisted of: mercury, fecal coliform bacteria, and bis(2-ethylhexyl)phthalate. Calibration for the second group used the same method employed for the metals. This was because the field sampling effort provided a sufficient number of spatial and temporal points to use the same time series analysis applied in the metals calibration.

1,4-dichlorobenzene was below detection limits for both field samples and SPMD studies and was not detected in mussel tissue. 4-methylphenol was below detection limits for the field samples and could not be tested on the SPMD because it is not lipophilic. However, it was detected in mussel tissue at the Duwamish/Diagonal site during the wet season and the Brandon site during the dry season. Both compounds were detected in CSO flow. Because of the dearth of field information for the two compounds, the calibration procedure was to compare model prediction against laboratory detection levels. Simulated concentrations of 1,4-dichlorobenzene were typically two orders of magnitude below the laboratory detection level of 0.14 µg/l compared to the simulated concentration of 0.002 µg/l. 4-methylphenol was typically an order of magnitude below the laboratory detection level of 0.24 µg/l compared to the simulated concentration 0.03 µg/l.

The mass calibration procedure for the organic compounds was simpler than the metals, because there were less data with which to work. Water samples drawn from the estuary and the bay showed that for all of the organic compounds except bis(2-ethylhexyl) phthalate, concentrations were below detection levels. Total water concentrations for TBT, fluoranthene, phenanthrene, chrysene, pyrene, benzo(b)fluoranthene, benzo(k)fluoranthene, and total PCBs were estimated from either SPMD or mussels or both. The SPMDs were analyzed at Battelle Marine Sciences Laboratory, and mussel tissue analyzed at King County Environmental Sciences Laboratory. Water concentrations were back-calculated from sorbed concentrations on the SPMD devices using a partitioning coefficient along with the assumption that the devices had been deployed long enough to come into equilibrium with the environment. Equilibrium occurs within a couple days for most compounds (Lefkovitz and Crecelius 1995). SPMDs were deployed for two weeks at two sites; one meter and three meters below the water surface at each site. Other studies showed SPMD data precede with observed data within a factor of three to ten, depending on the compound (Lefkovitz and Crecelius 1995), which is comparable to results by (Hofelt and Shea 1997).

Calculation of chemical data for PAHs and PCBs from mussel tissue data followed the methods outlined by (Neff and Burns 1996). Water concentrations were estimated from observed tissue concentrations using the regression curves proposed by Neff and Burns (1996). Their proposed methodology appears to agree with observed concentrations within a factor of five to ten (Neff and Burns 1996). The paper also explains that differences between observed and predicted concentrations are sensitive to mussel exposure time, in that mussels reflect exposures that occurred in the previous weeks and months. Analysis of the mussel data by a County scientist indicated that the mussels may not have come into equilibrium with the estuary for the period of deployment.

Water concentrations for TBT were estimated from mussel tissue using a bioconcentration factor (BCF) because TBT was not measured in field samples. A BCF of 3,000 was used as the "most representative" value (Cardwell 1988); BCF values can vary between 1,500 to 10,000.

Water concentrations estimated from the SPMD and mussel data represents a time average history of events that occurred over their deployment period. To compare model predictions of water concentrations to the SPMD and mussel data, model predictions

were saved at one-hour intervals for the duration of each deployment at each site. The arithmetic average of the one-hour samples were compared to the SPMD and mussel data for the mass calibration. Simulated and observed concentrations were plotted against each other to compare model results to observed. If simulated results match observed results perfectly, the points would lie on a straight line with a slope of one (Figure 5-1). The mass calibration entailed adjusting the mass inputs until a reasonable fit of predicted versus observed was obtained. All observed points for a specific organic compound were plotted in the same graph, whether at the different locations or times. Not enough data existed at each sample site to make a temporal comparison as was done for the metals.

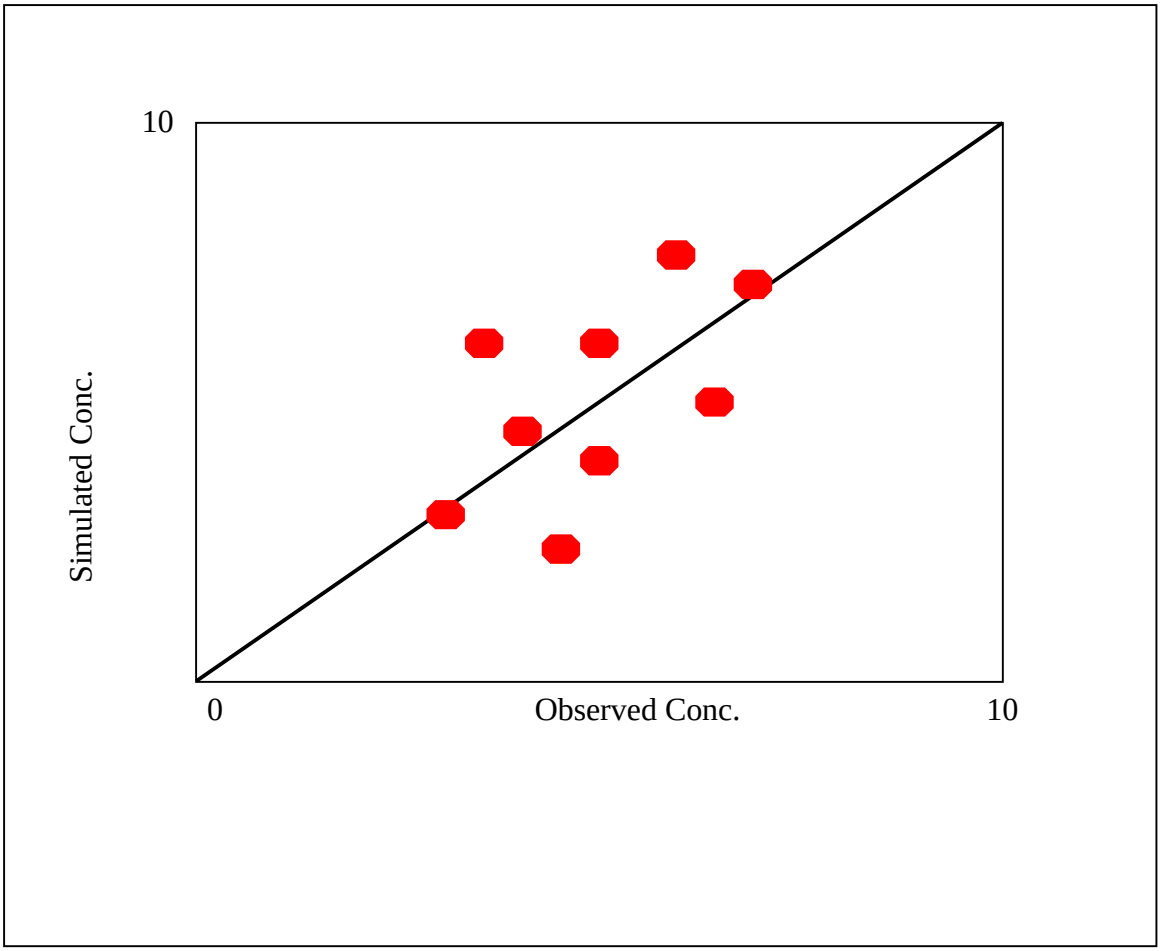

Figure 5-1. Plot of Observed Field Data Versus Simulated Against a Line With a Slope of One

Adjustment of the input loads for the organic compounds was performed differently than the metals. For example, benzo(b)fluoranthene was not detected in the CSO effluent and there was no historical evidence indicating it was measured in storm drains or other sources. As a result, one-half the MDL was used as the initial input concentration for both CSOs and other sources. Modeling results indicated that the source concentrations for benzo(b)fluoranthene needed to be adjusted to bring predicted concentrations in line

with observed. Since both CSO and other sources had been assigned an arbitrary value of one-half the MDL, both were adjusted simultaneously until predicted values reasonably matched observed values. This method was applied to benzo(b)fluoranthene, benzo(k)fluoranthene, total PCBs, and TBT, as these compounds were below detection levels in the CSOs and there was no known historical data for the other sources.

5.3.1 General Fitting of Model to Observed

Site names will be abbreviated as; turning basin, mid-channel Michigan CSO, mid-channel Brandon CSO, West Waterway Pier 10 (see Figure 2-1 for locations). SPMD and Mussel sample locations were near the Brandon CSO and the Duwamish/Diagonal Way storm drain.

Analysis of Run 1. Execution of the model with initial conditions for CSO and other sources over-predicted water concentrations for all eight organic compounds for group 1. Fl and Ph were fairly close, Chy was too high; pyrene was under; benzo(b)fluoranthene, benzo(k)fluoranthene, and TBT were about same order of magnitude over; and PCBs were about two orders of magnitude over. Concentrations for CSO inputs and other sources were adjusted downward or upward as needed.

Fecal coliform bacteria (fecals) were over-predicted on JDs 341, 442, 477, and 518 in which large CSO discharges occurred. Fecal concentrations were approximately an order of magnitude too high at some sample locations. Other source concentrations were reduced by an order of magnitude. The model under-predicted concentrations on JDs 394 and 422, on which no CSO discharges occurred. Persistence of the under-prediction throughout the model domain indicated that the effect may be boundary driven at the Green River end. Therefore, the Green River boundary for JDs 394 and 422 was adjusted.

While bis(2-ethylhexyl)phthalate was detected in a considerable number of samples, a large portion of the data was qualified as having high blank contamination and thus discarded from use in the mass calibration. For those points that did not have significant blank contamination, bis(2-ethylhexyl)phthalate was over-predicted on JD 518 throughout the model and appeared to be driven by boundary conditions (BC) at the Green River. Green River BCs were decreased accordingly. The model tended to over-predict westside concentrations so, westside sources were reduced by half. The model under-predicted concentrations on JDs 476 and 477 at a number of sample sites. Concentration time series for other sources were increased by an order of magnitude for the period JD 476 to 477.

Mercury concentrations were fairly good, but there were fewer data points for the mass calibration than other chemicals. Therefore, it is much more difficult to assess discrepancies between modeled and observed concentrations. However, simulations indicated that mercury concentration were a little high and thus concentrations for other sources were decreased.

Analysis of Run 2. Adjustment of the eight organic compounds improved predicted concentrations, however, all concentration were too high. TBT and PCBs were reduced about one order of magnitude; all others were reduced by a factor of two or less.

Decreasing fecal concentrations in the other sources did not significantly reduce over-prediction at JDs 341, 442, 477, and 518. Comparing the estimated annual discharge volumes of CSOs and other sources to average fecal concentrations for each source indicates that CSOs could contribute 50 times more fecals to the estuary than other sources (Table 5-1). Given this and the fact that reducing the fecal concentration from other sources had no effect when comparing model prediction to observed, it was decided to adjust fecal concentrations in the CSOs to match observed. Fecal concentrations for other sources remained constant. Therefore, fecal concentrations for other sources were set back to initial values and concentrations for CSOs were reduced a factor of ten. It needs to be noted that fecal inputs from the other sources are important during periods of no CSO discharge, and that comparisons between simulated and observed concentrations during these periods are comparable.

Table 5-1. Comparison of Fecal Inputs from Other Sources and CSOs

Fecal Source	Annual Volume (MG)	Fecal Count/100ml	Relative Load (Load/CSO Load)
Other Sources	9,857	1,100	.019
CSOs	1,221	473,476	1.0

Inclusion of additional Green River BC fecal concentrations on JDs 394 and 422 improved comparisons between predicted and observed concentrations.

Reducing JD 518 bis(2-ethylhexyl)phthalate concentration at the Green River boundary improved comparisons between predicted and observed concentrations. Lowering westside concentrations had a moderate improvement. No further adjustments were made for JD 518 and westside inputs. Increasing concentration around JDs 476 and 477 showed no noticeable improvement between predicted and observed. The peak concentrations occurred at the east Michigan and mid-channel Chelan stations in the surface sample on JD 476, but a peak did not occur at the Brandon station located between the two. The observed concentration at east Michigan and mid-channel Chelan was approximately 23 and 10 (µg/l), respectively. In addition, a peak concentration also occurred at the east Connecticut station on JD 303 with a value of 8 (µg/l). Two hydrographs were developed for JDs 476 and 303 and placed in the cells just upstream of east Michigan and east of east Connecticut with a fecal concentration of 200 (µg/l). Mercury predictions were comparable to observed data given the limited number of data points. Model predictions were considered adequate; no further adjustments were made to mercury inputs for Run 3.

Analysis of Run 3. Predictions for four of the eight organic compounds were fairly good and required no further adjustments. The four that required further adjustment were TBT, chrysene, benzo(k)fluoranthene, and PCB. TBT and PCB input concentrations for both CSO and other sources were set to zero (no source contribution to the estuary). chrysene and benzo(k)fluoranthene were reduced by a factor of two for both sources.

Reduction of all CSO source concentrations greatly improved comparison between the predicted and observed fecal concentrations on JDs 341, 442, 477, and 518. The model generally under-predicts concentrations in the upper reach of the estuary and near the Denny Way. Thus, CSO concentrations for Norfolk, 8th Avenue, and Michigan were increased a factor of two. Denny was increased by a factor of eight. Simulations in the east waterway near the Hanford and Lander CSOs indicated the model over-predicted concentrations. Concentrations at Hanford and Lander were decreased by a factor of five.

Introduction of the two hydrographs for bis(2-ethylhexyl)phthalate on JDs 476 and 303 showed a slight improvement in the bottom layer, but little improvement in the surface layers. Bis(2-ethylhexyl)phthalate concentrations were increased by a factor of ten for Run 4.

Analysis of Run 4. Chrysene and benzo(k)fluoranthene comparisons between simulated and observed were comparable and no further adjustments were required. TBT is still over-predicted by an order of magnitude even with all source components set to zero. PCBs were over-predicted by approximately a factor of 5. This indicated that the sediments are the major source component to the estuary for both TBT and PCBs. The methods used to estimate TBT and PCB concentrations from mussel and SPMD data can vary between a factor of three to ten for PCBs, and a factor of ten or more for TBT. Also given the effect of errors from approximations and simplifications in the model formulation of the equations and segmentation of the area, further refinement of model parameters to achieve a better fit between simulated and observed would suggest more accuracy than is presently available. No further adjustments were made.

Increasing fecal concentrations at Norfolk, 8th Avenue, and Michigan improve the comparison between predicted and observed concentrations. However, review of the data indicated that the model slightly under-predicted concentrations along the shore channel compared to the center. Reduction of concentrations at Hanford and Lander greatly improved comparisons between predicted and observed in the bottom layer, however it significantly under-predicted concentrations during peak CSO loads in the bottom layer of the upper estuary. As the model is currently configured, Hanford and Lander significantly influence fecal loads into the salt wedge, which travel up the estuary to sites Brandon and Michigan, but not at the Chelan site. The model also slightly over-predicted concentrations in the surface layer during periods of minor CSO discharges. Concentrations were also under-predicted at depth at the east and west Connecticut sites. It was also observed that the model under-predicted fecals on JD 422 at all estuary sties, indicating a Green River boundary source. Actions taken were to decrease other source fecal concentrations by 20 percent, increase Connecticut CSO by 30 percent, and include a Green River source on JD 422.

Calibration for bis(2-ethylhexyl)phthalate was focused on matching peak concentrations on JD 303 at Connecticut and JD 476 at Michigan and Chelan. Increasing the concentration by a factor of ten did not improve results sufficiently. The horizontal discharge location for the Michigan peak was moved from cell (93) to cell (96), which is a sample site location. Also, the vertical discharge locations were moved one layer closer to the surface; Michigan discharged into the upper three layers and Connecticut into the upper two for Run 5.

Analysis of Run 5. Modifications to fecal concentrations for other sources did reduce over-prediction during periods of minor CSO inputs, but the largest problem was on JD 516 when a major storm occurred. Comparing field data to simulated data indicated that the model correctly predicted concentrations at the Norfolk and Michigan sites, but over-predicted observed data at all other downstream sites by 1.5 times. All CSO-concentration time series were edited to reduce fecal concentrations between JDs 516 and 517.

Moving the source location for the Michigan site and raising the discharge location to the upper three layers in the water column improved modeled predictions compared to observed. Raising the discharge for the Connecticut site also improved comparisons. The vertical discharge locations for both sites were raised further; the discharge at the Michigan was set to the upper two layers, and the Connecticut site was set to the surface layer for Run 6.

Analysis of Run 6. Editing of the CSO concentration times series did not sufficiently reduce fecal concentrations on JD 516. Therefore, the JD 516 editing of the CSO concentration time series was removed and instead fecal concentrations at the Green River boundary were reduced by a 1,000 count. The Duwamish/Diagonal CSO/stormdrain effluent pipe discharges into bottom layers of the estuary at cell 129 and could act as a potential fecal source to the salt wedge. It serves an area similar to the Hanford and Lander CSOs. The concentration time series for the Duwamish/Diagonal CSO/stormdrain was assigned the Hanford time series to see if it would increase fecal concentrations in the bottom layers without affecting concentrations at the Hanford site. Fecal concentrations at the Denny Way CSO were over-predicted by three orders of magnitude on JD 516, but under-predicted at all other times. Concentrations were reduced by an order of magnitude at Denny.

The model over-predicted bis(2-ethylhexyl)phthalate concentrations at all three sites. Concentrations for hydrographs 303 and 476 were adjusted to bring concentration levels in agreement with observed concentrations for Run 7.

Analysis of Run 7. Modifying the Green River boundary for JD 516 did reduce fecal concentrations at sample sites located within the estuary. However, no significant reduction was observed at field sites within the bay. The model still over-predicted fecal concentrations on JD 516 at all sites except Norfolk and Michigan. Changes made to the Duwamish/Diagonal CSO/stormdrain input source significantly increased fecal concentrations at depth for sites Michigan, Brandon, and Chelan. It did not affect depth

concentrations at the Hanford site in the east waterway, but did influence concentrations in the surface.

Concurrent to the WQA, other personnel working on the basin run-off and conveyance system model for the Westpoint treatment facility (a separate project from the WQA), found that the Hanford/Rainer sewer line overflowed into Duwamish/Diagonal CSO/stormdrain overflow pipe at significantly greater rate than previously thought. Such circumstances could significantly influence fecal concentrations in the salt wedge near the Duwamish/Diagonal CSO/stormdrain outfall and upstream field sites. A new input hydrograph was constructed for the Hanford/Rainier and used as another CSO source at the Duwamish/Diagonal CSO/stormdrain site. The Hanford/Rainier connection serviced an area similar to the Hanford CSO basin, therefore the Hanford concentration time series was used for the new Hanford/Rainier hydrograph. The concentration time series for the Duwamish/Diagonal CSO/stormdrain was reset to the original fecal concentration time series.

Simulated bis(2-ethylhexyl)phthalate at the Michigan site on JD 476 closely matched the observed peak of 23 µg/l. However, review of predicted concentrations at the Brandon downstream site showed the model over-predicted bis(2-ethylhexyl)phthalate by several factors at all three transchannel sites, and under-predicted at the Chelan site. Predictions at the Connecticut site for JD 303 were too high in the surface layer and too low at depth. The discharge volume at the Connecticut site was redistributed over the vertical, discharging a larger portion into the second layer. No modifications were made to Michigan JD 476 inputs. The Green River concentration time series was modified to specify a bis(2-ethylhexyl)phthalate concentration of 0.07 µg/l, one-half the MDL value. This was done because bis(2-ethylhexyl)phthalate was detected at the Green River field sample site at levels above the MDL, indicating that bis(2-ethylhexyl)phthalate may have a persistent source, but is not detectable. Run 8 was then conducted.

Analysis of Run 8. Inclusion of the Hanford/Rainier CSO source did not significantly improve predictions of fecal concentrations at depth at upstream sites Michigan and Brandon.

Redistributing more of the Connecticut JD 303 discharge into the second layer slightly improved comparisons between predicted and observed results. Simulated concentrations decreased at the surface and increased at depth. No further adjustments were made to the fecal and bis(2-ethylhexyl)phthalate inputs. Final chemical time series concentrations for other sources and CSOs are listed in Subappendix A, Table 3, and calibration plots for the organic compounds of concern are shown in Subappendix C.

5.3.2 Assessment of Fecal Coliform Bacteria and Bis(2-ethylhexyl)phthalate Simulations

Fecal Coliform Simulations. There are several reasons why it may not be possible to improve the fecal calibration. The model is limited in describing how CSOs and other sources are discharged into the estuary. The first is that discharges must be assigned to a particular cell and layer depth. While the model allows the water elevation to change

with the tides, the location at which the CSO discharges is always in the same cell and layer. Therefore, the CSO discharge location moves up and down with the rising and falling tide levels. What actually happens is the CSO discharge is fixed and the rising and falling water levels move past the CSO. At high tide the CSO would be discharging into the lower water layers. At low tide it could discharge either just below the water surface, into the surface, or over a tidal flat into the surface. Because the model CSO always discharges into the same layer, at times it will be discharging into the wrong model layer. The possible ramifications are either over- or under-predicting fecal distributions within the model domain. This is one possible explanation for the difficulty in achieving a better match between simulated and observed fecal concentrations at depth.

It may also be that the model does not sufficiently simulate entrainment and mixing between the saltwater wedge and fresh water, tending to reduce fecals concentrations in the salt wedge. The same under-mixing was postulated in the metals mass calibration with arsenic, cadmium, and nickel.

There is also a large amount of variability in the fecal coliform concentrations for any CSO. Table 5-2 summarizes the statistics for fecal concentrations at the five CSO sample sites. The coefficient of variation for many of CSOs exceeded one, indicating a large variation in the data. This could significantly affect the mass calibration, as concentration inputs for fecals in the model were constant over time. If it is assumed that most of the data lie within two standard deviations of the mean and given a coefficient of variation greater than one, the model could, at times, differ from observed concentrations by a factor of two or greater.

Table 5-2. Fecal Coliform Statistics at the Sampled CSOs

CSO (count/100ml)	Arithmetic			Geometric Mean
	Mean	Std Dev	Coeff. Var	
Brandon	75,725	60,314	0.796	49,762
Hanford	961,700	1,601,277	1.66	479,037
Chelan	285,000	240,858	0.845	272,910
Connecticut	281,625	138,372	0.491	243,910
King	763,333	814,457	1.07	534,672

Bis(2-ethylhexyl)phthalate Simulations. The peak bis(2-ethylhexyl)phthalate concentrations observed on JDs 303 and 476 at sites Connecticut and Michigan may not be related to any discharge but could possibly be a sampling anomaly. Discussions with personnel at the King County Environmental Lab suggested that the observed peaks were unusually high and are probably from a small piece of plastic in the sample. bis(2-

ethylhexyl)phthalate is a fairly ubiquitous compound used as a plastizer and as a defoaming agent in detergents. Results of the mass calibration showed that the introduction of a point source load to create an equivalent peak value at the Michigan site adversely affects observations at the Brandon site, which showed no peak. It is possible that the sample was drawn right at the time of a discharge, not having had enough time to disperse downstream. This would have had to occur at all three peak observations, Michigan and Chelan on JD 476 and at Connecticut on JD 303. Considering comments from the Environmental Lab and results from the mass calibration, it did not seem likely that the observed peaks were a result of an unknown discharge, but were more likely a sampling anomaly.

Final chemical time series concentrations for other sources and CSOs are listed in Subappendix A, Table 3 and Table 4, and calibration plots for the bis(2-ethylhexyl) phthalate and fecals are shown in Subappendix D.

5.4 General Statements About Model Bias

The calibration was performed to reduce the mean bias of model predictions against mean field data to a zero value, that is a REM of zero. The estimated bias is only relative to field data, because the field data itself could be biased high or low compared to true conditions. The generally acceptable REM range for water quality modeling is ± 0.45 (U.S. EPA 1990, Table 5-15).

Tables at the beginning of each calibration appendix summarize REM values (in decimal form) at each field site. The tables for the metals and fecals clearly show that bias (non-zero REM values) varies at each site, and ranges between over- and under-prediction of observed field data, but most of the REM values are within the acceptable range of ± 0.45. Of the six metals, cadmium, lead, and zinc have REM values that exceed the 0.45 value. Cadmium exceeds 0.45 (over-predicts) at four sites near the Michigan CSO in the surface layer which represents 4 percent of the sample area. Lead exceeds 0.45 (over-predicts in the surface and under-predicts at depth) at five sites in the bay, representing 23 percent of the sample area. Zinc exceeds 0.45 (under-predicts at surface) at two sites in the bay, representing 15 percent of the sample area.

Also apparent is that the spatial distribution of bias is different for each chemical. Since source locations and discharge volumes within the model are the same for each chemical, the spatial differences between chemical types could imply that each chemical might have a different source location than that specified in the model. The differences could also be ascribed to spatial resolution of the model, field sampling methods, or laboratory error.

REM values for the organic compounds vary considerably between each compound and between each compound site. The model tends to significantly over predict TBT and total PCBs by –7.9 and –4.9 respectively, which will probably result in over-prediction of risk in the water or sediment columns. Calibration of the organic compounds was accomplished with much fewer samples than the metals and fecals, and thus have less

certainty. Results of the organic simulations should be used as an indication of concern, a means of flagging potentially harmful levels within the estuary. Results that show increased risk should require further, more intense field sampling and modeling efforts to better define spatial and temporal distributions and reduce the uncertainty.

How well the model performs over the whole sampling domain can be checked by looking at the mean REM of all the sample sites. The mean REM is computed by weighting each sample site REM by the cell area to account for the proportion of mass associated with each cell. Weight averaged REMs (for those constituents for which sufficiently large sample populations were obtained) are summarized in Table 5-3. Except for fecal coliforms, overall REM values are very small, and well within acceptable ranges. This implies that overall model bias is small for the listed constituents. The model generally over-predicts fecal coliform concentrations in the observed domain, and thus over-estimates potential risk.

For the given sampling areas, the model reasonably predicts overall, mean metals distributions for arsenic, cadmium, copper, lead, nickel, and zinc. At selected locations the model has a tendency to over-predict cadmium and lead in the surface layer, and under-predict zinc in the surface layer. The model tends to over-predict mean fecal coliform concentrations within the estuary.

Table 5-3. Weight Averaged REM for Metals and Fecal Coliforms

Constituent	Area Weighted REM
Fecal Coliforms	-0.51
Arsenic	0.04
Cadmium	-0.04
Copper	0.06
Lead	-0.02
Nickel	-0.06
Zinc	0.15

Given the limited data set for the organic compounds and mercury, results from the modeling effort should be used as an indication of possible chemical distributions within the estuary and bay. Results that indicate potential risk from a specific chemical should be used as a flag to collect additional field data to refine the spatial and temporal distributions and reduce uncertainty.

6. ASSESSMENT OF MODEL RESULTS

The purpose of the modeling effort was to estimate other source chemical loads into the Duwamish River and Elliott Bay, and to compare these sources to chemical loads from CSOs. This was accomplished by simulating conditions for one year with both CSO and other sources discharging (the baseline scenario), and comparing these results to the same year except with CSOs removed from the system (the "without CSO" scenario). The one-year simulation baseline simply entailed running the model with the chemical time series inputs developed from the mass calibration. The year without CSOs was simulated by setting all inputs from CSOs to zero. Both scenarios were simulated using the same Green River and Elliott Bay boundary conditions.

To show that the model is correctly simulating chemical transport and to explain some of the results, a single chemical at four sites within the estuary is selected to review model predictions. To review all 19 chemicals at all 5,120 cells would be unmanageable. Field data indicate that copper concentrations within the estuary are higher than ambient river and bay boundary concentrations, and that CSO and other source concentrations are an order of magnitude higher than ambient estuary concentrations. Because of this, changes to copper concentrations from CSOs and other sources in the estuary are more apparent. Four sites at model cells (45) near the turning basin, (95) mid-channel by the Michigan CSO, (110) mid-channel by the Brandon CSO, and (159) West Waterway by Pier 10 will be reviewed. The sites will give a sense of what happens along the length of the estuary. Items of review will be:

1. Total copper water concentrations
2. Suspended cohesive sediment water concentrations
3. Sediment bed mass concentrations
4. Copper sediments concentrations

The model divides the water column into ten layers and the sediments into a single layer. To review the four items above at the four sites in all layers would require 88 figures. To make the review manageable, only the surface layer in the water and the single sediment bed layer will be presented here.

Total copper water concentrations are shown in Figures 6-1 through 6-4 for baseline and without CSO conditions. Time averaged concentrations are presented in Table 6-1, and show that average copper concentrations decrease slightly when CSOs are removed. Comparisons of the time series indicate that peak copper concentrations during CSO events drop to ambient levels upon removal of the CSO. However at certain times, concentrations increase after the CSOs have been removed from the estuary. This is best illustrated by comparing JDs 413 and 444 of Figure 6-3 at the mid-channel Brandon site.

On JD 444 a storm occurred causing both CSO and other sources to discharge into the estuary. Copper concentrations on this day were lower without CSOs (11.6 µg/l) than

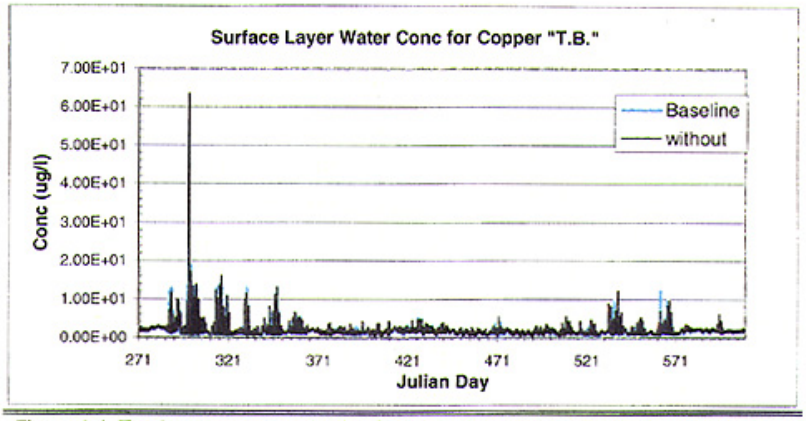

Figure 6-1 Total copper concentration in the surface water near the turning basin for baseline and without CSO discharge conditions.

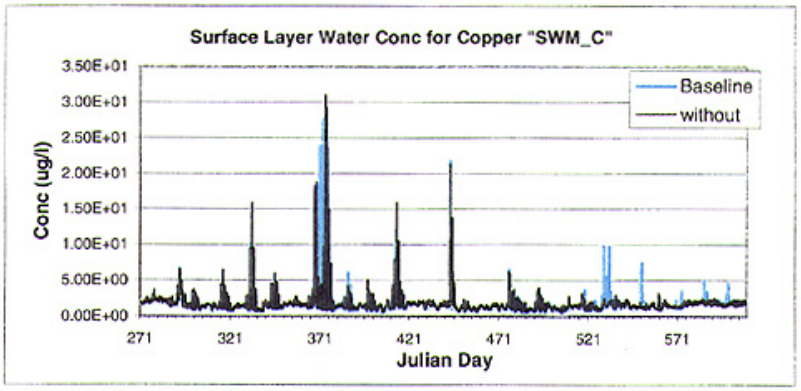

Figure 6-2 Total copper concentration in the surface water mid-channel by the Michigan CSO for baseline and without CSO discharge conditions.

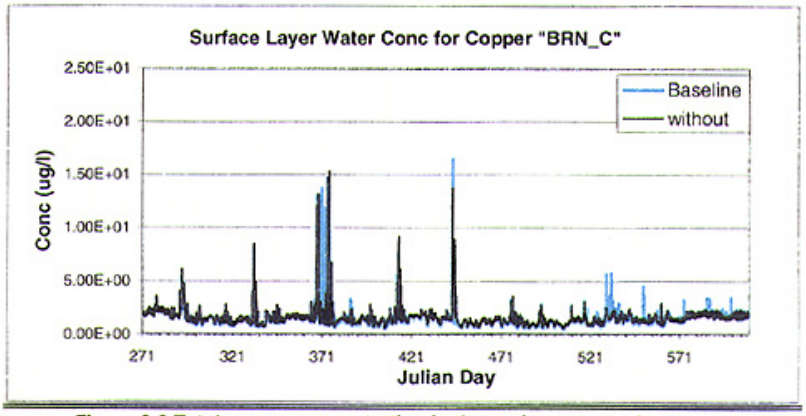

Figure 6-3 Total copper concentration in the surface water mid_channel by the Brandon CSO for baseline and without CSO discharge conditions.

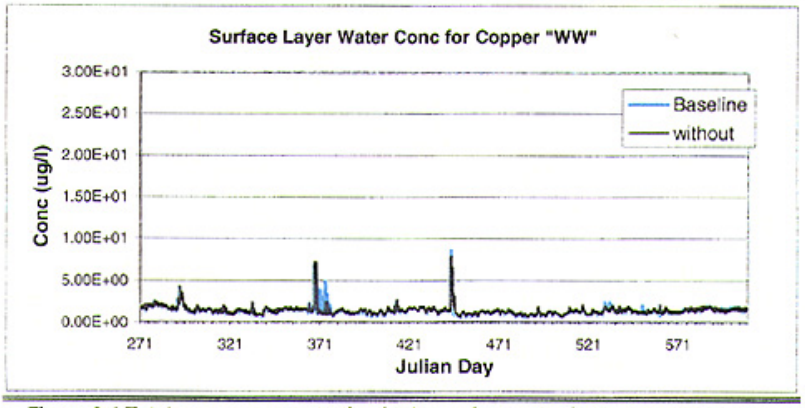

Figure 6-4 Total copper concentration in the surface water in the West Waterway by Pier 10 for baseline and without CSO discharge conditions.

Table 6-1. Annual Time Averaged Simulated Copper and Sediment Concentrations In Water Surface Layer and Sediment Bed

	Turning Basin	Michigan	Brandon	West Waterway		Turning Basin	Michigan	Brandon	West Waterway
Total Copper Concentration in Water					**Percent of Copper Sorbed to Suspended Sediments**				
Baseline	1.7 (µg/l)	1.7	1.57	1.45	Baseline	67.2 %	65.5 %	61.8 %	61.8 %
Without CSO	1.7 (µg/l)	1.63	1.54	1.42	Without CSO	66.4 %	64.6 %	61.5 %	61.7 %
Suspended Sediment Concentration					**Suspended Sediment Flux**				
Baseline	18.6 (mg/l)	17.3	14.7	14.7	Baseline	37.2 (mg/m^2s)	34.7	29.4	29.4
Without CSO	17.9 (mg/l)	16.6	14.5	14.6	Without CSO	35.9 (mg/m^2s)	33.2	29.1	29.3
Copper Concentration in Sediments					**Sorbed Copper Concentration in Water**				
Baseline	4.54 (mg/kg)	80.2	64.0	264	Baseline	62.4 (mg/kg)	64.3	66.0	60.9
Without CSO	4.68 (mg/kg)	81.3	64.6	265	Without CSO	62.9 (mg/kg)	63.5	65.2	59.8

with CSOs (16.6 µg/l). On JD 413, copper concentrations with CSOs were 7.75 µg/l and without CSOs 9.2 µg/l. But, on JD 413 no CSOs or other sources discharged into the estuary. However, Green River flows increased significantly from 58 cms on JD 410 to 172 cms on JD 413. The increased river flows caused significant amounts of copper-laden sediments to be suspended into the water, thus increasing copper concentrations in the water. Suspended cohesive sediment concentrations are shown in Figures 6-5 through 6-8 and show increased suspended sediment concentrations on JD 413. Since no CSO or other sources were discharging, the increased copper concentrations must be coming from the sediments.

Water concentrations are higher on JD 413 when the CSOs are not discharging, and if the copper is coming from the sediments, this implies that sediment concentrations are higher when CSOs are removed from the estuary. Table 6-1 shows that time averaged sediment copper concentrations are higher when CSOs do not discharge into the estuary. Figures 6-9 through 6-12 also show higher sediment copper concentrations under the without CSOs scenario.

Model results show sediment mass is greater with CSOs discharging into the estuary than without (Figures 6-13 through 6-16). CSOs increase the total mass of suspended sediments into the water and as a result, increase the total sediment mass that settles into the beds. Table 6-1 shows that the suspended sediment flux to the beds is slightly higher with the CSOs than without. Because copper sorbs to the suspended sediment mass, increasing the suspended sediment mass into the estuary increases the potential mass of copper that can settle into the beds. Therefore, with CSOs discharging more sediment mass and copper are available to settle into the beds, this condition increases the rate at which copper settles into the beds.

Review of Figures 6-9 through 6-12 shows that sediment copper concentrations decrease over time for both cases of baseline and without-CSO scenarios. This implies that existing sediment concentrations are higher than the supply of sorbed copper concentrations in the water that settle into the sediments. Even though copper concentrations in the water may be higher during peak CSO discharges, the sorbed copper concentrations settling into the sediment beds are less than observed copper concentrations. Thus with the increased sediment mass flux into the sediment bed from CSO discharges, existing sediment copper concentrations will dilute at a faster rate than they would if CSOs where removed.

Even though the model indicates that sediment copper concentrations will decrease at a faster rate with CSOs discharging into the estuary than they would if CSOs were removed, once sediment conditions come into equilibrium, sediment copper concentrations with CSOs discharging would be slightly higher than that without CSOs. Figure 6-17 illustrates how sediments might react to conditions baseline and without CSO discharges over many years. Concentrations with CSOs would be slightly higher, reaching equilibrium sooner because more suspended sediments settle into the beds. Table 6-1 shows that suspended sediment copper concentrations in the surface layer are

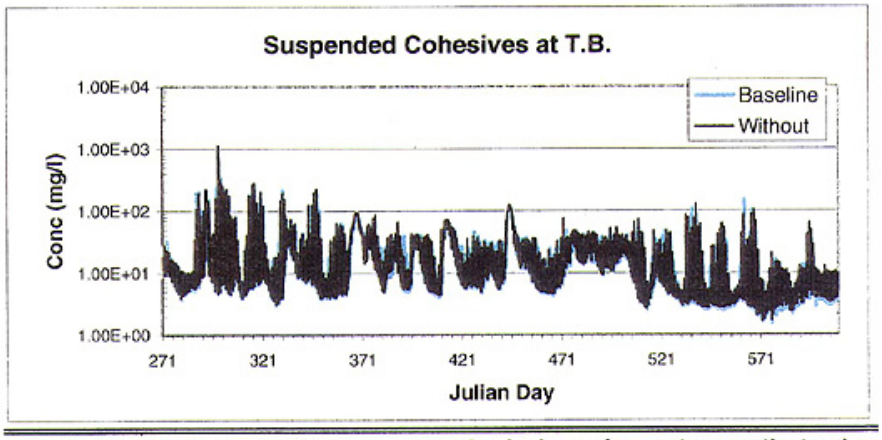

Figure 6-5 Cohesive sediment concentration in the surface water near the turning basin for baseline and without CSO discharge conditions.

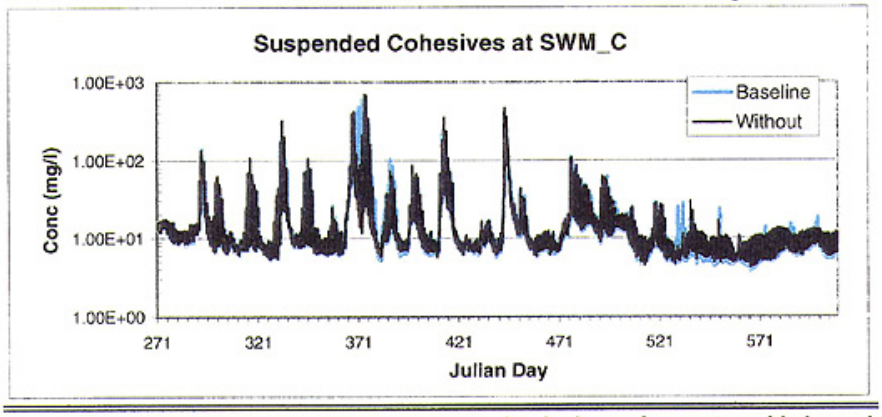

Figure 6-6 Cohesive sediment concentration in the surface water mid-channel Michigan CSO for baseline and without CSO discharge conditions.

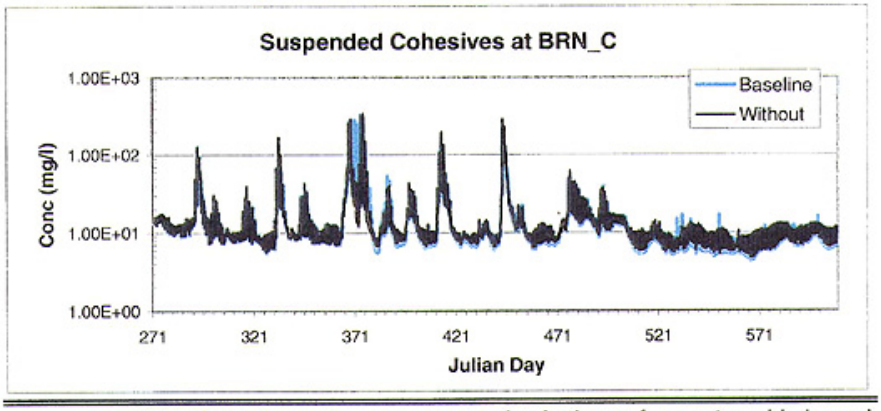

Figure 6-7 Cohesive sediment concentration in the surface water mid-channel Brandon CSO for baseline and without CSO discharge conditions.

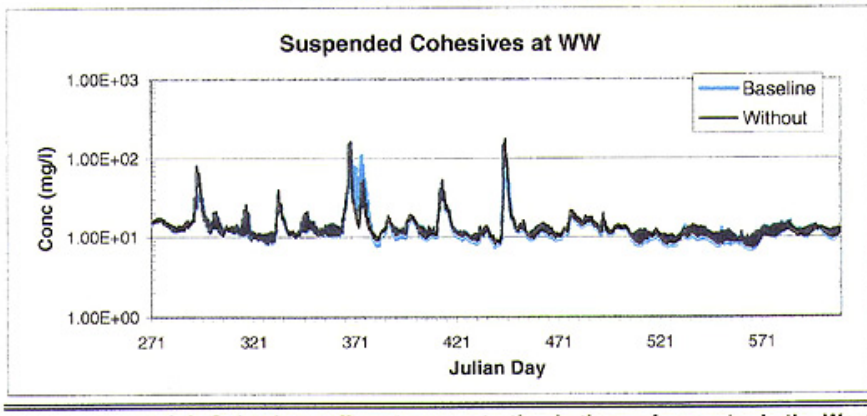

Figure 6-8 Cohesive sediment concentration in the surface water in the West Waterway for baseline and without CSO discharge conditions.

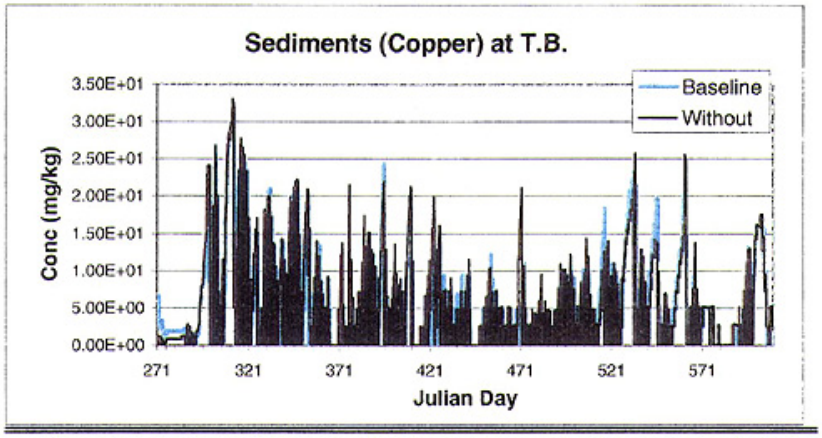

Figure 6-9 Copper sediment concentrations near the turning basin for baseline and without CSO discharge conditions.

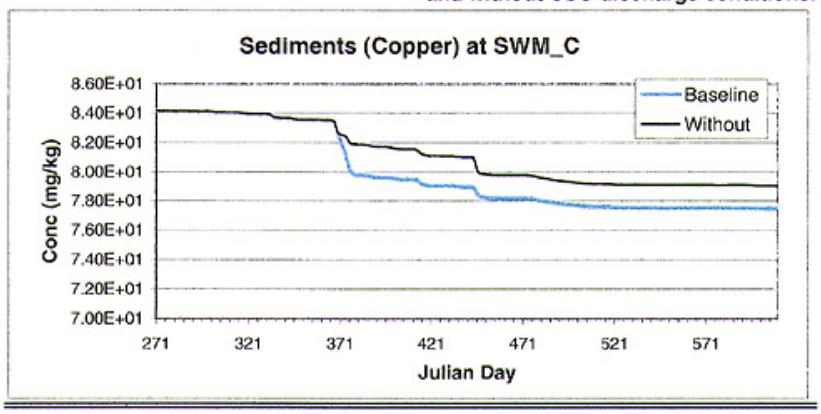

Figure 6-10 Copper sediment concentrations at mid-channel Michigan CSO for baseline and without CSO discharge conditions

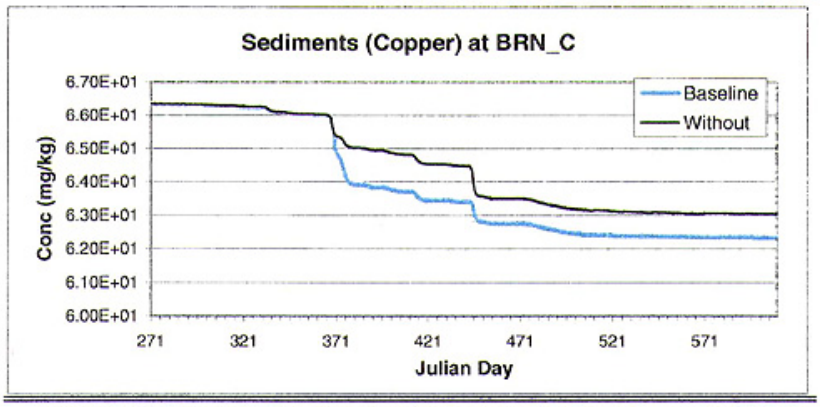

Figure 6-11 Copper sediment concentrations at mid-channel Brandon CSO for baseline and without CSOs discharge conditions.

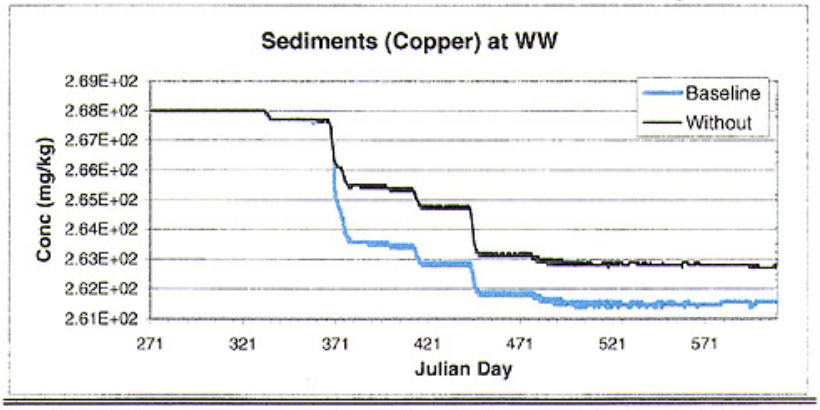

Figure 6-12 Copper sediment concentrations in the West Waterway by Pier 10 for baseline and without CSO discharge conditions.

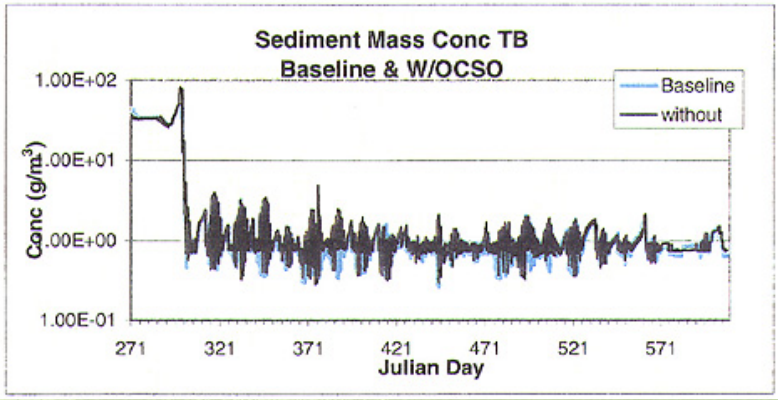

Figure 6-13 Sediment mass concentrations near the turning basin for baseline and without CSO discharge conditions.

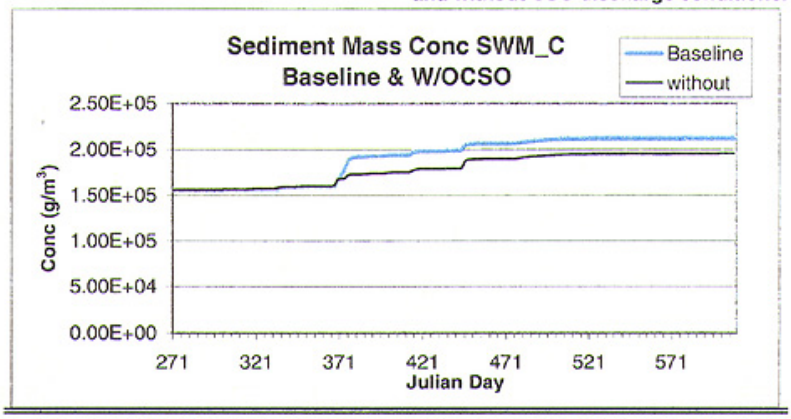

Figure 6-14 Sediment mass concentrations near at mid-channel Michigan CSO for baseline and without CSO discharge conditions.

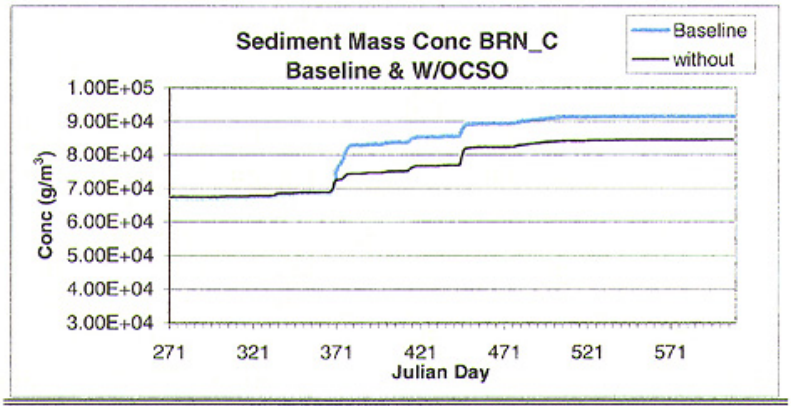

Figure 6-15 Sediment mass concentrations near at mid-channel Brandon CSO for baseline and without CSO discharge conditions.

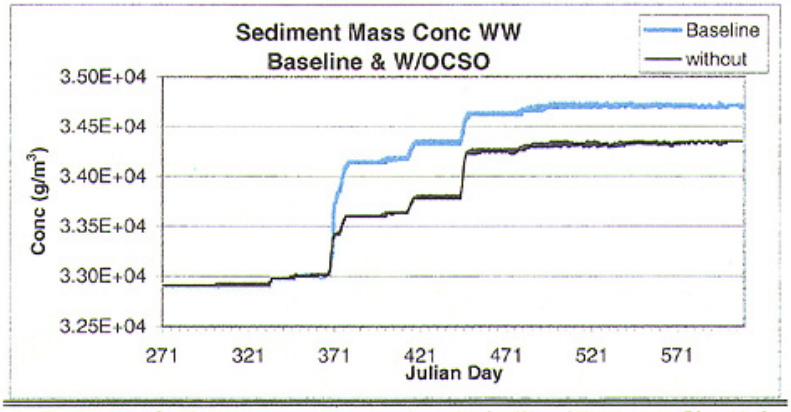

Figure 6-16 Sediment mass concentrations in the West Wtrwy near Pier 10 for baseline and without CSO discharge conditions.

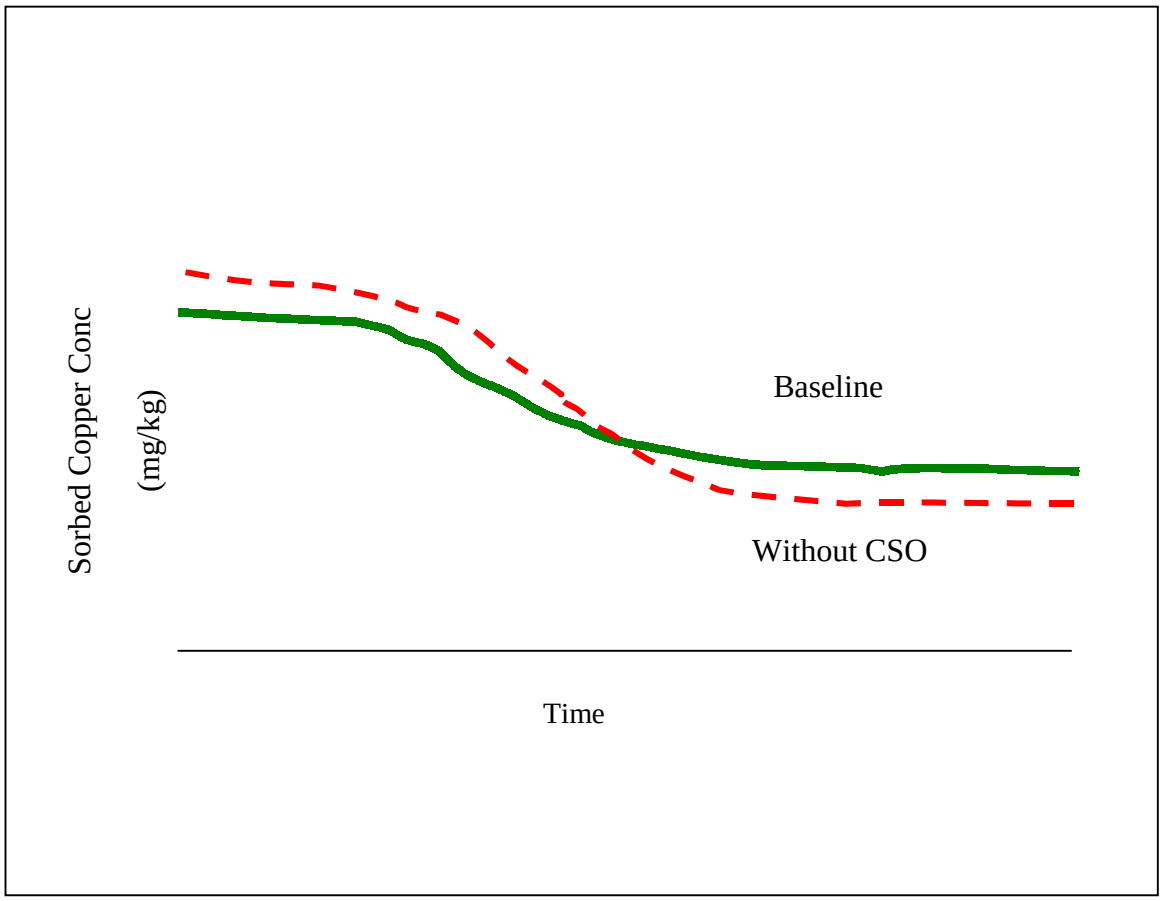

Figure 6-17. Change in Sediment Copper Concentrations for Conditions With and Without CSOs Over Many Years

slightly higher with CSOs. It should be noted that the estuary is very stratified and that the suspended sediment copper concentrations in the surface layer do not indicate what concentration is settling into the sediment beds. One could estimate long term sediment concentrations by reviewing sorbed copper concentrations to suspended sediments in the water layer directly above the sediment bed.

It appears that the model correctly simulated conditions with and without CSOs, showing a decrease in peak water copper concentration when CSOs are removed from the estuary. The model also indicates that initial sediment concentrations, as defined by information obtained from the SedQual database, appear to be historical in nature and will decrease over time to lower levels even with CSO discharging into the estuary.

6.1 Model Application to Risk Assessment

Results from the one year and ten year model simulations were used in the human health and aquatic life risk assessment to determine changes or differences in risk between conditions with CSOs discharging into the estuary and conditions without CSOs. The assessment investigated risks in the water and sediment column. Results of the risk assessment are summarized in report, "King County Combined Sewer Overflow Water Quality Assessment for the Duwamish River and Elliott Bay", Volume 1: Main Report and supporting appendices.

7. REFERENCES

Blumberg, A.F. and D.M. Goodrich. 1990. Modeling of wind-induced destratification in Chesapeake Bay. *Estuaries*. 13:236-249.

Cannon, C.A., N.P. Laird, and T.L. Keefer. 1979. Puget Sound Circulation: Final Report for FY77-78. NOAA Technical Memorandum ERL MESA-40. Marine Ecosystems Analysis Program. Boulder, Colorado.

Cardwell, R.D. 1988. Fate and effects of tributyltin in the marine environment: an update on knowledge. Prepared for Environmental Services, Envirosphere Company. Bellevue, Washington.

Cheng, R.T., V. Casulli, and J.W. Gartner. 1993. Tidal, residual, intertidal mudflat (TRIM) model and its application to San Francisco Bay, California. *Estuarine, Coast. Shelf Sci.* 36:235-280.

Cordell, J.R., L.M. Tear, C.A. Simenstad, and W.G. Hood. 1996. Duwamish River Coastal America Restoration and Reference Sites: Results from 1995 monitoring studies. Fisheries Research Institute, School of Fisheries, University of Washington, Seattle, Washington. FRI-UW-9612. 75 pp.

Curl, H.C., E.T. Baker, T.S. Bates, G.A. Cannon, R.A. Feely, T.L. Geiselman, M.F. Lamb, P.P. Murphy, D.J. Murphy, D.J. Pashinski, A.J. Paulson, D.A. Tennat. 1988. Contaminant transport from Elliott and Commencement Bays. NOAA Technical Memorandum ERL PMEL-78. Pacific Marine Environmental Laboratory. Seattle, Washington.

Devore, J.L. 1982. *Probability and Statistics for Engineering and the Sciences*. Brooks-Cole, Monterey, California.

Friedrichs, C.T. and J.M. Hamrick. 1996. Effects of channel geometry on cross-sectional variation in along-channel velocity in partially-mixed tidal estuaries. *In:* Buoyancy Effects on Coastal and Estuarine Dynamics. American Geophysical Union. Washington, DC.

Galperin, B. and G.L. Mellor. 1990. A time-dependent, three-dimensional model of the Delaware Bay and River system. Part 1: Description of the model and tidal analysis. *Estuarine, Coast. Shelf Sci.* 31:231-253.

Galperin, B., L.H. Kantha, S. Hassid, and A. Rosati. 1988. A quasi-equilibrium turbulent energy model for geophysical flows. *J. Atmos. Sci.* 45:55-62.

GeoSea Consulting. 1994. Sediment transport in Elliott Bay and the Duwamish River, Seattle: Implications to estuarine management.

Hamrick, J.M. 1979. Salinity intrusion and gravitational circulation in partially stratified estuaries. Ph.D. dissertation, University of California. Berkeley, California.

Hamrick, J.M. 1990. The dynamics of long-term mass transport in estuaries. *In:* R.T. Cheng, Ed. Springer-Verlag. pages 17-33. Residual Circulation and Long-Term Transport in Estuaries and Shallow Bays. New York, New York.

Hamrick, J.M. 1992. A three-dimensional environmental fluid dynamics computer code: theoretical and computational aspects. The College of William and Mary, Virginia Institute of Marine Science. Special Report 317. Williamsburg, Virginia.

Hamrick, J.M. 1996. A user's manual for the environmental fluid dynamics computer code (EFDC). The College of William and Mary, Virginia Institute of Marine Science, Special Report 331. Williamsburg, Virginia.

Hamrick, J.M. 1998. Personal Communication. Senior Modeler, Tetra Tech. Inc. Arlington, Virginia.

Hamrick, J.M. and T.S. Wu. 1997. Computational design and optimization of the EFDC/HEM3D surface water hydrodynamic and eutrophication models. Pages 143-156. *In:* G. Delich and M.F. Wheeler, Eds. Next Generation Environmental Models and Computational Methods, Society of Industrial and Applied Mathematics. Philadelphia, Pennsylvania.

Herrera Environmental Consultants. 1997. Denny Way/Lake Union CSO control project. Prepared for King County. Seattle, Washington.

Hess, K. and K. Bosley. 1992: Methodology for validation of a Tampa Bay circulation model. pages 32-94. *In:* M.L. Spaulding et al., Eds. Estuarine and Coastal Modeling, Proceedings of the 2nd International Conference. American Society of Civil Engineers. New York, New York.

Hofelt, C.S. and D. Shea. 1997. Accumulation of organochlorine pesticides and PCBs by semipermeable membrane devices and *Mytilus edulis* in New Bedford Harbor. Environ. Sci. Technol., 31, No. 1.

Howard, P.H., R.S. Boething, W.F. Jarvis, W.M. Meylan, E.M. Michalenko. 1991. Environmental degradation rates. Lewis Publishers Inc. Chelsea, Michigan.

King County Department of Natural Resources, Water Pollution Control Division (King County). 1996. Evaluating hydrodynamic and contaminate transport computer models. Seattle, Washington.

Lavelle, J.W., G.J. Massoth, and E.A. Crecelius. 1985. Sedimentation rates in Puget Sound from Pb^{210} measurements. NOAA Technical Memorandum ERL PMEL-61. Pacific Marine Environmental Laboratory. Seattle, Washington.

Lefkovitz, L.F. and E.A. Crecelius. 1995. Use of semipermeable membrane devices to monitor PAHs and PCBs in Elliott Bay, Seattle, Washington. Puget Sound Research 1995, Vol. 1, pg 372-376. Puget Sound Water Quality Authority. Olympia, Washington.

Leon, H. 1980. Terminal 107 environmental studies benthic community impact study for Terminal 107 (Kellogg Island) and vicinity. Prepared for Port of Seattle by Pacific Rim Planners, Inc. Seattle, Washington.

Liou, J.Y. and W.S. Chu. 1991. Numerical modeling of tides and currents in central Puget Sound and Elliott Bay. Technical Report No. 128. University of Washington, Department of Civil Engineering, Environmental Sciences. Seattle, Washington.

Meador, J.P. 1997. Comparative toxicokinetics of tributyltin in five marine species and its utility in predicting bioaccumulation and acute toxicity. Aquatic Toxicology. 37:307-326.

Mellor, G.L. and T. Yamada. 1982. Development of a turbulence closure model for geophysical fluid problems. *Rev. Geophys. Space Phys.* 20:851-875.

Municipality of Metropolitan Seattle (Metro). 1987. Duwamish Head baseline study. Seattle, Washington.

Neff, J.M. and W.A. Burns. 1996. Estimation of polycyclic aromatic hydrocarbon concentrations in the water column based on tissue residues in mussels and salmon: An equilibrium partitioning approach. Environ. Toxi. And Chem. Vol. 15, No. 12.

Norman, D.M., I. Moul, and A. Breault. 1989. Bald eagle incursions and predation in great blue heron colonies. Colonial Waterbirds. 12:215-217.

Oey, L.Y., G.L. Mellor, and R.I. Hires. 1985. A three-dimnesional simulation of the Hudson-Raritan estuary. Part II: Comparison with observation. *J. Phys. Ocean*. 15:1693-1709.

Peene, S., E. Yassuda, and D. Mendolsohn. 1998. Development of a waste load allocation model within Charleston Harbor estuary. Phase I: Barotropic circulation. pages 211-230. *In:* M.L. Spaulding and A.F. Blumberg, Eds. Estuarine and Coastal Modeling, Proceedings of the 5th International Conference. American Society of Civil Engineers. New York, New York.

Press, W.H., S.A. Teukolsky, W.T. Vetterling, and B.P. Flannery. 1992. Numerical recipes in FORTRAN, 2nd edition. Cambridge Unviersity Press. Cambridge, UK.

Ryskin, G. and L.G. Leal. 1983. Orthogonal mapping. *J. Comp. Phys.* 50:71-100.

Science Application International Corp. (SAIC). 1991. Untitled report prepared for the U.S. Army Corps of Engineers regarding PSDDA requirements for 1989. Unpublished.

Shen, J. M. Sisson, A. Kuo, J. Boon, and S. Kim. 1998. Three-dimensional numerical modeling of the tidal York River System, Virginia. *In:* M.L. Spaulding and A.F. Blumberg, Eds. Estuarine and Coastal Modeling, Proceedings of the 5th International Conference. American Society of Civil Engineers. New York, New York.

Sillcox, R.L., W.R. Geyer, and G.A. Cannon. 1981. Physical transport processes and circulation in Elliott Bay. NOAA Technical Memorandum OMPA-8. Office of Marine Pollution. Boulder, Colorado.

Stober, Q.J. and K.K. Chew. 1984. Renton treatment plant project Seahurst baseline study for the Municipality of Metropolitan Seattle. Seattle, Washington.

Strand, J.K., K. Stark, K. Silver, C. Laetz, T. Georgianna, D. McElhany, K. Li, S. Mickelson. 1998. Bioaccumulation of chemical contaminants in transplanted and wild mussels in the Duwamish River Estuary, Puget Sound Washington. *In:* Proceedings of Puget Sound Research '98. Puget Sound Water Quality Action Team. March 12-13. Seattle, Washington.

Thomann, R.V. 1982. Verification of water quality models. *J. Environ. Engrg. Div., ASCE*. 108:923-940.

Thomann, R.V. and J.A. Mueller. 1987. Principles of surface water quality modeling and control. Harper & Row. New York, New York.

U.S. Army Corps of Engineers (ACOE). 1981. Duwamish Waterways Navigation Improvement Study. U.S. Army Corps of Engineers. Seattle, Washington.

U.S. EPA. 1990. Technical guidance manual for performing waste load allocations. Book III Estuaries, Part 2, Application of estuarine waste load allocation models. EPA 823-R-92-003.

Vemulakonda, S.R. and N.W. Scheffner. 1994. Demonstration of the WES New York Bight hydrodynamic model in Long Island Sound. pages 309-332. *In:* M.L. Spaulding et al., Eds. Estuarine and Coastal Modeling, Proceedings of the 3rd International Conference. American Society of Civil Engineers. New York, New York.

Willmott, C.J. 1982. Some comments on the evaluation of model performance. *Bull. Am. Meteor. Soc*. 63:1309-1313.

Willmott, C.J., S.G. Ackleson, R.E. Davis, J.J. Feddema, K.M. Klink, D. Legates, J. O'Donnell, and C.M. Rowe. 1985. Statistics for the evaluation and comparison of models. *J. Geophys. Res*. 90:8995-9005.

SUBAPPENDIX A

CSO AND STORMWATER CHEMICAL CHARACTERISTICS

Table A-1. Initial Chemical Concentrations for Other Sources

Stormwater										
Source (mg/l)	**Arsenic**	**Cadmium**	**Copper**	**Lead**	**Nickel**	**Zinc**	**Mercury (ng/l)**	**TBT (µg/l)**	**Fecal Coliform (c/100ml)**	
Longfellow	0.00166	0.000703	0.00305	0.00237	0.0027	0.0097		0.011		
Hamm	0.0056	0.00085	0.0195	0.0289	0.0085	0.173		0.011		
Densmore	0.00268	0.000577	0.0148	0.0301	0.00533	0.100		0.011		
Arith Mean	0.00405	0.000738	0.0154	0.0248	0.00663	0.125	54.0 (CSO)	0.011	1100	
Source (µg/l)	**Bis(2-ethylhexl) phthalate**	**Chrysene**	**Fluoranthene**	**Phenanthrene**	**Pyrene**	**1,4-Dichloro benzene**	**4-Methyl phenol**	**Benzo(b) fluoranthene**	**Benzo(k) fluoranthene**	**Total PCB**
CSO	4.35	0.242	0.429	0.438	0.363	0.382	5.61	0.239	0.207	0.84
Hamm Creek	2.22		0.146	3.85	0.588	0.146	2.31			

Table A-2. Arithmetic Mean Chemical Concentrations for CSO

Source (mg/l)	Arsenic	Cadmium	Copper	Lead	Nickel	Zinc	Mercury (ng/l)	TBT (µg/l)	Similar Basin Type
Denny	2.44E-03	3.34E-04	4.42E-02	2.51E-02	4.82E-03	0.105	54.0	0.0	
King Street	2.00E-03	3.26E-04	4.58E-02	1.50E-02	2.30E-03	0.133	54.0	0.0	
Connecticut	2.31E-03	5.78E-04	3.83E-02	3.90E-02	8.30E-03	0.167	54.0	0.0	
Hanford	2.13E-03	4.40E-04	2.58E-02	2.10E-02	6.00E-03	0.109	54.0	0.0	
Lander	2.13E-03	4.40E-04	2.58E-02	2.10E-02	6.00E-03	0.109	54.0	0.0	Hanford
Harbor	3.33E-03	3.43E-04	2.32E-02	2.70E-02	7.90E-03	0.097	54.0	0.0	Chelan
Chelan	3.33E-03	3.43E-04	2.32E-02	2.70E-02	7.90E-03	0.097	54.0	0.0	
Brandon	3.40E-03	1.17E-03	4.87E-02	5.60E-02	1.60E-02	0.227	54.0	0.0	
8th Avenue	3.33E-03	3.43E-04	2.32E-02	2.70E-02	7.90E-03	0.097	54.0	0.0	Chelan
SW Michigan	3.40E-03	1.17E-03	4.87E-02	5.60E-02	1.60E-02	0.227	54.0	0.0	Brandon
Norfolk	3.33E-03	3.43E-04	2.32E-02	2.70E-02	7.90E-03	9.70E-02	54.0	0.0	Chelan
S. Magnolia	3.33E-03	3.43E-04	2.32E-02	2.70E-02	7.90E-03	9.70E-02	54.0	0.0	Chelan

Table A-2. Arithmetic Mean Chemical Concentrations for CSOs (continued)

Source (µg/l)	Bis(2-ethylhexl) phthalate	Chrysene	Fluoranthene	Phenanthrene	Pyrene	1,4-Dichloro benzene	4-Methyl phenol	Benzo(b) fluoranthene	Benzo(k) fluoranthene	Total PCB
Denny	3.17	0.216	0.483	0.464	0.385	0.335	1.18	0.015	0.0005	0.0
King St.	7.16	0.177	0.204	0.219	0.227	0.27	16.3	0.015	0.0005	0.0
Connecticut	6.28	0.576	0.931	0.873	0.736	0.423	5.89	0.015	0.0005	0.0
Hanford	4.92	0.18	0.255	0.346	0.22	0.404	15.8	0.015	0.0005	0.0
Lander	4.92	0.18	0.255	0.346	0.22	0.404	15.8	0.015	0.0005	0.0
Harbor	3.17	0.216	0.483	0.464	0.385	0.335	1.18	0.015	0.0005	0.0
Chelan	3.17	0.216	0.483	0.464	0.385	0.335	1.18	0.015	0.0005	0.0
Brandon	4.95	0.249	0.307	0.347	0.322	0.539	3.26	0.015	0.0005	0.0
8th Ave.	3.17	0.216	0.483	0.464	0.385	0.335	1.18	0.015	0.0005	0.0
S/W Michigan	4.95	0.249	0.307	0.347	0.322	0.539	3.26	0.015	0.0005	0.0
Norfolk	3.17	0.216	0.483	0.464	0.385	0.335	1.18	0.015	0.0005	0.0
S. Magnolia	3.17	0.216	0.483	0.464	0.385	0.335	1.18	0.015	0.0005	0.0

Table A-3. Final Other Sources Chemical Concentrations from the Mass Calibration

Source (µg/l)	Arsenic	Cadmium	Copper	Lead	Nickel	Zinc	Mercury (ng/l)	TBT	Fecal Coliform (c/100ml)
Eastside Inputs									
Pre-Julian day 400	4.64	0.95	22	22.8	0.0	134	5.4	0.0	1400
Post-Julian day 400	3.9	0.95	22	10.8	0.0	70.8	5.4	0.0	
Westside Inputs									
Pre-Julian day 400	4.64	0.9	22	26.2	7.1	156.8	5.4	0.0	900
Post-Juilan day 400	3.9	0.9	22	20.9	7.1	114	5.4	0.0	

Organic										
Source (µg/l)	**Bis(2-ethylhexl)**	**Chrysene**	**Fluoranthene**	**Phenanthrene**	**Pyrene**	**1,4 Dichloro-benzene**	**4-Methyl phenol**	**Benzo(b) fluoranthene**	**Benzo(k) fluoranthene**	**Total PCB**
Eastside	2.22	0.06	0.43	1.44	3.59	0.15	2.32	0.015	0.0005	0.0
Westside	1.11	0.06	0.43	1.44	3.59	0.15	2.32	0.015	0.0005	0.0

Table A-4. Final Fecal Coliform Counts From The Mass Calibration

Source	Fecal Coliform (count/100ml)
Denny	$2.8x10^6$
King Street	$3.8x10^5$
Connecticut	$1.4x10^5$
Hanford	$3.8x10^4$
Lander	$3.8x10^4$
Harbor	$1.4x10^5$
Chelan	$1.4x10^5$
Brandon	$3.6x10^4$
8th Avenue	$1.4x10^5$
S/W Michigan	$1.5x10^4$
Norfolk	$1.4x10^5$
S. Magnolia	$1.4x10^5$

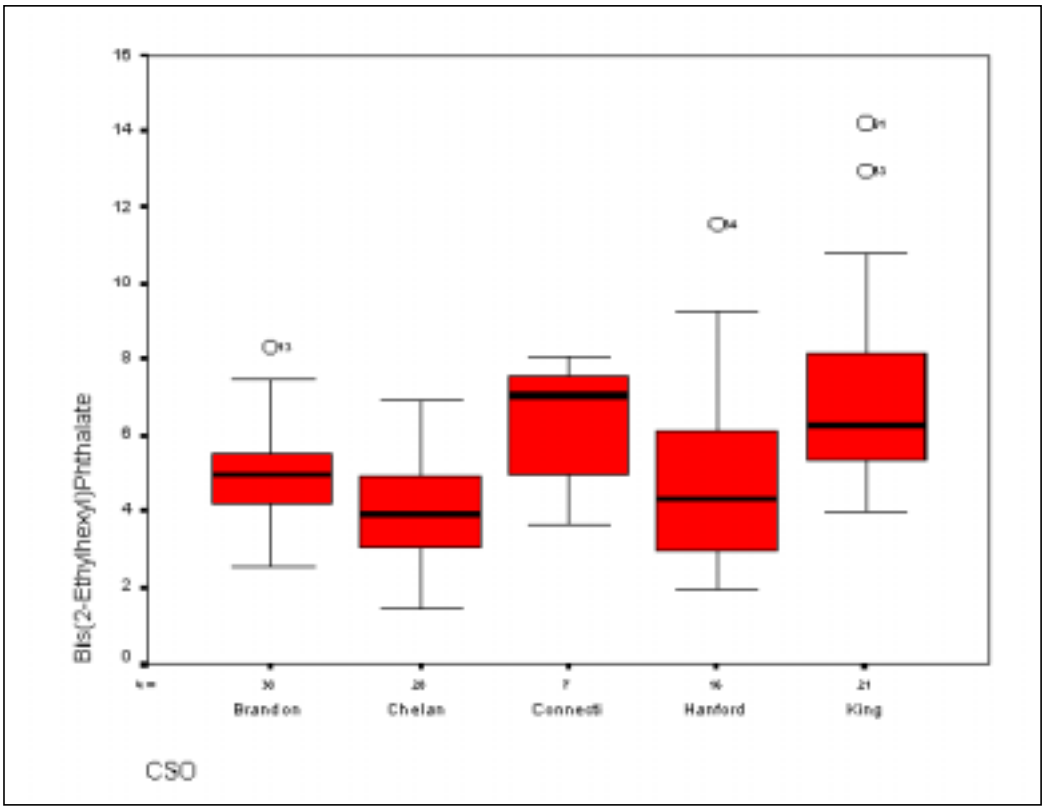

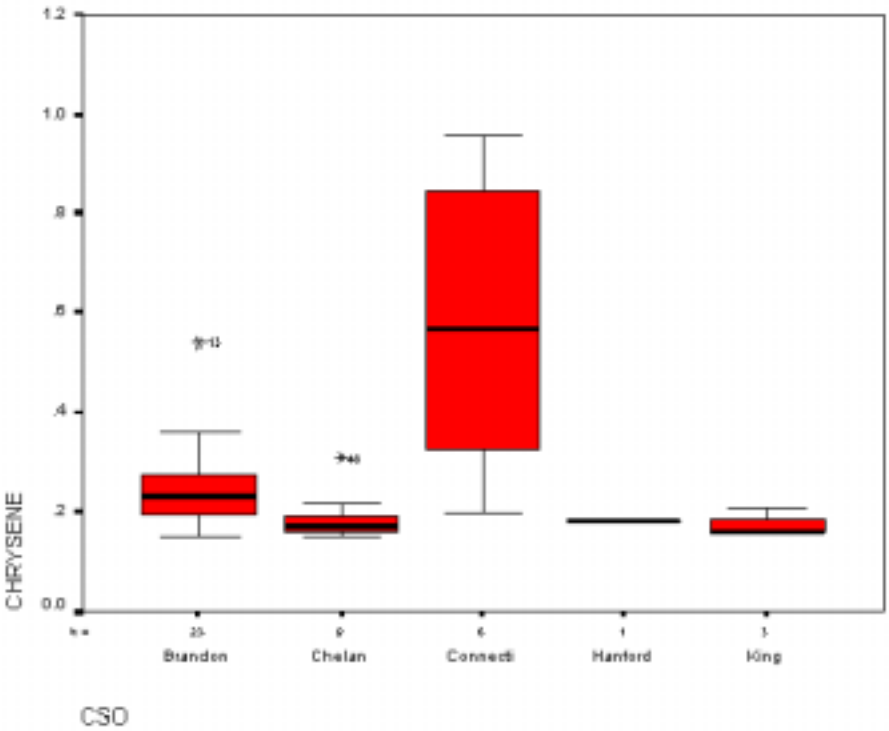

Note: box plots show cso statistics median, 25th and 75th percentile, and maximum minimum (organic (ug/l), metals (mg/l))

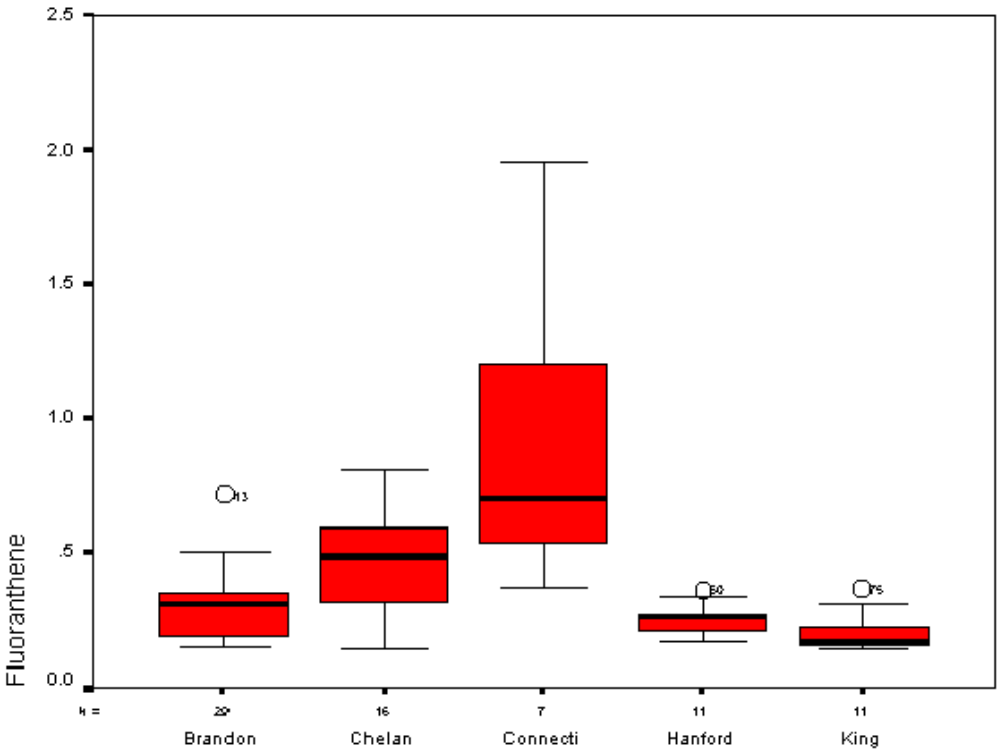

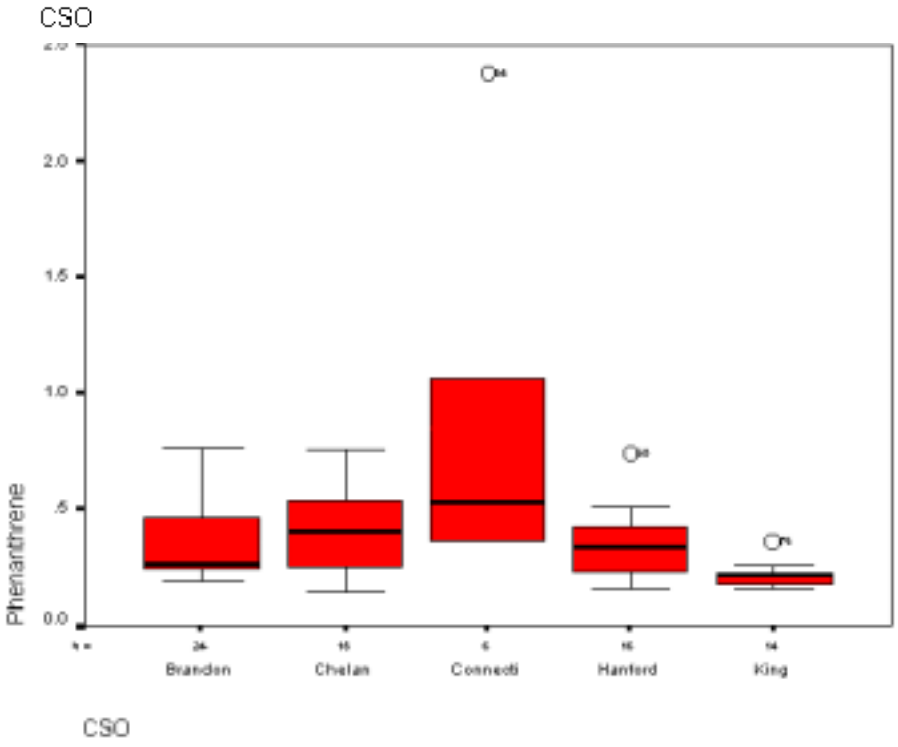

Note: Box plots show CSO statistics median, 25th and 75th percentile, and maximum minimum (Organic (ug/l), Metals (mg/l))

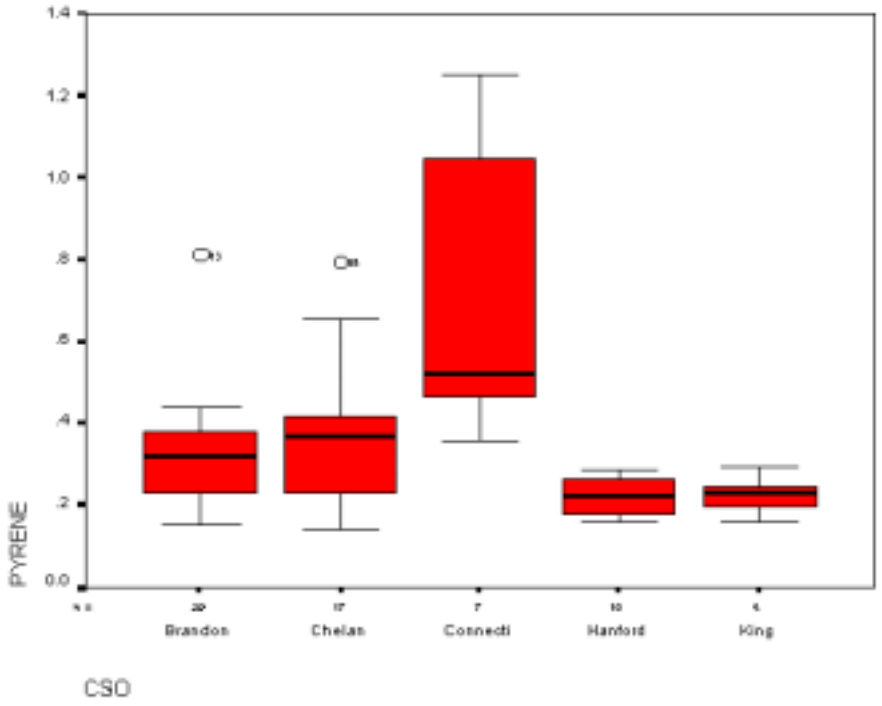

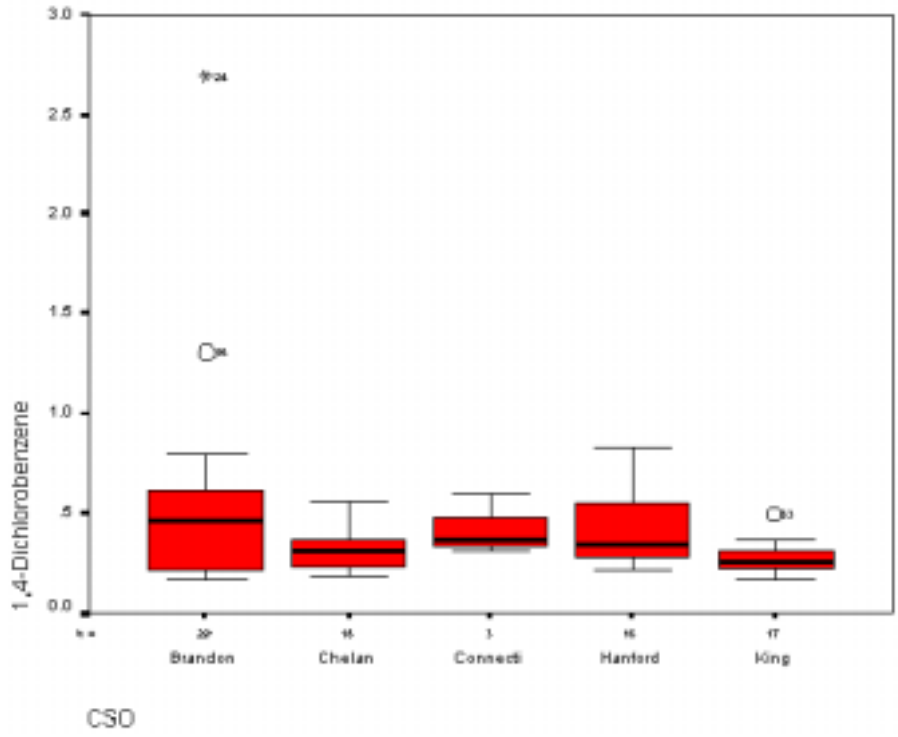

Note: Box plots show CSO statistics median, 25th and 75th percentile, and maximum minimum (Organic (ug/l), Metals (mg/l))

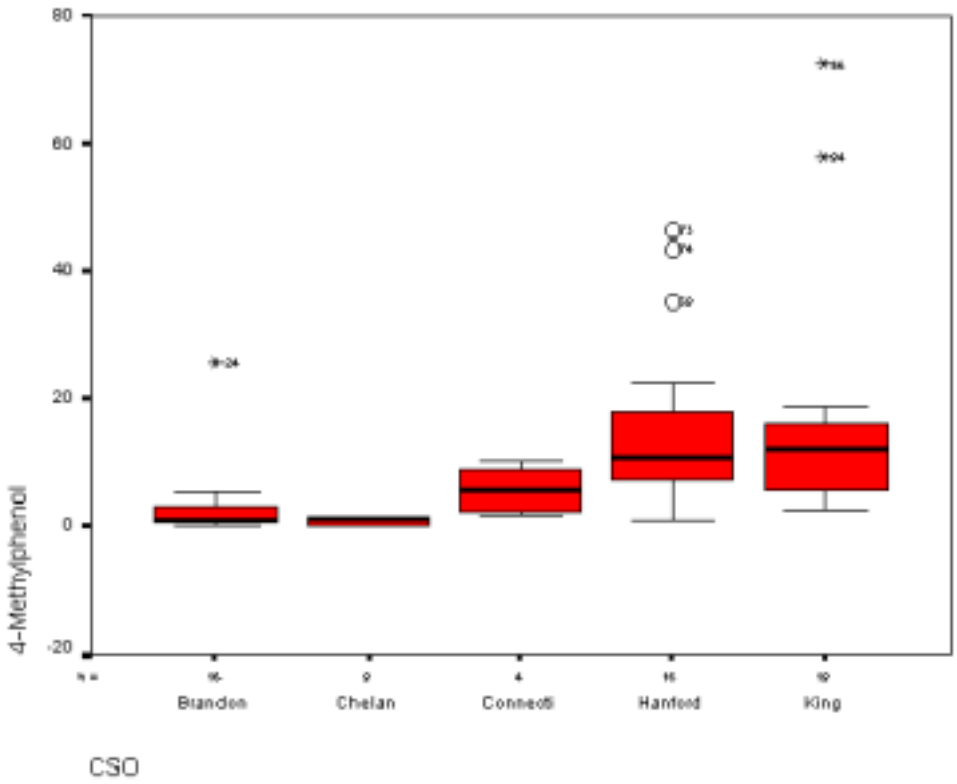

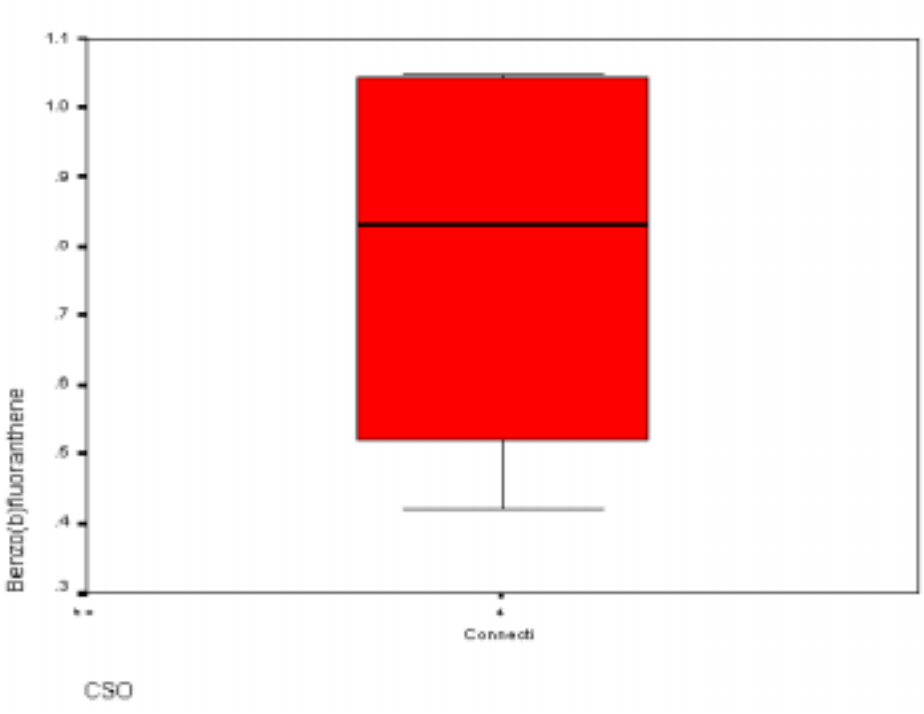

Note: Box plots show CSO statistics median, 25th and 75th percentile, and maximum minimum (Organic (ug/l), Metals (mg/l))

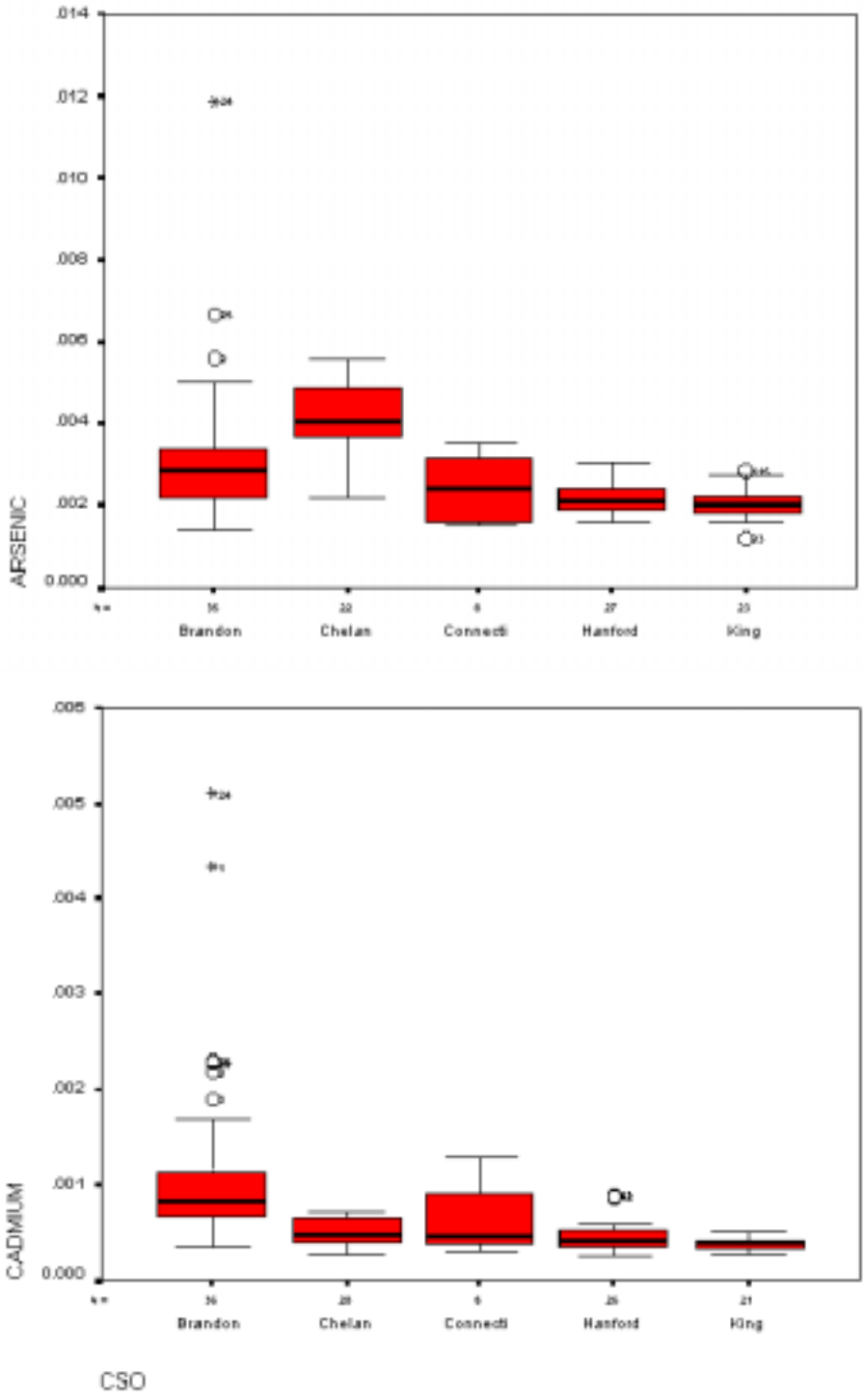

Note: Box plots show CSO statistics median, 25th and 75th percentile, and maximum minimum (Organic (ug/l), Metals (mg/l))

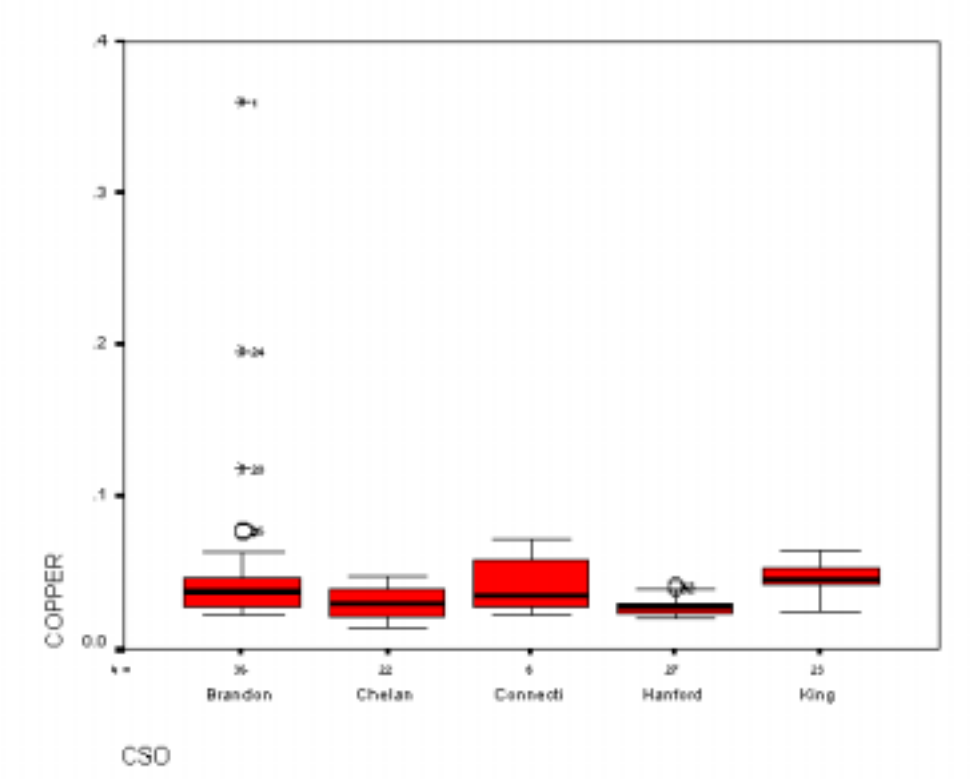

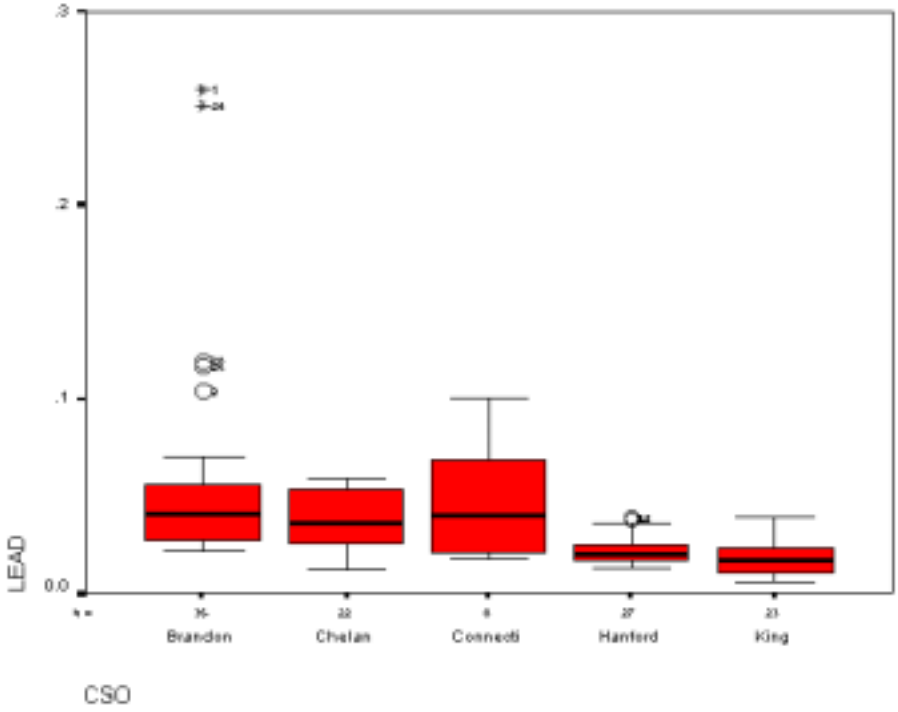

Note: Box plots show CSO statistics median, 25th and 75th percentile, and maximum minimum (Organic (ug/l), Metals (mg/l))

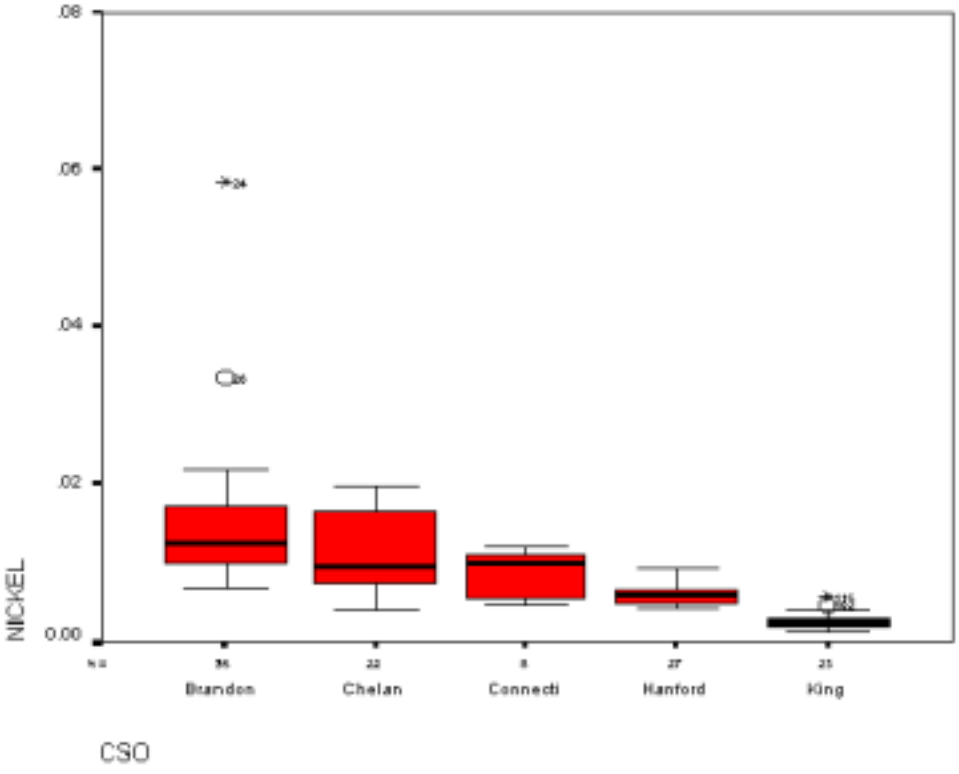

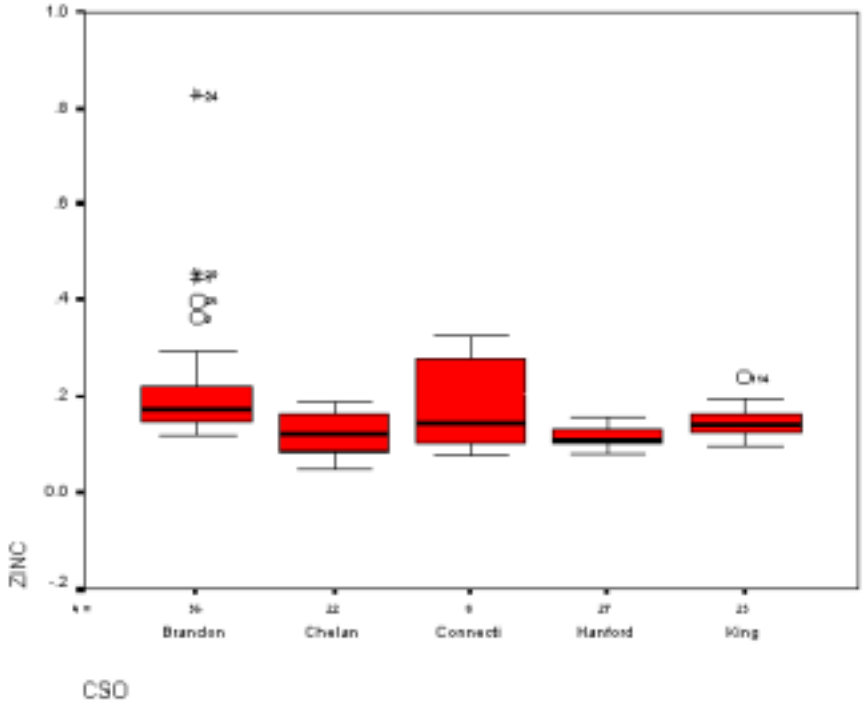

Note: Box plots show CSO statistics median, 25th and 75th percentile, and maximum minimum (Organic (ug/l), Metals (mg/l))

SUBAPPENDIX B

WATER SURFACE ELEVATION TIME SERIES PLOTS

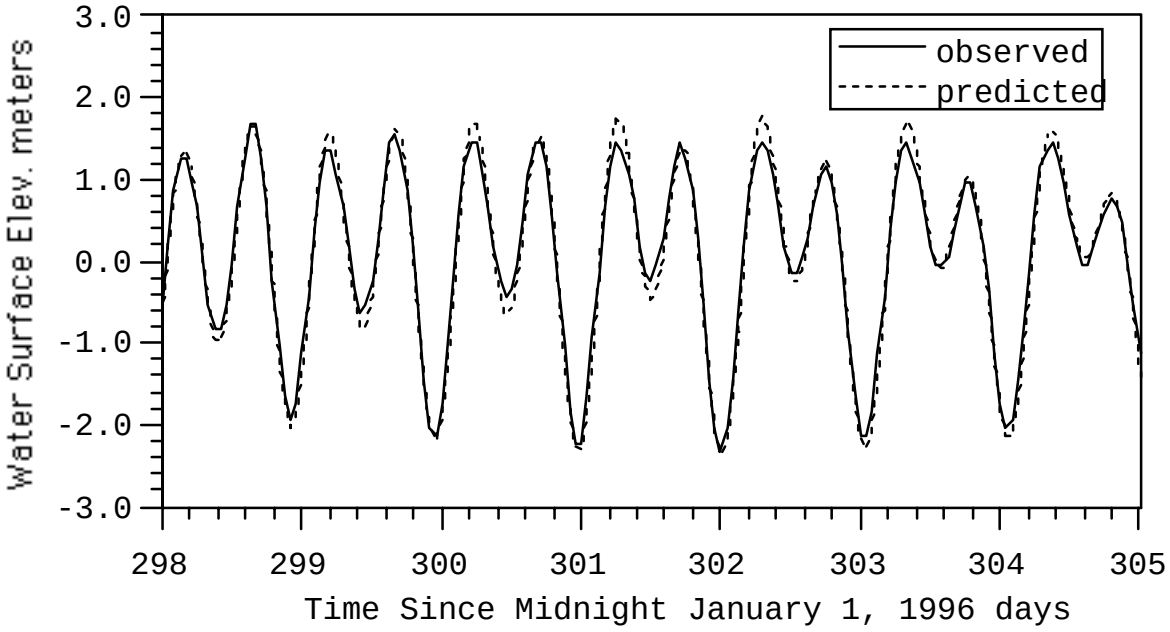

Figure B-1. Water Surface Elevation at Duwamish Yacht Club

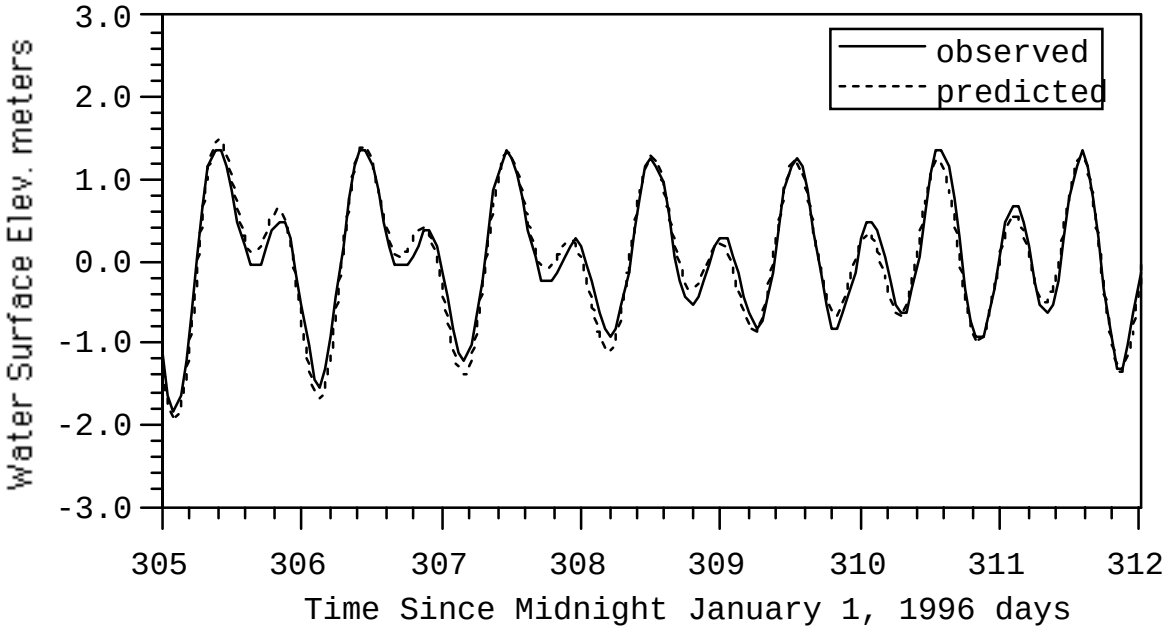

Figure B-2. Water Surface Elevation at Duwamish Yacht Club

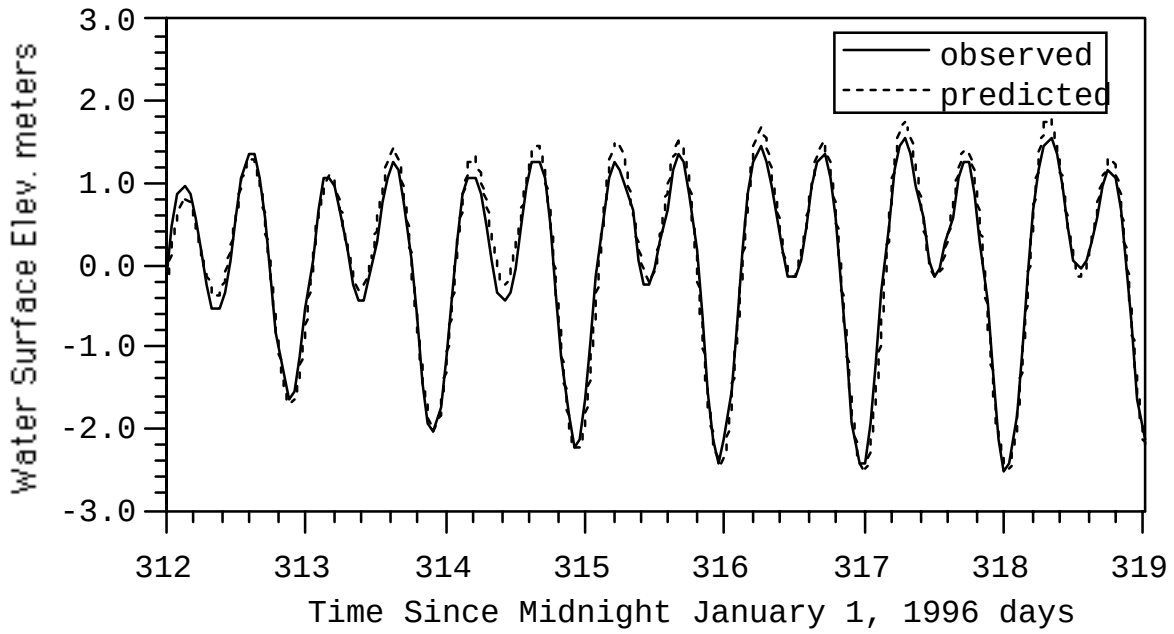

Figure B-3. Water Surface Elevation at Duwamish Yacht Club

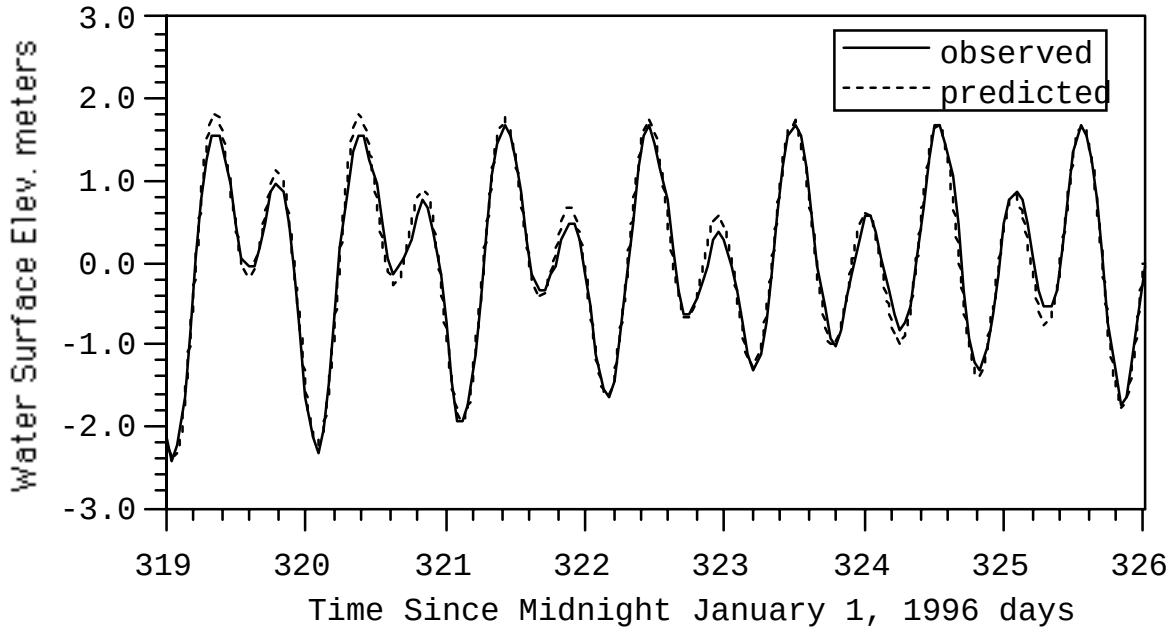

Figure B-4. Water Surface Elevation at Duwamish Yacht Club

SUBAPPENDIX C

VELOCITY HARMONIC ANALYSIS

INTRODUCTION

This appendix presents the results for least squares harmonic analysis of observed and model predicted horizontal currents at the ARC, BOE, SBW, Deep101 and Deep201 stations. The results are presented in tidal current ellipse format. Results for observed current in layers one and ten for the ARC, BOE, and SBW stations are questionable. For the two deep stations, results are not presented for layers one, nine and ten. The notation in the summary tables is as follows.

U MEAN	Mean across channel velocity (ARC, BOE, SBW) Mean eastward velocity (Deep101 and Deep201)
V MEAN	Mean along channel velocity, + seaward (ARC, BOE, SBW) Mean northward velocity (Deep101 and Deep201)
SYMBOL	Tidal constituent symbol
TCP	Period of tidal constituent, seconds
MAJ	Amplitude of major velocity ellipse axis, cm/sed
MIN	Amplitude of minor velocity ellipse axis, cm/sed
ANG	Major axis orientation angle, + counterclockwise 90 indicates along channel (ARC, BOE, SBW) Counter clockwise from east (Deep101 and Deep102)
PHE SEC	Time phase at which velocity vector aligns with major axis

c ARC observed layer 1

U MEAN=	-0.46	V MEAN=	-4.20		
SYMBOL	TCP	MAJ	MIN	ANG	PHE SEC
M2	44714.16	4.49	0.05	78.44	7504.14
S2	43200.00	1.14	0.07	73.00	24925.09
N2	45570.05	0.84	0.12	76.36	19449.91
K1	86164.09	1.78	0.06	72.00	45827.27
O1	92949.63	2.11	0.03	75.35	22737.50

c ARC predicted layer 1

U MEAN=	0.00	V MEAN=	-0.56		
SYMBOL	TCP	MAJ	MIN	ANG	PHE SEC
M2	44714.16	3.14	0.06	96.43	10229.76
S2	43200.00	0.60	0.02	94.98	24987.96
N2	45570.05	0.64	0.00	92.92	22982.58
K1	86164.09	0.91	0.00	93.89	52121.09
O1	92949.63	0.47	0.01	92.69	31719.21

c ARC observed layer 2

U MEAN=	-0.70	V MEAN=	-6.82		
SYMBOL	TCP	MAJ	MIN	ANG	PHE SEC
M2	44714.16	6.93	0.20	80.24	8403.49
S2	43200.00	1.77	0.14	81.43	25117.85
N2	45570.05	1.25	0.25	75.56	19084.80
K1	86164.09	2.66	0.00	75.15	45776.15
O1	92949.63	3.00	0.10	78.85	22506.66

c ARC predicted layer 2

U MEAN=	-0.08	V MEAN=	-0.33		
SYMBOL	TCP	MAJ	MIN	ANG	PHE SEC
M2	44714.16	5.12	0.01	92.13	11817.14
S2	43200.00	0.82	0.03	93.67	25915.82
N2	45570.05	0.87	0.02	94.34	23903.04
K1	86164.09	1.48	0.01	93.29	53789.98
O1	92949.63	0.70	0.00	95.61	33381.04

c ARC observed layer 3

U MEAN=	-0.54	V MEAN=	-6.62		
SYMBOL	TCP	MAJ	MIN	ANG	PHE SEC
M2	44714.16	7.31	0.05	80.96	9610.92
S2	43200.00	1.83	0.02	91.67	25336.80
N2	45570.05	1.34	0.35	71.06	18685.29
K1	86164.09	2.78	0.04	74.84	46149.21
O1	92949.63	2.74	0.07	83.15	21992.40

c ARC predicted layer 3

U MEAN=	-0.12	V MEAN=	0.08		
SYMBOL	TCP	MAJ	MIN	ANG	PHE SEC
M2	44714.16	6.02	0.07	91.56	13003.04
S2	43200.00	1.20	0.02	91.13	27801.90
N2	45570.05	1.14	0.03	91.96	24562.13
K1	86164.09	1.88	0.00	93.34	55212.94
O1	92949.63	0.89	0.02	96.65	35709.46

c ARC observed layer 4

U MEAN=	-0.40	V MEAN=	-5.51		
SYMBOL	TCP	MAJ	MIN	ANG	PHE SEC
M2	44714.16	7.45	0.61	82.77	10507.79
S2	43200.00	1.73	0.24	94.89	26087.19
N2	45570.05	1.45	0.50	74.35	18385.51
K1	86164.09	2.61	0.23	74.89	47176.85
O1	92949.63	2.09	0.04	91.28	21983.88

c ARC predicted layer 4

U MEAN=	-0.09	V MEAN=	0.30		
SYMBOL	TCP	MAJ	MIN	ANG	PHE SEC
M2	44714.16	6.34	0.10	92.01	13525.35
S2	43200.00	1.46	0.00	93.13	28849.23
N2	45570.05	1.37	0.01	91.83	24945.08
K1	86164.09	2.15	0.04	93.13	55018.66
O1	92949.63	1.13	0.06	91.81	35862.16

c ARC observed layer 5

U MEAN=	-0.35	V MEAN=	-3.84		
SYMBOL	TCP	MAJ	MIN	ANG	PHE SEC
M2	44714.16	7.41	1.08	84.31	11343.61
S2	43200.00	1.81	0.52	97.74	27167.43
N2	45570.05	1.45	0.74	78.41	18000.70
K1	86164.09	2.44	0.54	77.85	49371.27
O1	92949.63	1.36	0.02	101.12	21594.68

c ARC predicted layer 5

U MEAN=	-0.02	V MEAN=	0.18		
SYMBOL	TCP	MAJ	MIN	ANG	PHE SEC
M2	44714.16	6.39	0.17	92.18	13519.20
S2	43200.00	1.65	0.00	93.34	28880.76
N2	45570.05	1.51	0.01	93.12	24806.35
K1	86164.09	2.15	0.05	89.14	53154.76
O1	92949.63	1.37	0.05	88.66	33357.77

c ARC observed layer 6

U MEAN=	-0.49	V MEAN=	-1.65		
SYMBOL	TCP	MAJ	MIN	ANG	PHE SEC
M2	44714.16	7.35	1.21	85.45	12229.94
S2	43200.00	1.98	0.61	99.56	27911.47
N2	45570.05	1.40	0.98	95.37	16061.43
K1	86164.09	2.62	0.71	83.60	53141.07
O1	92949.63	0.98	0.15	119.76	19835.74

c ARC predicted layer 6

U MEAN=	-0.14	V MEAN=	0.73		
SYMBOL	TCP	MAJ	MIN	ANG	PHE SEC
M2	44714.16	6.76	0.17	93.93	15173.36
S2	43200.00	1.94	0.06	91.93	29841.66
N2	45570.05	1.46	0.00	92.06	26358.95
K1	86164.09	2.89	0.05	96.49	55259.10
O1	92949.63	1.41	0.03	97.28	37032.73

c ARC observed layer 7

U MEAN=	-0.59	V MEAN=	1.23		
SYMBOL	TCP	MAJ	MIN	ANG	PHE SEC
M2	44714.16	7.93	1.19	85.09	13213.46
S2	43200.00	2.17	0.51	96.95	28665.16
N2	45570.05	1.40	1.13	118.91	13196.74
K1	86164.09	3.23	0.72	84.10	56908.27
O1	92949.63	0.86	0.24	148.81	15397.88

c ARC predicted layer 7

U MEAN=	-0.09	V MEAN=	-0.50		
SYMBOL	TCP	MAJ	MIN	ANG	PHE SEC
M2	44714.16	7.64	0.03	92.25	16016.19
S2	43200.00	2.28	0.04	92.78	30101.41
N2	45570.05	1.42	0.01	93.31	27934.16
K1	86164.09	3.20	0.07	91.66	55607.57
O1	92949.63	1.18	0.02	89.49	36397.97

c ARC observed layer 8

U MEAN=	-0.76	V MEAN=	5.51		
SYMBOL	TCP	MAJ	MIN	ANG	PHE SEC
M2	44714.16	9.73	0.84	81.16	14024.05
S2	43200.00	2.69	0.21	91.07	30532.24
N2	45570.05	1.92	1.15	142.72	10041.37
K1	86164.09	4.41	0.88	84.81	60729.90
O1	92949.63	1.26	0.28	26.14	55425.09

c ARC predicted layer 8

U MEAN=	-0.25	V MEAN=	0.67		
SYMBOL	TCP	MAJ	MIN	ANG	PHE SEC
M2	44714.16	9.24	0.17	93.08	17158.40
S2	43200.00	2.77	0.07	92.90	32429.30
N2	45570.05	1.84	0.01	92.94	30684.03
K1	86164.09	4.03	0.05	94.54	55832.17
O1	92949.63	1.27	0.02	96.00	37486.49

c ARC observed layer 9

U MEAN=	-0.75	V MEAN=	14.19		
SYMBOL	TCP	MAJ	MIN	ANG	PHE SEC
M2	44714.16	13.35	0.01	84.22	14453.65
S2	43200.00	3.60	0.11	88.73	32718.71
N2	45570.05	1.83	1.52	90.25	18578.93
K1	86164.09	6.23	0.77	88.45	62178.24
O1	92949.63	1.96	0.06	74.02	45544.40

c ARC predicted layer 9

U MEAN=	-0.42	V MEAN=	6.74		
SYMBOL	TCP	MAJ	MIN	ANG	PHE SEC
M2	44714.16	10.83	0.03	93.57	17535.96
S2	43200.00	2.81	0.01	93.12	33906.49
N2	45570.05	2.08	0.01	93.20	29087.32
K1	86164.09	4.25	0.00	92.52	53655.06
O1	92949.63	0.39	0.02	86.89	42228.27

c ARC observed layer 10

U MEAN=	-1.31	V MEAN=	41.52		
SYMBOL	TCP	MAJ	MIN	ANG	PHE SEC
M2	44714.16	14.53	0.04	88.54	14394.66
S2	43200.00	4.89	0.16	88.63	33740.08
N2	45570.05	3.09	0.72	88.91	22740.65
K1	86164.09	7.62	0.74	92.74	65580.56
O1	92949.63	1.81	0.46	86.09	35140.89

c ARC predicted layer 10

U MEAN=	-0.87	V MEAN=	20.13		
SYMBOL	TCP	MAJ	MIN	ANG	PHE SEC
M2	44714.16	14.26	0.10	92.93	19666.10
S2	43200.00	4.10	0.06	92.64	36030.98
N2	45570.05	2.15	0.03	92.52	34194.33
K1	86164.09	7.51	0.03	92.46	58082.74
O1	92949.63	2.75	0.03	92.80	36395.60

c BOE observed layer 1

U MEAN=	0.02	V MEAN=	0.00		
SYMBOL	TCP	MAJ	MIN	ANG	PHE SEC
M2	44714.16	0.42	0.04	97.24	16074.02
S2	43200.00	0.10	0.01	93.00	8112.85
N2	45570.05	0.26	0.03	98.42	25845.99
K1	86164.09	0.21	0.02	95.16	1578.79
O1	92949.63	0.29	0.00	98.96	23889.11

c BOE predicted layer 1

U MEAN=	-0.23	V MEAN=	-0.95		
SYMBOL	TCP	MAJ	MIN	ANG	PHE SEC
M2	44714.16	3.36	0.27	86.17	9460.22
S2	43200.00	0.92	0.04	86.39	22181.07
N2	45570.05	1.00	0.04	84.48	25865.75
K1	86164.09	1.11	0.11	89.98	60052.08
O1	92949.63	0.84	0.12	85.07	57849.18

c BOE observed layer 2

U MEAN=	0.59	V MEAN=	-2.59		
SYMBOL	TCP	MAJ	MIN	ANG	PHE SEC
M2	44714.16	23.87	0.28	98.71	12228.22
S2	43200.00	4.88	0.09	98.91	30591.12
N2	45570.05	2.64	0.05	99.18	23786.96
K1	86164.09	7.53	0.06	98.91	56271.49
O1	92949.63	2.85	0.03	97.42	30405.14

c BOE predicted layer 2

U MEAN=	-0.33	V MEAN=	-1.61		
SYMBOL	TCP	MAJ	MIN	ANG	PHE SEC
M2	44714.16	10.12	0.07	85.58	10821.21
S2	43200.00	1.75	0.04	84.09	27563.08
N2	45570.05	1.50	0.00	86.49	23320.80
K1	86164.09	3.39	0.11	84.96	52903.41
O1	92949.63	1.95	0.18	85.85	37701.86

c BOE observed layer 3

U MEAN=	0.13	V MEAN=	-1.72		
SYMBOL	TCP	MAJ	MIN	ANG	PHE SEC
M2	44714.16	27.70	0.10	98.99	12605.46
S2	43200.00	5.33	0.06	98.78	31130.76
N2	45570.05	3.04	0.16	97.18	23410.35
K1	86164.09	8.44	0.28	96.65	56950.24
O1	92949.63	3.40	0.21	99.21	32293.26

c BOE predicted layer 3

U MEAN=	0.07	V MEAN=	0.56		
SYMBOL	TCP	MAJ	MIN	ANG	PHE SEC
M2	44714.16	17.00	0.05	86.58	12912.55
S2	43200.00	3.46	0.02	85.90	31547.37
N2	45570.05	2.43	0.02	85.84	24159.50
K1	86164.09	6.72	0.03	85.04	59068.11
O1	92949.63	4.53	0.05	84.14	46041.08

c BOE observed layer 4

U MEAN=	-0.22	V MEAN=	-0.18		
SYMBOL	TCP	MAJ	MIN	ANG	PHE SEC
M2	44714.16	31.42	0.38	98.61	13050.22
S2	43200.00	5.69	0.20	99.24	31034.77
N2	45570.05	3.66	0.02	97.72	22550.16
K1	86164.09	9.89	0.39	97.07	58256.90
O1	92949.63	4.05	0.17	97.27	35373.49

c BOE predicted layer 4

U MEAN=	0.17	V MEAN=	1.74		
SYMBOL	TCP	MAJ	MIN	ANG	PHE SEC
M2	44714.16	25.00	0.01	86.64	14671.62
S2	43200.00	4.63	0.01	86.47	32123.49
N2	45570.05	3.31	0.02	86.11	24190.75
K1	86164.09	8.41	0.01	86.72	61289.14
O1	92949.63	5.42	0.02	86.66	51690.71

c BOE observed layer 5

U MEAN=	-0.77	V MEAN=	2.08		
SYMBOL	TCP	MAJ	MIN	ANG	PHE SEC
M2	44714.16	33.78	0.63	98.12	13730.73
S2	43200.00	6.20	0.25	98.69	30549.38
N2	45570.05	4.46	0.08	98.26	21386.14
K1	86164.09	11.32	0.17	99.05	59072.59
O1	92949.63	4.78	0.32	97.76	37037.27

c BOE predicted layer 5

U MEAN=	0.24	V MEAN=	4.21		
SYMBOL	TCP	MAJ	MIN	ANG	PHE SEC
M2	44714.16	31.85	0.06	86.46	15985.94
S2	43200.00	6.35	0.08	86.30	32602.40
N2	45570.05	4.27	0.00	86.56	25697.66
K1	86164.09	10.31	0.05	86.67	60377.85
O1	92949.63	4.83	0.05	87.31	49010.88

c BOE observed layer 6

U MEAN=	-1.61	V MEAN=	7.04		
SYMBOL	TCP	MAJ	MIN	ANG	PHE SEC
M2	44714.16	32.84	0.75	96.02	14621.18
S2	43200.00	6.39	0.26	94.94	30205.20
N2	45570.05	5.29	0.20	95.28	20939.59
K1	86164.09	11.43	0.14	97.85	59237.04
O1	92949.63	5.12	0.74	95.67	35215.34

c BOE predicted layer 6

U MEAN=	0.51	V MEAN=	8.85		
SYMBOL	TCP	MAJ	MIN	ANG	PHE SEC
M2	44714.16	35.52	0.07	86.48	16629.92
S2	43200.00	7.75	0.06	85.99	31969.71
N2	45570.05	5.87	0.01	86.54	26941.51
K1	86164.09	11.90	0.12	86.57	58105.51
O1	92949.63	4.81	0.09	86.51	41763.07

c BOE observed layer 7

U MEAN=	-1.92	V MEAN=	14.89		
SYMBOL	TCP	MAJ	MIN	ANG	PHE SEC
M2	44714.16	28.25	0.37	95.11	14621.74
S2	43200.00	7.10	0.01	91.07	29441.12
N2	45570.05	4.87	0.25	94.92	22408.78
K1	86164.09	10.65	0.20	94.66	58768.29
O1	92949.63	4.82	0.55	92.31	33688.70

c BOE predicted layer 7

U MEAN=	1.00	V MEAN=	15.18		
SYMBOL	TCP	MAJ	MIN	ANG	PHE SEC
M2	44714.16	35.44	0.05	86.39	16693.92
S2	43200.00	8.45	0.06	86.05	31185.61
N2	45570.05	6.74	0.05	86.02	27920.94
K1	86164.09	13.00	0.11	86.09	56009.02
O1	92949.63	5.83	0.09	86.17	35636.51

c BOE observed layer 8

U MEAN=	-2.01	V MEAN=	23.14		
SYMBOL	TCP	MAJ	MIN	ANG	PHE SEC
M2	44714.16	23.52	0.02	94.86	13324.81
S2	43200.00	7.62	0.09	93.79	28739.71
N2	45570.05	4.41	0.04	94.34	24772.25
K1	86164.09	8.64	0.29	94.89	57585.44
O1	92949.63	3.19	0.29	91.61	29491.58

c BOE predicted layer 8

U MEAN=	1.41	V MEAN=	21.69		
SYMBOL	TCP	MAJ	MIN	ANG	PHE SEC
M2	44714.16	32.53	0.02	86.34	16261.22
S2	43200.00	7.93	0.01	86.46	30816.08
N2	45570.05	7.28	0.06	86.54	28513.67
K1	86164.09	12.95	0.07	86.37	53801.20
O1	92949.63	6.59	0.01	86.58	34011.84

c BOE observed layer 9

U MEAN=	-2.17	V MEAN=	28.18		
SYMBOL	TCP	MAJ	MIN	ANG	PHE SEC
M2	44714.16	19.41	0.03	94.63	12520.83
S2	43200.00	6.63	0.03	96.12	28828.71
N2	45570.05	3.68	0.08	94.27	24761.79
K1	86164.09	7.18	0.28	96.94	57619.65
O1	92949.63	2.58	0.26	91.09	25474.64

c BOE predicted layer 9

U MEAN=	1.37	V MEAN=	26.34		
SYMBOL	TCP	MAJ	MIN	ANG	PHE SEC
M2	44714.16	29.09	0.01	86.63	15633.82
S2	43200.00	7.10	0.04	86.92	30819.07
N2	45570.05	7.23	0.01	86.94	28651.85
K1	86164.09	11.43	0.09	86.73	52968.25
O1	92949.63	5.91	0.07	86.37	32998.35

c BOE observed layer 10

U MEAN=	-0.63	V MEAN=	31.97		
SYMBOL	TCP	MAJ	MIN	ANG	PHE SEC
M2	44714.16	16.48	0.23	96.48	12037.76
S2	43200.00	6.37	0.20	97.94	30724.30
N2	45570.05	2.53	0.16	88.97	23199.33
K1	86164.09	6.21	0.45	102.95	59881.73
O1	92949.63	1.91	0.78	87.34	26618.64

c BOE predicted layer 10

U MEAN=	2.38	V MEAN=	30.12		
SYMBOL	TCP	MAJ	MIN	ANG	PHE SEC
M2	44714.16	27.51	0.17	85.84	15093.29
S2	43200.00	6.59	0.02	86.73	30420.73
N2	45570.05	6.58	0.09	86.06	28270.55
K1	86164.09	9.89	0.06	86.20	53095.73
O1	92949.63	4.66	0.01	84.78	32011.69

c SBW observed layer 1

U MEAN=	0.09	V MEAN=	-0.82		
SYMBOL	TCP	MAJ	MIN	ANG	PHE SEC
M2	44714.16	2.19	0.12	91.19	16430.53
S2	43200.00	0.94	0.05	91.20	33480.33
N2	45570.05	0.75	0.07	90.27	26335.84
K1	86164.09	0.95	0.02	91.22	61118.50
O1	92949.63	0.45	0.02	95.79	17837.31

c SBW predicted layer 1

U MEAN=	-0.47	V MEAN=	-1.67		
SYMBOL	TCP	MAJ	MIN	ANG	PHE SEC
M2	44714.16	6.80	0.39	93.08	10679.04
S2	43200.00	1.60	0.04	92.73	26387.28
N2	45570.05	1.73	0.07	91.63	24456.15
K1	86164.09	1.52	0.07	92.47	53505.98
O1	92949.63	0.78	0.05	87.44	37045.05

c SBW layer observed layer 2

U MEAN=	0.17	V MEAN=	-5.72		
SYMBOL	TCP	MAJ	MIN	ANG	PHE SEC
M2	44714.16	24.24	0.29	87.79	11796.07
S2	43200.00	6.93	0.10	87.23	28874.54
N2	45570.05	3.52	0.18	88.52	21278.28
K1	86164.09	7.35	0.01	87.15	54008.87
O1	92949.63	2.94	0.13	90.99	25668.19

c SBW predicted layer 2

U MEAN=	-0.83	V MEAN=	-2.05		
SYMBOL	TCP	MAJ	MIN	ANG	PHE SEC
M2	44714.16	11.78	0.77	91.00	10840.26
S2	43200.00	2.46	0.18	91.13	26421.62
N2	45570.05	1.93	0.11	96.22	23495.17
K1	86164.09	2.51	0.28	92.69	52787.24
O1	92949.63	1.13	0.21	89.67	35368.04

c SBW layer observed layer 3

U MEAN=	0.08	V MEAN=	-5.32		
SYMBOL	TCP	MAJ	MIN	ANG	PHE SEC
M2	44714.16	28.17	0.29	86.21	12136.09
S2	43200.00	7.87	0.02	85.45	29043.63
N2	45570.05	4.27	0.12	85.28	21183.01
K1	86164.09	8.42	0.02	85.70	53881.87
O1	92949.63	3.68	0.13	88.09	26027.19

c SBW predicted layer 3

U MEAN=	-0.80	V MEAN=	-1.98		
SYMBOL	TCP	MAJ	MIN	ANG	PHE SEC
M2	44714.16	15.33	0.47	89.79	11341.83
S2	43200.00	3.30	0.17	89.64	27452.76
N2	45570.05	2.74	0.25	92.10	23748.97
K1	86164.09	3.57	0.31	90.87	52663.06
O1	92949.63	1.60	0.22	91.54	38052.72

c SBW layer observed layer 4

U MEAN=	0.26	V MEAN=	-3.58		
SYMBOL	TCP	MAJ	MIN	ANG	PHE SEC
M2	44714.16	31.78	0.09	84.92	12619.32
S2	43200.00	8.62	0.10	83.99	29201.72
N2	45570.05	4.97	0.04	85.40	21257.03
K1	86164.09	9.57	0.00	84.33	53864.35
O1	92949.63	4.43	0.06	84.42	26716.88

c SBW predicted layer 4

U MEAN=	-0.78	V MEAN=	-2.09		
SYMBOL	TCP	MAJ	MIN	ANG	PHE SEC
M2	44714.16	17.74	0.36	89.28	12265.68
S2	43200.00	4.24	0.08	88.20	28579.86
N2	45570.05	4.13	0.24	90.67	24966.08
K1	86164.09	4.20	0.24	89.97	52387.20
O1	92949.63	1.91	0.16	90.17	36150.66

c SBW layer observed layer 5

U MEAN=	0.49	V MEAN=	-1.00		
SYMBOL	TCP	MAJ	MIN	ANG	PHE SEC
M2	44714.16	34.21	0.15	85.00	13068.64
S2	43200.00	9.11	0.15	84.22	29209.44
N2	45570.05	5.89	0.37	86.01	21632.26
K1	86164.09	10.02	0.20	83.56	54190.20
O1	92949.63	4.79	0.05	80.94	28062.73

c SBW predicted layer 5

U MEAN=	-0.69	V MEAN=	-1.48		
SYMBOL	TCP	MAJ	MIN	ANG	PHE SEC
M2	44714.16	19.96	0.45	89.83	13399.32
S2	43200.00	5.04	0.09	89.11	29148.62
N2	45570.05	5.08	0.10	89.61	26474.98
K1	86164.09	4.79	0.15	90.71	52448.33
O1	92949.63	1.81	0.03	91.76	36198.00

c SBW layer observed layer 6

U MEAN=	0.63	V MEAN=	2.55		
SYMBOL	TCP	MAJ	MIN	ANG	PHE SEC
M2	44714.16	33.61	0.71	86.75	13556.33
S2	43200.00	9.27	0.10	86.37	29814.50
N2	45570.05	6.89	0.38	87.45	22260.51
K1	86164.09	10.06	0.40	84.96	56262.03
O1	92949.63	4.43	0.16	84.17	30436.24

c SBW predicted layer 6

U MEAN=	-0.55	V MEAN=	-0.14		
SYMBOL	TCP	MAJ	MIN	ANG	PHE SEC
M2	44714.16	22.34	0.38	90.16	14475.34
S2	43200.00	5.82	0.03	90.24	30065.76
N2	45570.05	5.31	0.03	89.76	27034.93
K1	86164.09	5.85	0.07	91.13	53819.14
O1	92949.63	2.12	0.08	92.15	37845.25

c SBW layer observed layer 7

U MEAN=	0.91	V MEAN=	7.93		
SYMBOL	TCP	MAJ	MIN	ANG	PHE SEC
M2	44714.16	29.67	0.93	88.16	13995.15
S2	43200.00	9.31	0.09	88.08	30561.64
N2	45570.05	6.68	0.06	89.10	23600.52
K1	86164.09	10.04	0.65	87.72	57033.98
O1	92949.63	4.83	0.19	87.70	31189.85

c SBW predicted layer 7

U MEAN=	-0.36	V MEAN=	2.71		
SYMBOL	TCP	MAJ	MIN	ANG	PHE SEC
M2	44714.16	25.04	0.07	90.06	15497.60
S2	43200.00	6.48	0.04	90.15	31185.45
N2	45570.05	5.54	0.09	89.15	27111.14
K1	86164.09	7.54	0.10	90.63	55046.77
O1	92949.63	3.02	0.13	90.94	38576.34

c SBW layer observed layer 8

U MEAN=	0.87	V MEAN=	14.04		
SYMBOL	TCP	MAJ	MIN	ANG	PHE SEC
M2	44714.16	24.88	0.62	88.74	13855.03
S2	43200.00	8.65	0.12	87.35	30779.12
N2	45570.05	4.63	0.11	89.84	25290.63
K1	86164.09	9.26	0.48	89.56	56668.73
O1	92949.63	5.17	0.21	87.85	32141.01

c SBW predicted layer 8

U MEAN=	0.17	V MEAN=	7.91		
SYMBOL	TCP	MAJ	MIN	ANG	PHE SEC
M2	44714.16	28.13	0.01	90.06	16342.66
S2	43200.00	7.17	0.06	90.76	32027.78
N2	45570.05	5.58	0.05	90.80	27668.15
K1	86164.09	9.77	0.05	90.38	55368.45
O1	92949.63	4.35	0.08	90.38	38138.47

c SBW layer observed layer 9

U MEAN=	0.69	V MEAN=	18.81		
SYMBOL	TCP	MAJ	MIN	ANG	PHE SEC
M2	44714.16	19.88	0.25	90.44	13238.32
S2	43200.00	6.78	0.04	90.84	30704.37
N2	45570.05	3.02	0.09	89.63	25206.32
K1	86164.09	7.81	0.12	92.31	57828.72
O1	92949.63	4.38	0.11	88.50	33216.12

c SBW predicted layer 9

U MEAN=	0.00	V MEAN=	15.45		
SYMBOL	TCP	MAJ	MIN	ANG	PHE SEC
M2	44714.16	30.16	0.05	89.60	16719.30
S2	43200.00	7.47	0.09	89.81	32547.73
N2	45570.05	5.49	0.03	89.58	29502.90
K1	86164.09	11.88	0.02	89.65	54584.83
O1	92949.63	6.19	0.05	89.68	36571.01

c SBW observed layer 10

U MEAN=	3.75	V MEAN=	27.38		
SYMBOL	TCP	MAJ	MIN	ANG	PHE SEC
M2	44714.16	17.79	0.79	90.80	11317.16
S2	43200.00	5.29	0.37	95.49	30458.80
N2	45570.05	3.34	0.55	88.51	24448.36
K1	86164.09	6.94	0.54	94.68	63654.66
O1	92949.63	3.36	0.27	80.66	39160.59

c SBW predicted layer 10

U MEAN=	-0.26	V MEAN=	23.56		
SYMBOL	TCP	MAJ	MIN	ANG	PHE SEC
M2	44714.16	31.08	0.05	90.26	16715.65
S2	43200.00	7.80	0.03	90.20	33051.18
N2	45570.05	6.32	0.08	90.13	31646.71
K1	86164.09	13.40	0.06	90.39	53822.77
O1	92949.63	7.55	0.02	90.23	35772.61

c Deep101 obs layer 2

U MEAN=	-1.03	V MEAN=	0.07		
SYMBOL	TCP	MAJ	MIN	ANG	PHE SEC
M2	44714.16	4.28	0.47	164.94	17754.18
S2	43200.00	2.26	0.27	175.83	33072.40
N2	45570.05	1.08	0.15	178.77	25467.17
K1	86164.09	0.83	0.24	154.35	56552.05
O1	92949.63	2.27	0.05	3.66	19103.38

c Deep101 prd_37 layer 2

U MEAN=	-3.57	V MEAN=	1.13		
SYMBOL	TCP	MAJ	MIN	ANG	PHE SEC
M2	44714.16	0.66	0.13	177.15	12187.16
S2	43200.00	0.16	0.01	145.03	28375.90
N2	45570.05	0.16	0.05	142.62	19091.78
K1	86164.09	0.08	0.02	123.98	46783.05
O1	92949.63	0.15	0.01	95.84	36993.16

c Deep101 obs layer 3

U MEAN=	-0.83	V MEAN=	0.10		
SYMBOL	TCP	MAJ	MIN	ANG	PHE SEC
M2	44714.16	4.05	0.58	164.24	15316.16
S2	43200.00	2.00	0.42	173.38	33217.69
N2	45570.05	1.49	0.41	174.55	23630.88
K1	86164.09	0.72	0.15	154.46	63594.80
O1	92949.63	2.51	0.14	176.02	69128.65

c Deep101 prd_37 layer 3

U MEAN=	-2.95	V MEAN=	1.02		
SYMBOL	TCP	MAJ	MIN	ANG	PHE SEC
M2	44714.16	0.79	0.05	3.11	34028.21
S2	43200.00	0.16	0.05	152.34	27034.70
N2	45570.05	0.20	0.05	164.28	20441.55
K1	86164.09	0.18	0.01	14.95	44111.67
O1	92949.63	0.22	0.20	112.69	39173.53

c Deep101 obs layer 4

U MEAN=	-0.56	V MEAN=	-0.01		
SYMBOL	TCP	MAJ	MIN	ANG	PHE SEC
M2	44714.16	4.26	0.78	159.01	13807.36
S2	43200.00	1.62	0.16	167.60	32456.12
N2	45570.05	1.80	0.43	169.21	23868.65
K1	86164.09	1.12	0.10	153.99	66555.81
O1	92949.63	1.93	0.08	172.65	71954.95

c Deep101 prd_37 layer 4

U MEAN=	-1.58	V MEAN=	0.34		
SYMBOL	TCP	MAJ	MIN	ANG	PHE SEC
M2	44714.16	0.97	0.02	10.96	31604.21
S2	43200.00	0.16	0.07	153.75	28986.45
N2	45570.05	0.26	0.07	4.63	1572.01
K1	86164.09	0.12	0.07	155.00	78670.72
O1	92949.63	0.38	0.13	147.79	46374.91

c Deep101 obs layer 5

U MEAN=	-0.13	V MEAN=	0.10		
SYMBOL	TCP	MAJ	MIN	ANG	PHE SEC
M2	44714.16	4.28	1.08	153.74	12393.51
S2	43200.00	1.59	0.24	154.07	30680.69
N2	45570.05	2.07	0.50	164.71	24499.59
K1	86164.09	1.40	0.28	156.40	67766.84
O1	92949.63	0.98	0.22	163.37	75386.47

c Deep101 prd_37 layer 5

U MEAN=	-0.07	V MEAN=	-0.78		
SYMBOL	TCP	MAJ	MIN	ANG	PHE SEC
M2	44714.16	1.03	0.16	12.57	30050.04
S2	43200.00	0.21	0.08	139.21	36589.51
N2	45570.05	0.42	0.03	175.71	27129.65
K1	86164.09	0.35	0.01	145.17	65968.48
O1	92949.63	0.34	0.02	148.97	42247.57

c Deep101 obs layer 6

U MEAN=	0.44	V MEAN=	0.15		
SYMBOL	TCP	MAJ	MIN	ANG	PHE SEC
M2	44714.16	4.67	1.20	153.82	11729.88
S2	43200.00	1.60	0.32	156.64	30334.16
N2	45570.05	2.20	0.51	165.56	24673.86
K1	86164.09	1.39	0.49	161.81	64948.75
O1	92949.63	0.49	0.16	72.02	52974.81

c Deep101 prd_37 layer 6

U MEAN=	2.15	V MEAN=	-2.56		
SYMBOL	TCP	MAJ	MIN	ANG	PHE SEC
M2	44714.16	0.80	0.26	7.81	31779.17
S2	43200.00	0.14	0.06	174.11	34930.46
N2	45570.05	0.41	0.01	171.09	24990.94
K1	86164.09	0.30	0.14	160.33	69604.98
O1	92949.63	0.25	0.03	41.02	74672.96

c Deep101 obs layer 7

U MEAN=	1.11	V MEAN=	-0.25		
SYMBOL	TCP	MAJ	MIN	ANG	PHE SEC
M2	44714.16	5.05	1.38	151.73	11688.89
S2	43200.00	1.43	0.25	172.79	31260.27
N2	45570.05	1.85	0.62	167.26	24766.72
K1	86164.09	1.29	0.75	163.11	60023.50
O1	92949.63	1.17	0.25	0.23	71052.39

c Deep101 prd_37 layer 7

U MEAN=	2.90	V MEAN=	-3.17		
SYMBOL	TCP	MAJ	MIN	ANG	PHE SEC
M2	44714.16	0.97	0.39	1.63	33461.55
S2	43200.00	0.24	0.14	152.09	42584.72
N2	45570.05	0.61	0.06	160.27	27591.03
K1	86164.09	0.44	0.21	175.64	65758.27
O1	92949.63	0.31	0.01	28.57	73881.14

c Deep101 obs layer 8

U MEAN=	2.02	V MEAN=	-0.89		
SYMBOL	TCP	MAJ	MIN	ANG	PHE SEC
M2	44714.16	5.08	2.02	149.81	12444.55
S2	43200.00	1.59	0.22	156.64	29737.23
N2	45570.05	1.93	0.50	169.74	24561.93
K1	86164.09	1.40	1.15	92.92	72702.39
O1	92949.63	2.07	0.24	164.27	23074.62

c Deep101 prd_37 layer 8

U MEAN=	3.58	V MEAN=	-3.36		
SYMBOL	TCP	MAJ	MIN	ANG	PHE SEC
M2	44714.16	1.33	0.27	11.17	36413.04
S2	43200.00	0.24	0.17	178.91	38976.17
N2	45570.05	0.56	0.04	167.49	28301.40
K1	86164.09	0.38	0.23	175.00	71438.28
O1	92949.63	0.25	0.00	101.70	72964.65

c Deep201 obs layer 2

U MEAN=	-1.38	V MEAN=	2.08		
SYMBOL	TCP	MAJ	MIN	ANG	PHE SEC
M2	44714.16	2.00	1.29	62.05	17693.19
S2	43200.00	1.04	0.66	25.10	41148.66
N2	45570.05	0.40	0.16	88.91	35373.92
K1	86164.09	0.84	0.55	42.55	54592.52
O1	92949.63	2.68	0.65	1.75	16761.84

c Deep201 model layer 2

U MEAN=	0.99	V MEAN=	1.35		
SYMBOL	TCP	MAJ	MIN	ANG	PHE SEC
M2	44714.16	1.04	0.04	7.05	34689.77
S2	43200.00	0.19	0.00	173.61	27051.93
N2	45570.05	0.17	0.08	93.39	15598.21
K1	86164.09	0.32	0.09	115.79	37306.11
O1	92949.63	0.46	0.12	95.87	10369.54

c Deep201 obs layer 3

U MEAN=	0.07	V MEAN=	2.46		
SYMBOL	TCP	MAJ	MIN	ANG	PHE SEC
M2	44714.16	3.40	0.05	38.33	19067.81
S2	43200.00	1.61	0.69	32.45	40760.58
N2	45570.05	0.83	0.32	32.20	35149.30
K1	86164.09	0.80	0.10	39.66	54379.73
O1	92949.63	2.54	0.35	2.85	20363.79

c Deep201 model layer 3

U MEAN=	0.84	V MEAN=	0.64		
SYMBOL	TCP	MAJ	MIN	ANG	PHE SEC
M2	44714.16	1.02	0.05	7.88	35266.19
S2	43200.00	0.20	0.00	168.74	27041.93
N2	45570.05	0.16	0.09	78.31	12082.14
K1	86164.09	0.29	0.11	117.80	37430.57
O1	92949.63	0.45	0.08	100.33	6882.30

c Deep201 obs layer 4

U MEAN=	1.26	V MEAN=	2.59		
SYMBOL	TCP	MAJ	MIN	ANG	PHE SEC
M2	44714.16	4.12	1.32	34.01	20580.45
S2	43200.00	1.97	0.52	23.04	39661.21
N2	45570.05	1.25	1.01	177.00	17177.50
K1	86164.09	0.53	0.39	141.60	45074.47
O1	92949.63	2.09	0.15	172.32	69831.70

c Deep201 model layer 4

U MEAN=	0.62	V MEAN=	-0.05		
SYMBOL	TCP	MAJ	MIN	ANG	PHE SEC
M2	44714.16	0.99	0.07	8.18	35660.55
S2	43200.00	0.19	0.04	175.92	28295.80
N2	45570.05	0.16	0.07	32.51	4168.99
K1	86164.09	0.23	0.21	164.29	46164.41
O1	92949.63	0.37	0.02	112.81	1879.73

c Deep201 obs layer 5

U MEAN=	1.68	V MEAN=	1.81		
SYMBOL	TCP	MAJ	MIN	ANG	PHE SEC
M2	44714.16	3.99	2.70	26.59	22347.00
S2	43200.00	1.77	1.04	18.49	38022.95
N2	45570.05	1.81	1.06	160.56	19505.36
K1	86164.09	1.14	0.40	159.35	44338.75
O1	92949.63	1.16	0.44	18.03	31856.04

c Deep201 model layer 5

U MEAN=	0.47	V MEAN=	-0.59		
SYMBOL	TCP	MAJ	MIN	ANG	PHE SEC
M2	44714.16	0.98	0.09	9.13	35944.26
S2	43200.00	0.23	0.06	27.36	9682.93
N2	45570.05	0.20	0.02	29.71	2813.34
K1	86164.09	0.30	0.13	37.78	14682.27
O1	92949.63	0.33	0.12	102.65	87881.38

c Deep201 obs layer 6

U MEAN=	1.67	V MEAN=	0.42		
SYMBOL	TCP	MAJ	MIN	ANG	PHE SEC
M2	44714.16	3.79	3.66	21.39	23687.85
S2	43200.00	1.31	0.81	39.95	36300.29
N2	45570.05	1.65	0.53	153.97	20677.62
K1	86164.09	1.48	0.82	153.27	46162.95
O1	92949.63	1.06	0.62	54.94	41887.27

c Deep201 model layer 6

U MEAN=	0.43	V MEAN=	-1.01		
SYMBOL	TCP	MAJ	MIN	ANG	PHE SEC
M2	44714.16	0.97	0.07	11.59	35896.30
S2	43200.00	0.24	0.03	32.32	10500.88
N2	45570.05	0.22	0.01	29.10	2297.88
K1	86164.09	0.40	0.01	48.45	15689.25
O1	92949.63	0.38	0.09	88.61	82020.94

c Deep201 obs layer 7

U MEAN=	1.60	V MEAN=	-0.79		
SYMBOL	TCP	MAJ	MIN	ANG	PHE SEC
M2	44714.16	4.37	3.54	146.88	8718.18
S2	43200.00	1.22	0.63	71.33	36778.45
N2	45570.05	1.58	0.22	161.17	23258.23
K1	86164.09	1.33	0.86	16.70	80048.98
O1	92949.63	1.11	0.63	135.03	25935.77

c Deep201 model layer 7

U MEAN=	0.46	V MEAN=	-1.27		
SYMBOL	TCP	MAJ	MIN	ANG	PHE SEC
M2	44714.16	0.94	0.05	14.73	35837.23
S2	43200.00	0.28	0.03	34.17	11274.13
N2	45570.05	0.27	0.05	29.89	1633.40
K1	86164.09	0.51	0.14	56.32	14929.64
O1	92949.63	0.45	0.01	84.32	78627.99

c Deep201 obs layer 8

U MEAN=	1.22	V MEAN=	-1.59		
SYMBOL	TCP	MAJ	MIN	ANG	PHE SEC
M2	44714.16	4.64	3.53	152.41	9204.79
S2	43200.00	1.42	1.21	136.76	29973.95
N2	45570.05	1.76	0.08	175.42	22924.34
K1	86164.09	1.18	0.45	24.82	73052.77
O1	92949.63	1.73	0.65	130.97	23505.25

c Deep201 model layer 8

U MEAN=	0.42	V MEAN=	-1.28		
SYMBOL	TCP	MAJ	MIN	ANG	PHE SEC
M2	44714.16	0.92	0.02	16.64	35656.99
S2	43200.00	0.29	0.02	22.82	11560.49
N2	45570.05	0.29	0.10	33.45	45557.84
K1	86164.09	0.66	0.25	61.81	13447.54
O1	92949.63	0.50	0.07	86.37	78795.21

SUBAPPENDIX D

HARMONIC AND RESIDUAL VELOCITY PROFILE PLOTS

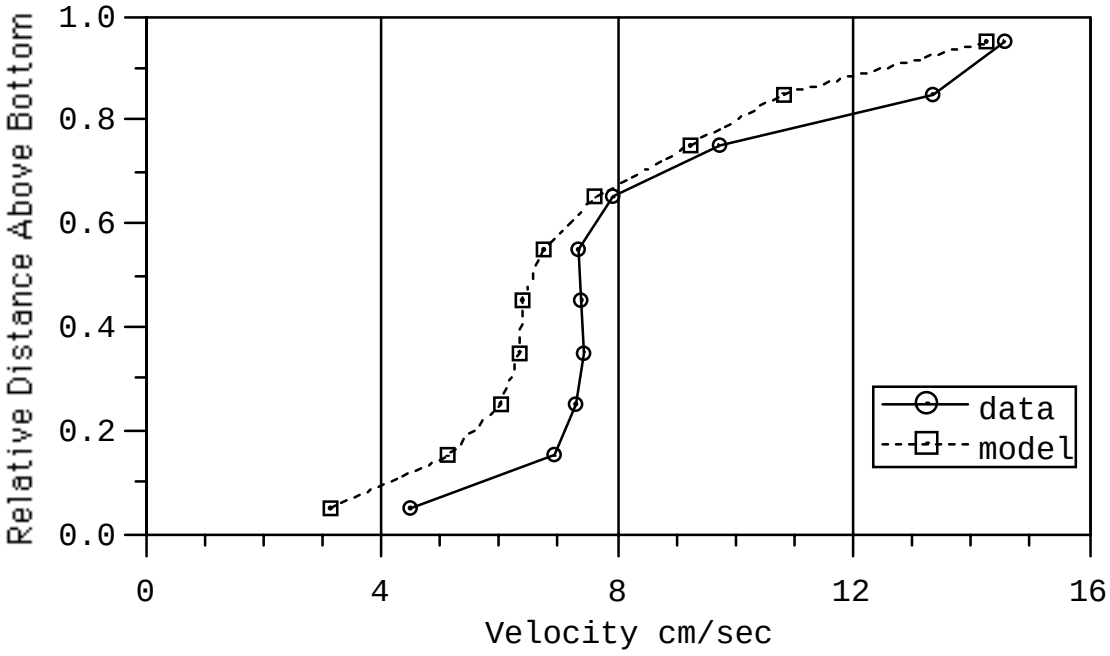

Figure D-1. Amplitude of M2 Harmonic Component of Longitudinal Velocity at Station ARC

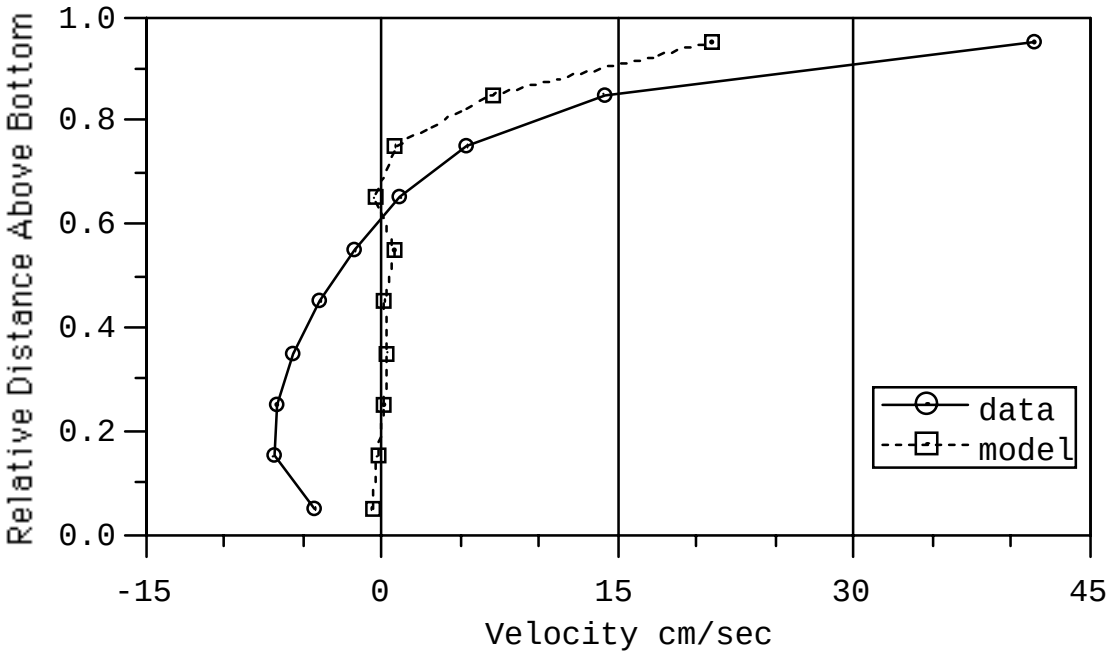

Figure D-2. Mean Longitudinal Velocity at Station ARC

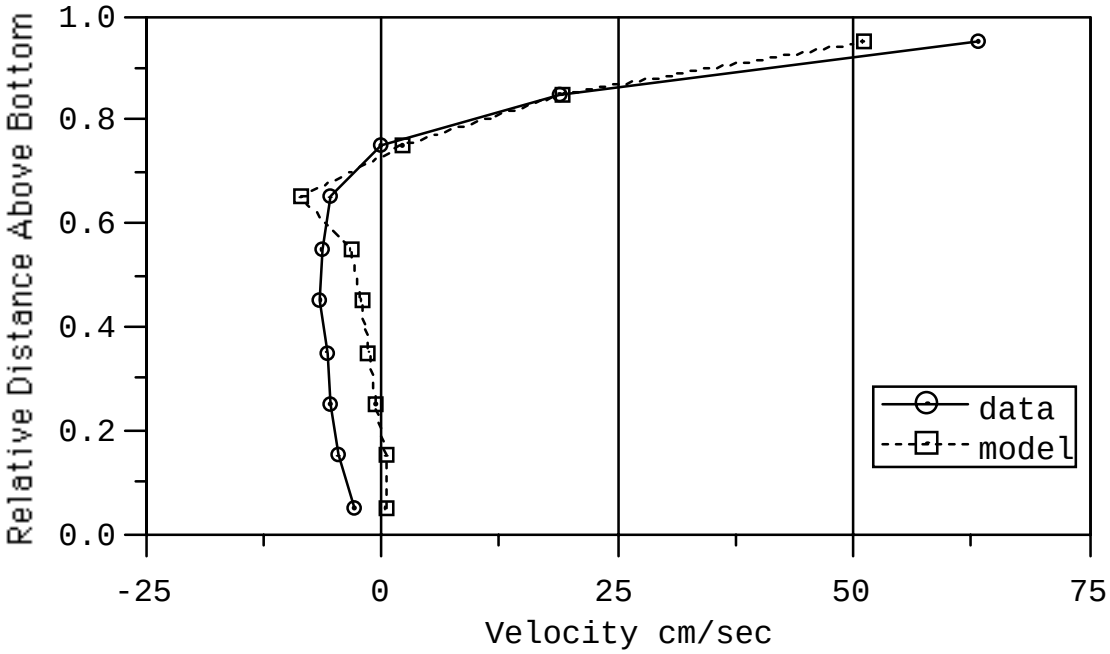

Figure D-3. Mean Longitudinal Velocity at Station ARC

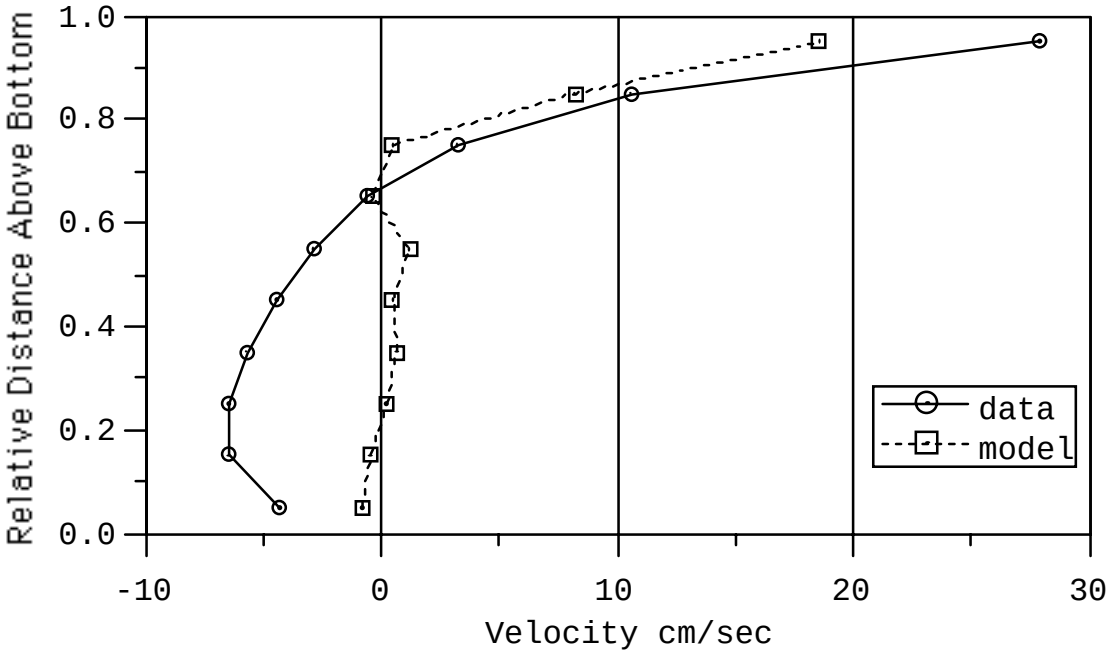

Figure D-4. Mean Longitudinal Velocity at Station ARC

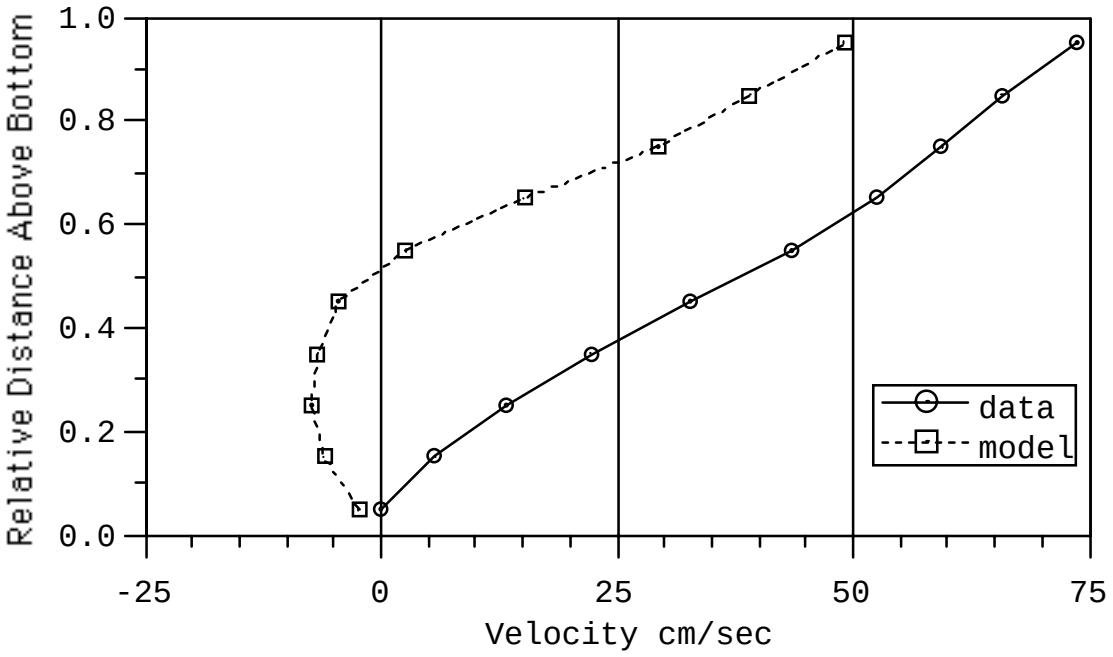

Figure D-5. Mean Longitudinal Velocity at Station EWW

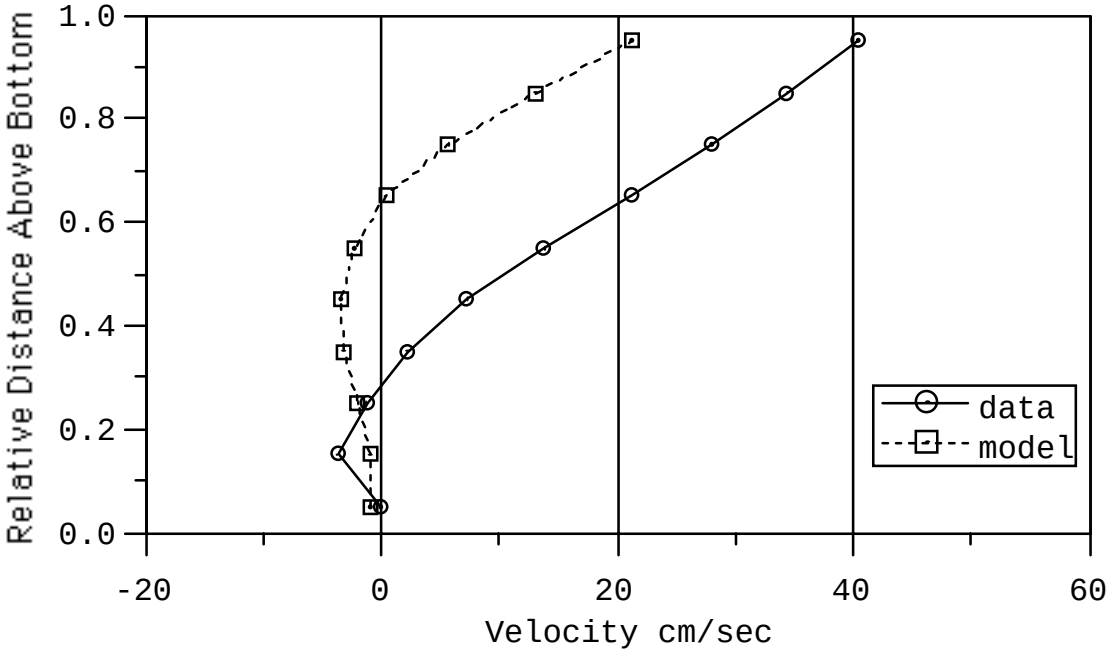

Figure D-6. Mean Longitudinal Velocity at Station EWW

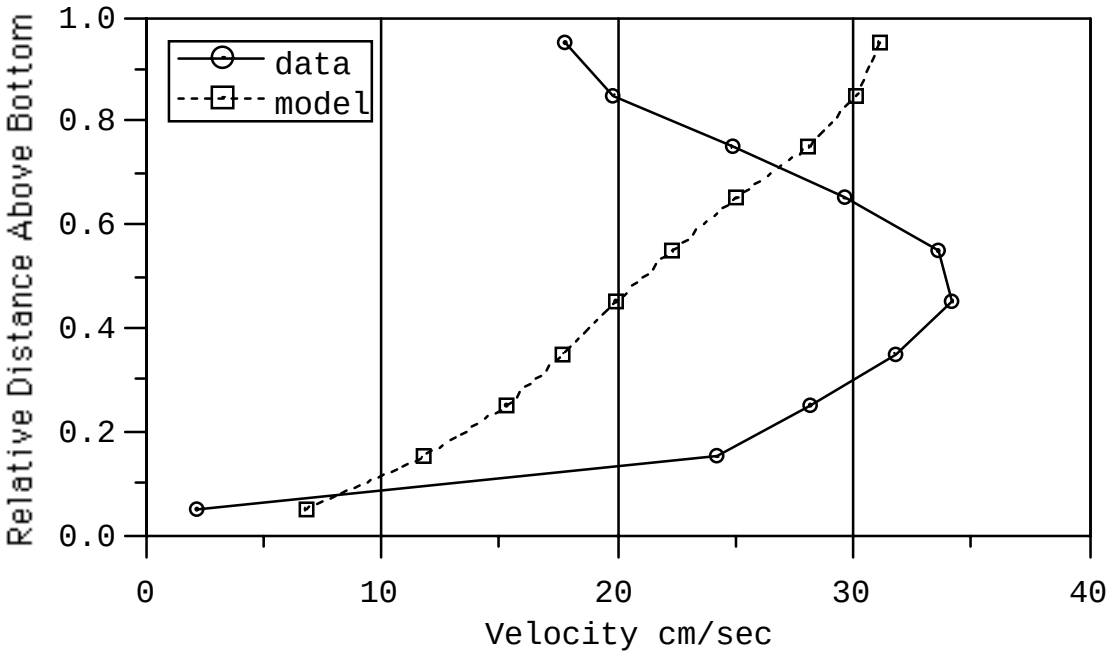

Figure D-7. Amplitude of M2 Harmonic Component of Longitudinal Velocity at Station SBW

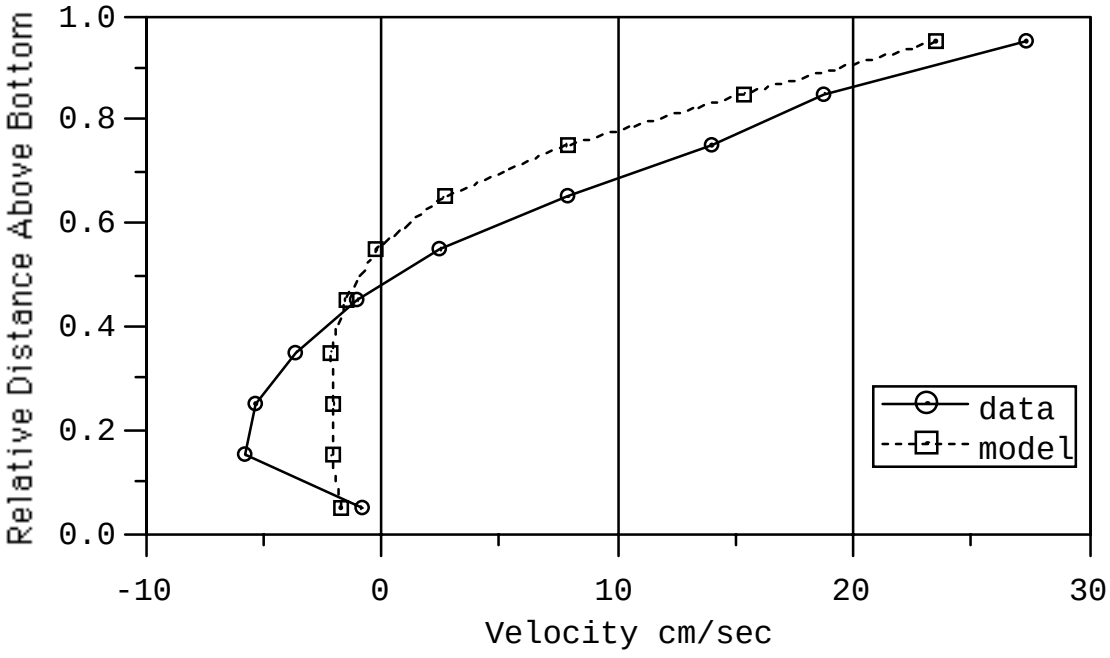

Figure D-8. Mean Longitudinal Velocity at Station SBW

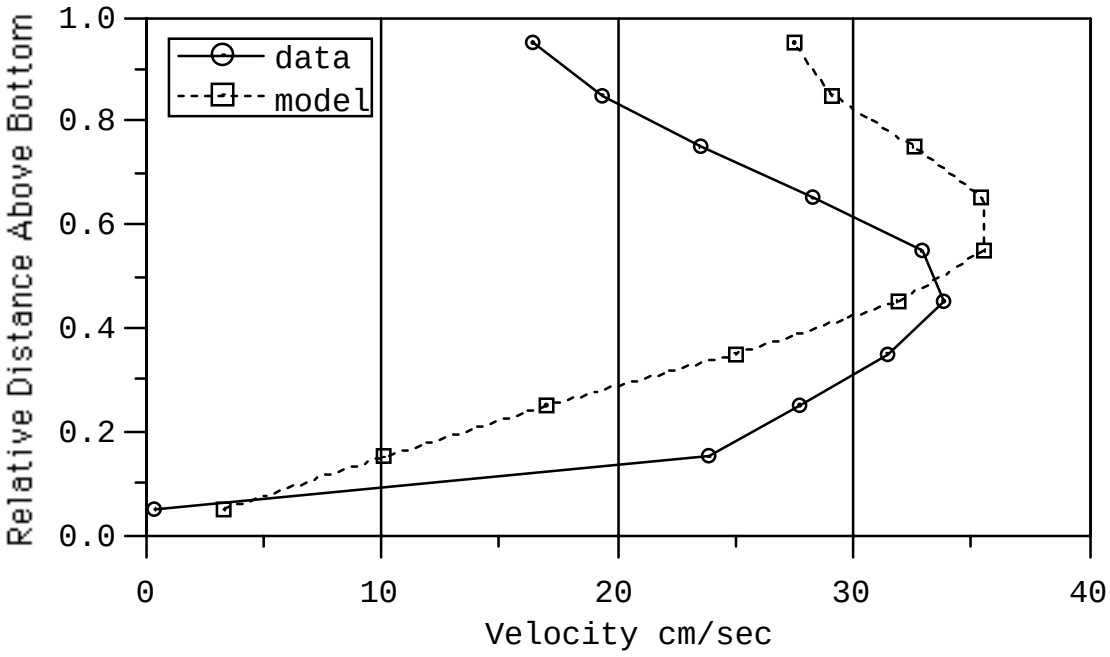

Figure D-9. Amplitude of M2 Harmonic Component of Longitudinal Velocity at Station BOE

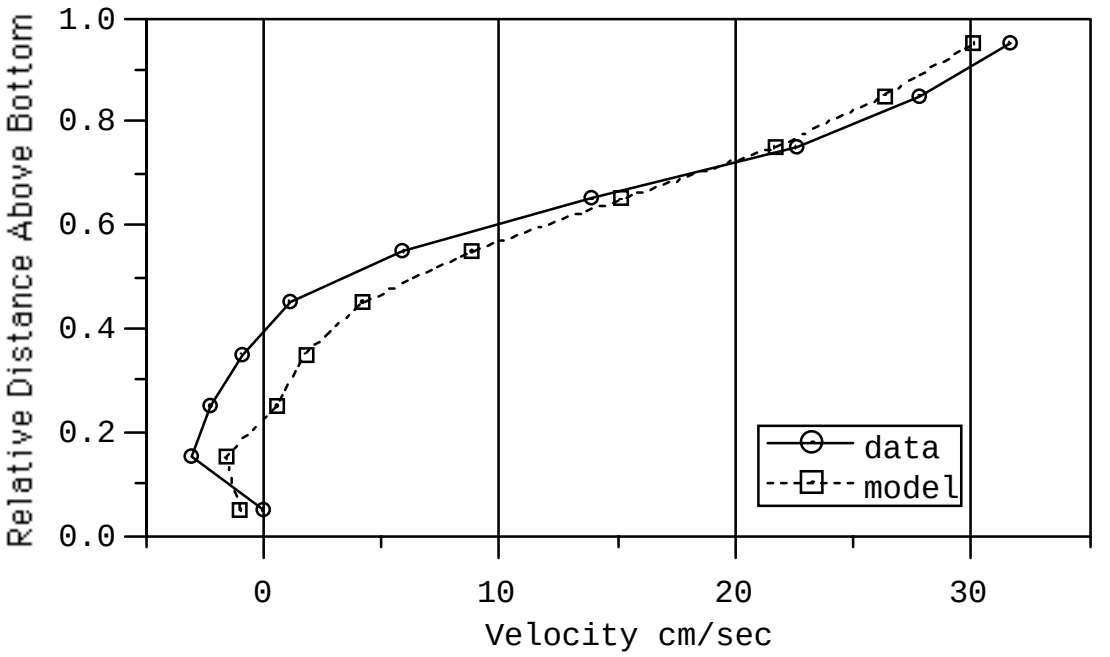

Figure D-10. Mean Longitudinal Velocity at Station BOE

SUBAPPENDIX E

EFFECT OF CROSS SECTION SHAPE AND LATERAL POSITION ON THE VERTICAL DISTRIBUTION OF TIDAL AND RESIDUAL LONGITUDINAL VELOCITY

INTRODUCTION

The purpose of this appendix to illustrate the effect of channel cross section shape and lateral position on the vertical distribution of the tidal and residual longitudinal velocity in an estuary. The analysis is based on Hamrick (1979) and Friedrichs and Hamrick (1996).

Consider a simple model for the tidal velocity in an estuary. The momentum equation is:

$$\partial_t u = -g\partial_x z_s + \partial_z\left(A_v \partial_z u\right) \qquad \text{(Equation E-1)}$$

where z_s and u are the water surface elevation and longitudinal velocity and A_v is the kinematic eddy viscosity. The x and z coordinates are seaward and upward respectively. Introducing harmonic representations

$$\begin{aligned} u &= \mathrm{Re}\left(U e^{i\omega t}\right) \\ z_s &= \mathrm{Re}\left(Z e^{i\omega t}\right) \end{aligned} \qquad \text{(Equation E-2)}$$

Equation E-1 becomes:

$$\partial_z\left(A_v \partial_z U\right) - i\omega U = g\partial_x Z \qquad \text{(Equation E-3)}$$

The solution for constant A_v is:

$$U = U_1 \cosh\left((1+i)\delta\frac{z}{h}\right) + U_2 \sinh\left(-(1+i)\delta\frac{z}{h}\right) + i\frac{g}{\omega}\partial_x Z \qquad \text{(Equation E-4)}$$

where

$$\delta = \sqrt{\frac{\omega h^2}{2A_v}} \qquad \text{(Equation E-5)}$$

A no stress condition is assumed at the mean free surface, z=0,

$$\partial_z u = \partial_z U = 0 \quad : \quad z = 0 \qquad \text{(Equation E-6)}$$

which allows the constant U_2 to be evaluated giving

$$U = U_1 \cosh\left((1+i)\delta\frac{z}{h}\right) + i\frac{g}{\omega}\partial_x Z \qquad \text{(Equation E-7)}$$

A no slip condition is applied at the bottom, $z=-h$, where h is the local depth

$$u = 0 \quad : \quad z = -h \qquad \text{(Equation E-8)}$$

Evaluating the constant U_1 gives:

$$U = i\frac{g}{\omega}\partial_x Z\left(1 - \frac{\cosh\left((1+i)\delta h^{-1} z\right)}{\cosh\left((1+i)\delta\right)}\right) \qquad \text{(Equation E-9)}$$

For a triangular cross section, h is given by:

$$h = h_o\left(\frac{y}{b}\right) \qquad \text{(Equation E-10)}$$

where b is the channel width. Equation E-5 then becomes:

$$\delta = \sqrt{\frac{\omega h_o^2}{2A_v}}\left(\frac{y}{b}\right) = \delta_o\left(\frac{y}{b}\right)$$
$$\delta_o = \sqrt{\frac{\omega h_o^2}{2A_v}} \qquad \text{(Equation E-11)}$$

Introducing dimensionless coordinates:

$$\zeta = \frac{z}{h}$$
$$\eta = \frac{y}{b} \qquad \text{(Equation E-12)}$$

Equation E-9 becomes:

$$U = i\frac{g}{\omega}\partial_x Z\left(1 - \frac{\cosh\left((1+i)\delta_o \eta\zeta\right)}{\cosh\left((1+i)\delta_o \eta\right)}\right) \qquad \text{(Equation E-13)}$$

Defining the surface velocity at the deepest point of the cross section as:

$$U_s = U\left(\zeta = 0\,,\, \eta = 1\right) = i\frac{g}{\omega}\partial_x Z\left(1 - \frac{1}{\cosh\left((1+i)\delta_o\right)}\right) \qquad \text{(Equation E-14)}$$

allows normalization of Equation E-13 to the form:

$$\frac{U}{U_s} = \left(1 - \frac{1}{\cosh((1+i)\delta_o)}\right)^{-1}\left(1 - \frac{\cosh((1+i)\delta_o\eta\zeta)}{\cosh((1+i)\delta_o\eta)}\right) \qquad \text{(Equation E-15)}$$

It can be readily shown that the magnitude of the complex quantity Equation E-15 is the ratio of the current harmonic amplitude at a point in the cross section to that at the reference location. Likewise the argument of Equation E-15 is the phase lag between a point in the cross section and the reference location.

Figures E-1 and E-2 show vertical profiles of current amplitude ratios and phase lags for δ_o equal to one at the deepest lateral position and a lateral position having a depth of 80 percent of the deepest position. Figures E-3 and E-4 show similar profiles for δ_o equal to two. Note a doubling of δ_o is equivalent to doubling the depth or decreasing the vertical eddy viscosity by a factor of four. The value of δ_o equal to one produces vertical phase lags on the order of those observed at station SBW, while vertical phase lags observed at station ARC are better represented by the value of two. Observed vertical phase lags at station BOE are intermediate, but somewhat closer to δ_o equal to one. Table E-1 summarizes various depth average measures of difference between amplitude and phase properties in the deep section and section having a depth of 80 percent of that in the deep

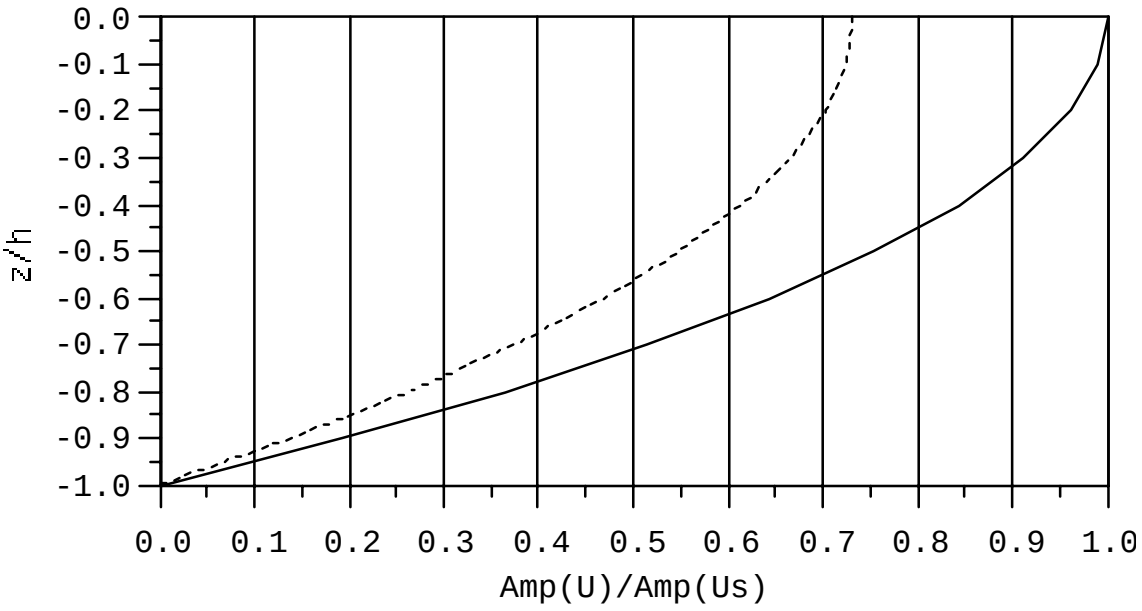

Figure E-1. Vertical Profiles of Normalized Tidal Velocity Amplitude for a Triangular Cross Section for δ_o =1. (solid line corresponds to lateral position of maximum depth, dashed line corresponds to lateral position having a local depth of 80% of maximum depth)

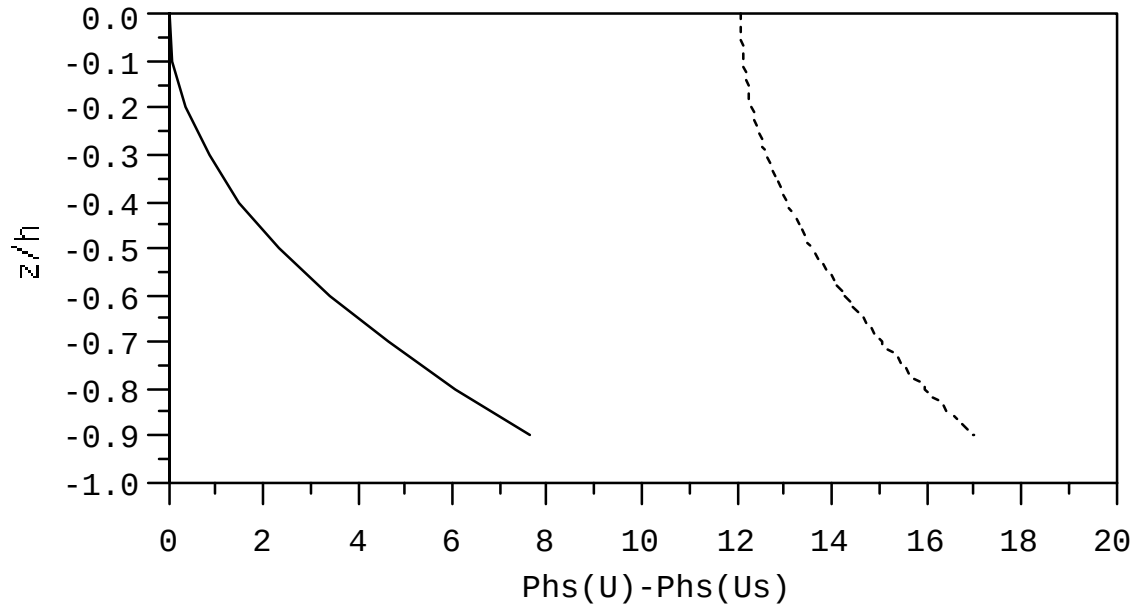

Figure E-2. Vertical Profile of Phase Lag Corresponding to Figure E-1

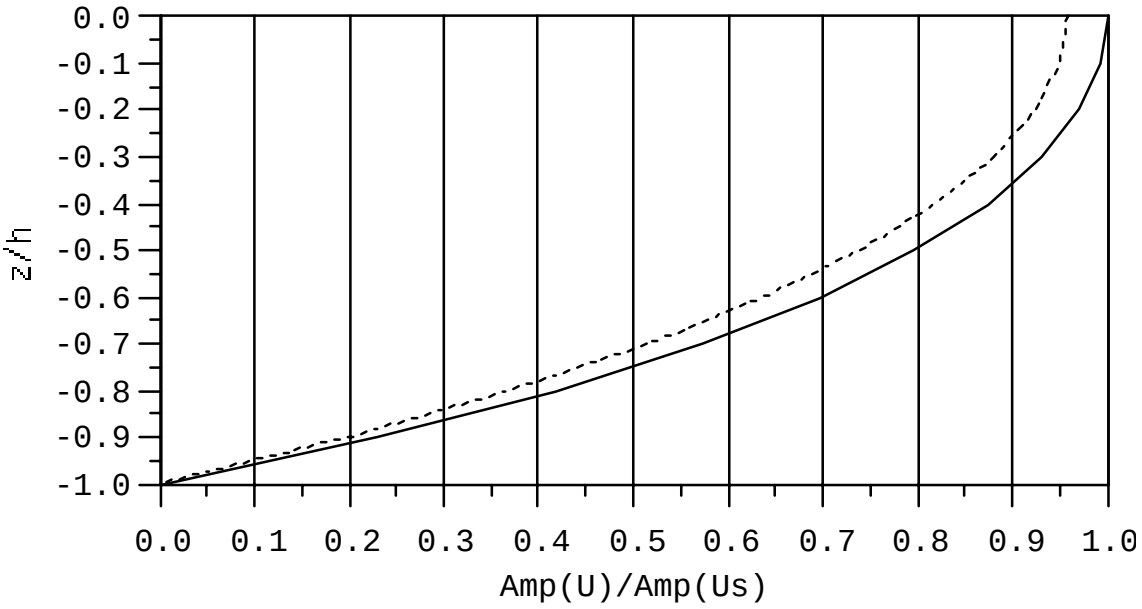

Figure E-3. Vertical Profiles of Normalized Tidal Velocity Amplitude for a Triangular Cross Section for δ_0 =2. (solid line corresponds to lateral position of maximum depth, dashed line corresponds to lateral position having a local depth of 80% of maximum depth)

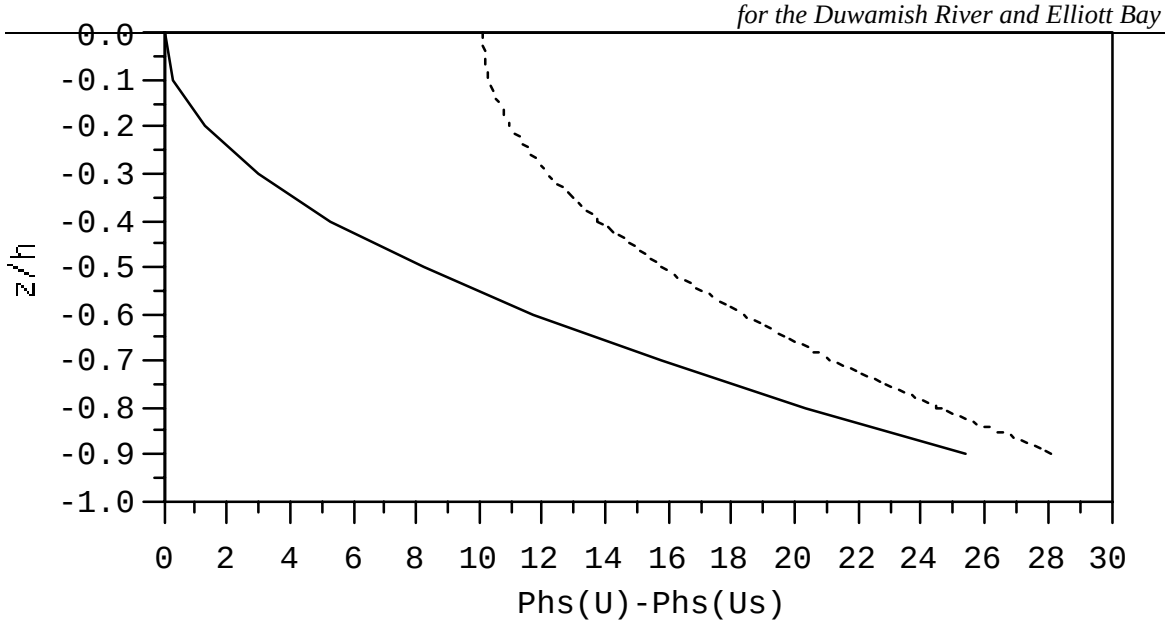

Figure E-4. Vertical Profile of Phase Lag Corresponding to Figure E-1

Table E-1. Differences Between Deep Section and 80% Depth Section Tidal Velocity Amplitudes and Phases

	$\sqrt{\frac{\omega h_o^2}{2A_v}} = 1$	$\sqrt{\frac{\omega h_o^2}{2A_v}} = 2$
Depth Avg of Udeep Udeep(surface)	0.65	0.68
Depth Avg of Abs(Udeep - U80%) Udeep(surface)	0.176	0.044
Depth Avg of Abs((Udeep - U80%)/Udeep)	0.25	0.07
Depth Avg of Abs(Phasedeep-Phase80%))	10.1 deg	6.7 deg

section. The third line of the table indicates absolute differences in velocity amplitude range from 4 to 18 percent of the deep section surface velocity amplitude. The fourth line indicates that the depth average of the relative difference between velocity amplitudes ranges from 7 to 25 percent. The final line indicates that the depth average of phase differences range from 7 to 10 degrees.

Now consider a simple model for the density driven residual circulation in an estuary. The residual momentum equation is:

$$0 = -\frac{1}{\rho_o}\partial_x\langle p\rangle + \partial_z\left(A_v\partial_z\langle u\rangle\right) \qquad \text{(Equation E-16)}$$

where <*p*> and <*u*> are residual components of the pressure and longitudinal velocity and A_v is the kinematic eddy viscosity. The *x* and *z* coordinates are seaward and upward respectively. The residual hydrostatic pressure balance is:

$$0 = -\frac{1}{\rho_o}\partial_z\langle p\rangle - g\frac{\langle\rho\rangle}{\rho_o} \qquad \text{(Equation E-17)}$$

Introducing a dimensionless density variable

$$\theta = \frac{\langle\rho\rangle - \rho_o}{\rho_o} \qquad \text{(Equation E-18)}$$

and eliminating the pressure between Equations E-16 and E-17 gives:

$$\partial_{zz}\left(A_v\partial_z\langle u\rangle\right) = -g\partial_x\theta \qquad \text{(Equation E-19)}$$

Assuming a constant eddy viscosity, as appropriate for simple analytical models gives:

$$\partial_{zzz}\langle u\rangle = -\frac{g\partial_x\theta}{A_v} \qquad \text{(Equation E-20)}$$

Integrating (Equation E-20) twice gives:

$$\partial_{zz}u = -\frac{g\partial_x\theta}{A_v}z + c_1 \qquad \text{(Equation E-21)}$$

$$\partial_{zz}\langle u\rangle = -\frac{g\partial_x\theta}{A_v}z + c_1 \qquad \text{(Equation E-22)}$$

A no stress condition is assumed at the mean free surface,

$$z{=}0, \partial_z\langle u\rangle = 0 \quad : \quad z = 0 \qquad \text{(Equation E-23)}$$

which allows the constant *c2* to be evaluated giving:

$$\partial_z\langle u\rangle = -\frac{g\partial_x\theta}{A_v}\frac{z^2}{2} + c_1 z \qquad \text{(Equation E-24)}$$

A final integration gives:

$$\langle u \rangle = -\frac{g\partial_x \theta}{A_v}\frac{z^3}{6} + c_1\frac{z^2}{2} + c_3 \qquad \text{(Equation E-25)}$$

A no slip conditions is applied at the bottom, z=-h, where h is the local depth

$$\langle u \rangle = 0 \quad : \quad z = -h \qquad \text{(Equation E-26)}$$

Evaluating the constant *c3* gives:

$$\langle u \rangle = -\frac{g\partial_x \theta}{6A_v}\left(z^3 + h^3\right) + \frac{c_1}{2}\left(z^2 - h^2\right) \qquad \text{(Equation E-27)}$$

The constant *c1* is determined by the integral continuity conditions

$$\int_0^b \int_{-h}^0 \langle u \rangle \, dz dy = Q_f \qquad \text{(Equation E-28)}$$

where *b* is the width of the channel and *Qf* is the net seaward freshwater discharge. For a triangular cross section with

$$h = h_o\left(\frac{y}{b}\right) \qquad \text{(Equation E-29)}$$

the constant *c1* is given by:

$$\frac{c_1}{2} = -\frac{g\partial_x \theta}{6A_v}\frac{9}{10}h_o - Q_f\frac{2}{h_o b}\frac{3}{h_o^2}$$
$$\frac{c_1}{2} = -\frac{g\partial_x \theta}{6A_v}\frac{9}{10}h_o - u_f\frac{3}{h_o^2} \qquad \text{(Equation E-30)}$$

where u_f is the average freshwater discharge velocity since the cross sectional area is $bh_o/2$. Equation (Equation E-27) now becomes:

$$\langle u \rangle = -\frac{g\partial_x \theta}{60A_v}\left(10z^3 + 9h_o z^2 + 10h^3 - 9h_o h^2\right) - u_f\frac{3}{h_o^2}\left(z^2 - h^2\right) \qquad \text{(Equation E-31)}$$

Or:

$$\langle u \rangle = -\frac{g\partial_x \theta h_o^3}{60A_v}\left(10\frac{z^3}{h_o^3} + 9\frac{z^2}{h_o^2} + 10\frac{h^3}{h_o^3} - 9\frac{h^2}{h_o^2}\right) - 3u_f\frac{h^2}{h_o^2}\left(\frac{z^2}{h^2} - 1\right) \qquad \text{(Equation E-32)}$$

Introducing dimensionless coordinates:

$$\zeta = \frac{z}{h}$$
$$\eta = \frac{y}{b} \qquad \text{(Equation E-33)}$$

and noting that:

$$h = h_o \eta \qquad \text{(Equation E-34)}$$

allows (Equation E-17) to be written as:

$$\langle u \rangle = -\frac{g \partial_x \theta h_o^3}{60 A_v} \left(10\eta^3 \left(\zeta^3 + 1\right) + 9\eta^2 \left(\zeta^2 - 1\right)\right) - 3u_f \eta^2 \left(\zeta^2 - 1\right) \qquad \text{(Equation E-35)}$$

The coefficients in (Equation E-35) can be estimated from residual velocity observation at two locations in the cross section, for example:

$$\langle u \rangle (z = 0, h = h_o) = -\frac{g \partial_x \theta h_o^3}{60 A_v} + 3u_f \qquad \text{(Equation E-36)}$$

$$\langle u \rangle \left(z = -\frac{3}{4}, h = h_o\right) = -\frac{g \partial_x \theta h_o^3}{60 A_v} \left(\frac{118}{64}\right) + u_f \frac{21}{16} \qquad \text{(Equation E-37)}$$

which are the surface and 1/4 quarter water column depth above the bottom velocities at the deepest point in the cross section.

The SBW and BOE mean velocity profiles, Figures D-8 and D-10 in Subappendix D, can be fitted to (Equation E-36) and (Equation E-37) giving:

$$-\frac{g \partial_x \theta h_o^3}{60 A_v} = 12.85 \ cm/s$$
$$3u_f = 43.8 \ cm/s \qquad \text{(Equation E-38)}$$

Figure E-5 shows the vertical profiles corresponding the values given by (Equation E-38) at *y=b* and *y=0.9b*. Note that a slight lateral shift form the deepest point in the cross section significantly alters the near bottom landward transport.

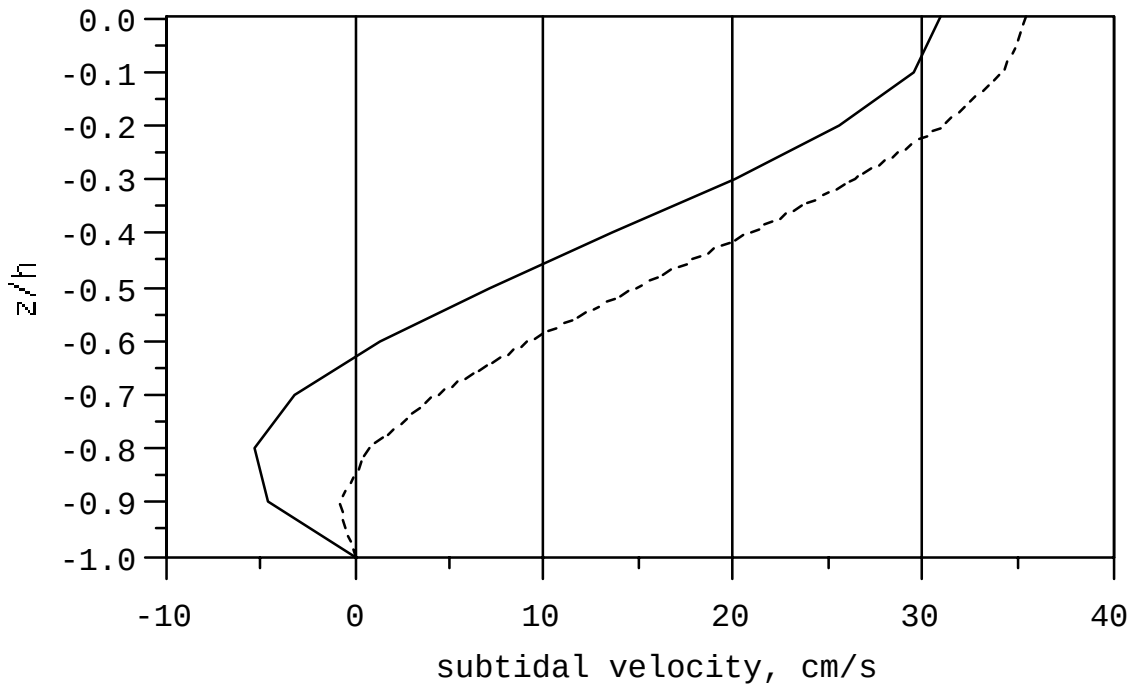

Figure E-5. Vertical Profiles of the Residual Longitudinal Velocity for a Triangular Cross Section. (solid line corresponds to lateral position of maximum depth, dashed line corresponds to lateral position having a local depth of 90% of maximum depth)

REFERENCES

Friedrichs, C.T. and J.M. Hamrick. 1996. Effects of channel geometry on cross-sectional variation in along-channel velocity in partially mixed tidal estuaries. Buoyancy Effects on Coastal and Estuarine Dynamics, D.G. Aubrey and C.T. Friedrichs, Eds. American Geophysical Union. Washington, D.C.

Hamrick, J.M. 1979. Salinity intrusion and gravitational circulation in partially stratified estuaries. Ph.D. dissertation, University of California. 451 pp.

SUBAPPENDIX F

INSTANTANEOUS SALINITY TIME SERIES PLOTS

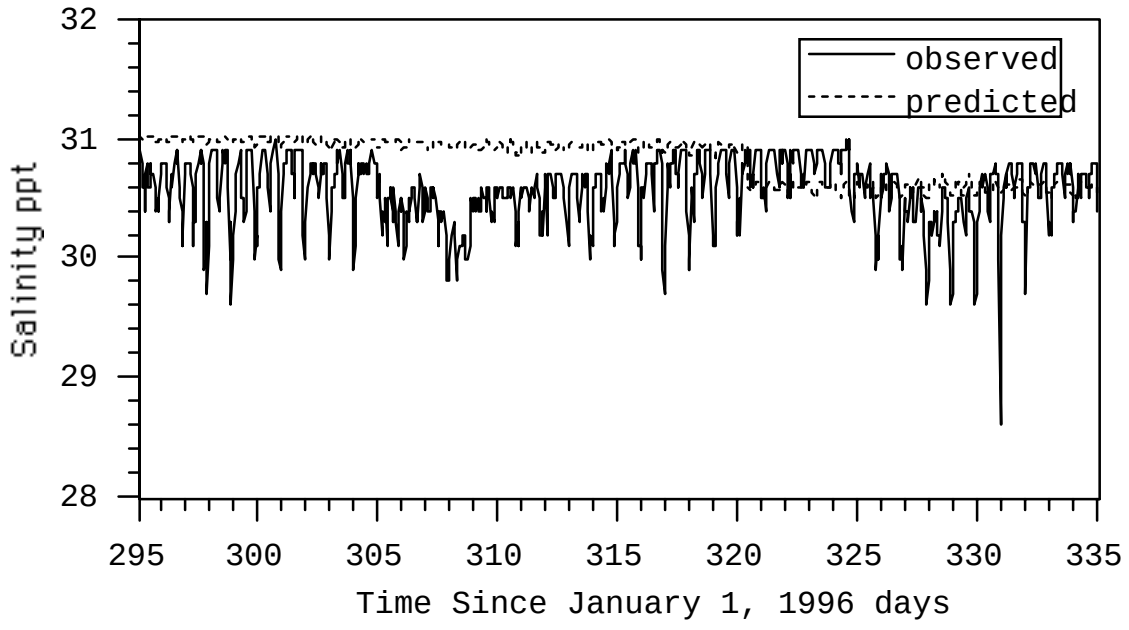

Figure F-1. Salinity at Station S-Bottom-1

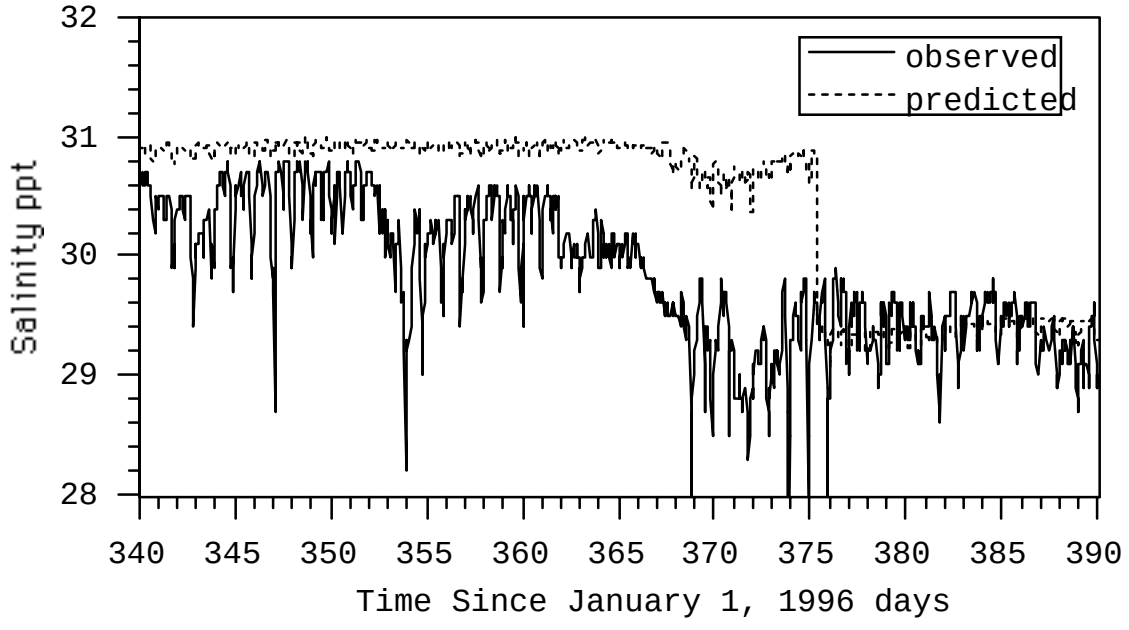

Figure F-2. Salinity at Station S-Bottom-2

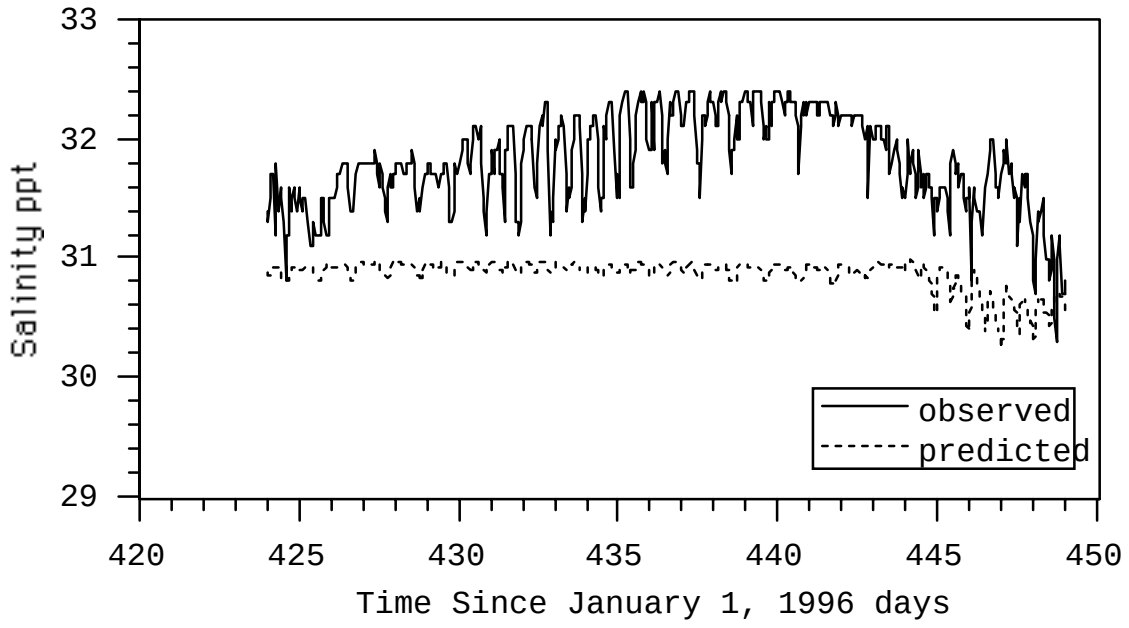

Figure F-3. Salinity at Station S-Bottom-3

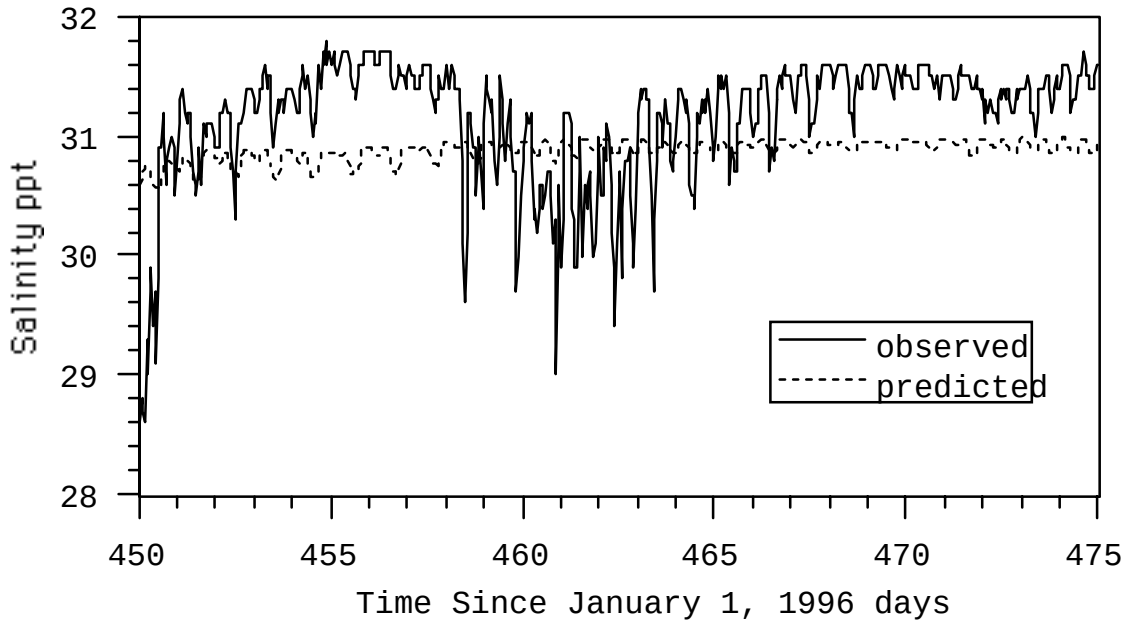

Figure F-4. Salinity at Station S-Bottom-4

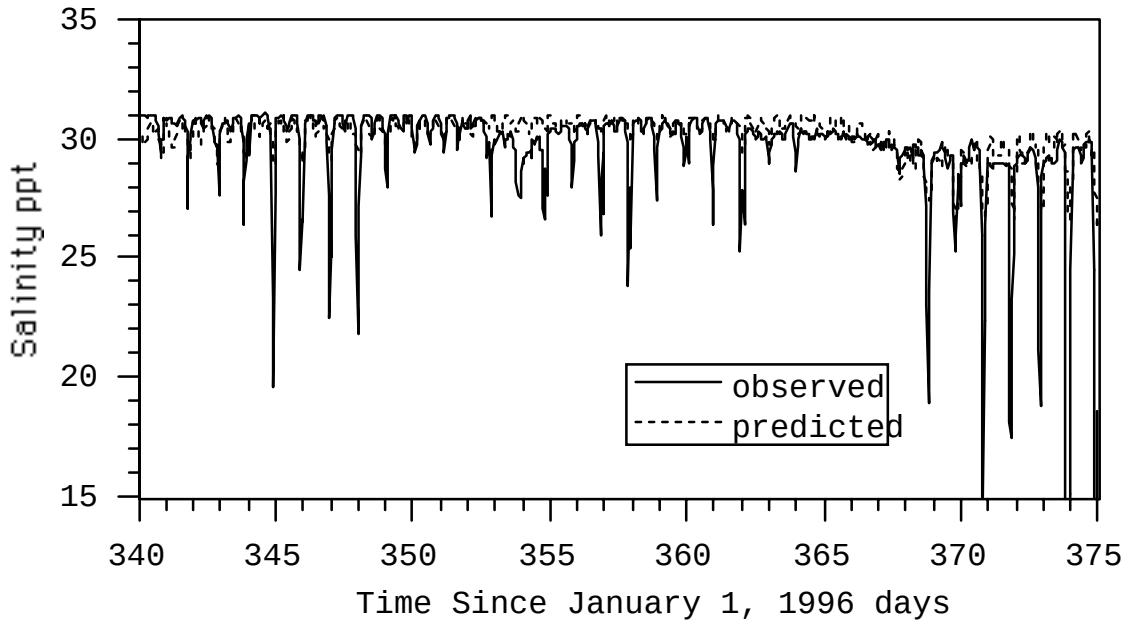

Figure F-5. Salinity at Station S-Middle-1

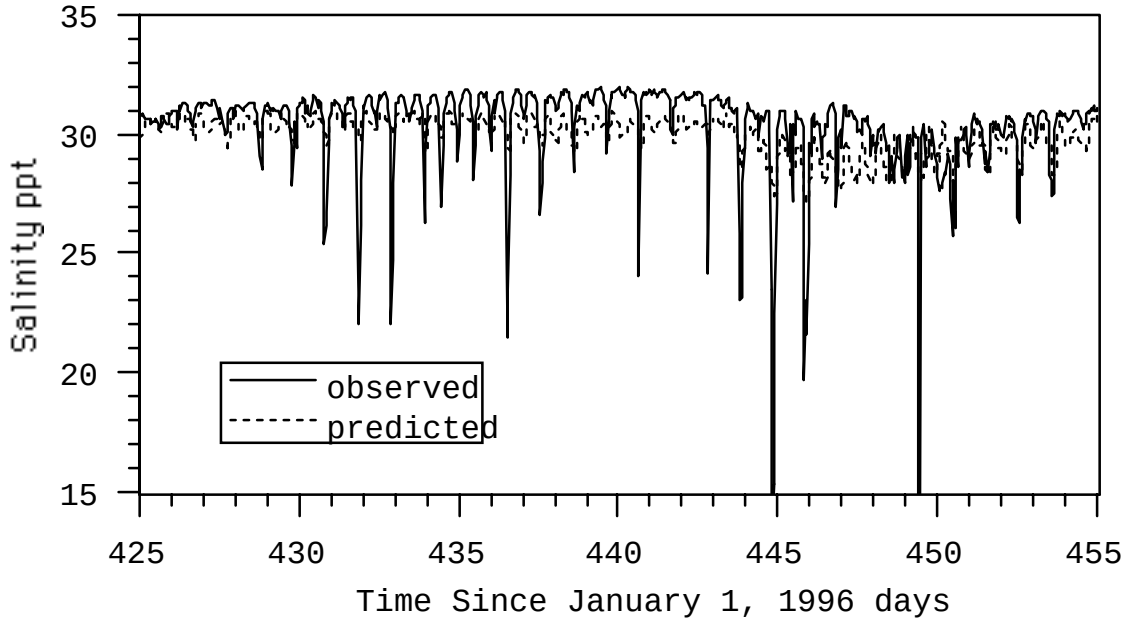

Figure F-6. Salinity at Station S-Middle-2

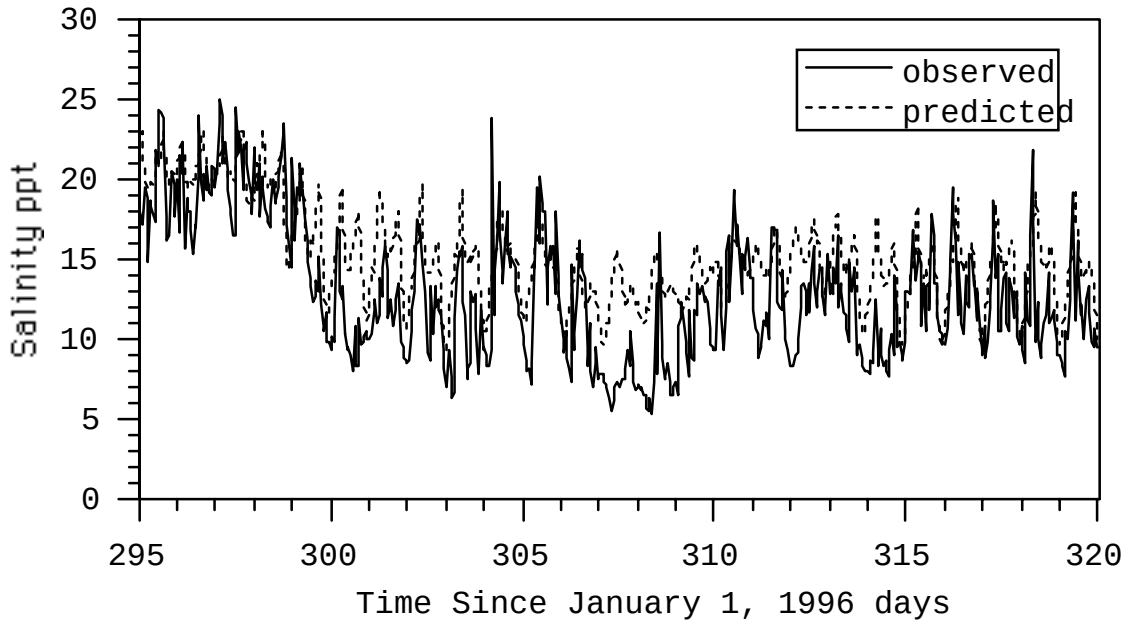

Figure F-7. Salinity at Station S-Surface-1

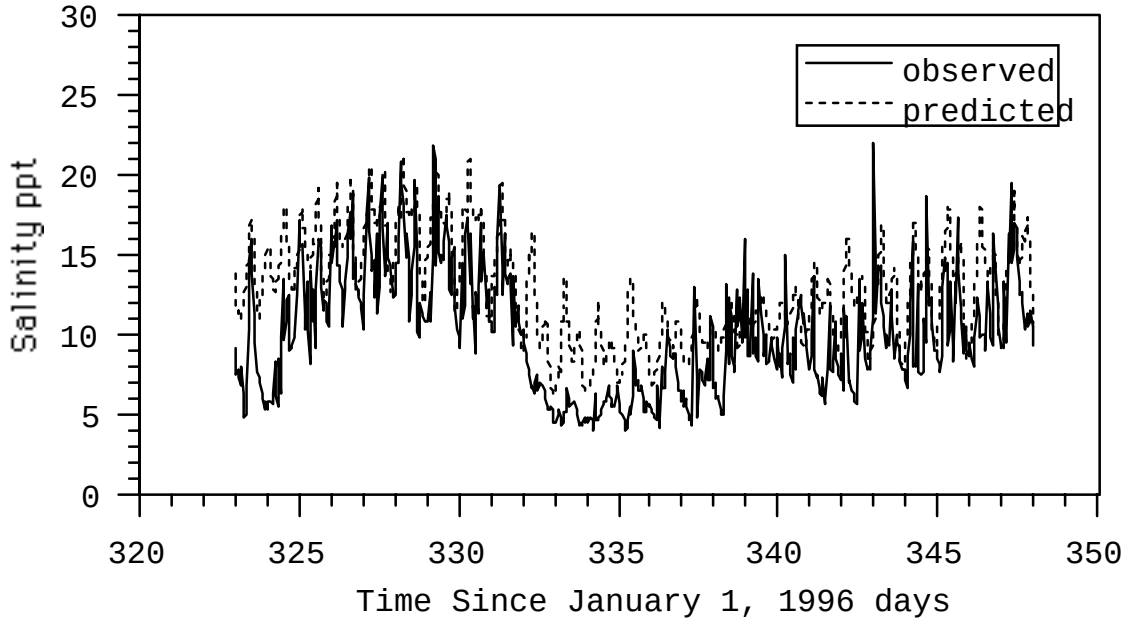

Figure F-8. Salinity at Station S-Surface-2

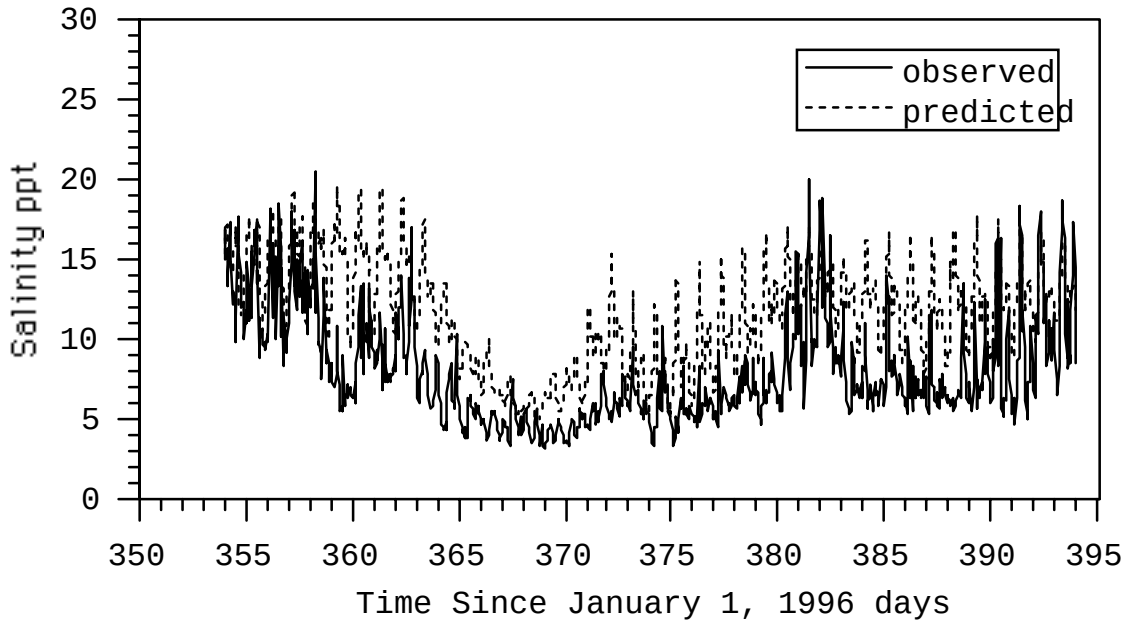

Figure F-9. Salinity at Station S-Surface-3

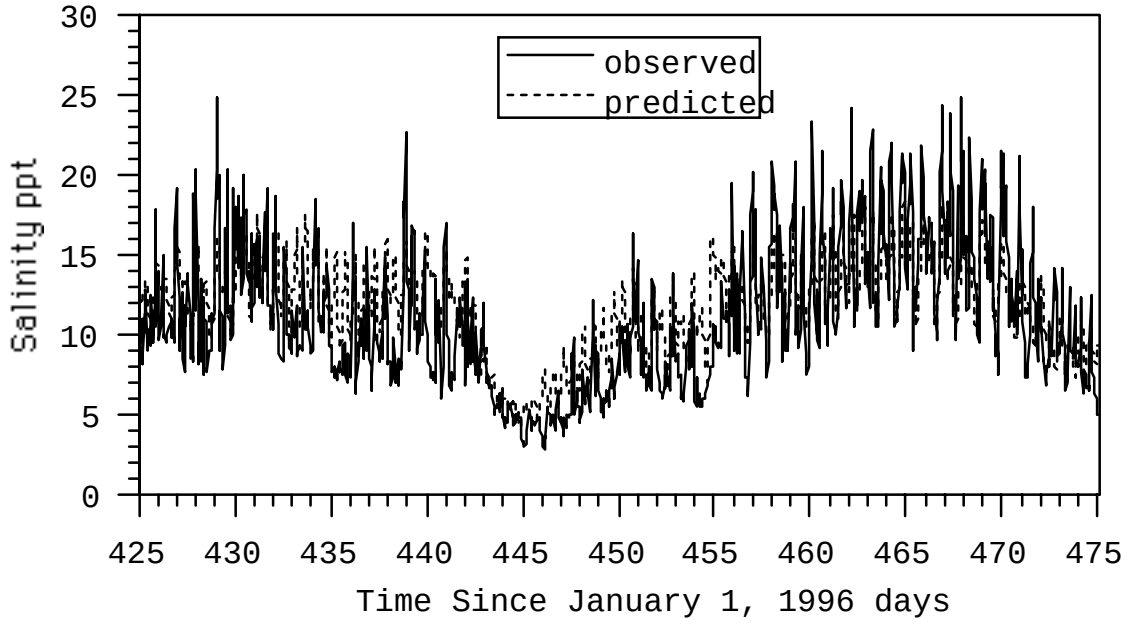

Figure F-10. Salinity at Station S-Surface-4

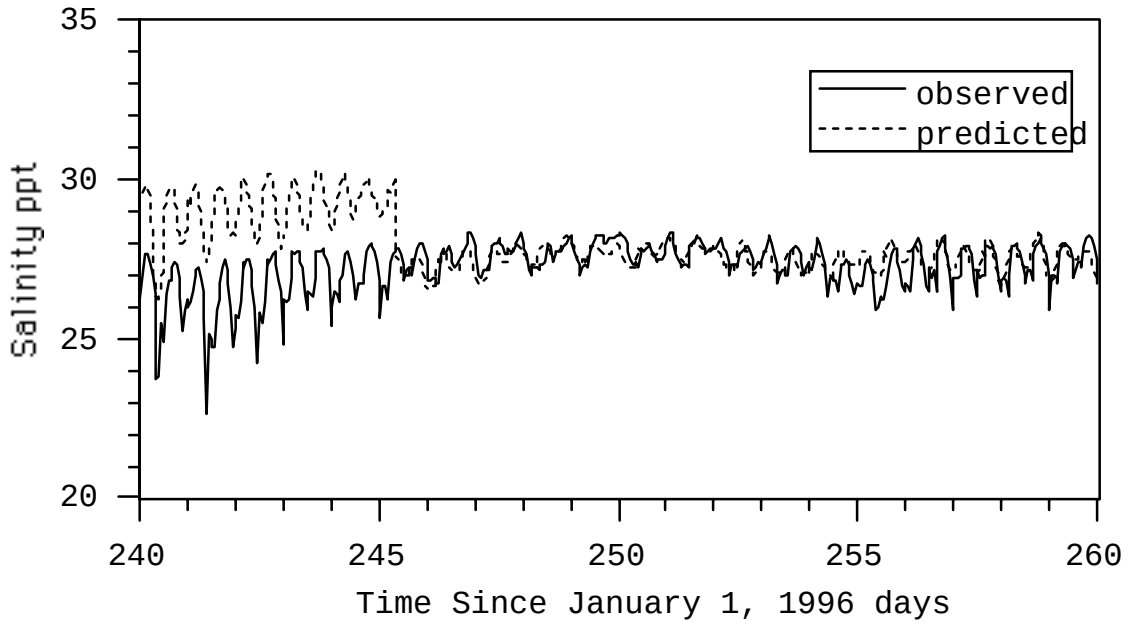

Figure F-11. Salinity at Station B-Bottom-1

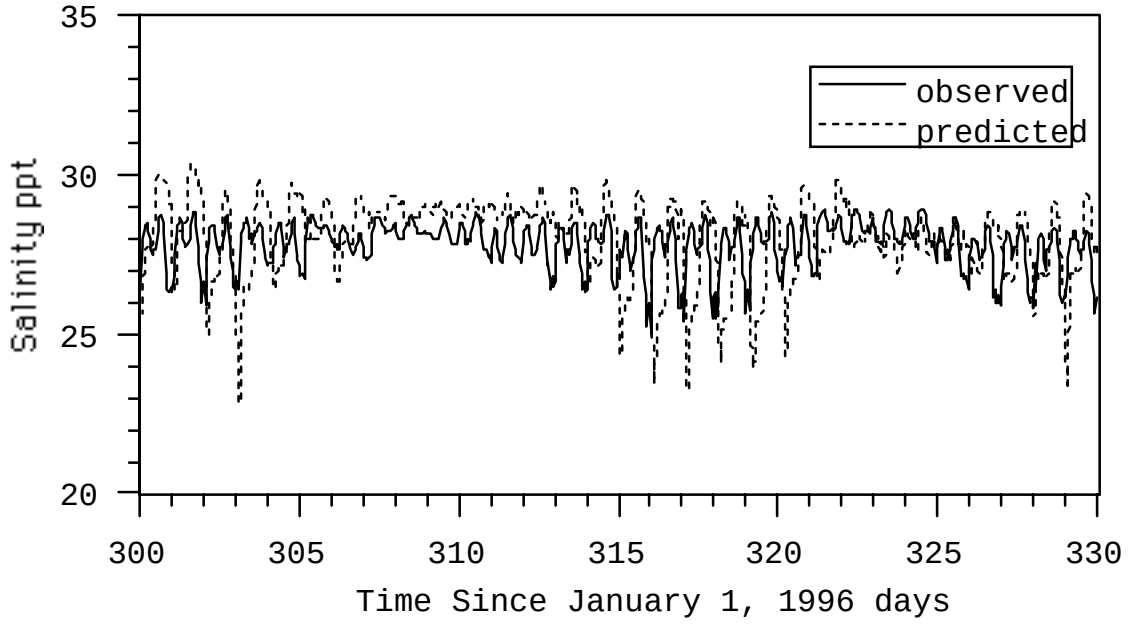

Figure F-12. Salinity at Station B-Bottom-2

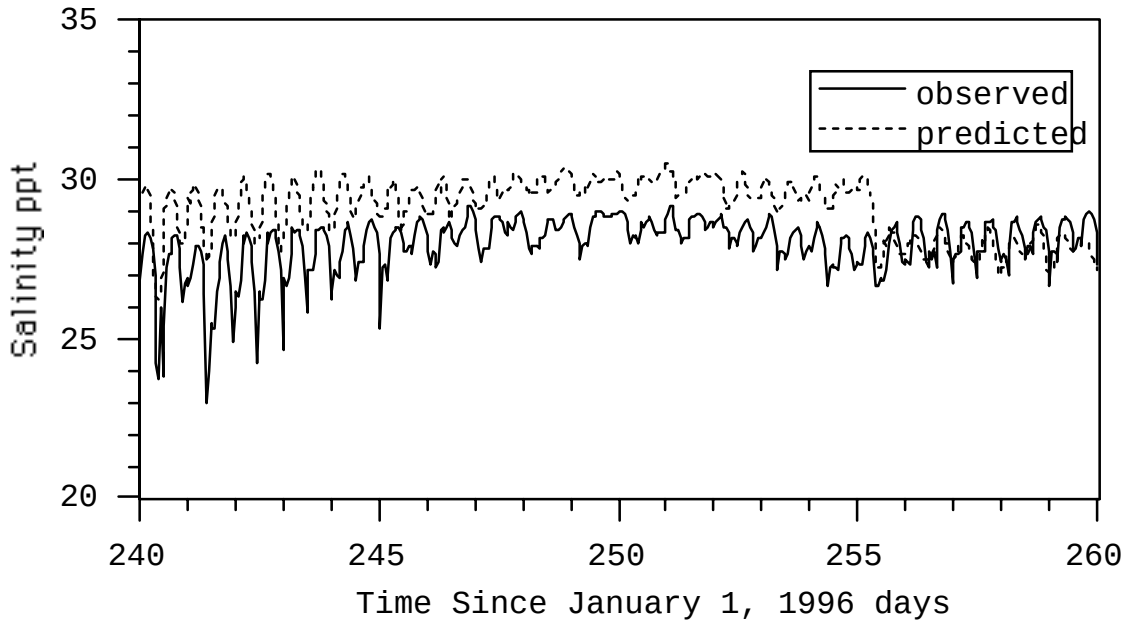

Figure F-13. Salinity at Station B-Middle-1

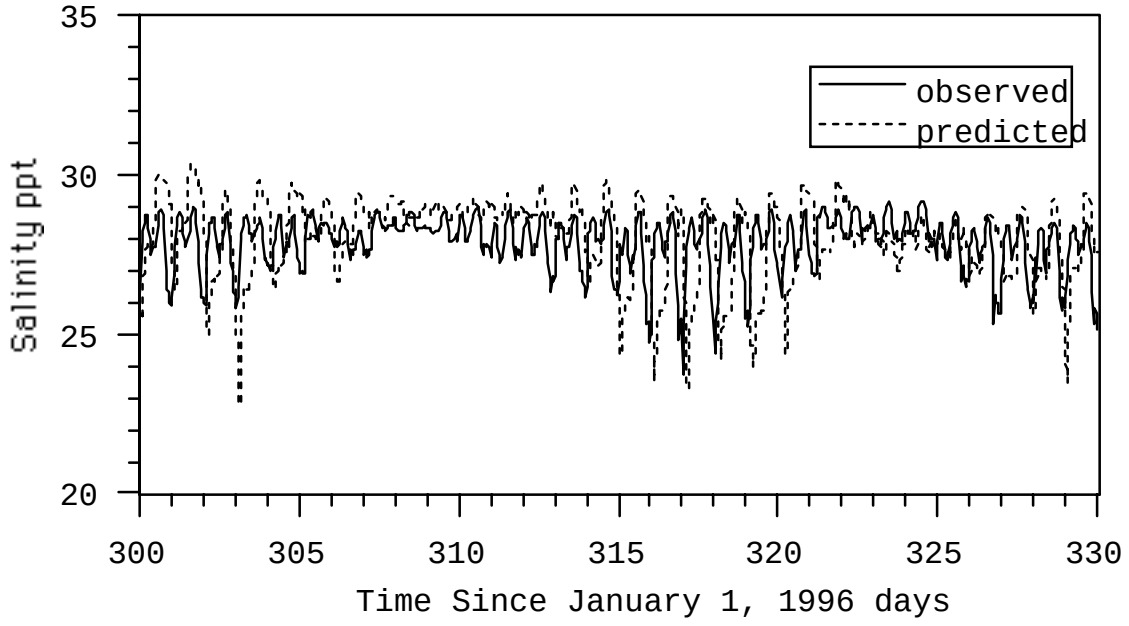

Figure F-14. Salinity at Station B-Middle-2

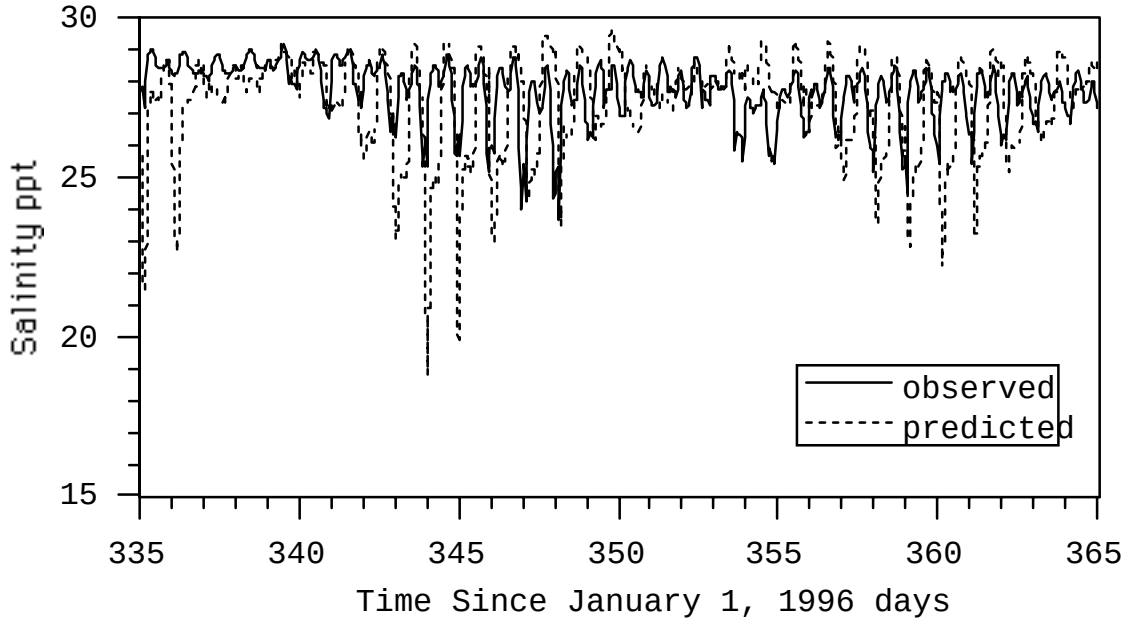

Figure F-15. Salinity at Station B-Middle-3

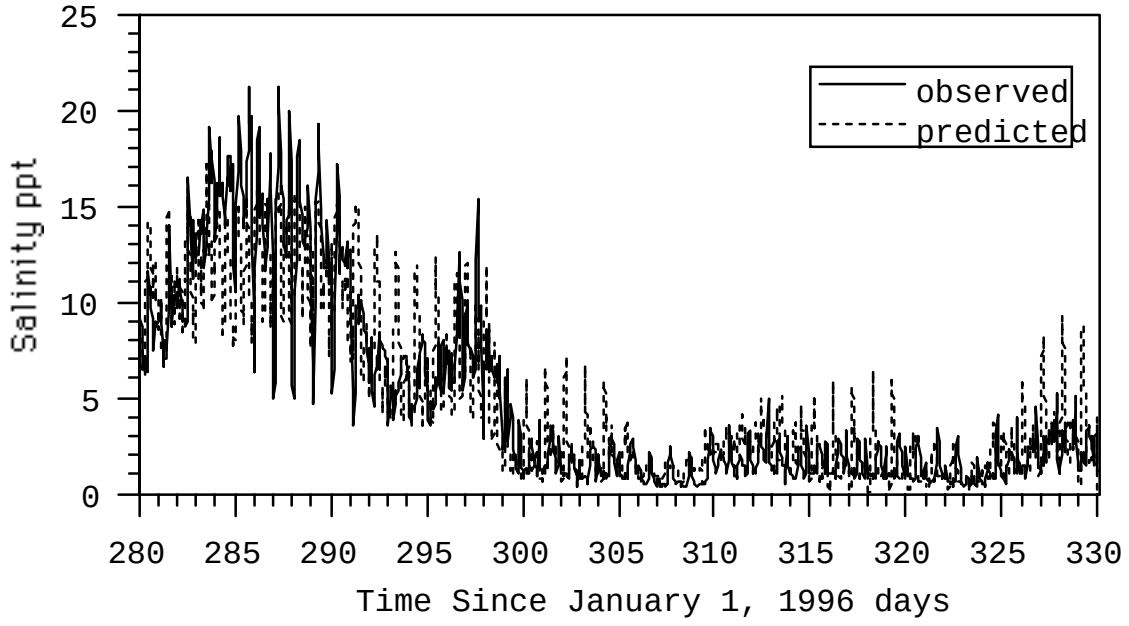

Figure F-16. Salinity at Station B-Surface-1

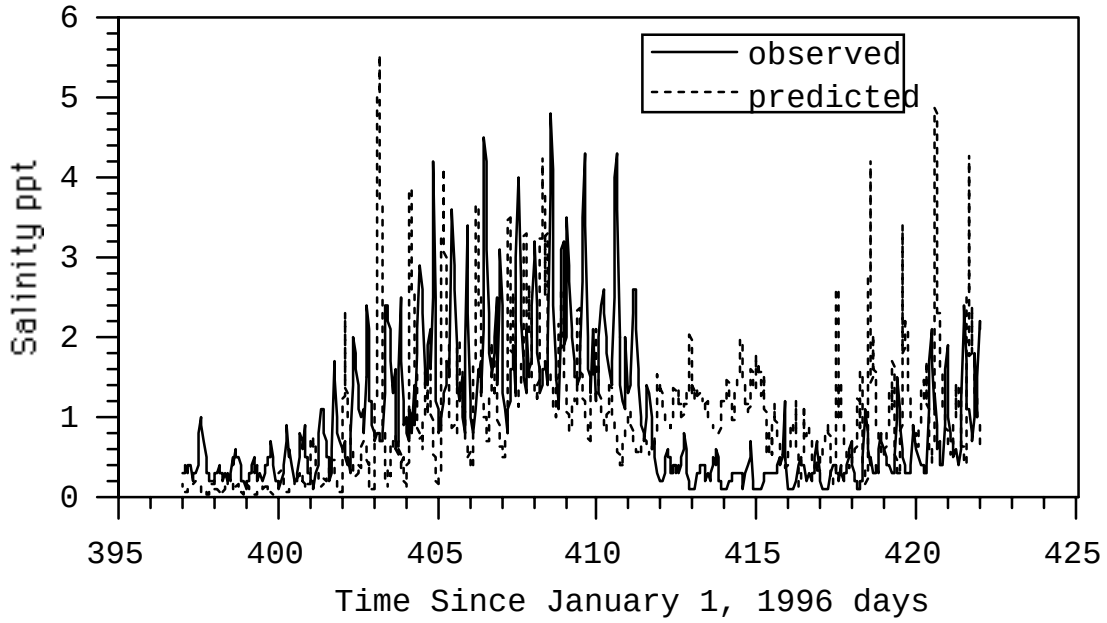

Figure F-17. Salinity at Station B-Surface-2

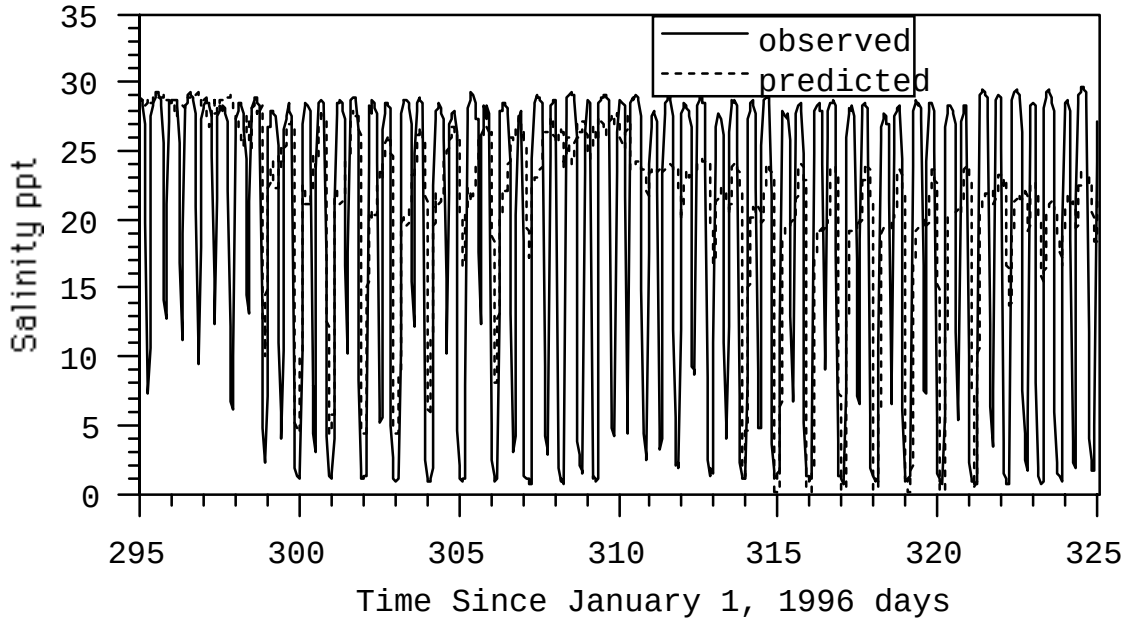

Figure F-18. Salinity at Station D-Bottom-1

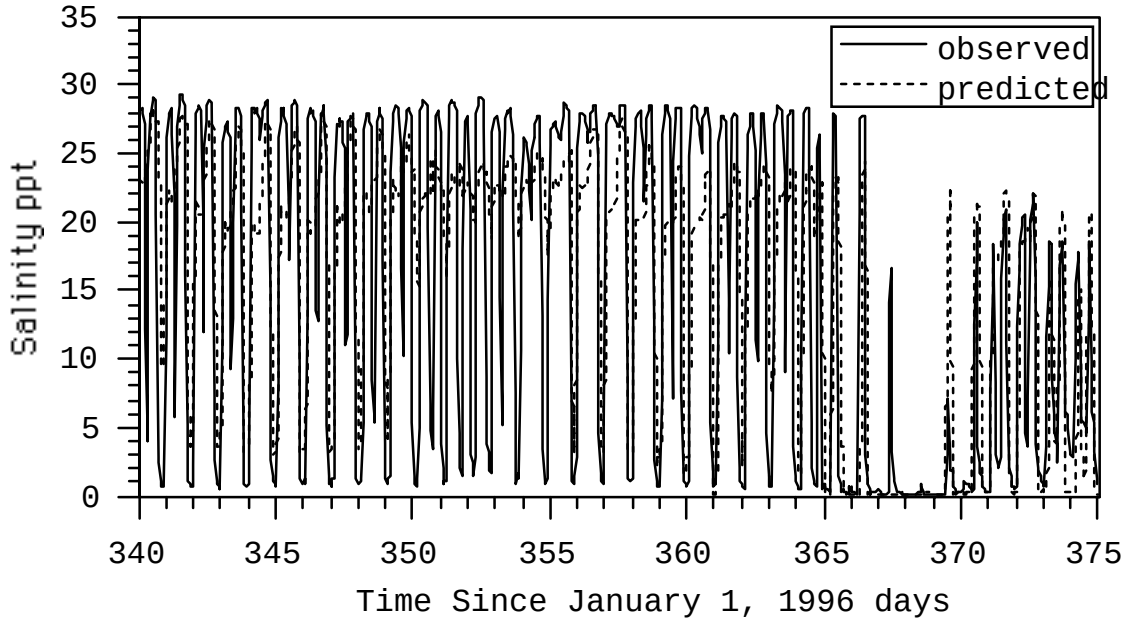

Figure F-19. Salinity at Station D-Bottom-2

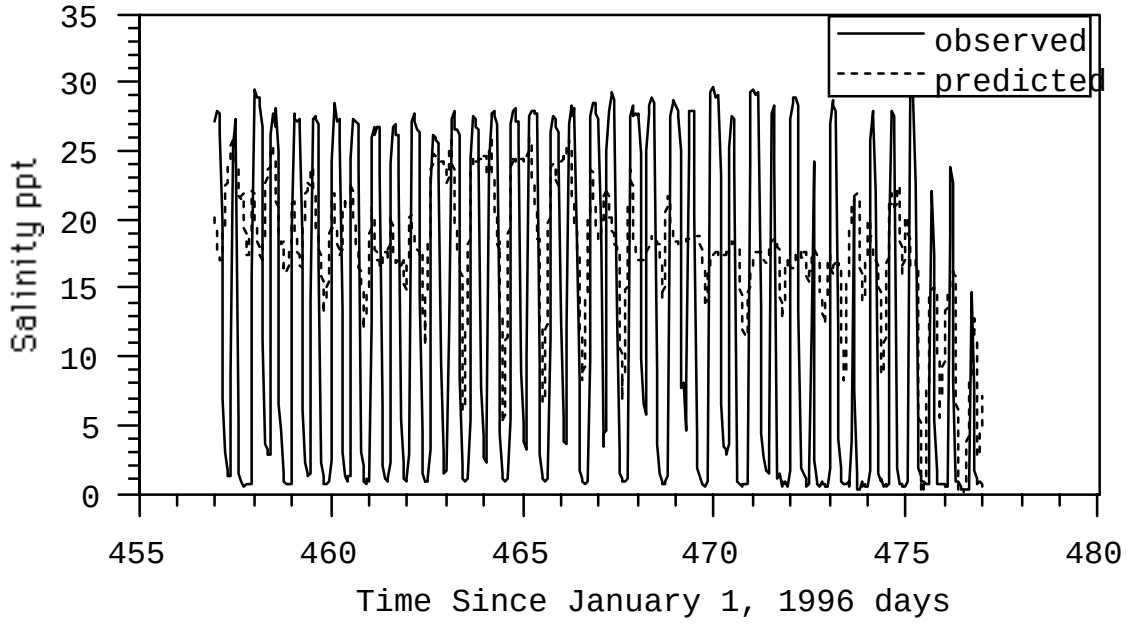

Figure F-20. Salinity at Station D-Bottom-3

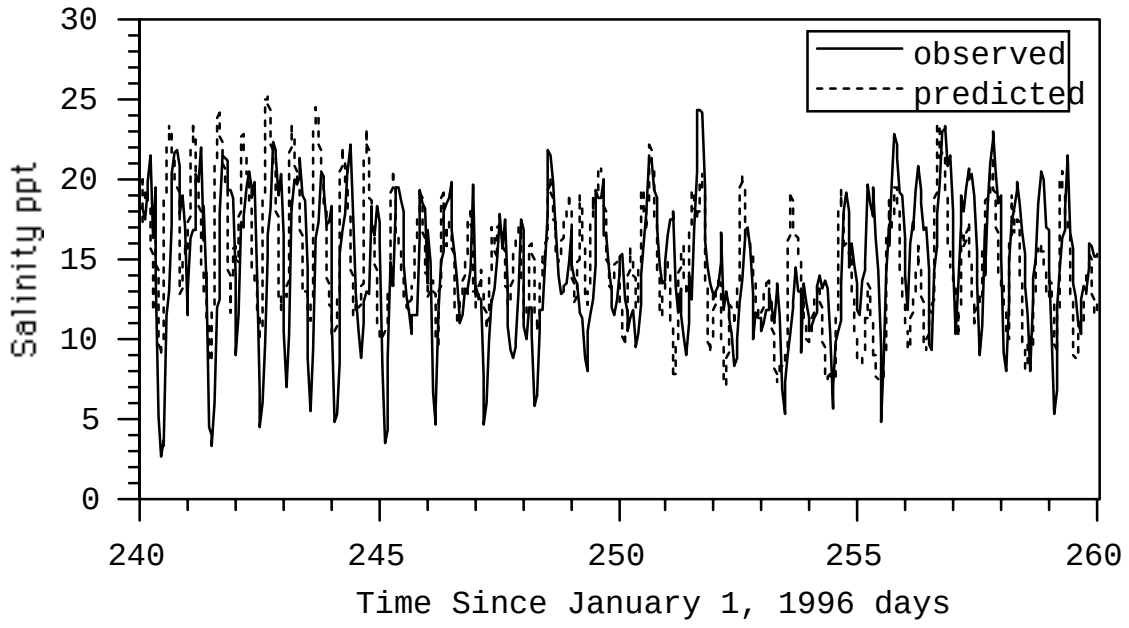

Figure F-21. Salinity at Station D-Surface-1

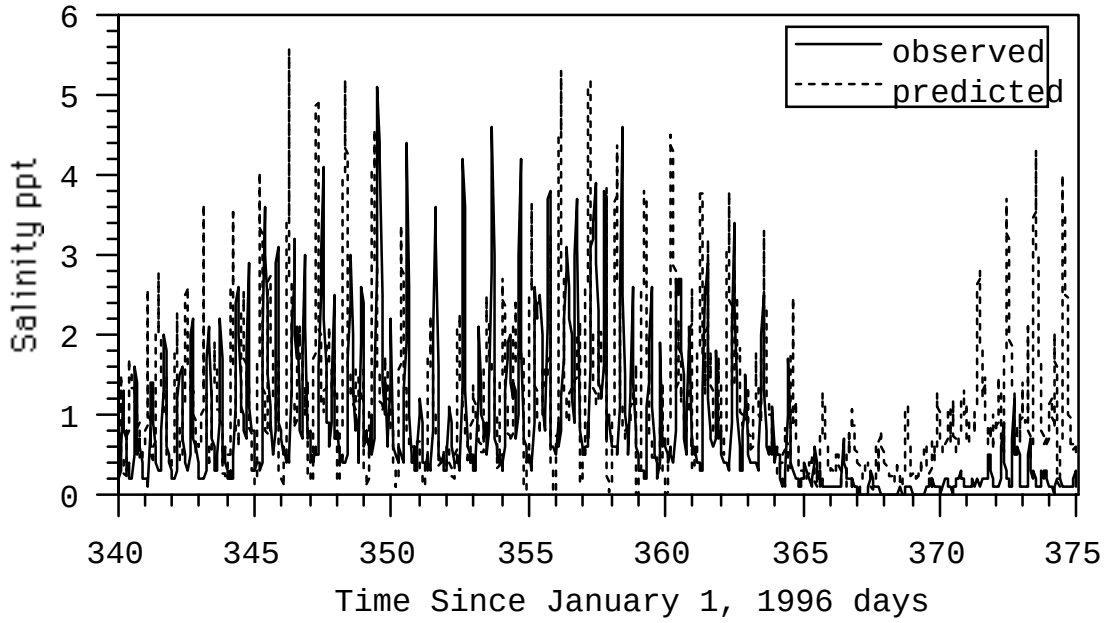

Figure F-22. Salinity at Station D-Surface-2

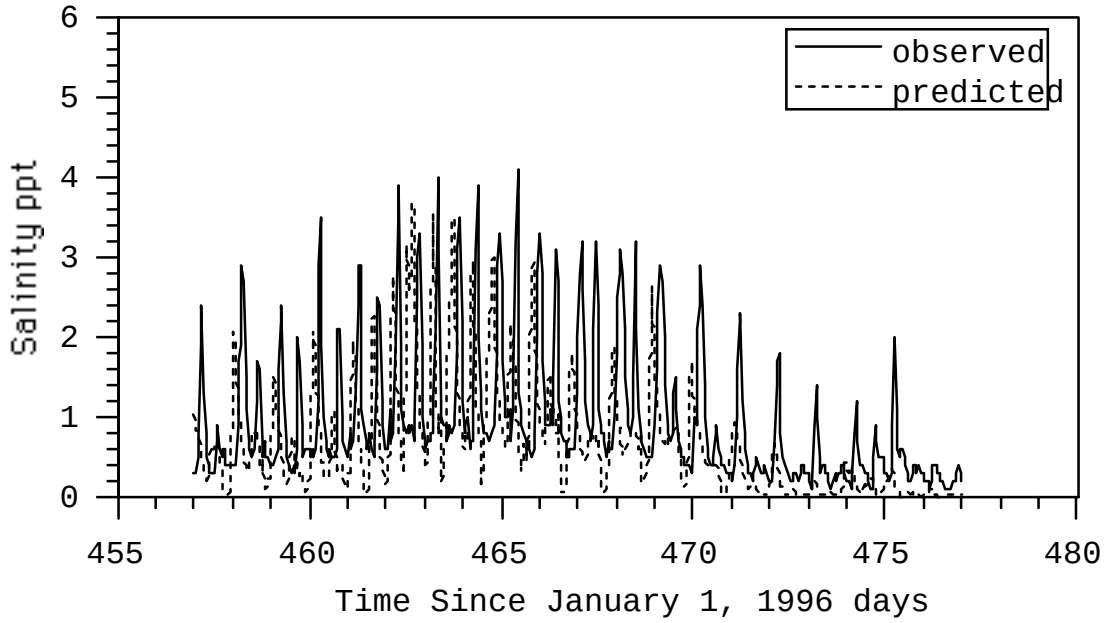

Figure B-23. Salinity at Station D-Surface-3